ELECTRODEPOSITION AND HOT CORROSION OF CERMETS

Thesis

Presented for the degree of Doctor of Philosophy

in the

University of London

by

John Adeyemi Carew

Nuffield Research Group, Department of Metallurgy

Royal School of Mines

Imperial College

December, 1979

CONTENTS

****

ABSTRACT

Electrodeposited cermets have been produced from a Watt's nickel bath containing Al_2O_3, ZrO_2 and HfO_2 particles (0.05 to 0.1 μm) held in suspension by mechanical stirring and air-agitation. The effects of particle concentration and plating conditions on microstructure and physical properties of the deposits were studied. Using submicroscopic Al_2O_3, ZrO_2 and HfO_2 particles, the room temperature yield strength increased from 11.2 kg/mm^2 for as-deposited nickel to 67.8 and 75.2 kg/mm^2 for nickel deposites containing 2.02 wt % Al_2O_3 and 3.92 wt % ZrO_2, respectively. The corresponding average hardness of nickel deposit not containing ceramic oxide was 170.8 VHN compared to 275.4, and 420.4 VHN for Ni.Al_2O_3 (2.02 wt.%) and Ni.ZrO_2 (3.92 wt.%) respectively. Heat treatment at 750^{o}C for 1 h resulted in a drop in average micro-hardness and yield strength of all specimens.

Oxidation behaviour of electrodeposited cermets of Al_2O_3, ZrO_2, and HfO_2 with nickel has been studied at 700^{o}C and 900^{o}C in SO_2:O_2 environments. Comparisons are made of the oxidation behaviour of cermet coated and duplex coatings of Ni-Co/Cr/cermet on Ni-base superalloys - Nimonic 105 and IN 738. Oxidation of specimens pre-coated with

Na_2SO_4 + NaCl mixture, and electrochemical studies of the various coatings in molten Na_2SO_4 and Na_2SO_4 + NaCl (5 wt.%) were also carried out.

The corrosion kinetics in SO_2 + O_2 mixtures falls into two categories: electrodeposited nickel and pure rolled nickel which oxidised faster than the duplex coatings of Ni-Co/Cr/Cermet; Al_2O_3 cermets in the range of 3.5 vol. % to 14 vol. % ZrO_2 and HfO_2 cermets, which showed slower oxidation rates. The overall effect of specimens pre-coated with Na_2SO_4 and Na_2SO_4 + NaCl mixture on the oxidation kinetics and the morphology of the scale varied according to the type of cermet coatings (Al_2O_3 ZrO_2 or HfO_2). Parabolic rate constants have been calculated for each type of coating and are in the range of 0.01 $mg^2/cm^4/h$ to 517 $mg^2/cm^4/h$. The corrosion products (NiO, Cr_2O_3, CrS, CoO and Co_3O_4) were studied by optical microscopy, SEM, TEMSCAN, and X-ray analysis.

CHAPTER 1 : INTRODUCTION

A.1. Background to the problem

The majority of turbine blades now in service in the more aggressive situations are given a surface coating prior to use, in order to improve their corrosion resistance. Most of these coatings are based on aluminium, but aluminium/chromium, chromium, and silicon have also been used with limited success. The Problems encountered in coated superalloys are usually due to degradation of the coating by interdiffusion with the base alloy, or by corrosive attack through pores and cracks in the coating itself. The problems of maintaining efficient coatings on nickel-base alloys have been examined by many workers (Llewelyn 1967; Ubank 1970; Goward 1970) and the properties of some of the Nimonic series of alloys after coating have been examined by Samuel and Lockington (1964) who concluded that suitable diffusion coatings of chromium and aluminium would prove beneficial under some circumstances, although the improvement in corrosion resistance might be offset in some cases by reduction of mechanical properties, particularly fatigue resistance. The search for materials able to withstand high temperatures, particularly in cyclic oxidising environments continues, and the large amount of research now being focussed onto the problem has been previously unparalleled.

Interest in dispersion-strengthened alloys for high-temperature applications has steadily increased since the introduction of the first such materials 25 years ago. This interest has resulted in the recent accelerated development of dispersoid-metal mixtures involving nickel, copper, chromium, iron and other base metals or alloys with various oxide or other dispersed phases (Zwilsky and Grant 1957; Feisel and Cochardt 1959; Snyder 1959; Stuart 1963).

Nickel and cobalt-base superalloys are the major high-temperature construction materials in industrial and aircraft gas turbines. These superalloys retain useful strengths to temperatures above 980°C (1800°F). However, the alloy additions that confer these high temperature strengths generally lower the superalloy's resistance to surface degradation by oxidation, hot corrosion or thermal fatigue. For this reason, surface protection by means of coatings is used to improve environmental resistance and retain alloy strength. Aluminium, with or without the addition of other elements, is the major coating constituent used, and aluminide coatings formed by interaction with the base metal are the major coatings in use. These coatings greatly increase the life of a part with service temperatures up to

925°C (1700°F) according to Dalder and Talboom (1964/65), while Geyer and Lane (1974) report the upper temperature limit for reasonable life to be 980°C (1800°F).

Conventional methods for the production of the various dispersion - strengthened composites may be divided into two general categories : 1) mechanical mixing followed by compaction and sintering, and 2) Chemical reactions. This includes a variety of procedures such as: (i) internal oxidation of the matrix metal, (ii) surface oxidation of matrix metal powder, (iii) preferential chemical reduction of mixed oxides, (iv) and co-precipitation of matrix and dispersed phase compounds followed by preferential chemical reduction of the matrix metal phase, with consolidation by standard powder metallurgy techniques (Bunshah and Goetzel 1959) as a final step. The literature abounds with reports of the difficulties of obtaining optimium dispersion - strengthened composites by these conventional processes. For example Feisel and Cochardt (1959) using mechanical mixing procedures for preparing dispersion-strengthened nickel and nickel-cobalt, found that the dispersoid particles tend to agglomerate during mixing and then segregate as oxide clusters in the composite, making alloys of structural quality difficult to obtain at best.

Gimpl and Fuschillo (1966) found that the fluidised bed process produces alloys with good oxide particle distribution; however, production rates are low and carbon contamination is a major problem for nickel and chromium alloys made by vapour phase decomposition of carbon containing compounds.

The major difficulty in alloy development for hot-corrosion resistance lies in achieving a balance between corrosion and oxidation resistance, alloy phase stability, and mechanical properties to meet the requirements of a particular application. Rather than rely on the superalloy itself to develop a protective scale, a corrosion-resistant coating may be applied to the surface. The coating and structural alloy, however, must be compatible to achieve the desired stability and corrosion protection. Such a coating should, like scale of good protective properties, be characterised by satisfactory compactness and adherance. The rate of interdiffusion between the two elements of the coating-metallic substrate system must, therefore, be low compared with the required service life. The protective layer and metal should also have approximately thermal expansion coefficients in order to avoid cracking and exfoliation of the coating during temperature changes. The protective coating should be relatively easy to apply, and the defects which may have occured in exploitation should be able to be repaired without causing adverse effects on

sound neighbouring areas. Coatings have been used successfully in jet engines, but their value in industrial gas turbines, where long parts lives are required, remains to be demonstrated.

2. Nickel-base Superalloys.

In the late 1930s, nickel-base superalloys development was underway in England, France, Germany and United States, prompted by the need for more heat-resistant materials in aircraft engines. It has been paced, since the early 1940s, by the increasing demands of advancing gas turbine engine technology. Nickel-base alloys are the bulwark of high-temperature metallurgical technology in gas turbines, nuclear reactors, furnaces, and a myriad of highly specialised modern products. Although their physical metallurgy is the most complex and subtle of any alloys, the relationships of properties to structures in the systems is certainly the most well known of all materials for use over the range 650 - 1093°C. This allows their use to extend to the highest homologous temperature of any competitive materials.

Nickel-base superalloys containing small additions of zirconium and boron were first made in 1948 (Skelton), although a full study of the effects of these additions was not made until some years later, and quite independently, by Decker, Rowe and Freeman (1957). New or modified alloys have been introduced from time to time, not only to meet

TABLE 1 COMPOSITION OF ALLOYS (Wt. %)

Alloy designation	Type	C	Fe	Ni	Cr	Co	Mo	Ti	AL	W	Nb	Ta	Zr	B
Nimonic 80A	Wrought	.10		Balance	19.5			2.3	1.4				.10	,008
Nimonic 81	Wrought	.05		Balance	30			1.8	0.9				.06	.003
Nimonic 105	Wrought	.20	2.0 max	Balance	14.5	20.0	5.0	1.2	4.7					
Nimonic 90	Wrought	.07	3.0 max	Balance	19.5	18.0		2.5	1.5					
IN 100	Cast	.18		Balance	10.0	15.0	3.0	4.7	5.5				.06	.015
IN 713 LC	Cast	.05	0.35	Balance	12.0		4.5	0.6	5.9		2.0		.10	.01
IN 738 LC	Cast	.11		Balance	16.0	8.5	1.75	3.5	3.5	2.6	.85	1.75	.05	.01
IN 939	Cast	.15		Balance	22.5	19.0		3.7	1.9	2.0	1.0	1.4	.10	.01
MAR M246	Cast	.15		Balance	9.0	10.0	2.5	1.5	5.5	10.0		1.5	.05	.015
Ud 500	Cast	.07		Balance	18.0	19.0	4.2	3.0	3.0				.05	.007
X - 40	Cast	0.5		10.5	25.5	Balance				7.5				
FSX 414	Cast	0.25		10	30	Balance				7.0				

the continued demands from engine designers for alloys capable of operating at higher temperatures, but also to satisfy particular requirements associated with the form required or the manufacturing process to be adopted. The complete list of nickel-base alloys now commercially available under the 'Nimonic' trade mark is thus extensive. The alloys numbered 80A, 81, 90 and 105 form the main development stream of alloys for wrought turbine blades. They have progressively increasing high temperature strength obtained by compositional changes in combination (Table 1) with optimisation of heat-treatment. In addition the higher-strength alloys Nimonic 105, 108, 109, 115 and 120 are all vacuum - refined. Nimonic 108 and 109 are similar to Nimonic 105 with slightly modified compositions to meet special requirements of certain engines.

By the late 1950s turbine blades operating temperatures, which were always challenging, were clearly limited by the capability of the best available wrought alloys. Further, these alloys were forgeable only with great difficulty. Chemical compositions of alloys with great strength appeared available, but were impossible to forge by any available methods. The needed strength was found by turning to investment cast alloys. Cast nickel-base alloys, the present mainstay of the hottest

stages of gas turbines, include 1N-100, Udimet 500 and 700, 1N 738, 1N 792, Rene'80 and Mar-M432.

Nickel-base superalloys are generated principally from Ni-Cr-Co ternary system. Aluminium and Ti additions contribute to the formation of a precipitation-hardenable Ni_3Al (gamma prime) phase which precipitates coherently with the matrix. Refractory metal elements are added as solid-solution strengtheners for the matrix and also for substitution in gamma prime. Carbides of Cr, Ti, and/or the refractory elements are also present. The demand for higher-strength alloys has been met by increased Al and Ti to develop more gamma prime, as well as by increased amounts of refractory elements. Elements such as chromium, molybdenum, and tantalum form a series of carbides, which contribute to grain boundary strengthening. Aluminium and chromium provide oxidation resistance, while chromium and titanium are effective in imparting hot-corrosion resistance. Increasing the chromium content, however, decreases the gamma prime - solvus temperature and the maximum temperature to which the alloy can retain useful strengths. The Cr content, however, has been concurrently decreased to prevent the formation of embrittling TCP phases (Sims 1966). This lowering of the Cr content has contributed much to the problem of surface stability - the

ability of superalloys to resist the various forms of environmental attack. A delicate compositional balance is necessary in some alloys to achieve all the needed properties, that is, maximum strength, oxidation resistance, and hot-corrosion resistance, while maintaining resistance to the formation of micro-structural phases in service may weaken or embrittle the alloy. Cast nickel-base superalloys have the combination of high-temperature capability and intermediate - temperature strength required of turbine blades. They also demonstrate good ductility, oxidation and hot-corrosion resistance, microstructural stability, and castability, This combination of properties has led to widespread use in turbine blades, vanes, and integral wheels.

The development of dispersion-strengthened nickel-base alloys was made possible because powder metallurgy came into use as a preparation technique. Commercially produced dispersion-strengthened nickel was introduced by Du Pont in 1962 as TD Nickel, an alloy of 2 v/o ThO_2 in an unalloyed nickel matrix (Anders et al 1962). Attempts have been made to produce alloys containing more stable particles such as refractory metal oxides, in order to maintain strength to higher temperatures. These alloys retain outstanding strength at temperatures above

980°C (1800°F) owing to the presence of fine stable well-dispersed oxide particles, but at lower temperatures have less strength than conventional wrought or cast gamma prime - hardened nickel-base alloys (Betteridge and Heslop 1974). The technique used to produce these dispersion-strengthened alloys does not lend itself to the addition of reactive elements such as aluminium and titanium, so these alloys could not be successfully strengthened by gamma prime. A variety of methods have been used in attempts to achieve the optimum dispersoid size and distribution (Leszynski 1960; Rice 1965; Ansell et al 1966). The simplest approach has been mechanical mixing of alloy matrix and dispersoid powders prior to compaction. Nimonic alloys MS 753 and 754, similar in composition to Nimonic 80A but containing about 1.3% yttrium oxide, are made in production quantities by this process.

3. Oxidation Characteristics of nickel-base superalloys in SO_2 : O_2 atmospheres

The most serious form of corrosion in nickel-base superalloys is that due to reaction with sulphur or sulphur compounds. The corrosion is particularly severe due to the formation of a nickel/nickel-sulphide (Ni_3S_2) eutectic which melts at about 645°C. Sulphur attack is

only rarely due to elemental sulphur, but usually due to sulphur-bearing gases SO_2, SO_3 and particularly H_2S in reducing conditions.

In the corrosion of Ni-based alloys which are used in aero-engine turbine blades at high temperatures, the rate of oxidation is considerably enhanced by the presence of sulphur dioxide in the atmosphere. In Atmospheres containing no free oxygen, Alcock et al (1969) and Fontaine (1969) found very rapid but irregular attack by sulphur dioxide on nickel. Pre-oxidation in pure oxygen was found by Alcock et al to reduce the sensitivity to sulphur dioxide and where layers thicker that 2000°A were formed no effect of SO_2 was subsequently observed. This was confirmed by Wootton & Birks (1972) in their study of the oxidation of nickel in atmosphere containing SO_2. Alcock et al studied the corrosion of pure Ni sheet by controlled mixtures of SO_2 + Oxygen in the temperature range 500 - 750°C. At a given temperature the rate of attack passed through a maximum value for SO_2 - rich gas mixtures. The authors also observed that the mechanism was usually of parabolic diffusion-controlled type, but at the highest rates of attack the process had linear kinetics. And in accordance with the views of Kubaschewski and Hopkins (1962), and Kofstad (1966) the process is controlled by the rate of diffusion of the

reactants through the growing layers, except at the highest reaction rates. Increasing reaction rate with temperature up to about 700°C, above which it began to decrease, had also been found in earlier similar studies by Alcock and Hocking (1966). They suggested that this behaviour is due to the decrease in stability of the products, such as sulphates or sulphides in the corroding atmospheres of constant total pressure as the temperature is raised.

The sensitivity of nickel to oxidation in sulphurous atmospheres at elevated temperature is appreciated by workers such as Vernon (1932); Ramyantsev and Chizhikov (1955); Ipatev and Zhellukin (1958); Hancock (1961); Arkharov et al (1963); Pennetier and Davignon (1964); Seybolt and Betram (1967); Fontaine (1969); Alcock et al (1969); Vasantasree and Hocking (1976). Much of the work done on nickel based alloys has been concerned with the conditions under which turbines operate in generating plant and experience of corrosion by fuel ash when most of the sulphur is present as sulphates.

Wootten and Birks (1972) studied the reaction occuring between nickel and argon atmospheres containing 10% sulphur dioxide over the temperature range 475-900°C. They found the reaction kinetics to be complex and not conforming th any single rate law over the whole course

of the reaction period. However, in most cases the reaction rate settles down to a more or less constant value, which is thought to be controlled by a reaction step at the scale-gas interface and which varies with temperature in a complex manner, showing a maxima at 600° and 750°C. The authors used microprobe analysis to indicate that substantial concentrations of sulphur (up to 5%) is dissolved in NiO. They suggested that the development of the relatively complex microstructures is an indication that the dissolved sulphur migrates quite rapidly through the NiO and also enhances cation diffusion rates. This is an agreement with the findings of Alcock et al (1969). They reported the mobility of the S in the NiO layer since an Ni_3S_2 layer was found beneath it, having grown by the inward diffusion of S ions to the receding metal surface. Vasantasree (1971); Vasantasree & Hocking (1976) studied the growth scale on specimens of Ni, Cr and Ni-Cr (0.1 - 50 at %) in the temperature range 600° - 1000°C in flowing SO_2 and SO_2/O_2 mixtures at 1 atmospheres total pressure. At 700° to 800°C there were two layers in the corrosion product; an outer compact layer of NiO containing Ni_3S_2 islands and an inner porous layer of Cr_2O_3 with CrS and Ni_3S_2 islands. Vansantasree's report includes a brief review up to the year 1970, of the research work involving reaction with

SO_2/SO_3 of a number of metals of interest in high temperature corrosion.

Mckee et al (1976) investigated the effect of surface treatments, such as grit-blasting and mechanical indentation, on the resistance of some Ni-Cr alloys and the Ni-base superalloy IN 738 to Na_2SO_4 induced hot corrosion at 900°C in a 0.1% SO_2 - 76% O_2 - Bal. N_2 atmosphere. They observed that when deformed-and-annealed specimens of Ni-5Cr, Ni-15Cr and IN 738 were placed directly in contact with molten Na_2SO_4, the grain boundaries facilitated sulphur penetration and enhanced metal wastage. The deleterious effects of mechanical treatments could, in the case of Ni-15Cr, be offset by suitable thermal treatments such as pre-oxidation prior to Na_2SO_4 exposure. The increased grain boundary density created by the grit-blasting promoted the formation of a dense, continuous Cr_2O_3 scale during the pre-oxidation treatment. This scale, rather insoluble in Na_2SO_4 equilibrated with the 0.1%SO_2 - 76% O_2 - bal N_2 atmosphere (Chatterji et al 1975), and effectively isolated the alloy from the salt and resisted corrosion. The former authors supported the contention that the hot corrosion behaviour of an alloy depends not only on chemical consideration (Goebel et al 1973 , Chatterji et al 1975), but also on microstructural characteristics of the alloy. The study was, however, limited to alloy

compositions likely to produce Cr_2O_3 - rich scales in purely oxidising environments. Whether or not the hot corrosion behaviours of Al_2O_3 - forming alloys depends on mechanical and thermal history remains an open question.

Strafford et al (1977) found that small additions ($\sim$ 0.5 - 5 W/o) of certain elements to a Ni/15 Cr control alloy can considerably reduce the corrosion experienced in an SO_2/O_2 atmosphere, particularly the additions of Gd, U, Zr, or V. These elements are also effective in controlling sulphidation. Additions of Gd and Zr improve oxidation performance, but V appears to be detrimental and U appears to induce excessive intergranular oxidation.

4. Oxidation behaviour of dispersion strengthened Nickel alloys.

Researchers in the area of alloy development are continually striving to obtain materials which possess good strength and creep resistance at elevated temperatures. Such efforts have led to the development of dispersion-strengthened alloys, which exhibit both a resistance to recrystallization at temperatures near the melting point of the matrix metal and a stress-rupture response which is nearly temperature independent. The first commercial dispersion-strengthened Ni-base alloy was thoriated Ni,

which is strengthened by submicron ThO_2 particles uniformly distributed throughout the microstructure. However, the oxidation behaviour of this alloy does not differ substantially from that of pure Ni, thus requiring that it be coated for elevated temperature use. As a result, Cr has been added as an alloying addition to improve the high temperature oxidation resistance. An additional effect of Cr is to reduce the high temperature steady-state creep rate (Wilcox and Clauer 1969).

The effects of dispersion thoria particles on the oxidation behaviour of Ni-20% Cr alloys at temperatures above 800°C have been well documented (Grisaffe and Lowell 1969; Wallwark and Zed 1971; Giggins and Pettit 1971; Lowell et al 1970; Davis, Graham and Kvernes 1971; Lowell 1971; Gilbreath 1971; Sanders and Barrett 1971; Centolanzi et al 1971; Seltzer, Wilcox and Jaffee 1972), and in summary are: (1) to promote the selective oxidation of chromium to form a continuous Cr_2O_3 scale; (2) to reduce the rate of growth of the Cr_2O_3 compared to particle-free alloys; (3) to greatly improve the adhesion of the Cr_2O_3; and (4) to change the location of the scale-forming reaction to the scale-metal interface in the alloys containing a dispersion, from the scale-oxygen interface in the dispersion-free alloys.

A Ni - 13.5% Cr - 1 vol % ThO_2 alloy in some cases showed the same oxidation behaviour as the Ni - 20% Cr - 2 Vol.% ThO_2 alloy (Davis, Graham and Kvernes 1971), but a dispersion of 2.5% Sm_2O_3 had no effect on the oxidation of a Ni - 7.5% Cr alloy (Stringer and Hed 1971), so that the minimum alloy chromium content at which an oxide dispersion can make a useful contribution to the oxidation resistance of Ni-Cr alloys apparently lies in the range of 7.5 to 13.5 wt %.

The mole fraction of Cr which must be present in a thoriated Ni-Cr alloy to ensure selective oxidation of Cr is uncertain. In binary Ni-Cr alloys, approximately 30 wt.% Cr is required (Giggins and Pettit 1969) for selective oxidation to occur at 0.1 atm. oxygen. Also uncertain is whether the ThO_2 particles remain inert with respect to the oxidation reactions, or whether they influence the oxidation behaviour. In a review paper, Rapp (1969) reported that dispersion-strengthened metals similar to thoriated Ni exhibit oxidation behaviour which differs very little from that of the matrix metal. Other types of metal-particle combinations were shown to affect the oxidation resistance.

Giggins and Pettit (1969) prepared specimens of Ni-Cr alloys containing a fine dispersion of Al_2O_3 by electroplating a layer of pure nickel onto alloy specimens in a bath containing a suspension of Al_2O_3 particles: these specimens

were then annealed to diffuse chromium into the nickel layer. The Oxidation rate at 900°C was greatly reduced by the dispersion, and a thin continous scale apparently consisting of Cr_2O_3 was formed. In addition, an alloy of Ni-10 wt.% Cr containing 1% scandium was produced. Unlike the alloys containing the oxide dispersion, the grain size of this specimen was quite large. Again, the oxidation rate at 1100°C was greatly reduced; however, at 900°C some portions of the specimen had a thick external NiO layer and an internal oxide subscale, although again most of the specimen was covered with a thin adherent Cr_2O_3 scale.

Stringer and Hed (1971) studied the effect of a dispersion of Sm_2O_3 on the oxidation of a Ni-7.5 wt % Cr alloy over a wide range of oxygen pressures and at 900 and 1100°C. The samaria was present as (a) a small number of large agglomerates (10-30 μm); (b) many small agglomerates (1-3 μm); (c) a uniform fine distribution of oxide particles throughout the matrix. The results indicated that the samaria distribution had no effect on the oxidation process, and the mechanisms of oxidation was controlled by diffusion through the nickel oxide. The rates of oxidation agreed closely with Giggins and Pettit's (1969) values for electrodeposited specimens.

However, contrary to the results of Giggins and Pettit for the plated specimens containing Al_2O_3, not only has the oxide dispersion had no effect, but the very considerable difference in grain size has had no effect either. It is possible, therefore, that the oxidation behaviour of the electroplated specimens differs significantly from that of specimens prepared in the bulk, possibly due to the existence of a chromium gradient as well as the oxide distribution.

Davis, Graham and Kvernes (1971) investigated the oxidation behaviour of Ni - 13.5 - 33.7 Cr-1 ThO_2 alloys in flowing oxygen at 150 Torr in the temperature range 1000 - 1200°C. These workers combined gravimetric measurements of the oxidation kinetics with microstructural studies of the reacted samples in order to evaluate the reaction mechanisms. The oxide products formed on the alloys were a function of Cr content, sample surface preparation, reaction time, and temperature. The presence of ThO_2 appeared to produce two effects during alloy oxidation. First, enhanced Cr diffusion to the alloy surface resulted in rapid formation of Cr_2O_3 subscale beneath NiO_2 on Ni - 13.5 Cr - 1 ThO_2 and selective oxidation of Cr for Ni - 22.6 Cr - 1 ThO_2. Second, the mechanism of formation of Cr_2O_3 was apparently different from that for simple Ni-Cr alloys, resulting in about an

order of magnitude reduction in the Cr_2O_3 growth rate. The oxidation-vaporization of Cr_2O_3 to CrO_3 became rate controlling for the higher Cr alloys after only a few hours of exposure at 1200°C. David, Graham, and Kvernes, observed that during the period of rapid weight gain, NiO grows as the main reaction product at both 1000 and 1200°C. However, X-ray diffraction results showed both Cr_2O_3 and $NiCr_2O_4$ spinel to be present in small quantities. The oxidation of TD NiCr (Ni-20wt %Cr - $2ThO_2$) was studied between 900 and 1200°C by Wallwork and Hed (1971). The authors compared the oxidation behaviour with that of Ni-30 Wt % Cr and Co - 35 wt % Cr alloys. They found that all alloys developed Cr_2O_3 scales but the weight changes obtained for the Ni Cr and CoCr alloys showed an increase with time whereas above 1000°C the TD NiCr showed a progressive loss in weight from the evaporation of CrO_3 from the scale, and the reaction products appeared to be formed mainly at the alloy-scale interface.

The oxidation behaviour of Ni-20Cr alloys containing approximately 3 Vol % Y_2O_3, ThO_2, and Al_2O_3 as dispersed particles was examined by Wright, Wilcox and Jaffee (1975), in the temperature range 900 to 1200°C in slowly flowing oxygen at 100 Torr. The results showed that the oxidation behaviour of the Y_2O_3-, ThO_2-, Al_2O_3-, and CeO_2-containing alloys was very similar and that some anomalies

in the behaviour of the ThO_2 - containing alloy might be explained by the slower rate of chromium diffusion in this coarse-grained alloy. Two Al_2O_3 containing alloys were studied. One with a relatively coarse dispersoid size behaved in a manner analogous to a dispersion-free Ni-30% Cr alloy at 1100°C. The other alloy contained a dispersion of fine Al_2O_3 particles and behaved exactly like the Y_2O_3 containing alloy at 1000 and 1100°C, but at 1200°C oxidised at a faster rate.

Improvements in oxidation resistance have been reported for Ni-20% Cr - 3 vol % Y_2O_3 and Ni-20% Cr - 3 vol % CeO_2 alloys, Stringer et al (1971), Stringer, Wilcox and Jaffee (1972), at 900 to 1200°C in 100 Torr oxygen. Interestingly, other workers found that dispersions of Cr_2O_3, Al_2O_3, TiO_2, and ZrO_2 have little effect on the oxidation rate of Ni-20% Cr oxidised at 800 and 900°C in air for long times, Kravchenko and Zhuk (1969). Michels (1976) prepared nickel - 20 wt.% chromium alloys containing ThO_2, Y_2O_3, La_2O_3, Al_2O_3 and Li_2O, by the mechanically alloying technique. These alloys were examined for isothermal and cyclic oxidation resistance in dry air at 1000, 1100 and 1200°C. TDNiCr, a commercial electrical heating element alloy (Com Ni-20Cr) and a laboratory melted alloy (Giggins and Pettit 1969) (Lab Ni-20Cr) were also tested. The workers found that Y_2O_3, La_2O_3, Al_2O_3 and ThO_2

dispersoids markedly increased both isothermal and cyclic oxidation resistance compared to Lab Ni-20Cr at all temperatures; in contrast Li_2O additions gave no improvement in protection. Com Ni-20Cr was in between Lab Ni-20Cr and the Y_2O_3, Al_2O_3 and ThO_2 containing alloys in both cyclic and isothermal oxidation performance.

Michels' (1976) results on the oxidation resistance of Ni-20 wt % chromium alloys containing ThO_2, Y_2O_3, La_2O_3, Al_2O_3 and Li_2O, as prepared by the mechanical alloying technique, indicated that the dominant oxide was Cr_2O_3, although NiO and $NiCr_2O_4$ were also occasionally observed. This was in agreement with the observations of Wallwork and Hed (1971) who reported that the oxidation product of TDNiCr is mainly Cr_2O_3 together with some $NiCr_2O_4$. Giggins and Pettit (1971) observed NiO in TDNiCr scale, but emphasized that a continuous Cr_2O_3 layer was always underneath. Kravchenko and Zhuk (1969) indicated that $NiCr_2O_4$ was a transient phase while Giggins and Pettit (1969) stated that once a continuous Cr_2O_3 scale was formed, NiO ceased to grow.

Several alloying elements, when added as either metals or oxides such as Si and Mn in Ni-20Cr or as ThO_2 in TDNiCr, have been shown to improve cyclic and isothermal oxidation resistance (Douglas and Armijo 1970; Lowell 1973). Other elements including Ca, Ce, La, Zr and Mg are also known to have an influence (Rustman 1950;

Pfeiffer and Sommer 1966). Also small additions of reactive metals, e.g. Y, Th, Ca, Ce, Sm, etc., are very benificial and provide good oxidation resistance or scale adherence or both. Kvernes and Kofstad (1970) added up to 0.7wt.% yttrium to a Ni-9Cr-6Al alloy and found improved scale adherence and a reduction in the oxidation rate. Yttrium existed in the grain boundaries of the alloy in the form of Ni-Y intermetallics that oxidised preferientially, giving rise to a "Keying-on" effect of the oxide scale. There was no yttrium found in the scales.

Except for a few relatively minor differences, the oxidation of alloys containing dispersed oxide particles formed by internal oxidation is reasonably analogous to the oxidation of pure metals containing dispersed oxide particles, so that certain alloy oxidation studies may be used to predict the expected oxidation behaviour for yet uninvented dispersion strengthened metal.

5. Electrochemical behaviour of Ni-base superalloys in Molten Salt environment.

The performance of nickel base superalloys at high temperatures depends, in part, on the formation of an oxide film to prevent extensive oxidation or other forms of detrimental corrosive attack. The intensity of the corrosion is usually a function of the environment to which the material is exposed and the nature of the

oxide film. Danek (1965) established that hot-section components of gas-turbine engines, especially in marine applications, are susceptible to deterioration by a form of catastrophic oxidation stimulated by the presence of molten salts, the main corrosive constituent being Na_2SO_4. Although Na_2SO_4 is present in sea salts, it can also be formed by the reactions between NaCl and sulphur impurities (Cutler et al., 1971).

$$2NaCl + H_2O + SO_3 \longrightarrow Na_2SO_4 + 2\ HCl$$

The sulphates can then form molten deposits on the high temperature metal surfaces.

Wheatfall et al (1966) investigated the effect of molten salt behaviour at 900°C of oxide films on two nickel base superalloys (AMS 5391A and AMS 5384) and pure nickel. In the initial experiments, Na_2SO_4 and NaCl were reacted with Cr_2O_3 and NiO in both oxidising and reducing atmospheres. The authors found that half-cell potential measurements correlate well with sulphidation attack. A sustained rise in the half-cell potential was observed whenever sulphidation occured. Alloy AMS 5391A was attacked in both Na_2SO_4 and Na_2SO_4/NaCl mixtures, while alloy AMS 5384 suffered sulphidation in Na_2SO_4/NaCl mixtures only. Increasing the oxide thickness lengthened the time to a sustained rise in half-cell potential.

Reactions of NiO and Cr_2O_3 with Na_2SO_4 and NaCl occured only in the presence of carbon, a reducing agent. The products of such reactions were found to be nickel, NiS, Ni_2S_3, and CrS.

Cutler and Grant (1972) carried out electrochemical measurements of corrosion rates of several commercial nickel-base and cobalt-base gas turbine alloys as a function of time in the ternary Li/Na/K eutectic sulphate melt at 725°C under 1 atm oxygen and 3.23×10^{-4} atm SO_3. The alloys used were Nimonic 90, 105, 115, IN 738, X-40, Stallite 7 and 8. The corrosion rates for the Nimonic nickel-base alloys were all appreciably greater than the rates for the cobalt-base alloys, with the corrosion rate decreasing in the order Nimonic 90 > Nimonic 115 > Nimonic 105. The corrosion behaviour of IN 738 nickel-base alloy showed a different pattern from the other alloys. Instead of the gradual decrease in the mean corrosion rate as a function of time which was observed for the Nimonic alloys and the cobalt-base alloys, the corrosion rate for the IN 738 alloy remained relatively high for the first few hours before falling sharply to a relatively low value which compared favourably with the cobalt-base alloys. After the corrosion experiments, the authors observed a grey colouration in the molten sulphate, with Nimonic 115, 105 and IN 738 suggesting traces of a finely divided oxide precipitate. The

intensity of the discolouration was less for the alloys lower corrosion rates, and was hardly detectable with IN 738.

The literature on electrochemical behaviour of nickel-base alloys in molten salt is very scant. There has been a number of studies in this field carried out under contract to the Admiralty Materials Labs. of the M.O.D. Hocking et al (1973), and also studies of the high temperature behaviour of superalloys in KCl and NaCl melt by Mansfeld et al (1973), reported the results of corrosion studies of Nimonic 105, Ni-15Cr, Ni-10Cr, Ni-Cr alloys with three Hf additions of 0.16, 1.22, and 2.54 Wt.% and Ni, between 700°C and 900°C in various molten Na_2SO_4 and NaCl mixtures under air atmosphere. In general, the authors reported the increasing corrosion rates due to the presence of NaCl, and that in the case of preoxidised Ni-10Cr and Ni-15Cr in Na_2SO_4 + 18 to 25% NaCl, the corrosion rates are low.

Mansfeld et al (1973) found that the corrosion rates of superalloys in molten NaCl at 820°C are highly dependent on oxygen pressure and to some extent on the water content of the melt. The damaging effect of moisture reported by Mansfeld (1973) was also observed by Gurovich (1954) who concluded in a study of the action of fused chloride on nickel, copper, and certain steels that fresh and

dehydrated salt should always be used for testing metals in salts as the presence of even traces of moisture in the salt appreciably increases corrosion losses.

In electrochemical tests samples are exposed to an environment of fused salts, such as Na_2SO_4 or Na_2SO_4/NaCl mixtures at an elevated temperature. The experimental arrangement involves an electrochemical cell comprising of a fused salt as the electrolyte, a reference electrode, a working electrode, and perhaps auxillary electrodes. The purpose of the experiment may be either to. investigate the properties of the salt mixture (Brown et al 1970) or to determine the corrosion resistance of the specimen - working electrode (Doering 1969; Seybolt 1970; Davis and Kinnibrugh 1970; Baudo et al 1970). In all such measurements, a reliable reference electrode is essential.

6. Electrode Processes in Molten Salts

Molten Salts are a class of high-temperature liquids which range from the simplest ionic liquids, such as the alkali metal halides, through the less simple oxy-anion melts such as the alkali metal sulphates, nitrates, and carbon ates to the often complex assoicated liquids such as molten phosphates, borates, and silicates. In each case, the ionic charactor of the solid crystalline form persists in the molten state, although local association

reactions may take place. The principal constituents of these systems are free ions, complex ions, and free volume. The physical properties of a wide range of molten salts have been tabulated by Janz et al (1964).

A limitation to the range of molten salt systems arises from acid-base reaction. These are most significant in relation to oxyanion melts and are associated with the concentration of oxide ions, which Lux (1939) and Flood et al (1952) identified as the principal base, i.e.,

$$\text{Base} \rightleftharpoons \text{Acid} + O^{2-}$$

The species O^{2-} being a constituent of all oxyanion - containing melts and also of halide melts containing aqueous contaminants (Littlewood 1961). Hence basicity can be defined as:

$$pO^{2-} = -\log a_{O}2- \text{ or } -\log C_{O}2-$$

Lux (1939), Flood (1952), and Lui (1962), Inman and Wrench (1966) considered the fact that Na_2SO_4 and NaCl being oxyanionic and ionic respectively may indicate their diffusion characteristics. The salts are capable of both chemical and ion-associated reactions. The halides, being simple ionic liquids in the molten state, do not give rise to complicated redox reactions and are generally considered to be wholly ionised. On the other hand, the authors noted that several reductions are feasible in the

case of molten sulphates (oxyanionic in nature) while the oxidation reaction is limited to one. The reactions are as follows:

$$\text{anodic: } SO_4^{2-} = \tfrac{1}{2}O_2 + SO_3 + 2e^- \qquad (1)$$

$$\text{cathodic: } SO_4^{2-} + 2e^- = SO_3^{2-} + O^{2-} \qquad (2)$$

$$SO_4^{2-} + 6e^- = S + 4O^{2-} \qquad (3)$$

$$SO_4^{2-} + 8e^- = S^{2-} + 4\,O^{2-} \qquad (4)$$

Corrosion reactions and cathodic processes in molten sulphates and nitrates have been investigated by Liu (1962), Johnson and Laitinen (1963), Swofford and Laitinen (1963), Brough and Kerridge (1965). The SO_3 equilibrium concentration and the rate of decomposition of sulphate anions are both low in sulphate melts. Decomposition is slight even in the absence of vapour buffering of the acid-base level of the melt. This is not so for carbonate melts where carbon dioxide containing atmospheres are needed to suppress dissociation.

Electrode processes in molten salts account for a major part of the electrochemistry of melts. Studies in the field of the electrochemistry of molten salts have been extensively reviewed by Delimarskii and Markov (1961), and Graves et al (1966). Graves et al summarised the electrode processes in molten salts under two categories. The first is concerned with relatively slow processes, invariably involving gas evolution and which can be studied by simple dc techniques. The second category dealt with fast metal $\rightleftharpoons$ metal ion reactions which require

relaxation methods for their investigation. Special complexities of certain slow processes, and the importance of some interfacial configuration in metal -melt systems with regard to the Kinetics of fast electrode processes, were high-lighted.

7. Mechanism of hot corrosion of Nickel-base superalloys

Marine hot corrosion is the form of surface attack caused by combination of sulphur from the fuel and sea salt from the air. While neither alone is overly detrimental, their combination in hot gas turbines can lead to catastrophic attack. Hot corrosion has been the subject of considerable investigation in the past two decades (Simons et al 1955, Graham et al 1967, Seybolt and Beltran 1967, Hardt et al 1967, De Crescente and Bornstein 1968, Seybolt 1968, 1970, Stringer 1972, Beltran and Shores 1972, Goebel et al 1973 McKee and Romeo 1973,74,75.).

All investigators of the hot corrosion phenomenon are in agreement that the formation of a condensed film of Na_2SO_4 on the hot nickel alloy parts is responsible for hot corrosion attack. The mechanism of hot corrosion has not yet been entirely clarified, and probably a generalised explanation for this type of phenomenon cannot be expected due to the variety of alloy compositions and environmental situations that can lead

to similar corrosion morphologies. The turbine environment is composed of a high-temperature, high-pressure, high-velocity gas containing O_2, H_2O, N_2, CO_2, SO_2, SO_3 as well as gaseous, liquid or solid impurities such as Na_2SO_4, NaCl, MgO, $MgSO_4$, and possibly other compounds carried or formed in the airstream. Many impurities have been identified as playing a role in hot corrosion but the most important of these are sodium, chloride, and sulphur in gas turbines.

Although there is still considerable debate on the details of the reaction mechanism it is generally agreed that the formation of a deposit of molten sodium sulphate on the blades is an essential first step. Bowers (1966) reported the attack to be much less severe if the temperature is outside the range 700°C to 850°C within which sodium sulphate is molten. Simons et al (1955) suggested that the reactions may be of type:

$$Na_2SO_4 + 3R = Na_2O + 3RO + S \qquad (5)$$

$$M + S = MS \qquad (6)$$

$$Na_2SO_4 + 3MS = 4S + 3MO + Na_2O \qquad (7)$$

$$4M + S = 4MS \qquad (8)$$

where R represents some reducing species, and M is a metal atom. The sodium sulphate may be from ingested sea spray but may also form by the reaction:

$$2NaCl + S + 2H + 2\,O_2 = Na_2SO_4 + 2HCl \qquad (9)$$

Whether or not these reactions are thermodynamically compatible and will proceed at a considerable rate will depend on the temperature and the availability of the various reactants.

DeCrescente and Bornstein (1968) pointed out that the reaction.

$$2NaCl_{(g)} + SO_{2(g)} + \tfrac{1}{2}O_{2(g)} + H_2O_{(g)} \rightleftharpoons Na_2SO_{4(g)} + 2\,HCl_{(g)} \qquad (10)$$

would be displaced very much to the right in a gas turbine, and Tschinkel (1972) agreed, noting, however, that another reaction

$$NaCl_{(g)} + H_2O_{(g)} = NaOH_{(g)} + HCl_{(g)} \qquad (11)$$

would become important above 1100°C. From this it would appear that NaCl is not itself important in the actual hot-corrosion reaction, and indeed the salt deposits found on blades removed from turbines do not contain appreciable amounts of chloride ions. Conde (1972) quoted unpublished work by Hanby and Beer which showed that the short residence time in the hot zone ($\sim$ 5 ms) prevent the gas phase sulphation of NaCl. However, sodium halide salts when molten (Seybolt 1970) and Halogen gases (Elliot 1972) have been shown to cause very severe attack in nickel-base alloys, by breaking down the protective Cr_2O_3 scale followed by selective removal of chromium. The very marked

effect of chloride contamination on the stability of oxide scales has also been demonstrated by Hancock and Hurst (1971).

Numerous studies have been preformed to examine the mechanism for hot corrosion induced by Na_2SO_4 (Simons et al 1955; Seybolt, 1968; Bornstein and DeCrescente 1969; Goebel and Pettit, 1970), mixtures of Na_2SO_4 and NaCl (Greenert, 1962; Lewis and Smith,1961), V_2O_5 (Sachs, 1958; Lucas et al, 1955), as well as salt mixtures containing V_2O_5 (Cunningham and des Brasunas, 1956; Dooley et al, 1971); Elliott and Hampton, 1972; Moller, 1972). Many such studies have generally contributed to the understanding of the hot corrosion mechanisms in a qualitative sense. However, as indicated earlier in this review, a variety of conflicting opinions have been developed concerning the critical processes necessary for the initiation of hot corrosion as well as related topics.

Simons et al (1955) and Seybolt (1968), proposed for the case of Na_2SO_4 - induced hot corrosion that sulphur in the Na_2SO_4 is the important species. Virtually all the models proposed for the presumed detrimental effect of sulphur involved the formation of sulphur phases in the alloy which presumably destroy or prevent the formation of a protective oxide scale. Betteridge et al (1955) proposed

that Cr_2S_3 is formed as an initial step and is then oxidised along with the nickel matrix, freeing the sulphur for further penetration into the alloy. Bergman (1964) suggested that the formation of chromium sulphide leads to depletion of chromium in the surrounding matrix, becomes oxidised, and then scale flaking occurs which exposes fresh material. Hancock (1961) suggested that Ni_3S_2 is also formed at the operating temperature, and because this is molten, rapid penetration by oxygen can occur. On cooling any remaining Ni_3S_2 is reduced by chromium diffusing from the bulk of the alloy. This last mechanism would explain why areas of the chromium sulphide often appear to have been molten even though temperatures have not been high enough to cause fusion of chromium sulphide itself.

Bornstein and DeCrescente (1969) and Goebel and Pettit (1970), agreed that although during Na_2SO_4 - induced hot corrosion sulphur enters the alloy and sulphide phases are formed, the critical process for the hot corrosion reaction is considered to be the resulting increase in the activity of Na_2O (or oxide ions) in the Na_2SO_4, since oxide-ion enriched Na_2SO_4 as well as other similar salts are efficient fluxes for oxide scales.

The following mechanism for the hot corrosion of

nickel-based alloys has been suggested from the mechanistic studies by Pettit and Co-workers (1969, 1970), and on results and related experiments by Bornstein and Decrescente (1969). As shown in Figure 1, the surface of the metal is initially covered by a nickel oxide (NiO) film, and a molten layer of Na_2SO_4 is deposited, Sulphur diffuses through the oxide to form sulphides beneath the oxide, and this raises the oxygen ion concentration in the salt layer adjacent to the oxide. Eventually, oxidation of the NiO to form nickelate ions NiO_2^{2-} takes place; these ions are soluble to a limited extent in the salt. The nickelate ions move outward towards the air/salt interface, and eventually the oxygen ion concentration falls sufficiently low for the nickelate ions to be reduced again to nickel oxide. Thus the protective oxide layer is dissolved and re-precipitated in a loose non-protective form within the molten salt layer. In the case of pure nickel, the sulphide formed is a liquid phase which decomposes on cooling to form nickel metal and a eutectic of Ni and Ni_3S_2, and the system quickly approaches a steady state in which a protective oxide layer is once again established. However, the presence of certain metals can prevent the re-establishment of a protective oxide, and these are capable of forming stable complexes with sodium oxide, Na_2O, in oxidising environments; chromium (Na_2CrO_4), molybdenum (Na_2MoO_4), and tungsten (Na_2WO_4),

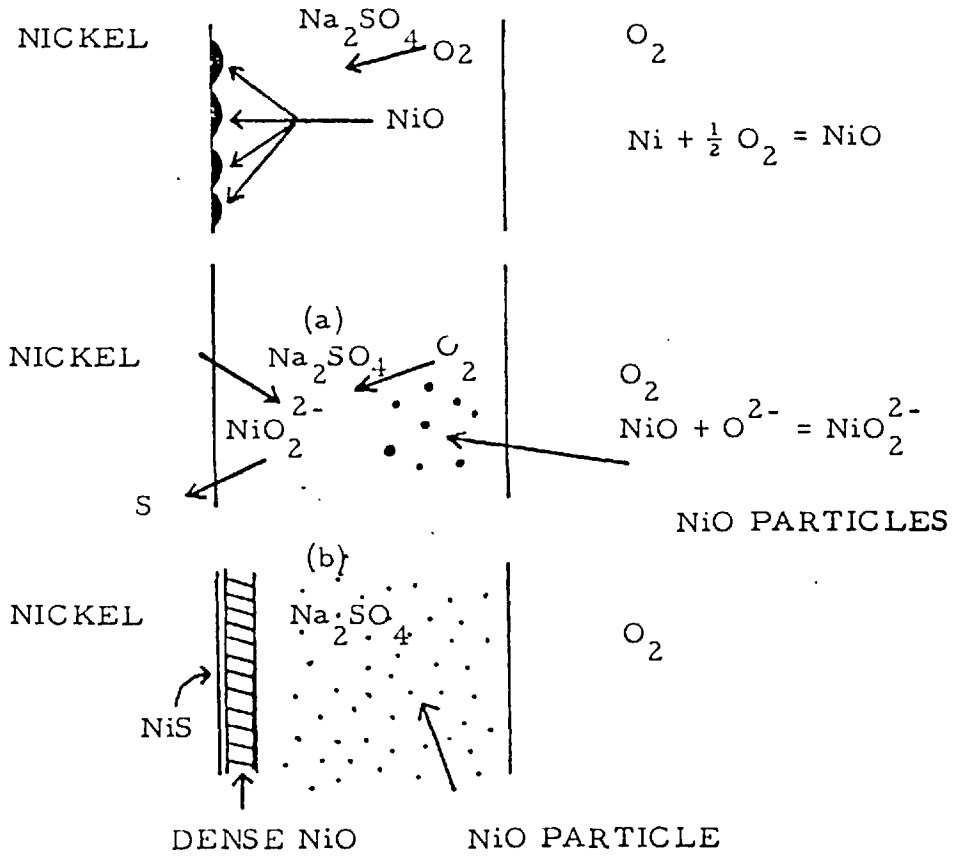

Fig. 1 A model proposed by Pettit et al (1969; 1970) for the hot corrosion of nickel by sodium sulphate. Initially, the metal oxidisesto form a layer of NiO, liberating sulphur. This diffuses through the oxide to form nickel sulphidé. Continuing sulphidation produces an increase in oxygen ion activity in the salt adjacent to the oxide surface, eventually allowing solution of the oxide as nickelate ions (basic fluxing). Towards the salt/atmosphere interface the oxygen ion activity falls and the ions are reduced to form a loose non-continous oxide. Eventually, however the reaction achieves a steady state in which a continuous oxide layer again develops by transport of oxygen through the salt..

are the most obvious examples. Small amounts ($\sim$ 5 at.%) of these metals can result in the development of a continuing rapid reaction rate. However, if there is sufficient chromium to form continuous Cr_2O_3 layer, the reaction rate is usually slow because of the low solubility of this oxide in the molten salt.

This model is capable of explaining the sensitivity to hot corrosion of alloys forming Al_2O_3 oxides, and a very clear summary has been presented by Goebel et al (1972) - Figure 2. Because of the amphoteric nature of alumina, it can be dissolved in either acid (low oxygen ion activity) or basic sodium sulphate, in the first case forming Al^{3+} ions (Figure 2) and in the second AlO_2^- ions. In addition, the same authors (1973) have discussed the reactions which may occur between Al_2O_3 and MoO_3 in molten Na_2SO_4, and have shown that the reaction products are either soluble in Na_2SO_4 or are themselves liquid. These various fluxing reactions thus prevent the formation of a protective layer and allow rapid attack of the substrate.

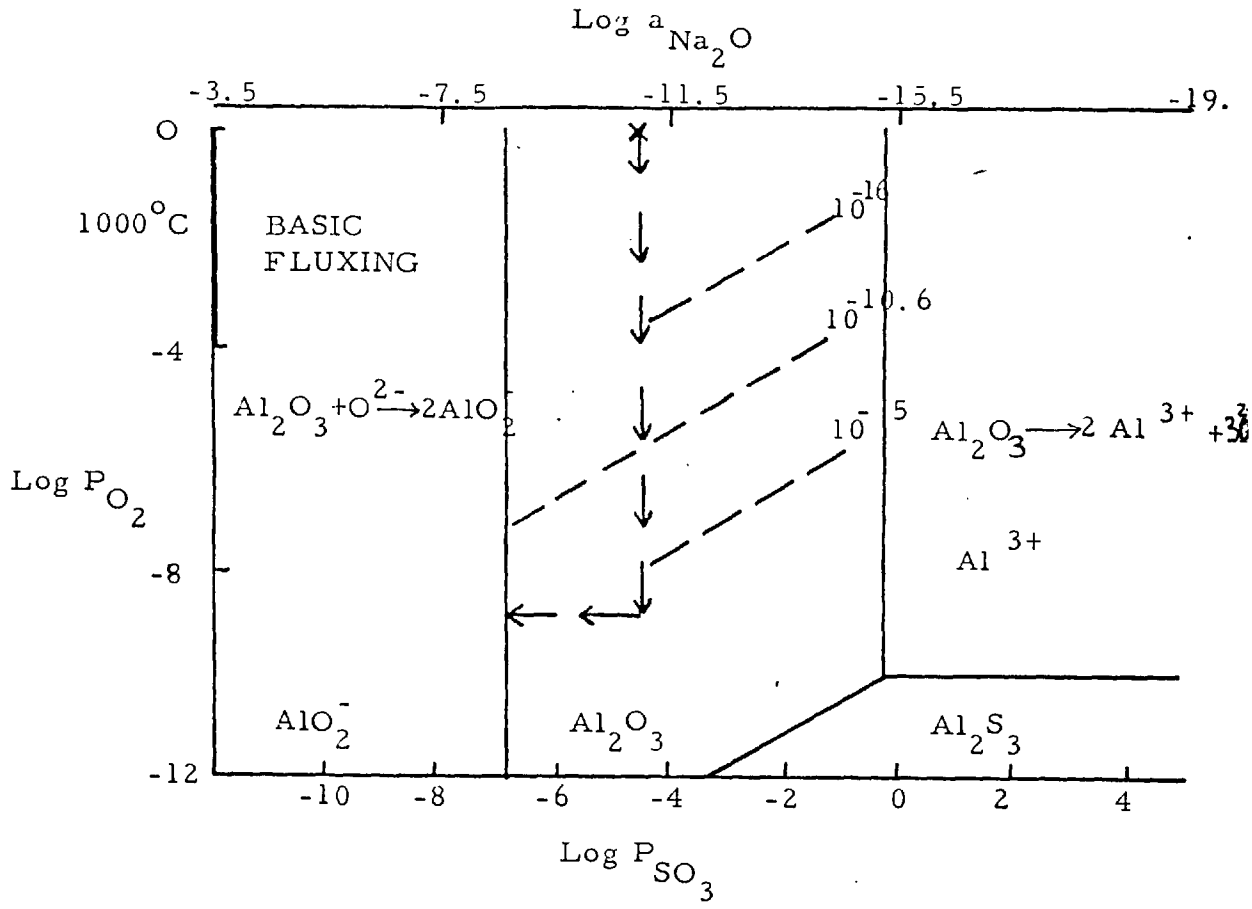

Figure 2. Stability diagram showing the phases of aluminium that are stable in Na_2SO_4 at 1000°C. The arrows show how the composition of Na_2SO_4 can change because of removal of oxygen and sulphur. The broken lines are sulphur isobars and the isobars of $10^{-10.6}$ is the sulphur pressure required to form aluminium sulphide beneath an Al_2O_3 scale on a Ni-31 wt % Al alloy. This diagram shows that Al_2O_3 is stable in Na_2SO_4 for certain compositions, and that Al_2O_3 reacts with Na_2SO_4 which has either high or low activities of Na_2O (after Goebel et al 1972).

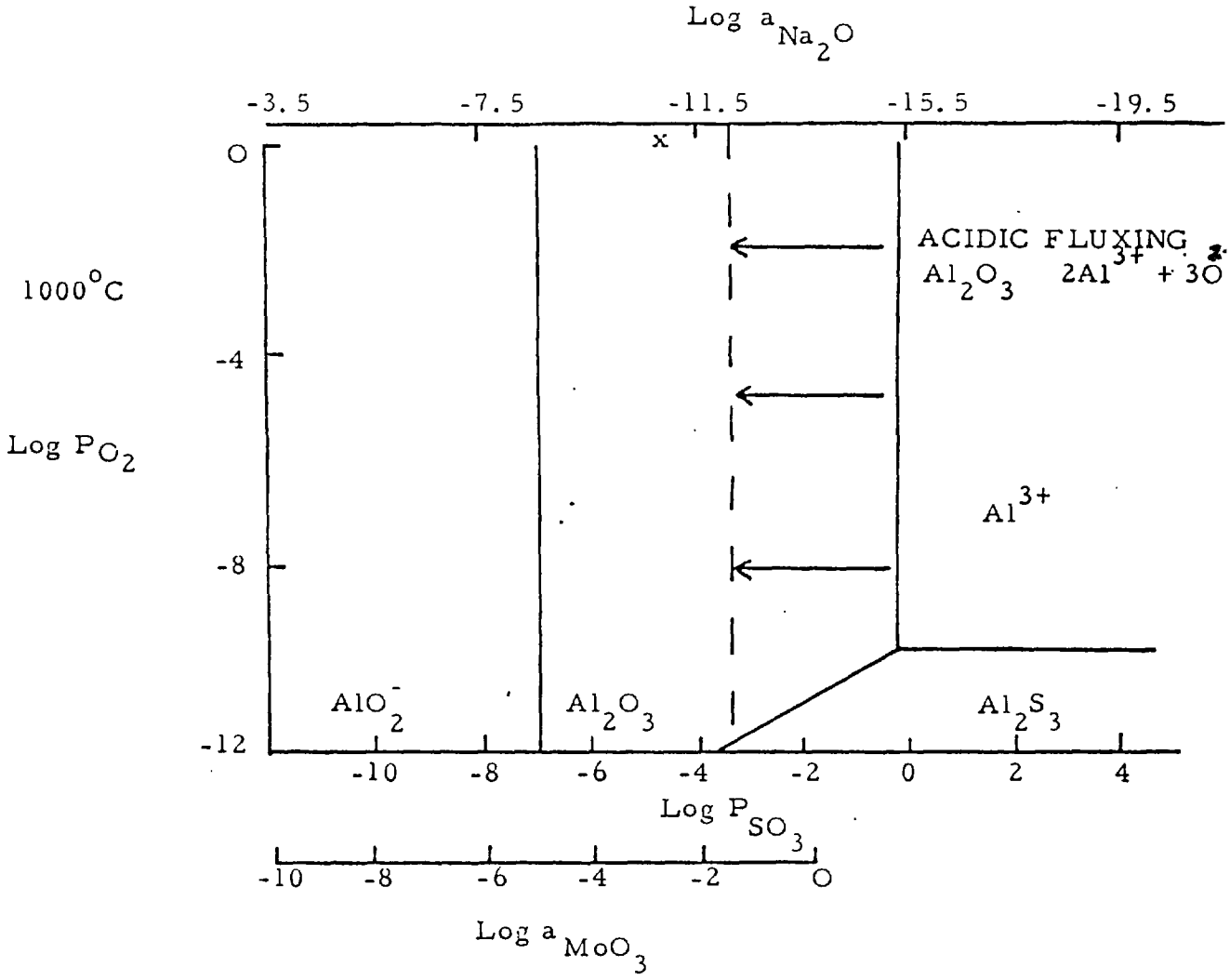

Figure 3. Stability diagram showing the displacement of the boundary (arrows) at which acidic fluxing of Al_2O_3 can occur for the case where Na_2SO_4 contains MoO_3 in solution such that the MoO_3 activity is 0.1 at a mole fraction of Na_2SO_4 of 0.99 (after Goebel et al 1972).

It can be seen that in these mechanisms sulphur may not play as important a role as the basic corrodant Na_2O with its fluxing action.

The crucial point is that the molten salt contains two oxidants, so that the removal of one, by reaction with the metal, produces an increase in the activity of the other. Na_2SO_4 is important because (a) it is very stable, so that a very small change in stoichiometry produces a large change in the activity of the ionic species, and (b) it is molten in the temperature range of interest, Bornstein and DeCrescente (1969) have shown that in certain circumstances hot corrosion may be produced by salts in which the second oxidant is not sulphur, but nitrogen or carbon. However, this view is not universally held. In the past, it has been suggested that sulphur may be important either because it forms a low melting point nickel sulphide which then penetrates the metal grain boundaries, allowing rapid access of the oxidant, or because it removes the chromium from the matrix as stable chromium sulphides, allowing rapid attack of the depleted matrix. The evidence in favour of the first of these mechanisms is that in the hot-corrosion reaction a thick layer of oxide containing metal particles may form, and in detail the structure suggests that the oxidation front follows the sulphide

(figure 3).

However, in blades taken from engines it is very unusual to detect nickel sulphide; the only sulphides formed appear to be high melting point chromium - rich sulphides, and because of the higher stability of chromium sulphide one would not expect nickel sulphide to be formed until the chromium has been depleted - possibly by the oxidation reaction. Hancock (1961) suggested that a very rapid exchange reaction may take place during cooling, so that the phases observed in the blades may not be representative of those present at temperature.

The mechanism of Pettit et al is primarily concerned with the destruction of the initial protective oxide and the prevention of its re-establishment. In the practical situation the system is thermally cycled, and this can result in the local failure of the protective oxide. There is no general aggreement on the effect of chloride, but it seems possible that it could reduce the scale/metal adhesion, leading to removal of the protective layer.

8. Scope of the Present investigation.

Protection of high temperature materials, to be used in contact with high velocity gases, requires a coating that has a combination of properties. It must provide erosion and corrosion resistance, good adherence under both mechanical and thermal stresses and have minimal effect

on the mechanical properties of the base alloy. It must be sufficiently stable to give an acceptable lifetime. Optimization of these characteristics may not be simultaneously available and compromises are frequently necessary.

Coating systems are of at least three types: (1) Metallic (diffusion) (2) Ceramic (non-diffusion) and (3) cermet (combination of (1) and (2)). The present study has primarily been in the area of category (3). The coatings have been produced by electrodeposition, and this is the first in a series of experiments planned for a systematic study of the hot corrosion resistance of single and duplex overlay coatings on nickel-base superalloys.

Generally, coatings are aluminium-rich, most commonly produced by pack techniques. These types of coatings have been well - reviewed by Goward (1970, 1971). Investigations into the use of chromium and aluminium, and duplex chromium/aluminium coatings for high temperature protection of alloys in air, have been carried out by Morrison (1966). Development work by others into complex alloy coatings has been reported in a recent review by Goward (1976).

Based on a combination of a moderate amount of fundamental understanding resulting from research on

oxidation and hot corrosion of nickel-base alloys containing rare-earth additions, and practical experience, development of improved coatings containing Al_2O_3, ZrO_2 and HfO_2 has been undertaken. Other oxide additions such as TiO_2, CrO_2 and Y_2O_3 are planned for further studies.

B. Principles of Electrodeposition

1. Potentials of metals in aqueous solution

Aqueous electrodeposition involves solutions containing chemical compounds of the metal to be deposited, which have good electrical conductivity. When a metal is immersed in a solution of its ions, an interaction occurs between the metal and the solution such that the metal releases ions into the solution, whilst conversely, the solution discharges ions on the metal which are incorporated into a metal lattice. Because the ions are at the same time charge-carriers, this passage of ions creates an electrical double layer at the metal - solution interface. The potential is a result of the equilibrium of chemical and electrical forces.

The electrode equilibria most relevant to electrodeposition are:

$$M^{z+} + Ze \rightleftharpoons M \qquad (12)$$

$$H^{+} + e^{-} \rightleftharpoons \tfrac{1}{2}H_2 \qquad (13)$$

$$\tfrac{1}{2}O_2 + H_2O + 2e \rightleftharpoons 2OH^{-} \qquad (14)$$

In the case of equation (12), e.g. $Cu^{2+} + 2e \rightleftharpoons Cu$, or $Zn^{2+} + 2e \rightleftharpoons Zn$, the metal attains a specific electrical potential which are characteristic of that particular metal and the concentration of metal ions (Muller 1960). These

systems are reversible and can be treated thermodynamically, which means that they conform with the Nernst equation that has been derived from thermodynamic considerations:

$$E = E^{o}_{M^{z+}/M} + \frac{RT}{zF} \ln a_{M^{z+}} \qquad (15)$$

where E is the electrode potential at 25°C, (V), R is the gas constant (8.315 J deg C^{-1} mol^{-1}), T is the absolute temperature, and F is the Faraday constant (96,500 coulombs). Thus the electrode potential of copper in copper sulphate solution varies logarithmically with the activity of cupric ions as predicted by the Nernst equation. The values for electrode potentials normally quoted in reference tables, the so called e.m.f. series, are the standard reversible electrode potential E^{o} for $M^{z+} + Ze = M$, which is defined as the potential of a metal in equilibrium with a sclution of its ions at unit molar activity, at a temperature of 25°C.

2. Ion migration and transport

If a direct voltage is applied to the electrodes in an electrolyte a force acts on the ions, which accelerates them towards the anode or cathode, depending on their charge. Thus, there is an electric field between the electrodes in the cell, apart from the tremendous field in the small region of the double layer. Because of friction

with the ambient molecules and ions and the drag exerted by a water envelope around the ion, the accelerated motion is transformed after a brief acceleration into a steady motion termed the migration velocity of the ion. The migration velocity is defined as the constant velocity of an ion in dm/sec at a field intensity of 1 v/dm. It is a characteristic constant for the particular ion involved. Its magnitude depends also on certain external conditions, such as pressure, temperature, nature of the solvent, and concentration. The migration velocities U_C of the cations and U_A of the anions are of the same order of magnitude, only those of the hydrogen and hydroxyl ions being considerably greater than those of the other. As long ago as 1853, J.W. Hittorf concluded on the basis of observed concentration changes during current passage that different ionic species have different migration velocities. If one (or two) oppositely charged ions migrates at a higher velocity than the other a greater impoverishment must occur at the electrode from which the faster ion migrates. Such concentration shifts in an electrolyte were termed, transport phenomena by Hittorf. These effects are possible without violation of the neutrality conditions in the electrolyte because more ions of one kind can be discharged at an electrode than are transported in the electrolyte. The migration in the electric field

represents only a prefered component of the motion, since owing to the thermal motion of the ions, both anion and cation species are always present in the vicinity of both electrodes.

The quantity of electricity transported by each ion species is proportional to the velocity of the ions. Thus, of the cations having migration velocity U_c, the proportion

$$N_c = \frac{U_c}{U_c + U_A} \qquad (14)$$

and of the anions having migration velocity U_A, the proportion

$$N_A = \frac{U_A}{U_c + U_A} \qquad (15)$$

is transported. Hittorf termed these proportions the cation transport number N_c and the anion transport number N_A. The relation $N_A + N_c = 1$ always applies.

3. Polarisation.

When an electrode (either an anode or cathode) is immersed in an electrolyte with no current flowing. a potential exists between the electrode and the electrolyte. This potential is called

the static or steady state electrode potential (E_s). When a particular metal is immersed in an aqueous solution of its ions of unit molar activity at 25°C, this potential is called the standard reversible electrode potential (E^o), for the metal.

When, however, two electrodes are connected in series with an external electromotive force, the potentials are displaced from their steady-state value. The potential of the cathode becomes more negative and that of the anode, more positive; the decomposition potential is reached, current begins to flow and irreversible electrode reactions occur at a finite rate. Metal is deposited or hydrogen released at the cathode, and at the anode dissolution occurs or oxygen is released

When these processes occur at an electrode and its potential departs from the static value, that electrode is said to be polarised (E_p). The polarisation occuring during electrolytic metal deposition depends on the kind of metal, the type of electrolyte, any special additions which have been made, and the cathodic current density. While, for example, copper, zinc and cadmium are deposited from a sulphate electrolyte with low activation polarisation, nickel is deposited from sulphate electrolyte with a high

activation polarisation. Thus a nickel electrode whose potential is made more negative in sulphuric acid is said to be polarised, the polarisation being due to the overpotential of the reaction:

$$H^+ + e \longrightarrow \tfrac{1}{2}H_2 \qquad (16)$$

On the other hand, if the nickel electrode is made cathodic in a Watts bath, the overpotential will be due to the reaction:

$$Ni^{2+} + 2e \longrightarrow Ni \qquad (17)$$

All effects that cause an electrode to depart from (Es), its unpolarised value to (Ep) its polarised value, are called 'Overpotentials'.. The value of (Ep) is the sum of the overpotentials due to one or more electrode processes that are occuring. The most significant are:

1. Concentration overpotential (η_{conc})
2. Activation overpotential (η_{act})
3. Ohmic overpotential (η_{ohmic})

$$Ep = Es + \eta_{conc} + \eta_{act} + \eta_{ohmic} \qquad (18)$$

η total = Ep - Es which is - for cathodic processes and + for anodic processes.

3.1 Concentration overpotential

Concentration overpotential or polarisation is due to the variation in the concentration of metal ions around the electrodes and accounts for a large part of

the total polarisation at the current densities used in industrial plating. At the cathode the solution close to the actual surface becomes depleted of metal ions and further deposition becomes more difficult as the potential becomes more negative. The greater the current density the lower the conc. of metal ions near the cathode and the greater the polarisation. If the C.d. is further raised a fundamental limiting current density can theoretically be reached where there is zero metal at the cathode surface, but before this point is reached, alternative electrode reactions such as the discharge of H_2 at the cathode, called H_2 overpotential, takes place. At the anode the reverse of all these facts applies and high concentrations of metal ions build up which are unable to diffuse away, and oxygen liberation (oxygen overpotential) occurs. These concentration gradients are known as anode and cathode diffusions layers respectively and can be minimised by raising temp., agitation and the concentration of solution.

Increasingly, the temperature increases ionic mobility and thus lets more metal ions diffuse in and out from the electrodes, lowering the overpotential. This is the reason why most modern solutions are used warm.

Agitation by air or movement decreases the thickness of the diffusion layers by physically moving the ions into the bulk of the solution, also reducing conc. overpotential.

The metal concentration can be raised and a more active anion used, all of which help ion mobility.

3.2 Activation overpotential.

This refers to the energy needed to move ions across the interface between electrolyte and electrode and to build the discharged atom (adatom) into the crystal structure of the cathode deposit, or remove it from the anode. There are also other electrode reactions that need activation energy to make them proceed. These include the hydration and dehydration of ions, the discharge of ions at electrodes, and the formation of crystals or molecular gases from absorbed atoms. Deposition never occurs unless a certain amount of activation polarisation is present. Its value depends upon many factors, such as : whether ions are complexed, the presence of other ions in the solution, the addition agents present in the solution.

3.3 Ohmic overpotential

The presence of ionically conducting films on the surface of electrodes produces additional polarisation. These films can range from non-liquid films such as metallic oxides to the complex films containing organic compounds which cause the brightening and leveling properties of many solutions.

Anode electrode reactions are often impeded by the formation of poorly conducting films. These usually cause a change in the appearance of the anode such as discolouration or even encrustation of salts on it. In cyanide solutions the effect is greatly increased by lack of 'free' cyanide, and the addition of a small quantity of sodium or potassium cyanide will restore the bath to normal condition almost immediately. Anode polarisation may also be caused by the presence of impurities in the electrolyte.

The voltage that must be applied between the anode and cathode of an electroplating bath to produce a finite current, is called the cell voltage and is composed of a number of factors given in the relationship below :

$$V = E_{cell} + \text{total cathodic polarisation} + \text{total anodic polarisation} + IR$$

E_{cell} is the minimum voltage needed to cause the electrode reactions to take place and plating to commence. This is equivalent to the decomposition potential.

Both anode and cathode polarisation opposes the applied voltage so they are both added to E_{cell} regardless of sign.

The IR drop, or resistive overpotential, is the basic Ohm's law voltage drop derived from the current I and the resistance R of the electrolyte; contributions to cell voltage drop due to thin film of electrolyte near the electrode surface are considered as part of the anode and cathode polarisation.

The potential drop across the bulk electrolyte, between anode and cathode, largely depends upon dissolved salts in the aqueous solution, the greater their concentration, the lower the solution resistance. Because of this lower resistance, the voltage (IR) drop across the solution is less and consequently a lower voltage is needed to pass a given current. (There is however, a limit to which a salt concentration can be increased and above a certain value the ionic mobility is reduced which increases resistance. This only applies to higly concentrated solutions such as sulphamate nickels and certain chromium plating solutions).

4. Metal deposition from solutions of simple salts

The simple salts form hydrated cations in aqueous solutions : the hydrated metal ion has the same positive valency as the free metal ion. In electrolytes containing hydrated metal ions, the concentration of metal ions which can be discharged is generally high. For deposition from

hydrated metal ions, the dehydration must be taken into account as a preliminary reaction. This removal of the water molecules takes place mainly in the external, diffuse layer of the Helmholtz double layer and normally occurs in several steps. The energy necessary for the removal of the hydrated envelope depends on the nature of the metal ion - it is very high, for example, for nickel ions (which gives rise to a high activation polarisation).

If the deposition mechanism is to be elucidated it is necessary to trace the path of the metal ion from the interior of the electrolyte to the cathode surface. The hydrated metal ion present in the electrolyte arrives at the cathode under the influence of the imposed electric field as well as by diffusion and convection. At the cathode it enters the diffusion layer, in which its migration velocity is determined by the concentration gradient. The field strength in the diffusion layer is not yet sufficient to liberate the metal ion from its hydrated envelope. At most, the loosely bound H_2O molecules are aligned by the field. The metal ion then passes through the diffuse part of the double layer and enters the external layer of the fixed double layer. The field strength in the double layer is approximately 10^7 v/cm, and at this high field strength the metal ion is deprived of its hydrated envelope. The repelled

H_2O dipoles become components of the double layer. (Figure 4).

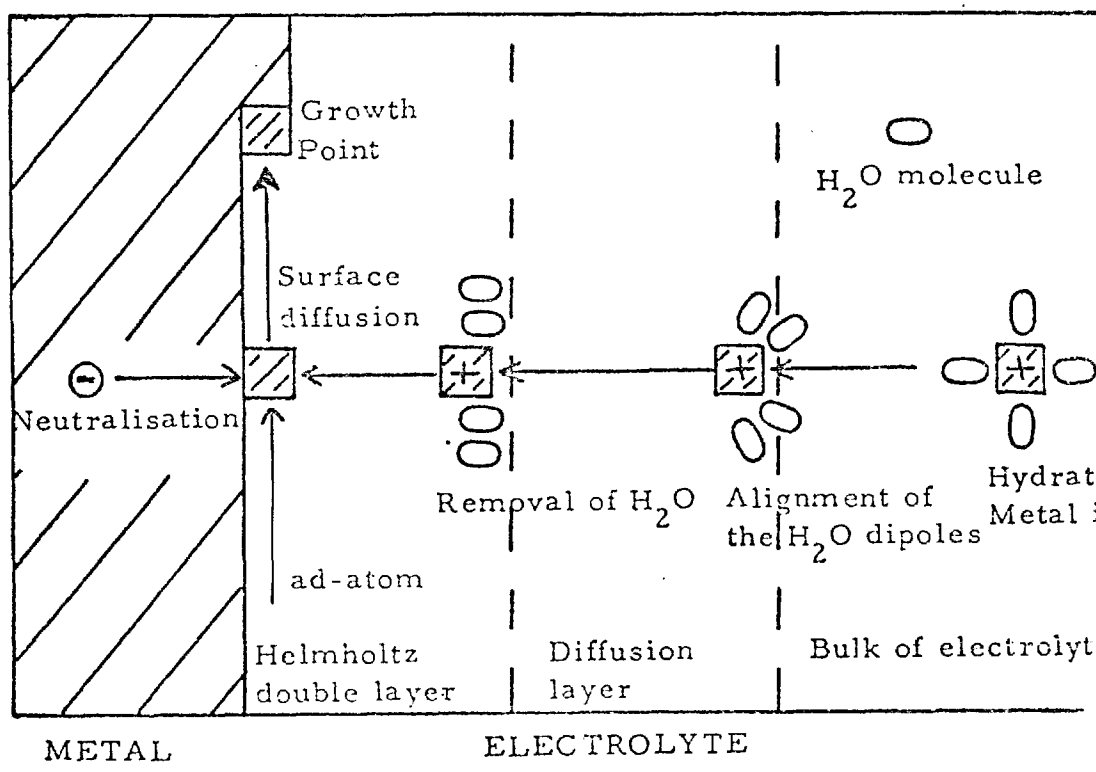

Figure 4. Schematic representation of the mechanism of cathodic metal deposition.

(after H. Gerischer).

According to the theory of H. Brandes (1927), Erdey-Gruz (1931), and Volmer (1934), the dehydrated metal ion migrates within the outer zone of the double layer to a point opposite an energetically favourable point (growth point) on the cathode surface. From this point the metal ion passes through the double layer, is neutralised, and deposited on the cathode. On the basis of more recent studies, however, this view is not tenable. The high field

strength within the double layer must be sufficient to retain the metal ion at whatever point in the outer zone of the double layer which it happens to occupy. A displacement within the double layer is also inhibited by the neighbouring cations with the same charge. According to Conway and Bockris (1960) the metal ion passes through the double layer at the point where contact first occurs. It is then neutralised and absorbed for the time being at the cathode surface (ad-atom). Migration of the ad-atom or ad-ion by surface diffusion to a growing edge, at which further co-ordination with respect to other metal atoms is achieved with further loss of solvent molecules of hydration. This theory is also supported by Lorenz (1929), Bockris and Mehl (1959), and Fleischmann and Thirsk (1963).

Gerischer and Tischer (1957, 58) reported that in the case of cathode metal deposition, the incorporation of a metal atom into the crystal lattice of the cathode proceeded independently of the passage and neutralisation of the metal ions i.e. the crystallisation proceeds via previously formed atoms (Figure 4). Thus the influence of the electric field strength cannot be as decisive as postulated in the theory of Brandes, Erdey-Gruz and Volmer.

5. Metal deposition from solutions of complex salts

Electrolytes in which the metal ion is bound in a complex predominate for metal deposition in electroplating

technology (Senderoff 1950). Metals such as copper, zinc, cadmium, silver and gold are deposited from cyanide electrolytes. In addition to the cyanide electrolyte types, electrolytes containing other complexes are used. In copper pyrophosphate electrolyte, the complex $(Cu(P_2O_7)_2)^{2-}$ is present, and stannate electrolytes contain the complex $(Sn(OH)_6)^{2-}$. In addition to copper and lead, tin deposits with good properties have recently been obtained using fluoborate electrolytes.

Even though the explanation of the deposition mechanism from solutions of simple salts is difficult, additional problems arise in the case of deposition from complexes because in these electrolytes the metal to be deposited is often bound to a negatively charged complex ion. Although a dissociation equilibrium exists betwwen these complex ions and the simple metal ions, the concentration of the simple hydrated ions is extremely low because of the generally high stability of the complexes. The exact composition of the complexes in the electrolyte is, in some cases, also unknown.

The formation of a complex ion may be represented as:

$$M^{n+} + qX^{p-} \longrightarrow MX_q^{n-pq} \qquad (19)$$

in which q is the coordination number and X is the complexing

ion of charge p; and the Nernst equation may be written:

$$E = E^{o}_{M^{n+}} - RT/nF\ln K_f + RT/nF\ln (a^{n-pq}_{MX_q}/a^{q}_{X^{p-}}) \quad (20)$$

Where K_f is the thermodynamic formation or stability constant (inverse of the dissociation constant) for the complex and 'a' represents activities of the species denoted by subscripts. In some instances, in which activity coefficients roughly cancel out, it is possible to obtain useful approximations by substituting concentrations for activities. The term involving K_f will usually determine the region in which the potential lies, and since K_f will be large for any stable complex, the potential will be shifted by a substantial negative quantity.

There is no difference in principle between discharge of complex and hydrated ions. In general, however, metal deposition from complex ions takes place with high overvoltage. Because of low concentration of dischargeable complexes, a high diffusion overvoltage is present at higher current densities. The formation of the dischargeable complexes in cyanide electrolytes is generally proceeded by reactions in which the complexes with higher coordination number, which predominate in the electrolyte, are dissociated to complexes with lower coordination number. In the Zinc cyanide electrolyte, the following reactions occur:

$$(Zn(CN)_4)^{2-} + 4\ OH^- \longrightarrow (Zn(OH)_4)^{2-} + 4CN^- \quad (21)$$

$$(Zn(OH)_4)^{2-} \longrightarrow (Zn(OH)_2) + 2OH^- \quad (22)$$

In the copper cyanide bath, the initial reaction is:

$$(Cu(CN)_3)^{2-} \longrightarrow (Cu(CN)_2)^- + CN^- \quad (23)$$

Similar reactions in other cyanide electrolytes also give rise to the formation of dischargeable ions. Inhibition of these reactions produce a higher reaction overvoltage (Lyons 1954).

Chromium occupies a special position with respect to the deposition mechanism (Morisset et al 1954, Reinkowski and Knorr 1954, and Dubpernell 1960). Although attempts to deposit chromium from solutions of simple salts proved that chromium can be deposited, for example, from solutions of salts of trivalent chromium (Kramer 1957), the practical solution of the difficulties involved has not yet been achieved. Chromium, therefore, is always deposited from aqueous solutions of chromic acid (Weiner 1960). These electrolytes differ in several respects from other plating baths. In order to obtain deposition of metallic chromium, the electrolyte must contain certain quantity of some other acid. This loosens the cathode film to such an extent through complex formation that chromium deposition is rendered possible. The effect of the sulphuric acid present

in a chromic acid electrolyte results from the fact that it forms an easily soluble complex with trivalent chromium, and hence tends to prevent the formation of a cathode film.

C. PHYSICAL PROPERTIES OF ELECTRODEPOSITS

1. Structure of electrodeposits.

The structure of an electrodeposit depends on the relative rates of formation of nuclei and the growth of existing ones. If the conditions favour the formation of fresh nuclei then fine-grained deposits are formed, while preferential growth of existing nuclei leads to the production of large-grained deposits. Usually fine-grained deposits are smoother, brighter, harder and less ductile than coarse-grained ones, although exceptions to this generalisation do occur. Fine-grained deposits produced by adding organic compounds to the plating solution can have a dull matt appearance instead of a smooth bright finish. Treed deposits produced by plating at a high current density appear coarse and rough, despite their small grain size, for the small grains form a coarse aggregate. In general, any change in the plating conditions that results in an increase in cathode polarisation leads to a reduction in grain size. Variation of the simple plating conditions without resort to addition to the solution, enables a certain amount of control to be exercised over the structure and physical properties of the deposit. An increase in current density causes a reduction of the metal ion concentration in the cathode film with a consequent increase concentration overpotential and decrease in grain size. If other factors remain constant,

an increase in the degree of agitation lowers the concentration overpotential and hence results in a larger grain size. An increase in temperature similarly leads to a reduction in cathode polarisation.

The type of solution and its composition also influences the characteristics of the deposit. Concentration overpotential will be high in a dilute solution and therefore the grain size will be small and the macro throwing power fairly good. However, in dilute solutions the limiting current density is so low that this type of solution is of only limited use commercially. Since fine-grained deposits are usually preferable to coarse-grained ones, it is necessary to devise solutions which provide this type of structure, but as dilute solutions are unstable other formulations are adopted. The normal procedure is to use the solutions which have a high concentration of metal compounds but a low metal ion concentration. Complex formation or the common-ion effect make this possible with the metal compounds serving as a reservoir of metal ions. Copper deposition provides an example of a metal which can be obtained by either technique, Fine-grained deposits are obtained from the double cyanide solution, much coarser deposits from the acid copper sulphate solution and even coarser deposits from solutions of copper sulphate containing no added sulphuric acid. Most of the coarse-grained deposits

have a columnar structure which can be revealed easily by etching and optical microscopy. The columnar grains are formed in the direction of the current flow lines and in thick deposits, planes of weakness can arise at features such as sharp corners, just as in castings having a columnar structure. Brenner, Zentner and Jennings (1952) have carried out an extensive programme to relate variations in structure to operating variables and bath compositions.

Growth can be defined as being epitaxial when the atomic arrangement in a crystalline substrate is perpetuated in the deposit. The effect of the substrate diminishes as the coating thickness increases. The rate at which this occurs is influenced by the type and state of the substrate and certain plating conditions. The effect of the substrate rapidly dimishes if the surface is mechanically polished and is prolonged when the substrate has a large grain size. An increase in current density, an increase in polarisation and the incorporation in the solution of surface active organic compounds are all factors which diminish the extent of epitaxial growth. Polycrystalline material is deposited at an early stage and lattice distortion occurs.

2. Heat Treatment of electrolytically deposited metals and alloys

Heat treatment of electrodeposited metals is not an important practical procedure, at least in the sense

of tonnage of products. Much has been learned of the relations between the structures of electrodeposits and their recrystallisation behaviour, but with the notable exception of the reflowing of tinplate, high-temperature treatments of deposits are rare. The value of studies on recrystallisation of deposits now lies in the field of general contributions to plating knowledge, particularly knowledge of metal structure. Recrystallisation has been extensively studied as a general metallurgical phenomenon, and this knowledge will be useful in gaining a better insight into many structural problems in electrodeposits. The purity of electrodeposited metals often leads to unexpectedly low recrystallisation temperatures. Low temperature heat treatments are fairly common, and their chief application is in the removal of hydrogen embrittlement by baking. Care must be taken here to employ only times and temperatures that will not alter desirable properties of the basis metal. Internal stress can be reduced by heat treatment at temperatures far below annealing temperatures. When properly executed, a stress-relief treatment does not alter to any great extent either the strength or ductility of the metal treated, but again, effects on the basis metal must be considered.

The properties of electrolytic deposits can often be considerably modified by subsequent annealing. The

modification of the properties of pure electrolytic metals during heat treatment is determined by relaxation and recrystallisation. For electrolytic metals containing appreciable amounts of impurities, the behaviour of these impurities during annealing is responsible for the modification of properties. The non-metallic impurities, in contrast to the foreign metal or hydrogen atoms in the lattice of the host metal, are not able to diffuse during annealing. They remain in the positions taken up during crystallisation until the annealing temperature attains the temperature of decomposition. Important modifications of properties do not take place below this temperature. The lattice strains produced by the impurities can at most be intensified by the differing thermal expansion coefficient of the impurity. The incorporated organic compounds, however, are not heat resistant. At a given temperature (which depends on composition) they normally decompose with formation of carbon and gases in which water vapour and carbon monoxide predominate. The deposited carbon can react with the host metal at high temperatures with formation of carbide (e.g. iron) and thus again give rise to property modifications when the annealing temperature is further increased. Inorganic impurities in electrodeposited metals decompose with gas evolution only when they contain water or easily evaporating or decomposing atomic groupings, usually in

in a complex bond. Other changes can occur when they melt or evaporate without decomposition. The decomposition temperatures of the impurities or the temperatures at which changes takes place in them, are usually so high that values are attained at which the metal atoms can freely migrate, so that in addition to the decomposition of impurities, the structure-sensitive properties of the metals are also subjected to sudden variations owing to rapid relaxation and recrystallisation.

Electrodeposited alloys can be brought into thermodynamic equilibrium by annealing. In addition to the structural changes which are to be expected, other properties are also greatly modified. Cathodically deposited hydrogen, which can be incorporated in the form of strongly super-saturated solution, or which is sometimes precipitated as hydride, as in chromium, occupies a special position among the alloying elements. By suitable heat treatment it is generally quite easy to expel all the hydrogen from the electrodeposited metal. As the space occupied by the hydrogen proton in the metal lattice is very small, hydrogen can be dissolved in an electrodeposited metal without modifying the structure-sensitive properties such as hardness. Thus, for example, Tammann and Jaacks (1926) showed that the hydrogen dissolved by chromium during electrodeposition can be expelled without affecting the hardness. It is very

difficult to assess correctly the effect of hydrogen on electrodeposited metals. Solutions that are strongly super-saturated hydrogen solutions do not normally occur with pure metals but in electrodeposited metals containing varying amounts of non-metallic impurities. These always produce lattice strains which are superimposed on a possible hydrogen effect. Hydrogen usually cannot be expelled without simultaneous decomposition or other change in the properties of other impurities in deposited metal. Hence, it has not yet proved possible to isolate the effect of hydrogen in nickel (a metal of particular importance in electroplating technology) from the certainly much greater effect of incorporated hydroxide, basic chloride, nickel sulphide and other impurities. This is particularly true of bright nickel. As in electrodeposited copper, the recrystallisation of electrodeposited nickel commences at the side which had been in contact with the cathode. Simultaneously with the recrystallisation of nickel, the hardness and tensile strength decrease from the initial to the final magnitudes. The tensile strength of nickel investigated by Koster (1928) did not decrease from 50Kp/mm^2 to the value (ca. 40Kp/mm^2) for annealed nickel but fell to 20 Kp/mm^2 at 700^{o}C and 11 Kp/mm^2 at an annealing temperature of 1100^{o}C. The cause of this was the unexpected loss in ductility during recrystallisation. Elongation, necking and number of bending cycles

decreased to very low values and finally to zero, so that complete brittle fracture occurred. This loss of ductility is due to an intercrystalline disintegration of the structure in nickel caused by H_2 gas evolution. The changes described above in electrodeposited nickel during heat treatment are typical for a nickel in which much impurity has been incorporated.

During the heat treatment of electrolytic alloys, the phases which occur in the alloys according to the phase diagram are formed with a composition corresponding to the equilibrium state. The results of heat treatment of strongly supersaturated electrolytic solid solution alloys also show that the lattice strains responsible for the great hardness are not due to the incorporation of foreign metals into the solid solution lattice, but to other independent causes, giving rise to lattice strains which are not or only partly eliminated during precipitation.

As the hardness variation during annealing shows, it is not possible to confer on supersaturated electrolytic solid solutions all the properties of cast or recrystallised alloys. The pronounced internal stress normally present in supersaturated solid solutions, which is independent of the lattice constant variation, prevents the reduction of the hardness to normal values. The stress

is at the same time responsible for the appearance of pronounced residual stresses, which can easily give rise to hairline cracking during soft annealing - this greatly reduces the strength of the deposit. These processes are clearly significant for the practical application of alloy deposits. Heat Treatment gives rise not only to changes in the properties of electrodeposited coatings through relaxation and recrystallisation or through other processes which take place in such coatings with impurity incorporation and in alloy deposits, but also to reactions between the coating and the base metal, and between the individual electrodeposited layers. An electrolytic coating, is deposited on the base metal with the formation of a sharp boundary. Alloy formation between the base metal and the deposit or between separate layers does not normally take place during electrocrystallisation, or with few exceptions, during storage at room temperature after electrodeposition. Only at sufficiently high temperatures can reactions take place at the base metal/deposited metal boundaries. If the two metals are mutually insoluble and do not form intermediate compounds alloy formation does not take place, even when high temperatures are attained. Cadmium plated iron for example, can be heated to the boiling point of cadmium without alloy formation between cadmium and iron. Iron and lead behave in the same manner.

Annealing for the purpose of promoting diffusion is often carried out for example, when an electrodeposited coating is to be strengthened or hardened. Corrosion protection can also be improved by the decrease in porosity of the coatings brought about by diffusion. Diffusion annealing is particularly useful with chromium plated steel. Thin chromium coatings can thus be transformed into a chromium-iron alloy coating with greater corrosion resistance and four or five times the original thickness. Heat treatment of electroplated parts for achieving diffusion (and thus alloy formation) between base metal and deposit or between the deposited metals in multilayer coatings, has achieved practical importance for the production of alloy coatings. It is employed for producing nickel-iron coatings, brass coatings on steel, and lead-tin or lead-indium coatings on the bearing faces of high duty friction bearings. The diffusion capabilities of electrodeposited coatings can thus have favourable effects in practical applications.

3. Hardness and adhesion of electrodeposits.

The hardness of electrodeposited metals can be varied both by a change in plating conditions and by the presence of additions in the plating bath. Of the mechanical properties of electrodeposited metal coatings, hardness is of special interest. It is relatively easy to measure

and can be related to significant and useful properties such as tensile strength and ductility. For electrodeposited metals even the quantitative relations commonly observed between hardness, tensile strength, and ductility do not always prevail. For example, the hardness of metals is normally expected to increase as tensile strength increases and as ductility decreases, but reverse effects are common among electrodeposited metals. It is particularly important therefore, in dealing with electrodeposits to be sure of the significance of hardness measurements.

The metals deposited in electroplating practice often contain intentionally introduced impurities to give the deposits certain properties required in their technical application. Impurity incorporation strongly influences the electrocrystallisation of metals and introduces strain into the metal lattice, thus greatly affecting the structure-sensitive properties, including hardness. The hardness of electrolytically crystallised metals, however, is in most cases much higher than that of cast or recrystallised metals even in the absence of detectable quantities of non-metallic impurities, attaining that of the fully cold-hardened state. Nickel and chromium, electrodeposits are usually relatively hard and it is not uncommon for their hardness to exceed that of the metal in the cold-worked condition.

Hardness is usually determined by an indentation technique but scratch tests and various types of abrasion or rubbing techniques can also be employed. Each category of test provides different results and so do different tests within a particular category. For example, in the case of a particular piece of metal, the value obtained using a Brinell ball indenter is different from that obtained using a Vickers or Knoop pyramid indenter. Consequently, hardness is not a fundamental property of metals since its determination is dependant on other properties and techniques employed. The essential feature of indentation techniques is that the size of the impression, made by applying a known load for a definite time, is measured using a microscope fitted with a calibrated eye piece. The hardness of electrodeposits is usually determined using a conventional microhardness technique employing a Vickers or Knoop pyramid indenter rather than by a macro technique. If the test is carried out on the surface of the deposit, the coating must be sufficiently thick to avoid the 'anvil' effect; otherwise, the substrate influences the hardness value obtained for the coating. The Knoop indenter is particularly suited for use on the surface of an electrodeposit since it produces a shallow depression. One diagonal is much longer than the other, and it is known that most of the elastic recovery takes place in the direction of the shorter diagonal. It is easy to measure

the longer diagonal accurately and it indicates the true size of the 'unrecovered' indentation. Frequently, microhardness determinations are carried out on the metallographically - polished cross section of the deposit, but the obvious limitation in this instance is that the coating must be thick enough (over 25μm) to accommodate the indentation. However, this procedure ensures that the impression is made on a smooth flat surface, whereas a certain amount of roughness may have to be tolerated if the indentation is made on the surface of the electrodeposit. Hardness can be calculated from the expressions given below.

a. The Brinell number (HB) equals load divided by the spherical area of the impressions:

$$HB = \frac{P}{(\pi D/2)\left\{D - \sqrt{(D^2 - d^2)}\right\}} \qquad (24)$$

where D is the diameter of the ball (mm), d is the diameter of the impression (mm) and P is the load applied (kgf).

b. The Vickers hardness number HV, (formerly V.P.N.) equals load divided by the contact area of the impression:

$$HV = \frac{1.845\ P}{d^2} \qquad (25)$$

where d is the length of diagonal of the impression (mm) and P is the load applied (kgf).

An important property of electrodeposited metals is their adhesion to the base metal. The adhesion should be such that the deposit is not stripped from the base metal by mechanical or thermal stresses acting on the electrolytically coated article. According to Hothersall (1937), adhesion can be defined as the force required for separation of the deposit from the base metal. The forces responsible for adhesion are of an atomic nature. In the interior of a solid, the forces exerted by an atom are saturated by the adjacent atoms. The forces of the surface atoms, however, partly extend into the environment. Thus, they can attract other particles (the atoms of a deposit, for example) with a force which is greater the more intimate the bond. The effect of these attraction forces is greatest at distances comparable with interatomic distances. Hence, to obtain good adhesion, the interference of foreign substances between the base and the deposited metal must be excluded - the surface to be electroplated must be metallically pure.

If the coating is deposited onto a cathode of the same metal and, under favourable conditions, the crystal lattice of the substrate is continued in the electrodeposit, and the distance between layers corresponds with the interatomic distance. In this case the bond and thus the adhesions are strongest. This phenomenon of epitaxy, which can also occur when the substrate is different from

the electrodeposit, has been discussed by numerous authors including Graham (1923), Blum and Rawdon (1923) and Finch, William and Yang (1947). The majority of electrodeposits are finely crystalline, physical evidence of epitaxy is the exception rather than the rule and that epitaxy is not necessarily the only criterion for good adhesion. Hothersall (1933 and 1935), using metallographic techniques, and depositing from a solution that gave coarsely crystalline deposits and a substrate of well-defined grain structure, has shown that the grain boundaries of the substrate can be continued in the deposit. Finch et al (1947) used electron diffraction to examine metals deposited at low current densities onto substrates of known crystal planes. They showed that the orientation of the substrate is continued up to a thickness of 30000 Å but at greater thicknesses epitaxial growth no longer occurred. This situation is unlikely to be encountered in many commercial applications as usually the coating and substrate are not the same metal. In this case, adhesion is represented by cohesive forces between metals. Hothersall (1935) stated that discharged ions take up their positions immediately adjacent to the basis metal lattice and within the field of molecular attraction. Interatomic forces involved are Van der Waal's forces, covalent forces, metallic bonding forces and ionic and polar forces. However, the theory of bonding is discussed in detail by Hume-Rothery (1960). The structure of a dissimilar basis metal is more

likely to be perpetuated in the coating at low current densities and consequently good adhesion is then most likely to result.

Strong adhesion is often obtained when alloy formation occurs as a result of diffusion between base metal and deposit. Atoms of one metal then occupy lattice sites of the other metal in the contact planes between the two metals - an alloy layer only a few atoms thick often has a good effect on adhesion.

The measurement of the adhesion between base metal and deposit is difficult, because only the tensile forces, required for separating the deposit from the base by failure, can be measured. The numerous testing methods which have been proposed permit only qualitative evaluation of the adhesion strength and the results thus obtained can only provide satisfactory and comparable measurements if a series of investigations is carried out-Sautter (1954). When adhesion strength is optimum, failure during the test takes place not at the interface between deposit and base metal, but within one of the metals, depending on which of them has the lower tensile strength.

D. PREPARATION FOR ELECTRODEPOSITION

1. Pre-treatment processes

The importance of perfect cleaning cannot be over-emphasised, since upon the efficiency of this operation depends the adhesion of the deposited metal. Of the various processes designed to give a clean surface suitable for plating, none is more important than the removal of grease, oil and other soils, whether left from machining, stamping, pressing or polishing. Plating on to a dirty or greasy surface inevitably leads to blistering or peeling of the deposit and fouls the electrolyte. The various cleaning and pretreatment processes through which an article must pass before it may be successfully electroplated can be classified under the following headings:

Preliminary cleaning or degreasing
Pickling or bright dipping
Hot alkaline cleaning.

Preliminary cleaning or degreasing involves the removal of heavy oils, greases and soils, and is necessary before a component can be pickled or bright dipped for the removal of oxide and scale. The pre-treatment processes immediately prior to plating generally take the form of hot alkaline cleaning, possibly followed by acid dipping to remove slight oxide films, then final cleaning to ensure that the component is perfectly clean.

The factors that influence the selection of cleaning materials are:

(a) Surface to be cleaned

(b) Dirt or soils to be removed

(c) Degree of cleanliness required

(d) Method of application of the cleaning material

The surface to be cleaned has a direct effect on the cleaning materials because of the possibility of excessive corrosion. For instance, strong alkaline cleaners may be used for steel, but for the non-etch cleaning of brass a solution having a low free alkalinity must be used. Electrolytic cleaning is more rapid in its action than ordinary immersion or soak cleaning. This is due to the scouring action of the gas evolved on the surface to be cleaned. Cathodic cleaning is more effective for the removal of greases and compositions than anodic cleaning, due to the fact that the volume of hydrogen evolved at the cathode is twice that of the oxygen evolved at the anode. Nickel surfaces and nickel base alloys must be electrocleaned cathodically to avoid passivation of the surface. The passivated surfaces will not plate satisfactorily.

Not all plating operations require the same degree of cleanliness of the basis metal. Lyons (1945) stated that an absolutely chemically clean surface is not required for production of an acceptable electroplate. By defination, a chemically clean surface is one that has no film on it

that might be detached by chemical or physical tests; obviously such a surface can be realised only with extreme difficulty, even in the laboratory. It is generally agreed, however, that surfaces substantially free of grease, oils and gross oxide films are needed for the best electroplates. Therefore it is a standard practice to clean as thoroughly as is economically feasible. A useful test for complete grease removal is to rinse well and observe how the work drains. De-wetting in patches and droplets indicate grease to be still present. Even drainage with no "break" appearing in the water film indicates freedom from hydrophobic soils.

Harris (1960) and Linford and Saubestre (1951) summarised the early literature on metal cleaning. Current recommended references are the Metal Finishing Guidebook, Metal Handbook, Volume II (1964), and Electroplating Engineering Handbook (1971). References by Blum and Hagaboom (1949), Spring (1962) and Myers (1959) cover recommended methods and procedures.

Ineffective cleaning and rinsing are together responsible for the majority of failures that occure in electroplating. If the various cleaning sequences are studied, it will be seen that articles must be swilled after nearly every operation. Cleanliness of the final rinse water used for articles after deposition is also of prime importance. With some solutions, particularly

the alkaline electrolytes, it is not easy to remove every trace by swilling in a single vat of water, and the articles should be rinsed first in one swill to free them from most of the solution and then in a second swill of cold water to remove the last traces. Finally they should be put through boiling water to raise the temperature and facilitate drying. To ensure stain-free drying it is now quite usual to employ de-ionised water at the final rinsing state.

2. Scale and Oxide removal.

It is essential that metal to be plated be free of scale and oxide for quality plating (Snavely and Faust 1962). Acid pickling is one of the most widely used. It has been reported that scale and oxide removal consumes 5% of all the industrial sulphuric acid, 25% of the hydrochloric acid, most of the hydrofluoric acid and a large quantity of nitric and phosphoric acids.

Sulphuric acid finds wide application for pickling steel, copper and brass, and is used with hydrofluoric or nitric acid or both for descaling nickel and its alloys. Hydrochloric acid has the advantage of being an effective pickle for many metals at room temperature. Nitric acid, however is an ingredient of many bright dips. It finds wide use in combination with hydrofluoric acid for removing heat scale from stainless steels, nickel - and - iron-base alloys, titanium, zirconium, and certain cobalt base alloys.

Some heat scales are not rapidly soluble in acids or may dissolve so slowly that attack on the basis metal occurs before the scale is removed. If this is the case, a pretreatment step can be used to change the scale so that it becomes readily soluble in dilute acids. Possel't et al (1968) found that a caustic soda - permanganate pretreatment made many types of heat treat scales easy to remove in regular acid pickling baths. Electric current is used to make pickling more effective. Cathodic pickling is practised on stainless steels. It increases the effectiveness of the pickling and is a good way of activating the surface so it will plate satisfactorily.

Many acid baths with varying concentrations and combinations of acids are used to obtain the desired descaling, brightening, and acid dipping qualities necessary for good plating. In the case of nickel and nickel alloys, the scale may be loosened by treatment for 10 to 30 minutes in the following solution:

Potassium permanganate	22.5 - 90 g/1
Soda ash	22.5 - 90 g/1
Temperature.	75 - 100°C

preferably with agitation, which is followed by a rinse and then by scale removal in any of the various combinations of sulphuric acid, phosphoric acid, and nitric acid. A typical bath contains 60% phosphoric acid, 20% suphuric acid, and 20% nitric acid, all by volume, Operates at room temperature.

E. GENERAL INFORMATION ON ELECTRODEPOSITION

1. Application of current during loading

Before loading the current should be switched on and the control panel set so that a low voltage is applied, sufficient to promote immediate deposition or to impart a high enough cathodic potential to the articles to prevent the surface of the metal from becoming attacked by the solution. As the loading proceeds the voltage applied should be increased, but must not be excessive, particularly at the beginning, otherwise the deposit will become 'burnt' or rough and granular in texture. This practice of applying a small voltage to the anode and cathode connections before introducing work is also essential in many cases to prevent contamination of the solution by displacement of metal with a lower negative value in the electro-chemical series by one higher in the series. For a similar reason articles should not be left in the bath after the current has been switched off.

The plating current should be maintained without interruption (except in specialised processes using interrupted current or periodic reverse sequences.) During nickel plating a break in the current supply could lead to laminated deposits and in the case of bright chromium plating to dull deposits.

2. Solution maintenance.

Great care should be taken to keep solution free from contamination. Frequent causes of contamination apart from carelessness or accidental introduction of foreign matter are:

(i) The use of unsuitable tanks or mixing vessels.

(ii) Failure to remove immediately any articles that fall from jigging wires to the bottom of the tank.

(iii) The carry over of acids and other solutions inside cup-shaped or hollow articles.

(iv) Failure to remove completely during the cleaning stages soils such as polishing residues.

(v) When solutions are not in use the tanks should be kept covered to minimise evaporation losses and prevent contamination of the solution with airborne particles.

(vi) Hot solutions should not be covered with fabric sheets as material extracted by the steam may contaminate the solution.

3. Anodes and anode bags.

The anode reaction in electroplating may be one of two types. The anode may be constructed of a metal which is oxidised to a metallic ion or complex ion under the conditions of the plating process. This is called the soluble

anode. The second type of anode is insoluble and simply provides a site that is at the required potential for the anode reaction, which generally results in the evolution of oxygen.

The anodes must operate in their optimum current-density range for good results. If the anode efficiency is significantly greater than the cathode efficiency, some insoluble anodes may be used concurrently to maintain proper metal concentration (West 1953).

The insoluble anode, which may be used alone or in combination with soluble anodes, causes a reduction in pH near its surface. The effects on the bath chemistry may be reduced by bagging the anodes or placing them in separate cells communicating with the main bath through an ion-permeable membrane (Jarczyk (1957)). An excellent summary of anode recommendations is given by Fishlock (1950).

Anodes should be checked regularly and replaced when necessary. When anode bags are employed they should be long enough to cover the anodes completely, and the tied ends must not hang below the solution level. Except when supplied in the pre-washed condition, new anode bags should be washed in hot water until they are free from dressing before being put into service. When in use they must be kept clean and should be regularly examined to see that they are free from holes.

4. Trouble shooting.

A fundamental procedure in trouble shooting is to observe the condition of the work after each step as it passes through the preparatory cleaning and plating operations. One should note where, if at all, the surface of the work exhibits any indications such as water breaks, stains, smut or films, etching or irregular surface colour or appearance. Frequently, the adhesion of solid foreign particles coming from a rinse or a process bath is a clue to a source of roughness. If the transfer time between processes is too long, drying may occur which often causes staining. The ability of subsequent treatments to remove stains should be noted.

4.1.1 Problems in nickel plating.

Nickel solutions are susceptible to metallic impurities. The general effect of metallic contamination is to cause loss of throwing power, diminish the brightness, and create a tendency for the deposit to crack. The most likely impurities are iron, copper, zinc and chromium.

4.1.2. Iron.

Iron causes the deposit to become less ductile, with a result that cracks may possibly develop. To prevent contamination, any articles that fall to the bottom of the tank should be recovered immediately, and all iron

and steel parts must be well rinsed in clean water after any acid dip, prior to their being placed in solution. The presence of iron may be indicated by a brown sludge of hydrated iron oxide on the anode bags.

To eliminate iron, the pH value of the nickel solution should be raised to 5.6 or just over by the addition of dilute sodium hydroxide solution or nickel hydroxide slurry, after which the bath should be vigorously air agitated for several hours and then filtered. After filtration, the pH of the solution must be restored to the normal value by the addition of either pure sulphuric or hydrochloric acid. With dull nickel plating solutions, it is usual to make an addition of 3 ml/ℓ of hydrogen peroxide (20 volume) or 1.5 g/ℓ of sodium perborate in order to oxidise the iron to ferric condition, before precipitation by the addition nickel carbonate or hydroxide slurry. Saubestre (1961 and 1963) pointed out that under correct conditions there is little nickel lost in the precipitate.

Where possible the purification treatment should be carried out in a separate tank. If necessary, the treatment can be carried out in the plating tank itself after the removal of anodes. After treatment, the solution is filtered out into storage containers and the tank cleaned out before the solution is returned.

4.1.3 Copper and zinc

Other impurities, such as copper and zinc, can be removed by electrolysing the solution for several hours at a current density of not more that 0.1. to 0.2 amp/dm^2 of cathode surface, using corrugated brass or mild steel cathode sheets. The voltage required is approximately 0.5 volt. New or stripped plating out sheets, should be flash nickel plated for a few minutes at 1 to 2 amp/dm^2. When a complete covering of nickel has been obtained, the current is then reduced to 0.1 to 0.2 amp/dm^2. It is essential that the solution be vigorously agitated and maintained at the plating temperature during this cleaning electrolysis, and the current be adjusted within the limits stated so that only a dark deposit is obtained at first. The cathode plates should be removed from the bath from time to time, rinsed in water, and brushed to remove any loosely adherent dark deposit. The plates should then be returned and the plating out process continued until all signs of darkness disappear.

4.1.4 Chromium

Contamination with hexavalent chromium may arise from the carry-over of chromium plating solution into the nickel plating solution. Its effect upon the deposit is to prevent deposition in the low current density areas.

Severe contamination may completely prevent deposition.

To remove chromium, the hexavalent chromium is reduced by the addition of ferrous sulphate in the proportion of 0.16 g/1 for every five parts per million (5 mg/1) of chromium (as Cr) present. The ferrous sulphate is dissolved in acidified water and added to the plating solution. The pH value of the solution is then raised to 5.8 to 6.0 by the addition of fresh nickel hydroxode prepared by adding 10 per cent solution of sodium hydroxide to an equal volume of nickel plating solution and adding the slurry so produced to the bath with stirring. The solution is air agitated for four hours with the temperature maintained at 60°C (140°F) and then filtered into a separate tank. After the purification treatment the pH value of the solution should be adjusted to its normal value.

4.1.5 Organic contamination

Organic contamination may occur in any type of nickel plating solution, as a result of extraneous organic matter entering the solution. With bright and semi-bright nickel plating solutions organic contamination can also occur as a result of the breakdown or organic addition agents incorporated in the solutions. Organic contamination can result in stress or brittleness in the deposit, pitting or patchy bright deposits from dull nickel solutions.

With dull nickel solutions, mild organic contamination may be removed by treatment with hydrogen peroxide or sodium perborate. The usual procedure is to add 6 ml/1 of 10 volume hydrogen peroxide of 3 g/1 sodium perborate to the nickel plating solution, stir well or air agitate, and then allow to react for twelve hours. After the hydrogen peroxide treatment, the solution should be worked at high current density on scrap cathodes for one hour in order to remove any excess peroxide remaining in the solution. For the treatment of plating solutions it is most important that the hydrogen peroxide used should be the sulphuric acid stabilised grade.

Where a dull nickel solution is heavily contaminated with organic matter, treatment with activated carbon may be necessary. Carbon treatment is preferably carried out in a separate tank fitted with heating and air agitation. The activated carbon is added directly to the plating solution, the quantity employed being between 3 to 10 g/1, depending upon the degree of treatment required. The plating solution is air agitated for several hours, allowed to settle, and then filtered into a separate storage tank. After the plating tank has been cleaned out, the solution is returned and any necessary additions made to restore the plating solution to its recommended composition.

4.2 Problems in chromium plating.

The spray resulting from efficient hydrogen evolution at the cathode in chromium plating baths causes hygiene problems. The spray may be reduced by use of plastic floats on the surface of the solution. Serota (1964) and several U.S. Patents, suggested a number of compounds as addition agents for the solution to reduce spray, among which is a trifluoroacetic acid salt of an oxyalkylated fatty amine.

4.2.1 Effect of metallic and organic impurities

Iron contamination in the chromium plating bath sequesters the chromium very efficiently. One unit weight of iron reacts with 7 unit weight of chromic acid, producing insoluble compounds. By this process the conductivity of the bath is reduced. Iron in the chromium plating solution causes increased resistance of the bath, reduces the throwing power and causes milky deposit.

Impurities in the nickel bath which precedes the chromium plating operation affect the quality of the chromium plate. Generally these impurities cause a reduction in nickel plate quality before an appreciable effect is noted on the chromium plate. Metallic and organic impurities cause poor plating in low current density areas in the nickel bath and even poorer plating in the following chromium bath.

Pitting of the chromium deposit is most frequently caused by corresponding faults in the basis material. The pit in the chromium plate will be larger than the pit on the basis metal, particularly in the presence of wetting agents. If wetting agents are not used and if the chromium deposit is of sufficient thickness, the pit may close up. Improper basis metal preparation is also responsible for poor adhesion. Although the thickness of the nickel underplate does not influence the chromium adhesion, the nickel plated parts should be chromium plated without delay to avoid oxide formation and the problems associated with its removal.

If the throwing power of the solution is poor and increased voltage has to be used to obtain satisfactory coverage, then a small addition of barium hydroxide is made to the solution, say about 1½ g/ℓ. The barium hydroxide must be dissolved in hot water and then added to the chrome solution, which must then be well stirred for at least ten minutes. The solution should be allowed to settle for one to three hours before recommencing plating. If some improvement results, further small additions of barium hydroxide can be made until the throwing power of the solution is restored. An excess must however, be avoided.

F. CERMET COATINGS

1. General

The improvement in the high temperature strength of metals by incorporating a dispersed phase of oxide, carbide or boride is well known, and there is considerable scope for the use of dispersion hardened materials in engineering. A number of methods exist for the preparation of dispersion-hardened metals and alloys e.g. internal oxidation, powder metallurgy, surface oxidation of powders followed by extraction, and each method has its advantages and limitations.

During the past two decades a great many workers, (Withers 1961, 62; Brown and Silman 1964; Williams and Martin 1964; Martin 1965; Williams 1966; Kedward and Martin 1967; Cole 1967; Greco and Baldauf 1968; Greco, Wallace and Cesaro 1969; Chen and Sautter 1971; Cameron and Forster 1976), on both sides of the Atlantic, made concerted efforts to produce commercially applicable electrodeposited composite coatings. Such coatings are produced by codeposition of fine inert particles and a metal matrix from electrolytic baths. The second phase particles are kept in suspension in a conventional electrolyte, and during the electrolytic crystallisation the particles come in contact with the cathode and are so embedded in the metallic deposit. Depending on the concentration and the size of the particles in suspension, dispersion hardened alloys of

various concentrations and interparticle spacings can be obtained.

Sautter (1963), gave a good historical account of the developments in electrolytic deposition of dispersion hardened metals, and Williams (1966) wrote a general review on electrodeposited composite coatings. The interest shown in these inclusion deposits was due to their applications for wear resistance, as dry lubricants, oxidation protection at elevated temperatures, dispersion strengthening and hardening. But despite the potential use of these deposits and more than a score of years of work, not many large-scale commercial baths have been developed to produce such coatings. Extensive work has been performed in Germany on electroless systems and in America by Browning et al (1964); Dunkerley, Leavenworth and Eichelmann (1966); Chen and Sautter (1971). Most of the work in the UK has been performed by Bristol Aerojet Ltd., Banwell, described by Kedward (1969, 1973,1977) for the production of Co-Cr_3C_2 coatings, and also by Neckarsulm (1970) for Ni-SiC coatings.

The technical applications of such composite coatings can be divided into three categories;

(1) as dry lubricant coatings or wear-resistant coatings, e.g. cobalt, tungsten carbide, nickel-silicon carbide;

(ii) as corrosion and oxidation resistant coatings, e.g. a nickel matrix containing a dispersed oxide phase;

(iii) as dispersion-hardened coatings, e.g. copper-alumina.

The development of industrial applications has been restricted so far mainly by two factors. Firstly, limited knowledge of the mechanism of codeposition of inert particles makes the choice of the right electrolysis conditions largely empirical. Secondly, information on the mechanical and physical properties of composite coatings is very limited. From a literature survey it is still impossible to deduce clearly the effect of different electrolysis conditions on the properties of composite coatings. Some hardness and ultimate tensile strength values are available for electrodeposited iron-alumina alloys (Brown and Gow, 1972). For example, the authors reported values of ultimate tensile strength of about 77 kg/mm^2 for heat-treated Fe-Al_2O_3 foil and average microhardness of about 415 KHN for as-deposited foil containing 2.5 and 4 wt % Al_2O_3 produced from baths containing 3 and 7 g/l Al_2O_3.

Values of hardness, yield strength and ultimate tensile strength have been published by Sautter et al (1974, 1976) and Roos et al (1978) for Cu-Al_2O_3 and for Co-Al_2O_3 alloys.

For electrodeposited Ni-Al_2O_3 and Ni-SiC alloys mechanical properties such as hardness, yield strength and wear resistance have been reported by Broszeit et al (1971). A composite of 4.5 wt% Ni.Al_2O_3 deposit was found (Broszeit et al 1971) to have a yield strength of 45 kg/mm^2 and a hardness value of 350 kg/sq mm. Hardness values of various nickel composites vary from 200 - 500 kg/sq mm.

2. Experimental methods and process development.

Interest in dispersion-strengthened alloys for high temperature application has steadily increased since the introduction of the first of such materials twenty years ago. Mixtures involving nickel, copper, chromium, iron and other base metals or alloys with various oxide or other dispersed phases are reported by Stuart (1963), Zwilsky and Grant (1957), Feisal and Cochardt (1959) and Ver Snyder (1959). Conventional methods for the production of the various dispersion-strengthened composites may be divided into two general categories;

1. Mechanical mixing followed by compaction and sintering.
2. Chemical reactions which include a variety of procedures such as internal oxidation of the matrix metal, surface oxidation of matrix metal powder, preferential chemical reduction of mixed oxides, and co-precipitation of matrix and

> dispersed phase compounds followed by preferential chemical reduction of the matrix metal phase, with consolidation by standard powder metallurgy techniques (Bunshah and Goetzel (1959) ? as a final step.

The literature abounds with reports of the difficulties of obtaining optimum dispersion-strengthened composites by these conventional processes. For example, Feisel and Cochardt (1959), using mechanical mixing procedures for preparing dispersion-strengthened nickel and nickel-cobalt, reported that the dispersoid particles tend to agglomerate during mixing and then segregate as oxide clusters in the composite, making alloys of structural quality difficult to obtain at best. As the important properties of dispersion-strengthened materials are mainly determined by the interparticle distance of the dispersed phase, it is important to obtain a homogeneous mixture. This is difficult to realise if powders of different sizes and specific weight have to be blended mechanically. In such cases, electrolytic co-deposition can be an attractive production method.

Smith (1963) reported a new technique for preparing dispersion-strengthened alloys, based upon work carried out at Watervliet Arsenal by Sautter (1962) on the codeposition of nickel and submicron sized Al_2O_3 particles. Three advantages of the electrodeposition process were cited:

the first was the case of dispersoid suspension in an aqueous solution and the resultant reduction of clustering and agglomeration of the small particles. The second was the elimination of the need for metal powders when making composites, which opens a much wider range of metal-metal oxides systems than was available for comminution by powder metallurgy techniques; and the third advantage was the possibility of making intricate shaped components directly by electroforming rather than by producing the dispersion-strengthened material first and then fabricating the components by various metal working processes.

Development work carried out by Bristol Aerojet Ltd., Banwell, and described by Kedward (1972, 1976) showed that good quality reproducible coatings could be achieved by the use of the liquid/air and plate pumping methods. All ancillary equipment used was of the conventional plating type. The experimental route adopted was simply to set up the unit and systematically examine the readiness of plating electrolytes to codeposit various ceramic additives.

Browning et al (1964) adopted other depostion processes which have been developed and proven as manufacturing methods for certain complex components including metal spraying, chemical vapour deposition, electrophoresis, and electrodeposition or modifications of these three. The basic electrodeposition equipment designed by these workers involved the use of recirculating pump to improve powder

dispersion by constant recycling. Withers (1962) has discussed the advantages that can be obtained with regard to the quality of electrodeposited composite coatings when periodic reverse current techniques are used.

Process development can be divided into three areas:

1. the plating bath and additives;
2. the dispersed phase; and
3. the methods of effecting optimum distribution of the particles in the bath to cause uniform codeposition of the dispersed phase in the plated matrix.

3. Selection of plating baths.

The electrodeposition method of fabrication showed good promise because commercial plating processes are available for pure matrix metals, such as chromium, copper, cobalt, nickel, silver and iron; and for certain nickel or cobalt-base alloys. Selection of the electroplating bath composition for a given metal-dispersoid system must be done with discretion, because the bath may contain organic or other chemical additives which will flocculate or otherwise adversely affect the behaviour of the dispersed phase during electrodeposition. Also, the concentration of particles in the bath may modify the mode of metal deposition.

TABLE 2 Properties of oxides of interest for dispersion - strengthening

(after Dunkerley et al 1966)

Oxide	Structure	Temperature of of lowest phase change (^{o}C)	(^{o}F)	F Kcal 1400^{o}K	Work of adhesion on Nickel in Vacuum dynes/cm^{2}	Molecular Weight	Comments
CeO_2	C_1	1950	3542	-168.0		172.1	Worth investigating
HfO_2	Monoclinic	2812	5094	-202.3		210.6	Worht investigating
Pr_2O_3	Monoclinic	d		-350.0		329.8	Poor
ThO_2	Monoclinic	3027	5481	-228.3	495	496.2	Good
WO_3	Monoclinic	1470	2678	-118.4		231.9	High Δ F
UO_2	Monoclinic	2176	3949	-201.9		270.1	Worth investigating
Mn_3O_4	C_4	1172	2142	-213.7		328.8	No advantage
TiO_2	Tetragonal	1572	2860	-165.3	264	79.9	Good
VO_2	Tetragonal	1967	3572	-225.0		82.9	Worth investigating
ZrO_2	Tetragonal	1205	2201	-198.2	540	123.2	Investigation interferes
MgO	B1	2810	506	-106.3	197	40.3	High ΔF
SrO	NaCl Type	2430	4406	-108.8		87.6	High ΔF
NiO	NaCl Type	2090	3794	- 26.4		74.7	Distorted below 150^{o}C
Mn_2O_3	$D5_8$	930	1706	-143.4		157.8	Poor
Sc_2O_3	bcc	----		-305.5		137.9	Worth investigating
Y_2O_3	bcc	2410	4370	-318.0		225.8	Worth investigating

Continued.....

MoO_3	$D5_{10}$	795	1463	-102.3		143.9	Poor
Nb_2O_5	Orthor-hombic	1512	2754	-309.7		265.8	Worth investigating
Re_2O_7	Orthor-hombic	296	565	-143.0		484.6	Poor
8-UO_3	Orthor-hombic			-206.5		286.1	Poor
V_2O_5	Orthor-hombic	670	1238	-240.5		181.9	Poor
AI_2O_3	$D5_1$	2045	3713	-293.1	480	101.9	Good
Cr_2O_3	Trigonal	2265	4109	-184.7		152.0	Worth investigating
Fe_2O_3	Trigonal	677	1251	-134.5		159.7	Poor
Ti_2O_3	Trigonal	100	392	-272.2		143.8	Poor
V_2O_3	Trigonal	1970	3578	-211.5		149.9	Worth investigating
Nd_2O_3	$D5_2$	----		-322.9		336.5	Worth investigating
Sm_2O_3	Trigonal	----		-341.0		348.8	Worth investigating
α -UO_3	Trigonal	----		-206.5		286.1	Poor
BeO	B_4(hex.)	4422	7763	-110.5	187	25.0	High ΔF
SiO_2	Quartz	575	1067	-150.3		60.1	Poor

Dunkerley et al (1966) reported that several of the common nickel plating baths, i.e. sulphate-chloride, chloride, sulpate, Fluoborate, sulphamate etc, can be used with good results. They obtained the most consistent results with the commercial sulphamate bath. Browning et al (1964) in their investigation of the properties of nickel dispersion hardening alloys, ultimately selected the Watt's nickel bath, after several other nickel baths were briefly reviewed for deposition efficiency, particle dispersion and uniformity of composite material produced.

4. Dispersoids - particle suspension

Any particle which can be held in suspension without reacting chemically with the plating bath can be dodeposited. A list of certain properties of possible candidate oxides is given in Table 2. Particle sizes suitable for dispersion strengthening fall within the range from 0.02 to 1.0 μm (Dupont 1964), and are considered to be in the colloidal range. Normally, oxide particles are comminuted and/or treated immediately before addition to the plating bath by ball-milling, resulting in the indivdual particles being given an electrostatic surface charge. Glasstone (1946) reported that when these particles were suspended in a liquid containing no ions, the like charge on the particles, usually positive for oxides, causes them to

repel each other and a fairly stable suspension results. Furthermore, addition of very small amount of electrolytes can add to the stability of such suspensions because of the formation of an electrical double layer of positive charge on the particles, and negative ions in the solution. This double layer results in a potential difference called the zeta potential (ζ), between the solution layer immediately adjacent to the particle and the main body of the solution because negative ions of the former are attracted preferentially to the positively charged electrostatic field on the particle surface. However, when the concentration of electrolyte exceeds a critical value, the magnitude of the zeta potential decreases drastically and the particles no longer have a sufficient charge to repel each other so that agglomeration and precipitation of particles result. O'Conner et al (1956), Modi and Fursteneau (1957), Forster and Kariapper (1973), Sykes and Alner (1974) reported on this relationship between the concentration of electrolyte and zeta potential. These results show that zeta potentials will be very small in strong solutions of electrolytes, but that the sign of this potential will depend on whether or not there are multivalent ions present of opposite charge to the particles. Thus, in a quiescent electroplating bath the dispersed particles inevitably precipitate because the concentration of electrolyte reduces the zeta potential below the critical value for particle suspension. For this reason, methods of increasing particle mobility and directing

particle migration towards the cathode in a uniform dispersion have to be considered for process development.

Forster and Kariapper (1973), Sykes and Alner (1974), and Foster and White (1978) have evaluated the techniques involving the application of an emf to a suspension of particles to effect their directional migration towards the cathode. The use of dc superimposed on the normal plating emf, with the solution current flow both parallel and perpendicular to the metal cation and particle flow, has been investigated. Other electrical methods such as dc plating current, and high-low voltage surge in the plating circuit, have also been tried in attempts to improve the codeposition of nickel and suspended dispersoid, Dunkerley et al (1966). None of these were reported to prove effective.

The reported methods by Dunkerley et al (1966) Brandes and Goldthorpe (1967) and Kedward et al (1976), of particle suspension in order to prevent particle agglomeration included :

1. bubble agitation and mechanical stirring both together and separated;
2. liquid/air process using a recirculating pump;
3. plate-pumper;
4. ultrasonic vibration and mechanical stirring combined.

Of these, only the liquid/air and plate-pumper systems are being used commercially in the U.K.

5. Mechanism of deposition

The mechanism of electrodeposition of inert particles and metals is far from being well understood. In order to explain the observed co-deposition, three mechanisms are generally proposed; namely, mechanical inclusion, electrophoresis, and adsorption of inert particles onto the cathode. The factors that influence the tendency for particles to be engulfed by the depositing metal are open to controversy; a number of investigators (Guglielmi (1972), Kariapper and Foster (1974), Celis and Roos (1977), Tomaschewski (1976), Roos et al (1977), Snaith and Groves (1977) (1978)) support the view that metal ion adsorption on the particles is a prerequisite for their entrapment whereas others (Lakshmina rayan (1976)) doubt the importance of this.

A more detailed account of the mechanism of electrolytic co-deposition has been given by some investigators and reference will be made to their work, Guglielmi (1972) is the only one who proposed a mathematical model for the electrocodeposition of inert particles.

The emphasis during the early days of research on cermet coatings was to concentrate not only on determining the optimum conditions for producing a good composite material, but also to obtain as much data as possible on the properties of such deposits. Few people appeared to

show interest in the theoretical aspects of such deposits, thus work explaining the mechanism by which inclusion takes place was pushed into the background.

There were opinions advanced by some of the early workers on what constitutes the mechanism by which codeposition occurs; that is to say, how the particles present in the plating solution migrate to and affix themselves to the deposit at the cathode. Tomaszewski, Clauss and Brown (1963), proposed a mechanism of inclusion based on the hypothesis that codeposition of particles with the metal matrix was the result of nickel and/or hydrogen ions being adsorbed on the surface of the particles present in the nickel plating bath. These adsorbed ions would thus impart a positive charge to the surface of the particle which would then, under the influence of an electric current, migrate to and be incorporated in the metal deposit at the cathode.

However, the codeposition of inert particles and copper seemed to be more difficult to realise. Sautter (1963) stated that the codeposition of alumina or silcon carbide and copper from acidified copper sulphate baths was not possible. According to Williams and Martin (1964) the codeposition of alumina, silicon carbide, or boron carbide and copper from a copper cyanide plating bath could readily be obtained. Chen et al (1971) pointed out the influence of the structure of the inert particles on the codeposition, α- alumina with a hexagonal structure could

be deposited from an acidified copper sulphate bath; while γ - alumina with a spinel-type cubic structure could not be codeposited from an analogous plating bath.. Additional work by Tomaszewski, Tomaszewski and Brown (1969) appears to give credibility to their earlier proposed theory that cation adsorption was the mechanism by which codeposition was accomplished. The afore-mentioned workers claimed that the addition of monovalent cations; such as Na^+, K^+, Rb^+, Cs^+, and Tl^+, to the plating baths promoted codeposition. Celis and Roos (1977) studied the influence of thallium sulphate which promoted codeposition of alumina in acid sulphate systems. They deduced that thallium, by some catalytic action, increased the rate at which metal ions were reduced at the particle-cathode interface and therefore speeded the establishment of the strong adsorption stage.

Snaith and Groves (1972) concluded that hydrodynamic transport to the cathode and mechanical entrapment of the particles were the most important factors in the codeposition process. Brandes and Goldthorpe (1967) proposed that the surface charge to particle size ratio and the micro-throwing power of the plating were important factors.

The two-step adsorption mechanism proposed and supported experimentally by Guglielmi (1972) has been recently validated by Celis and Roos (1977). In the first step the

inert particles are loosely adsorbed on the cathode and they are in equilibrium with the particles in suspension. The particles are still surrounded by adsorbed ions and the solvent molecules. In the second step this screen is broken through so that a strong electrochemical adsorption of the particles on the cathode takes place. The inert particles are now permanently bound to the cathode and are consequently embedded in the deposit. Guglielmi (1972) derived the following equation:

$$\frac{C}{\alpha} = \frac{Wi_o}{nFdv_o} \cdot e^{(A-B)\eta} \cdot \left(\frac{i}{K} + c\right) \qquad (26)$$

where C is the concentration of suspended particles, and α the volume fraction of particles in the deposit, W the atomic weight of the electrodeposited metal, and d its density, n the deposited gram metal valence, and F the Faraday constant. The parameters i_o and A are related to the metal deposition and are constants in the Tafel equation whibh gives a relation between the current density (i) and the overpotential (η):

$$i = i_o \cdot e^{A\eta} \qquad (27)$$

The parameters V_o and B play a symmetrical role with the parameters i_o and A but are related to the inert particle deposition. K is derived from Langmuir adsorption isotherm and depends essentially on the intensity of the interaction between particles and cathode. Guglielmi verified the validity of his model for the codeposition of titania and

silicon carbide with nickel from a nickel sulphamate bath. Celis and Roos showed the physical model, proposed by Guglielmi, to be valid for the codeposition of α - alumina and copper from a copper sulphate plating bath.

Foster and Kariapper (1973; 1974) concluded that metal ions were adsorbed onto the surface of the particle producing a surface charge which makes it possible for the particle to be attracted to the cathode surface and remain there long enough for it to be engulfed by the growing deposit, the adsorbed ions also assisting the formation of an efficient mechanical bond between particle and cathode surface. They also conclude that agitation and current density are major factors, the former having a two-fold effect in that it not only serves to bring particles into contact with the cathode surface, thereby increasing the particle/cathode collision frequency; but also influences the forces acting on the particle once they have come to rest on the cathode surface. The current density effect, however, would be to influence the rate of growth of the particle/metal interface; and thereby the strength of the physical bond between the two. The higher the current density, the greater the probability of a particular particle being codeposited. The authors also demonstrated that suspended particles in low pH systems acquire a positive charge and that an electrostatic force would be exerted on the particles

when they are in close proximity to the cathode surface. However, production of composite coatings from electroless systems makes the significance of electrostatic attraction in the electrodeposition of composite materials very doubtful.

CHAPTER II EXPERIMENTAL METHODS

G. ELECTRODEPOSITION.

1. The electrolyte for deposition

(i) Watts type nickel bath - analar grade of salts used were supplied by BDH Chemicals Ltd.

	g/l
Nickel sulphate	300
Nickel chloride	45
Boric acid	30
pH	4.0-4.5

Plating conditions:

Current density 2 A/dm^2

Temperature $50^{o}C$

The electrolyte was prepared by filling a litre beaker to two-thirds with distilled water and raising the temperature to about $40^{o}C$. The quantity of nickel sulphate (Analar Grade) required to make a litre of solution was dissolved in the hot distilled water followed by the quantity of nickel chloride needed. Then the required weight of boric acid was carefully added to the solution while stirring.

(ii) Nickel-Cobalt bath

	g/l
Nickel sulphate	240
Cobalt sulphate	15
Boric Acid	30

Nickel Chloride	45
Sodium formate	35
pH	4-4.3

Plating conditions:

Current density	2-4 A/dm^2
Temperature	54-60^{o}C

The electrolyte was made up by dissolving the salts, one after the other, and stirring thoroughly in warm distilled water as described above.

(iii) Chromium bath

	g/l
Chromic acid	250
Sulphuric acid	2.5

Plating conditions.

Current density	32 A/dm^2
Voltage.	6-12 V
Temperature	54^{o}C
Anode	Pb Alloy

The solution was prepared by carefully adding the sulphuric acid to cold distilled water, and then dissolving the chromic acid into the solution.

2. Blending of oxide particles

The electrolyte particle suspension was prepared by suspending the particles to be co-deposited in a small portion of nickel solution and stirred for

30 minutes with a high speed laboratory stirrer in order to ensure the break-up of clusters. The blended slurry was then added to the electrolyte concentrate and prepared for plating.

The oxides used to prepare the suspensions were:

$\gamma - Al_2O_3$	Particle size 0.05 μm (High purity powder supplied by BDH Chemicals Ltd.)
ZrO_2 (Yt stabilised)	particle size 1 μm (99.9% pure. Rare Chemicals, Metals & Ceramics Winconsin U.S.A.).
HfO_2	particle size 1 μm (99.7% pure Koch & Light Lab Ltd.)

3. Preparation of substrate for plating

(i) Brass

To obtain strippable deposits for mechanical tests as well as for gas phase studies, flat specimens of brass, dimensions 2" x 1" x $\frac{1"}{16}$ were cleaned as follows:

(a) Degrease with acetone
(b) Acid dip in 50% HNO_3 until gassing ensues.
(c) Passivate by immersing in a 10% chromic acid solution for 5 mins.

The specimens were thoroughly rinsed in between the stages. The water break test was used to judge whether the surfaces were properly cleaned.

(ii) Stainless Steel

Flat stainless steel cathodes which measured approximately 2" x 1" x $\frac{1"}{16}$ were first cleaned by soaking in a hot NaOH (50 g/l) and Na_2CO_3 (25 g/l) solution and scrubbed, followed by a hot water rinse. The test panels were then dipped in 10% H_2SO_4, and thorougly rinsed in distilled water.

(iii) Nickel-base Superalloys - Nimonic 105 and IN 738

Flat disc, specimens were cut from the alloys by a split grinding machine. Accurate dimensions of each specimen was measured with a micrometer screw gauge. The following cleaning system was used:

(a) Polish surface and edges of specimens with fine emery paper (grade 20).

(b) Wash in alcohol. Attach platinum wires to specimens by spot-welding.

(c) Vapour degrease in trichlorethylene.

(d) Anodic clean for 3 mins in 30% H_2SO_4: below boiling point with current density of about 30 A/dm^2; 6 volts across anode and cathode (stainless steel)

(e) In order to facilitate good adhesion, plate in a nickel sulphate strike bath for 5 mins. at 20 A/dm^2.

4. Apparatus for electroplating

The apparatus and set-up used for plating specimens in this investigation is shown schematically in figure 4. The basic design involved a circular glass tank (5), 1 litre in capacity, with the lower area funnel shaped (8), and sloping downwards towards a centre outlet, of diameter 12.6 mm. A sintered pyrex glass filter disc (7), 90mm in diameter (supplied by Scientific Supplies Ltd.,) is attached, as shown, in order to increase uniformity of air agitation. The bath temperature was maintained by means of a thermostatically controlled heater and pump unit (11) which pumps hot water round the glass jacket (3) surrounding the tank (5).

Rolled depolarised nickel anodes (1), 102mm x 32mm x 6mm in dimension, were used. The anodes were wrapped with bandage material so as to prevent particles, leached from the anodes during dissolution, from being codeposited.

The air needed to keep oxide particles in suspension was fed into the system by means of soft copper tubing (12), 20 gauge, with a control tap (14) and a pressure gauge (13) fitted. The copper tubing carrying the air was coiled round and allowed to rest at the bottom of the hot water tank (10), as shown, in order to ensure that warm air is supplied to the bath (3). The pressure of the air supplied was maintained at 4 lbs/in^2.

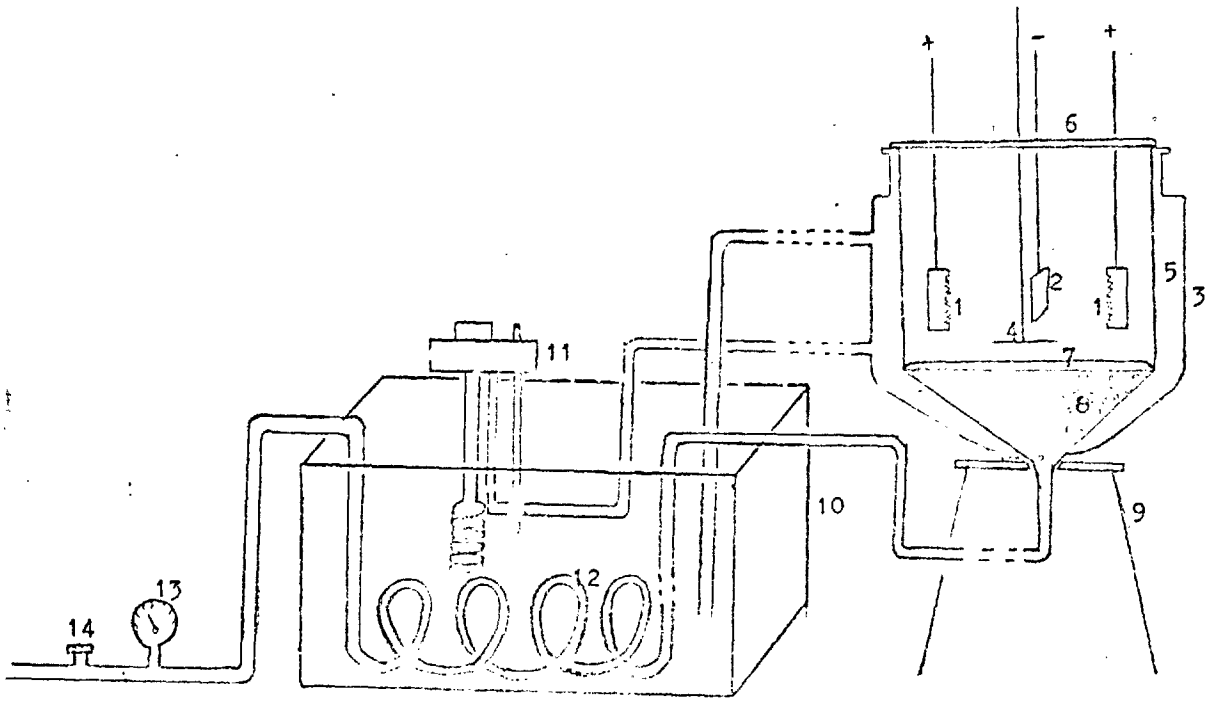

Figure 4 Schematic diagram of experimental set-up for electrodeposition.

Other equipment used included a Roband Varex Twin series II power supply.

The electrolyte temperature was maintained at 50°C throughout the electrodeposition process. The loss of electrolyte due to effervescence caused by air bubbling was minimised by adapting a perspex lid (6) to fit snugly on to the top of the plating bath. Slight losses due to evaporation can be replaced by periodically topping up the bath with distilled water.

The cathode (2) was centrally located in the bath in order to facilitate good distribution of current and ensure even distribution of particles along both faces of the cathode. A glass rod stirrer (4), 200 mm x 4.5 mm dimension, was used for intermittent stirring to ensure that the oxide particles were always in suspension in the solution.

Solution maintenance was carried out every fortnight by emptying the bath content into clean beaker, filtering to recover the oxide particles, and purifying the solution. The purification treatment (described earlier) involved adding 5 g/l activated carbon powder, raising the temperature to 60°C and agitating for 3 hours. The solution is allowed to settle overnight and then filtered using a whatmans 3 paper. The filtered solution is then electrolysed using a very small current (0.5A) for 2 hours. The pH is checked and the solution is then ready for use.

It is usual to keep stock solution so that this can be used while purification treatment is being carried out on the used solution.

5. Standardisation of plating conditions

Flat specimens 2" x 1" x 1/16" dimensions, were cut from brass sheet, and a number of tests were carried out.

(i) Nickel

A range of specimens were cleaned using the pretreatment cycle for brass mentioned earlier. The specimens were thoroughly rinsed in distilled water and electroplated in the modified watt's nickel solution at various current densities ranging from 0.5 A/dm^2 to 10A/dm^2 for plating time of one hour. The deposits produced were stripped from the brass matrix by filing the edges and peeling off the nickel deposits.

(ii) Nickel + Ceramic Oxide.

Similarly, a range of specimens were pre-treated using the cycle as for brass. The specimens were electroplated in the solution containing oxide particle contents ranging from 2 g/l to 10 g/l at various current densities ranging from 2 to 10 A/dm^2 for plating times of 1 and 2 hours respectively. The deposits produced were examined visually for any change in texture.

6. Duplex Coatings

A number of brass specimens were pretreated as aforementioned. A set of specimens were electroplated in the nickel-cobalt bath at the parameters stated in section 2.1 another set was plated in the chromium bath in order to assess the plateability of the solutions. A range of specimens were electroplated, firstly, in the nickel-cobalt bath, then in the chromium bath, and finally in the nickel +ceramic bath. The mounted and polished cross-sections of the deposits produced were examined under a microscope to assess the adhesion of the respective plates to each other.

7. Thickness determination

A variety of methods for measuring coating thickness are available, though a number of these do not find much use. The thickness of a coating is seldom measured with an accuracy of better than ± 5%, but this is usually sufficient.

7.1 Weight gain method

This method determines the average thickness of the deposits by gravimetric measurements on the basis of an assumed density.

Each specimen, 25 cm^2 in surface area, was put through the pretreatment cycle for brass, dried and carefully

weighed. It was then plated to conform to a nominal thickness, rinsed thoroughly in distilled water, dried, cooled to room temperature, and carefully reweighed. The thickness of the plating (nickel) was calculated by dividing the weight of the deposit in milligrammes, (i.e. the difference in weight of the test piece after and before plating) by the surface area of the plating in cm^2 x density.

i.e.

$$\frac{\text{Weight of nickel deposit (mg)}}{\text{Area } (cm^2) \times 8.90} = \text{Thickness (microns)}$$

7.2. Atomic adsorption spectroscopic analysis method

This method was used to cross-check the thickness values obtained by employing the weight gain method, as well as, for assessing the amount of nickel present in the nickel + ceramic coating. Thus, the intention was to indirectly estimate the amount of oxide particles in the cermet deposits. For nickel deposits, stock standard solution of nickel 1000μg/ml was prepared by dissolving 1.0g of nickel metal in minimum volume of (1 + 1) HNO_3. This was then diluted to 1 litre with 1% (v/v) HNO_3. The operating parameters are given in table 3 for nickel.

TABLE 3 Operating Parameters of the Instrument for Nickel Determination

Instrument	Perkin-Elmer 290B
Wavelength	232 UV
Slitting setting	0.2 nm
Light Source	Hollow cathode lamp
Flame type	Air-acetylene flame Oxidising (lean, blue).

The sensitivity for the standard conditions described above, is about 0.15 μg/ml nickel for 1% absorption. The working range for nickel is linear up to concentration of approximately 5 μg/ml in aqueous solution. A curve of absorbance versus concentration in μg/ml was plotted for the standard nickel solution.

Selected specimens 50mm x 25mm in dimension and 25μm thick, were each dissolved in a minimum (1+1) HNO_3 solution, and heated gently. The solution was cooled and diluted to 1 litre, A 10 ml. aliquot was taken and diluted to 100 mls in a standard flask. The percentage absorbance for each of the specimens was recorded and the respective nickel concentrations were determined from the standard graph.

8 Determination of the amount of oxide particles in deposits

In order to determine the amount of oxide particles in the deposits, the stripped deposits, 25 cm^2 in surface

area, were dissolved in hot 50% nitric acid. The oxide particles were separated from the nickel nitrate solution by centrifuging for 30 minutes and filtering through a microporous whatman's filter paper. After sufficient washing, the filter paper (0.00014 mg ash content) was then burned off. In determining the concentrations, a correction factor was used to compensate for the ashless filter paper.

The specific densities of the oxides were used for the conversion of weight per cent into volume per cent.

9. Heat Treatment of deposits.

Heat treatment of electrodeposits is not often practised, although it can be important in individual cases. Low temperature heat treatments are fairly common, especially as a means of relieving hydrogen embrittlement of the substrate metal. Internal stress can be relieved by heat treatments at temperatures much below those required for annealing.

Selected specimens were annealed in an O_2 free argon atmosphere. The specimens were put into a tube and flushed with O_2 free argon for 15 minutes. With the furnace temperature at 750°C, the tube was carefully inserted and left for an hour. Flushing with argon continued during the cooling period of 20 minutes.

10. Determination of hardness

Methods of measuring the hardness of metals are well known to metallurgists, and their application to electrodeposits is discussed by Read (1963) and Wilson (1960). The more useful methods involve making an indentation with an indenter of specific geometry under a specified load.

Micro-hardness tests were carried out on a number of specimens, as-plated and annealed in argon at $750^{0}C$ for 1 hr., using a Reichert micro-hardness tester. Four impressions were made on each specimen using an applied load of 60g and the arithmetic mean was then determined from the slightly deviating lengths of the indentation-diagonal thereby obtained. The micro-hardness was calculated by using the formula:

$$H_m = 1854.4 \cdot \frac{P}{d^2} \quad kg/mm^2 \qquad (28)$$

where H_m is the micro-hardness in kg/mm^2, P is the weight applied in grams, and d the indentation diagonal in microns.

11. Determination of ultimate tensile strength

The practice of investigators (Romanoff 1934; Brenner et al 1952) in the field of electrodeposition has been to isolate the plated coatings from its substrate and pull the coating in a tensile testing machine.

In order to obtain specimens which could be used for determination of tensile strength of the electrodeposited

material, stainless steel cathodes were used. The adhesion of nickel coatings on stainless steel is very poor without special surface treatment, and therefore it was very easy to strip the deposit from the cathode by filing the edges. The size of the cathode was 10 x 5 $cm.^2$, and by filing off the edges after plating, two sheets were obtained from which tensile specimens with a 2.54 cm (one in.) gauge length and 0.63 cm ($\frac{1}{4}$ in) in width were stamped out with a punch and die set. The thickness of the specimens varied between 80-120 μm.

The ultimate tensile strength was determined on an Instron Tensile Testing machine which was calibrated with a 100 kg weight such that full scale deflection was obtained on maximum sensitivity. The strain rate employed was 0.02 mm/mm/min and the chart speed selected was 1 cm/min. The yield strengths were determined at 0.2 per cent offset, and all tests were conducted at room temperature.

12. Examination of coatings.

The character of electrodeposits is influenced by plating conditions, nature of the substrate, composition of the solution and its purity. Extreme care is necessary in the design and operation of the experimental procedures, if consistent and reproducible results are to be obtained.

12.1 Optical microscopy

The examination of the nickel base superalloy substrates after pre-treatment was conducted using a metallurgical microscope. This instrument was also made use of during the course of standardisation of plating conditions to produce deposits of uniform structure and excellent coverage.

Micro-graphic observations and photography was done by using an Olympus Tokyo 203122 microscope with an Olympus PM-6 204898 camera attachment (courtesy of the Polytechnic of the South Bank, London). Micro-graphy of the sections was done after setting the required specimen in araldite and dry polishing through a series of 00 to 4/0 Oakey papers and giving a final polish with a 0.25 micron diamond abrasive.

12.2 Scanning Electron microscopy

In order to examine the morphology of the coatings in more detail, scanning electron microscopy was used. Several specimens were examined and photographs of the surface contours were recorded using a Stereoscan 600 (Cambridge Scientific Instrument Co).

12.3 TEMSCAN

Fractured sections of as plated and corroded stripped deposits of nickel and nickel + cermet were prepared and examined with JOEL'S Model100 CX TEMSCAN instrument. X-Ray spot analysis of the specimens were carried out to determine

the distribution of the cermet oxides in the deposits. The author gratefully acknowledges the excellent co-operation extended by Mr. P. Crawley (Joel Ltd) in the studies with the Temscan microscope.

H. HOT CORROSION

1. Electrochemical Studies

1.1 Preparation of molten salt electrolyte

A 50 ml platinum crucible was thoroughly cleaned with conc HCl, and then immersed in hot distilled water and finally degreased with acetone. The crucible, when cool, was filled with analar grade Na_2SO_4, or a weighed mixture of Na_2SO_4 + 5 weight per cent Nacl analar grade (both salts supplied by Hopkins and Williams Ltd), and lowered into the furnace. After electrochemical measurements were carried out on a specimen, the platinum crucible was quickly removed from the furnace. In order to prevent the solidifying fused salt from badly distorting the platinum crucible, the melt, on removal from the furnace, was immediately poured into an aluminium bowl. The crucible was then washed in hot water, cleaned and recharged with salts.

1.2. Preparation of specimens

Stripped specimens of electrodeposited nickel, and nickel + ceramic were cut into squares of approximately 10mm x 10mm. Platinum wires were attached to one end of the specimens by spot welding. Before testing each specimen was degreased in acetone, and then attached to a length of platinum wire protruding from an alumina sheath 450 mm long which formed the working electrode of the cell system.

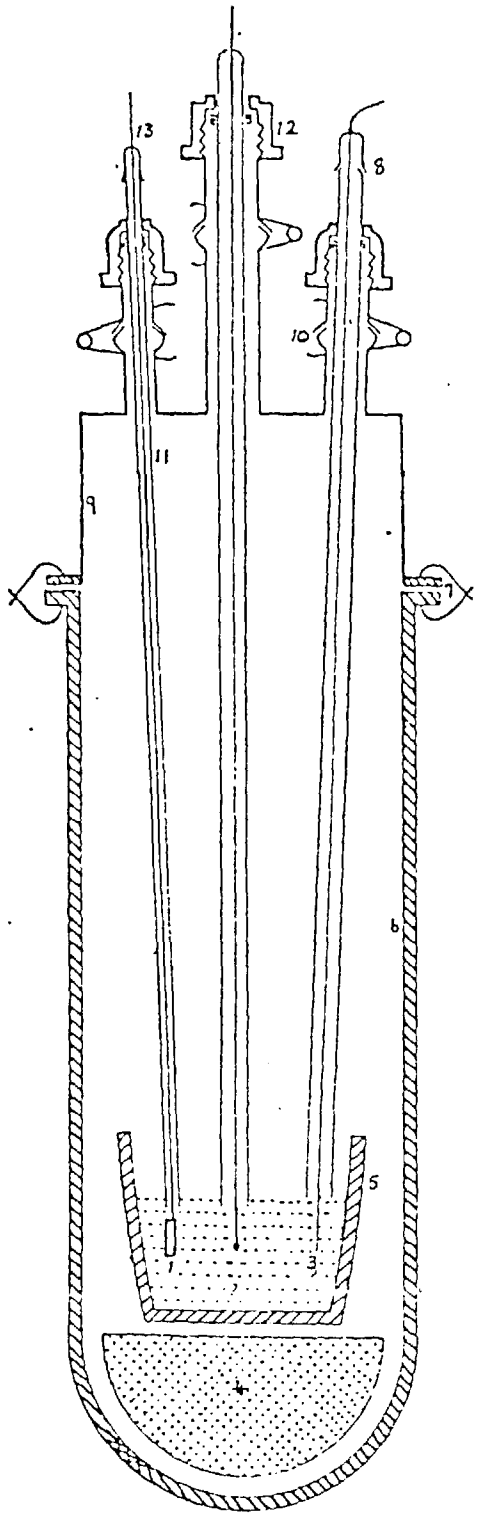

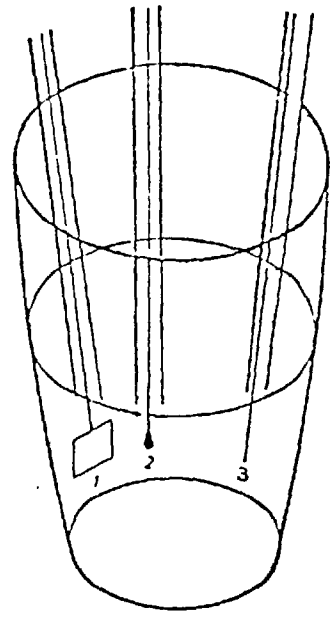

Key

1. Working electrode (specimen)
2. Platinum reference electrode
3. Platinum counterelectrode
4. Ordinary firebrick
5. Platinum melt container
6. Silica tube
7. Flange joints
8. Glass sockets
9. Pyrex manifold
10. Ball joint
11. Electrode support (alumina)
12. Screw cap adaptor
13. Platinum lead

Figure 5. High temperature cell assembly.

1.3. Experimental set-up

Figure 5 shows a schematic diagram of the furnace and the cell used for electrochemical measurement. A more comprehensive description of the set-up is being reported by Swidzinski (1980). The main features of this include:

(a) Furnace assembly - a closed end vertical furnace wound with 16 s.w.g. kanthal wire. A nichrome screen placed between the furnace winding tube and the closed end mullite reation tube. A Pt-Pt/13% Rh thermocouple, placed between the electrical screen and the reaction tube, to control the furnace temperature. Power was supplied from the mains through a Eurotherm temperature controller type LP96 DHS/PID/SCR 25. Lowering and raising of furnace carried out manually by making use of steel ropes, drums and a worm-gear mechanism.

(b) Cell assembly - a pyrex flange (12 cm O.D., 7 cm I.D.) cemented to the open end of the reaction tube. A fire brick placed inside the tube to ensure that platinum crucible was within the furnace hot zone. Alumina sheathed electrodes 450 mm in length, introduced into the furnace through a flanged manifold, were held in position by socket ended compression adapters, matching

ball joints on the pyrex manifold and spring clips. For free corrosion potential studies a two electrode arrangement was used.

(c) Electrodes - The working electrode was the specimen being tested. The counter and reference electrodes were platinum rods 4 cm x 0.1 cm diameter spot welded to platinum wires housed in an alumina sheath. Caution was taken to ensure that the alumina sheaths were above the melt during all electrochemical tests. The choice of platinum as reference electrode was influenced not only by its reversibility and unpolarizability in the selected salt media, but also by its stability, and the fact that electrode potential at a given temperature remains constant with time and is reproducible.

Both counter and reference electrodes were cleaned regularly by washing in distilled water, dipping into conc. HCl, and the surface heated in the oxidising flame of a Bunsen burner in order to remove all accumulated contaminants.

(d) Electrical instruments - An Ekco vibrating electrometer (type N616 B) placed in series in the measuring circuit to act as a null instrument and ensure accurate potential measurements ± 0.1 mV. An Amel 551 potentiostat- galvanostat used

to polarize the working electrode over a selected voltage range and to measure current passing through the cell against time (ΔV =-200mV). A ten speed gearbox, Multur M64, (Rayleigh Instruments Ltd) was used to drive the ten turn Potentostat potentiometer at the desired rate. An X - Y recorder Bryans 26000A4 was used to plot anodic polarisation curves and monitor the change in corrosion current with time at a constant applied anode potential. Free corrosion potential versus time was recorded on a Servoscribe 2S, (RE 571-20) x-t recorder. Chart speed used was 30 mV/hr, with a full scale deflection of 100 mV. Measurement of e.m.f. of the Pt-Pt/13% Rh thermocouples was carried out with a Cropico P4 thermocouple potentiometer supplied by Croydon Precision Instrument Company.

Electrodeposited nickel and nickel + ceramic coatings were cut into squares approximately 1 cm x 1 cm. Platinum wires were spot welded to one end of the specimens, and electrochemical tests were carried out. Two sets of experiments were performed to investigate the behaviour of the specimens in the presence of hot corrosive salts. The exposure temperature of 900°C was chosen for all experiments because it falls within the range of operating temperatures in many gas turbines where hot corrosion occurs readily.

In the first set of experiments, each specimen was degreased in acetone, attached to the electrode assembly and immersed in the melt (Na_2SO_4 or $NaSO_4$ + 5 wt % NaCl as the case may be). The potential difference between the working and reference electrode was adjusted to zero current, and the specimen anodically polarised with respect to the Pt - Pt/13% Rh reference electrode at a rate of 60 mV/min. Two forward and reverse sweeps were carried out on each specimen, and the resultant E/i curves generated were plotted on a Bryans X-Y recorder. After the second reverse sweep, the variation of specimen current with time (i vs t) at a fixed potential was observed and recorded. It was decided to confine the number of i vs t sweeps to two because of the hazard of losing the specimen in the melt. It would appear that the weld between the specimen and platinum wire is undermined after 2 sweeps to the extent of causing the specimen to fall off.

In the second set of experiments, a two electrode system was used; and the specimens were immersed in the respective molten salts at a temperature of 900°C in air. Free corrosion potentials of a specimen as a function of time was measured with an Ekco vibrating reed electometer, and the resultant curve plotted on a Servoscribe 2s x-t recorder at a chart speed of 30 mV/hr. The specimen was the working electrode and the reference electrode was Pt-Pt/13% Rh.

2. Gas phase studies

The corrosion kinetics and hot corrosion behaviour of various coatings, on their own, as well as on two industrial alloys, Nimonic 105 and IN 738 were investigated at 700° and 900°C in flowing SO_2: O_2 (2:1) gas mixtures using a microgravimetric technique similar to that used by Vasantasree (1971).

2.1. Gas train

The gas train used in sulphation studies is shown schematically in Figure 6. In order to register gas consumption, the liquified sulphur dioxide gas cylinder (supplied by I.C.I. Ltd.,) was rested on weighing scales. The gas train was entirely of pyrex glass with ball joints to permit flexibility, except for the cylinder-gas train connexion and about 100 cm connection to the reaction tube inlet. Many of the flexible connections like rubber, pvc etc are attacked by sulphur dioxide, but polythene tube (1mm wall thickness) had the best resistance. Shellac lacquer was used to seal polythene to glass connections. Adequate drying of gases was provided by anhydrous calcium chloride silica gel (8-14 mesh) and phosphorous pentoxide. Both gases used, sulphur dioxide and oxygen, were metered through conventional capillary flowmeters.

The "Blow-off" tubes contain dibutyl phthalate, and for SO_2 these were made of two concentric tubes with a

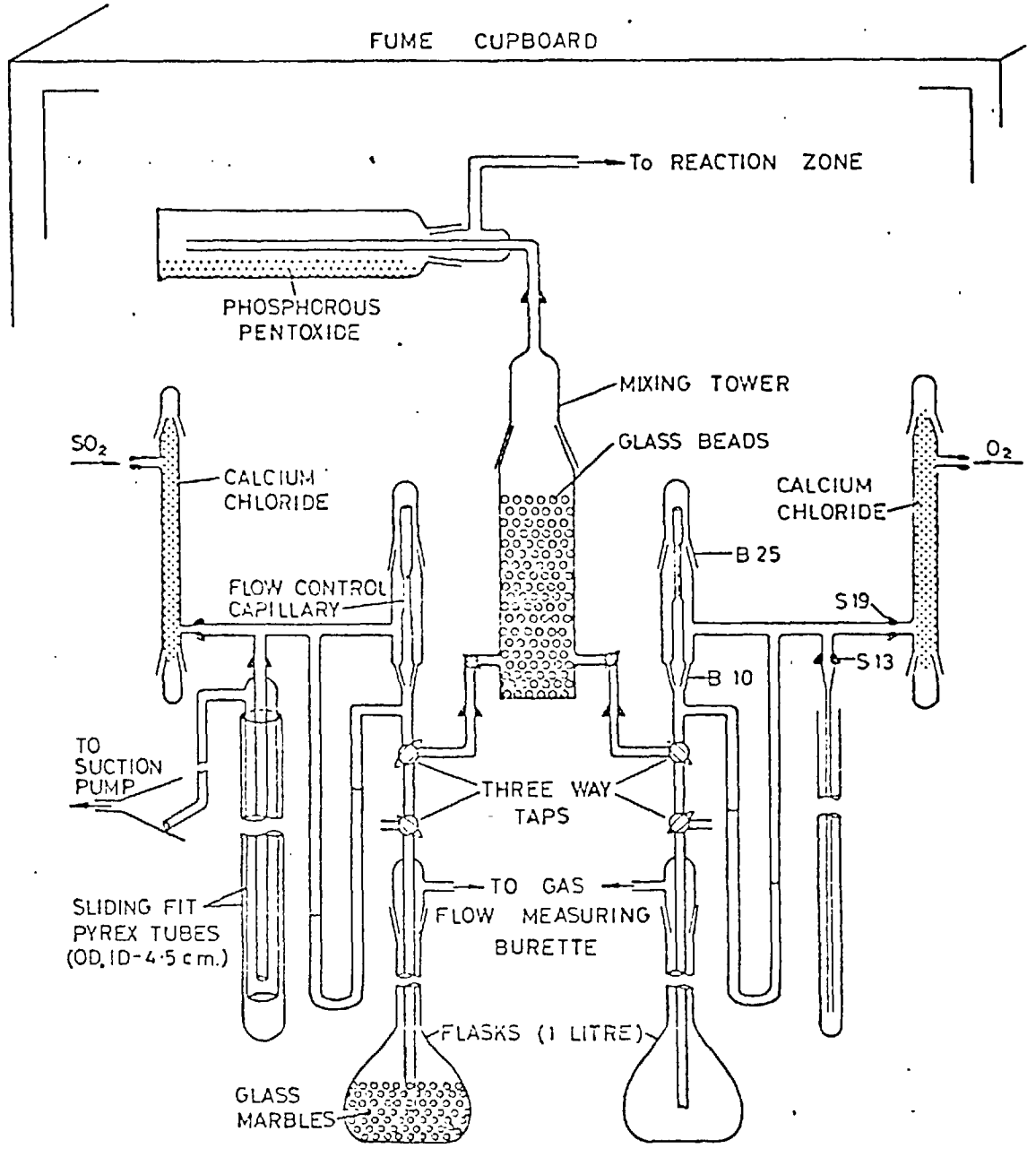

Figure 6. SCHEMATIC REPRESENTATION OF THE GAS TRAIN USED IN SULPHATION STUDIES.

sliding fit for adjusting the flow rates. Capillaries 2.5/2.5cm for SO_2/O_2 flowmeters gave the required flow ratio of 2/1, with a slight adjustment of the blow-off head. To obtain steady and reproducible rates it was necessary to saturate the dibutyl phthalate with sulphur dioxide by passing the gas for about half an hour. A conventional 100 ml burette, up which was swept a film of dilute teepol solution, was used for individually metering oxygen and sulphur dioxide. A 1-litre flask and a long glass tube connection acts as a reservoir between the gas train and the metering burette. This prevents any contact of the teepol film with the gas, otherwise the film breaks or becomes viscous and moves sluggishly. Additional preventive measure is taken by isolating the burette and flushing the connections and flask with oxygen between successive sulphur dioxide metering. Detection of any leaks in the gas train set-up could be carried out by shutting off the main inlet tap to the reaction tube and/or the individual gas taps and observing if the manometric liquid became level in the two limbs. A cotton wool soaked in ammonia causes the formation of thick white fumes of ammonium sulphate if leakage of the SO_2 gas occurs.

Mixing the two metered gases alters the manometer readings slightly because of the changes in the resistance of the individual outflows. By adjusting the blow-off heads the metered levels with respect to manometric heights can

be restored. Suitable selection of capillary flow-control tube and the liquid level in the blow off tubes makes for greater accuracy and ensures that the maximum possible manometric height was kept.

2.2. Thermobalance and furnace assembly

Figure 7 shows the apparatus used for sulphation kinetic studies. A mullite tube (50 cm long, 4.8 cm bore) differentially wound with 20 s.w.g. kanthal wire in an asbestos case 22 cm x 22 cm x 62 cm filled with alumina powder. The mullite reaction tube (90 cm long, 2.25 cm bore) tapered to standard B29 cones was supported inside the winding tube. Power was supplied from the mains through a Eurotherm temperature controller, model Lilliput LP96 DHS/PID/SCR. Between the winding tube and reaction tube is a controller thermocouple (Pt-Pt/13% Rh) which controls a steady temperature to within + 1 degree accuracy.

A B29 socket of a pyrex manifold (10.5 cm long) with a flange FG 35 at the other end, and a side tube about two-thirds the way up about 3 cm long with a S13 ball, was fitted on to the top mullite B29 cone of the reaction tube. A 12.5 cm long upper manifold with a B10 socket carrying a B10 drip cone, and a sloping tube (2 cm dia) at its neck that tapered to end with a S13 ball, was clipped onto the FG 35 flange. At the end of the gas train outlet is a two way tap with one fixed and one flexible S13 socket which could engage onto the S13 balls on the lower and upper inlet manifold respectively on the top of the mullite B29 cone. This provided two gas inlets to the

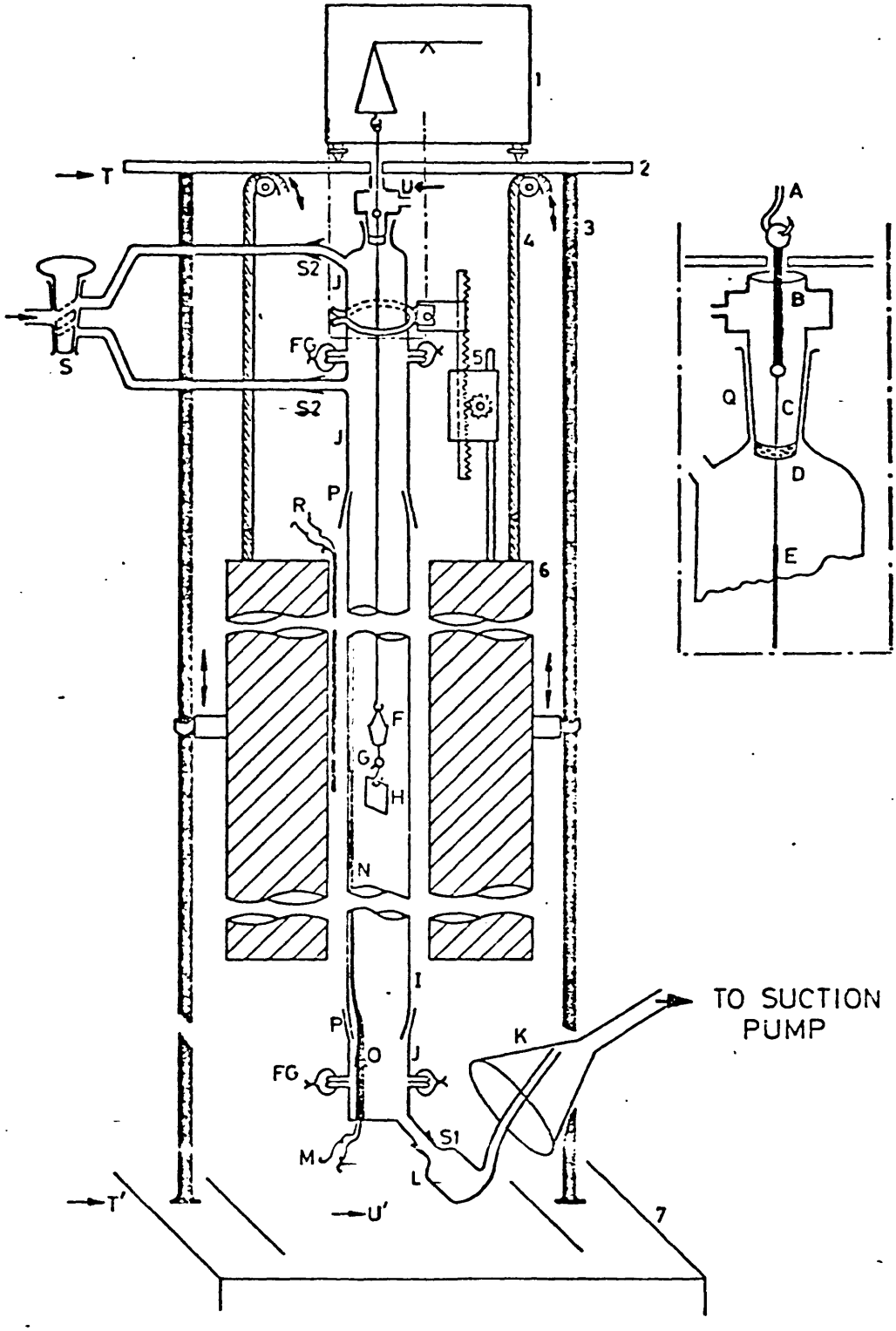

Figure 7. SCHEMATIC DIAGRAM OF APPARATUS USED FOR SULPHATION KINETICS STUDIES.

KEY TO FIG. 7.

1. RECORDING THERMOBALANCE.
2. ALLUMINIUM PLATE (71x56x1·3 cm.) SUPPORTED ON ANGLE IRON STAND.
3. STEEL GUIDE RODS (DIA. 1·3 cm.) TO LIFT AND LOWER FURNACE.
4. STEEL ROPES OVER PULLEYS CONNECTED TO FURNACE FROM A WORM DRIVE ASSEMBLY.
5. RACK AND PINION ASSEMBLY.
6. KANTHAL FURNACE (23x23x 63 cm.), Al SWG 2, 32 OHMS, CONSTANT TEMP ZONE LENGTH (6 cm.).
7. STAND BASE.

TT' WORKING HEIGHT BELOW ALUMINIUM PLATE, 191 cm.

UU' COMPLETE HEIGHT OF APPARATUS FROM B10 ORIP JOINT TO PYREX BOTTLE AT EXHAUST END, 128 cm.

A. STAINLESS STEEL HOOK (LENGTH 15 cm.)
B. PLATINUM HOOK (DIA. 1·3mm., LENGTH~7 cm.).
C. GOLD WIRE (DIA. 3 THOU. LENGTH~6 cm.).
D. LIQUID SEAL (HEIGHT ~ 0·2 cm.).
E. PLATINUM WIRE DIA. 0·3mm., LENGTH~55 cm.).
F. PLATINUM MICRO-CRUCIBLE (CAP 1·1 ml.).
G. SILICA HOOK
H. TEST SPECIMEN.
I. MULLITE TUBE MACHINED TO B 29 CONES (BORE 2·25 cm., LENGTH 90 cm.).
J. PYREX MANIFOLD.
K. 15 cm. GLASS FUNNEL CONNECTED TO SUCTION PUMP
L. PYREX BOTTLE AT OUTLET END.
M. Pt/Pt-Rh THERMOCOUPLE WITHIN REACTION TUBE.
N. CLOSED END SILICA SHEATH (ID 2 mm.) FOR THERMOCOUPLE M.
O. B 7 CONE AND SOCKET.
P. B 29 SOCKET.
Q B 10 SOCKET AND DRIP CONE.
R. Pt/Pt-Rh THERMOCOUPLE CONNECTED TO EUROTHERM FOR FURNACE TEMPERATURE CONTROL.

S1,S2 BALL JOINTS S 19, S13.

FG. FLANGE JOINTS FG 25.

reaction tube. For the exit of gases at the lower end of the reaction tube, pyrex manifolds were attached, leading into the mouth of a filter funnel connected to a filter pump. At Pt/Pt-13% Rh thermocouple was inserted into the hot zone via a B7 internal seal. The funnel and filter pump acted as an atmospheric exhaust unit at the lower end while a small drop of A.R. Conc. H_2SO_4 held in the B10 drip cone served as an effective top seal.

A Stanton microbalance (0.1 mg sensitivity), was placed on top of the aluminium plate (Figure 7), with a suspension from its rear pan passing vertically down through an 8 mm dia. hole in the aluminium plate. A small draft shield was positioned between the thermobalance and the aluminium plate. The composite suspension, which passes through the liquid seal into the centre of the reaction tube, consisted of a steel hook (14 cm long) hung from the balance rear pan carrying a thick platinum hook (7cm long, 1.3mm dia) and a Pt wire (55 cm long. 0.3mm dia) a gold wire (6cm long, 3 thou dia) connected the two Pt wires fused on to the wires over a 2 cm length. A platinum microcrucible (1.1 ml cap), with a loop beneath it, was suspended from the Pt-Au-Pt composite suspension With the furnace wound to the top position the suspension. was well within the constant temperature zone (4 cm).

Specimens were loaded and unloaded onto and from the suspension with the entire furnace and manifold assembly at the lowest position with respect to the micro-balance and suspension wire. The gas entered the manifold at the lower inlet, a glass disc covering the FG 35 flange. This allowed the upper manifold to be raised for insertion and removal of the sample. In the low position, with the end piece 10 cm above ground level, the crucible and specimen can be seen in the top piece of the manifold.

The use of sulphuric acid as a liquid seal did not in any way affect the corrosion performance of the specimen, and it precluded any contamination from unknown chemical products. It effectively shielded the thermo-balance from the reaction gas-sulphur dioxide and/or sulphur trioxide, itself remaining unaffected. The acid drop being a dehydrant, absorbed moisture from the laboratory atmosphere, and this increased the drop size over a period of time. This did not affect the experiments however, since this increase in size could be controlled.

The gas flow of 100 ml/min travelled down the length of the 2.25 cm bore reaction tube at an equivalent linear speed of 0.5 cm/sec approximately (Vasantasree 1971).

2.3. Specimen preparation

(i) Nickel based superalloys - A slip grinding machine, using carborundum wheels 4" dia.,

1" or ½" dia. centre hole, and ten thou. thick, was used to slit the nimonic 105 and IN 738 alloys into workable sizes. Accurate positioning and micrometer feed ensured cutting successive specimens of uniform thickness. The specimens were then polished on a series of Oakley polishing papers to Grade 4/0. This ensured the removal of the oxide coatings on the specimens, before subsequent washing with soap and water and degreasing in acetone. The accurate dimensions of each specimen was measured just before use, with a micrometer screw gauge.

(ii) 0.1M Na_2SO_4 and Na_2SO_4 + 24 wt % NaCl coated specimens ——

Each specimen was measured with a micrometer screw gauge and degreased in trichloroethylene for 5 minutes, cooled and weighed. A platinum wire (about 1 cm long) was spot welded to the specimen, weighed again, and then degreased. The platinum wire was bent into a hook and hung on a wire rail located inside a muffle furnace preheated at 400°C. After 5 minutes, the specimen was removed from the furnace and carefully sprayed with a fine mist of 0.1M Na_2SO_4 or a mixture of Na_2SO_4 + 24 wt % NaCl solution, as the case may be, using airless spray gun (supplied by Griffin

and George Ltd). The specimen was put back into the furnace to allow the salt to dry on the surface of the specimen, after which it was taken out, allowed to cool and weighed. This procedure can be repeated until about 1 mg/cm^2 of salt was covering the entire specimen surface.

(iii) Electrodeposited specimens - The accurate dimensions of each specimen was measured before use with a micro-meter screw gauge. Each specimen was degreased in trichloroethelye as mentioned above, and then weighed before and after spot welding a platinum wire (about 1 cm long) to it, and finally made use of in the sulphation studies carried out.

2.4 Experimental procedure

Mixtures of SO_2 and O_2 used at 700 and 900°C in this work were in the ratio 2:1 with the actual flow rates of approximately 100 ml/min., obtained by mixing metered flows from capillary flowmeters with $CaCl_2$ and self-indicating silica gel for the initial drying and P_2O_5 for final drying. The full equilibrium SO_3 pressure was obtained by positioning the platinum microcrucible (an effective catalyst) immediately upstream above the specimen as described in earlier studies by Hocking and Alcock (1966), and Vasantasree and Hocking (1976).

The weighed specimen, with its platinum wire (1 cm long) bent into a hook was attached to the loop below the platinum microcrucible. The top manifold was brought down to operating position and the gas mixture passed through the system for fifteen minutes. The balance was then poised to ensure that the weight registered on the chart was about 40 divisions. The Stanton recording balance used in this work is designed to register a full change of 100 milligrams and, a full scale chart traverse of 99-101 divisions for a 10 mg weight change.

When the furnace was raised, it took about 80 seconds for the specimen to attain the working temperature (Chattopadhyay and Wood 1970) and just about time for gas equilibration in the hot zone. The balance arrest action was switched on to automatic and the specimen was at the correct position well before reaction commenced. Generally, long runs greater than 7-8 hours were left to proceed overnight.

When the corrosion run was over, the furnace was lowered, and the specimen unloaded. The post-corroded specimen was weighed in a chemical balance, examined visually and later stored for further examination and analysis.

2.5. Examination of corroded specimens.

The surface morphology of the required specimen was examined in more detail and photographs taken with the Stereoscan 600 (Cambridge Scientific Instrument Co). Micrography of the sections was done after setting the required specimen in araldite and dry polishing through a series of Oakey emery papers and giving a final polish with a 0.25 micron diamond abrasive.

Polished sections were prepared of specimens corroded under various conditions. These were examined with a Hitachi S-450 S.E.M. (supplied by Perkin-Elmer) linked to a X-ray dispersion analysis system (link systems - pulse processor 2010 and Data General Corporation's Nava 2). This equipment was made use of by courtesy of the Polytechnic of the South Bank, London.

The surface oxide layers of the corroded specimens were analysed by x-ray using a Phillips wide range vertical goniometer type PW1050 in conjunction with a Phillips X-ray generator type PW 1310. A copper target with graphite monochrometer was used at 35mA and 40 KV operating conditions.

CHAPTER III RESULTS

I Electrodeposition

1. Codeposition of Al_2O_3, ZrO_2 and HfO_2 with Nickel

The effects of the concentration of dispersoids such as Al_2O_3, ZrO_2 and HfO_2 in the Watts nickel bath on the codeposition of the oxide particles in the nickel matrix is shown in Graphs 1 and 2. In general, the oxide content in the nickel matrix was found to increase linearly up to 10 g/l for Al_2O_3 HfO_2 and 20 g/l for ZrO_2. However, the amount of oxide content in the nickel matrix due to the increase in ZrO_2 dispersoids in the bath (from 15 g/l to 20 g/l) was less appreciable.

The weights and volumes per cent of Al_2O_3, ZrO_2 and HfO_2 in each of the 5 sections of the different deposits analysed is shown in Tables 4, 5 and 6.

The microscopic examination of the electrodeposited dispersion coatings of Ni-Al_2O_3, Ni-ZrO_2 and Ni-HfO_2 revealed that there exists loosely held particles as well as completely embedded particles on the deposited surface. The oxide particles incorporated into the nickel matrix were found to disperse uniformly over the entire cathode surface, however, they were partly aggregated forming a large inclusion. Electron micrographs of the surface obtained using a TEMSCAN reveal that the growth mechanism is modified by the presence of the oxide particles. The coarse grained

microstructure of the nickel deposits from a pure nickel bath was found to be altered by the incorporation of the oxide particles, and to have fine grained microstructure with an increase of the content of the oxide particles in the nickel matrix (Plate 1a-f).

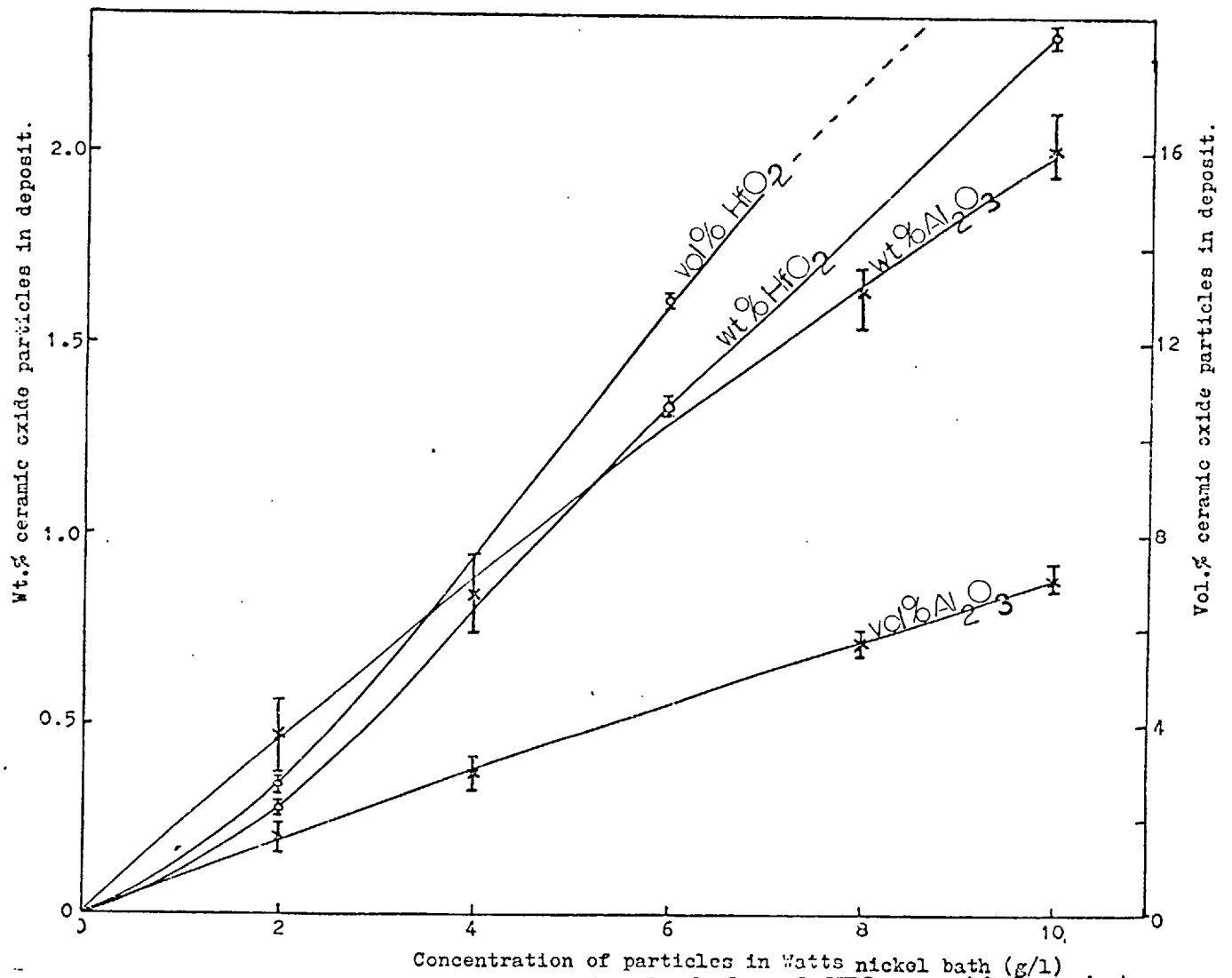

Graph 1. Variation of volume per cent of Al_2O and HFO_2 particles into nickel deposits with the concentration of the oxides in Watts nickel bath

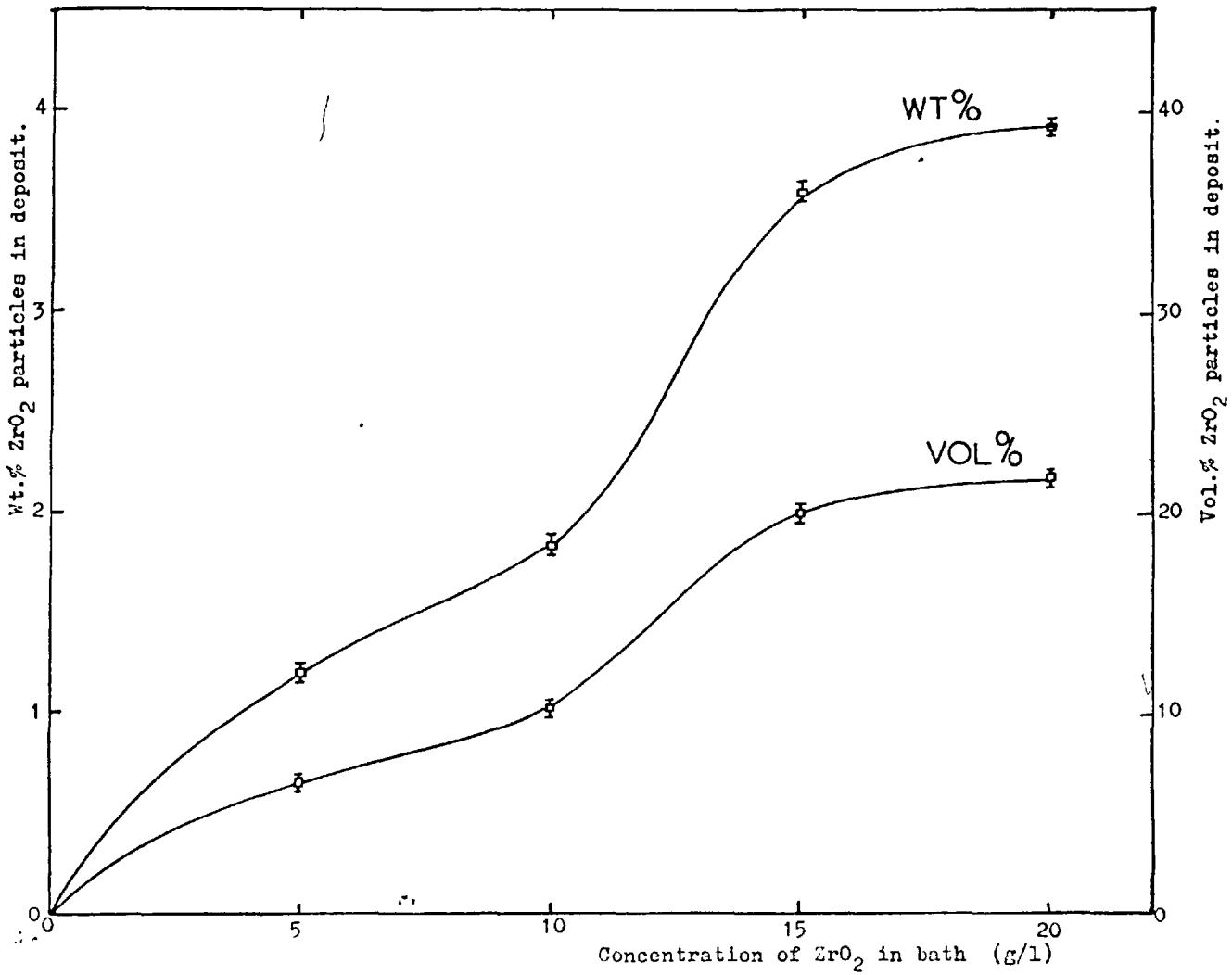

Graph 2. Variation of volume per cent ZrO_2 particles into nickel deposits with the concentration of ZrO_2 in Watts nickel bath.

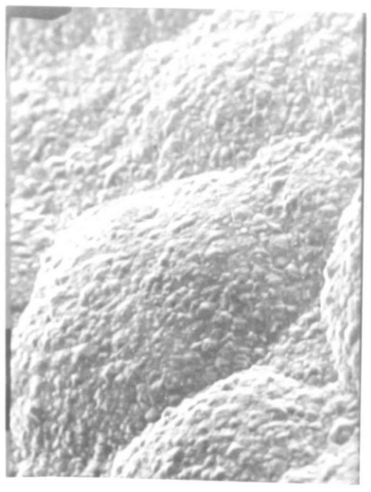

a. Surface profile of electrodeposited nickel; 25μm thickness, C.D. 2A/dm^2, SEM(x1000).

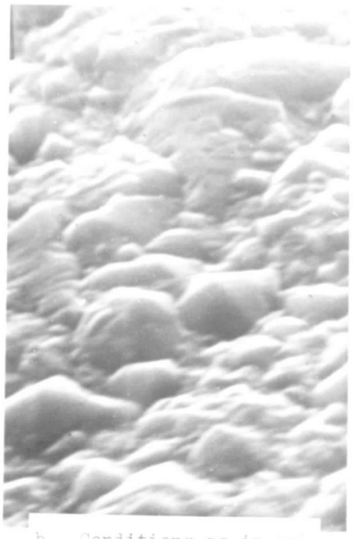

b. Conditions as in (a), SEM(x10000).

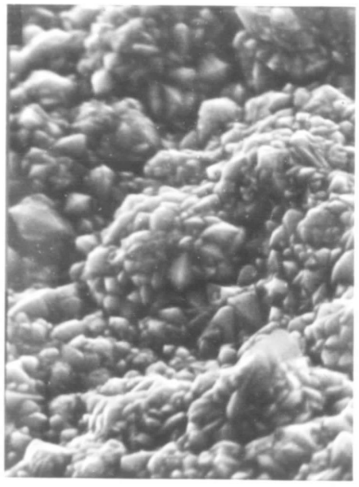

c. Surface morphology of electrodeposited Ni-Al_2O_3 (0.47 wt.%); 25μm thickness. C.D. 2A/dm^2. SEM(x5000).

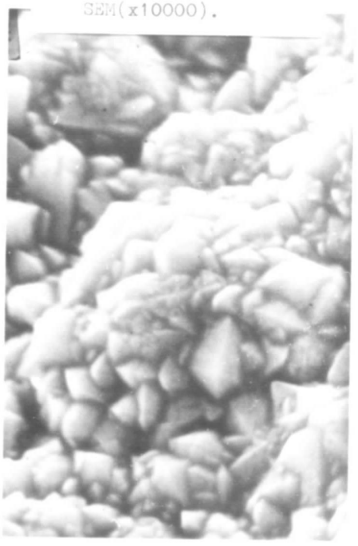

d. Conditions as in (c), Ni-Al_2O_3 (0.83 wt.%). SEM(x10000).

e. Conditions as in (c), Ni-Al_2O_3 (1.56 wt.%). SEM(x5000).

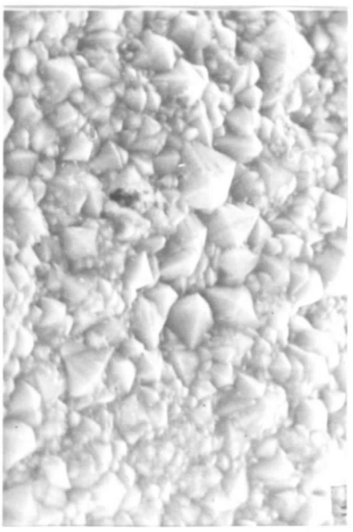

f. Conditions as in (c), Ni-Al_2O_3 (2.06 wt.%). SEM(x5000).

PLATE I

Plate 2(a-d) shows the effect of annealing for 1 hour at 750°C in argon atmosphere on the surface profiles of electrodeposited nickel and Ni-Al_2O_3 containing varying oxide content in the nickel matrix. The plating conditions were as for specimens in Plate 1 (i.e. current density 2 A/dm^2, temp 50°C). Plates 3(a-c); 4(a-c) and 5(a,b) show the comparison of the surface morphologies and the X-ray dispersive analysis of various oxide incorporated nickel electrodeposits. The current density and deposition rate was higher in the case of Ni-ZrO_2 (i.e. 4 A/dm^2). The number of ZrO_2 particles in suspension per unit volume of bath solution was more than that for Al_2O_3 and HfO_2 and as such the build up of ZrO_2 particles on the cathode surface was much faster.

Plate 5(a and b) shows the X-ray analysis obtained for the Ni-ZrO_2 (3.9 wt %) and that for Ni-HfO_2 (2.35 wt%).

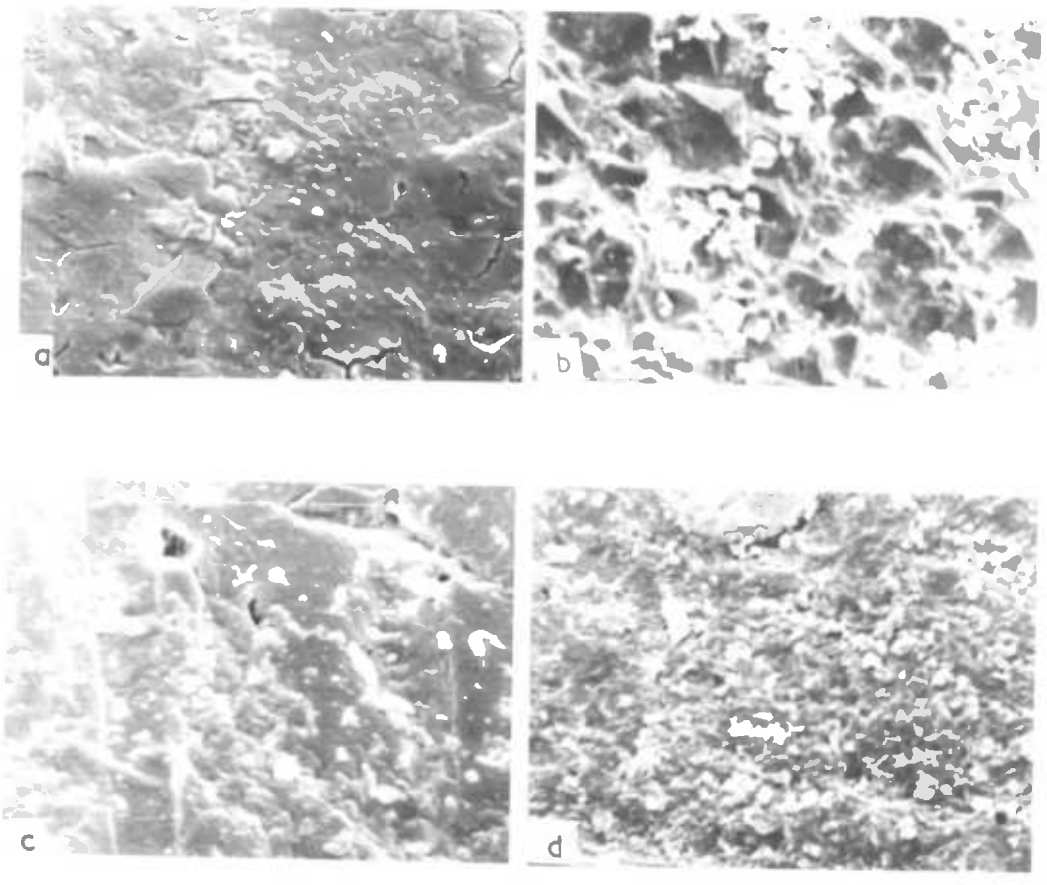

Surface profiles of the different electrodeposits after annealing in argon for 1 hour at 750°C. (x500).

a. Electrodeposited nickel.
b. Ni-Al_2O_3 (0.47 wt. %).
c. Ni-Al_2O_3 (1.06 wt.%).
d. Ni-Al_2O_3 (1.02 wt.%).

PLATE 2

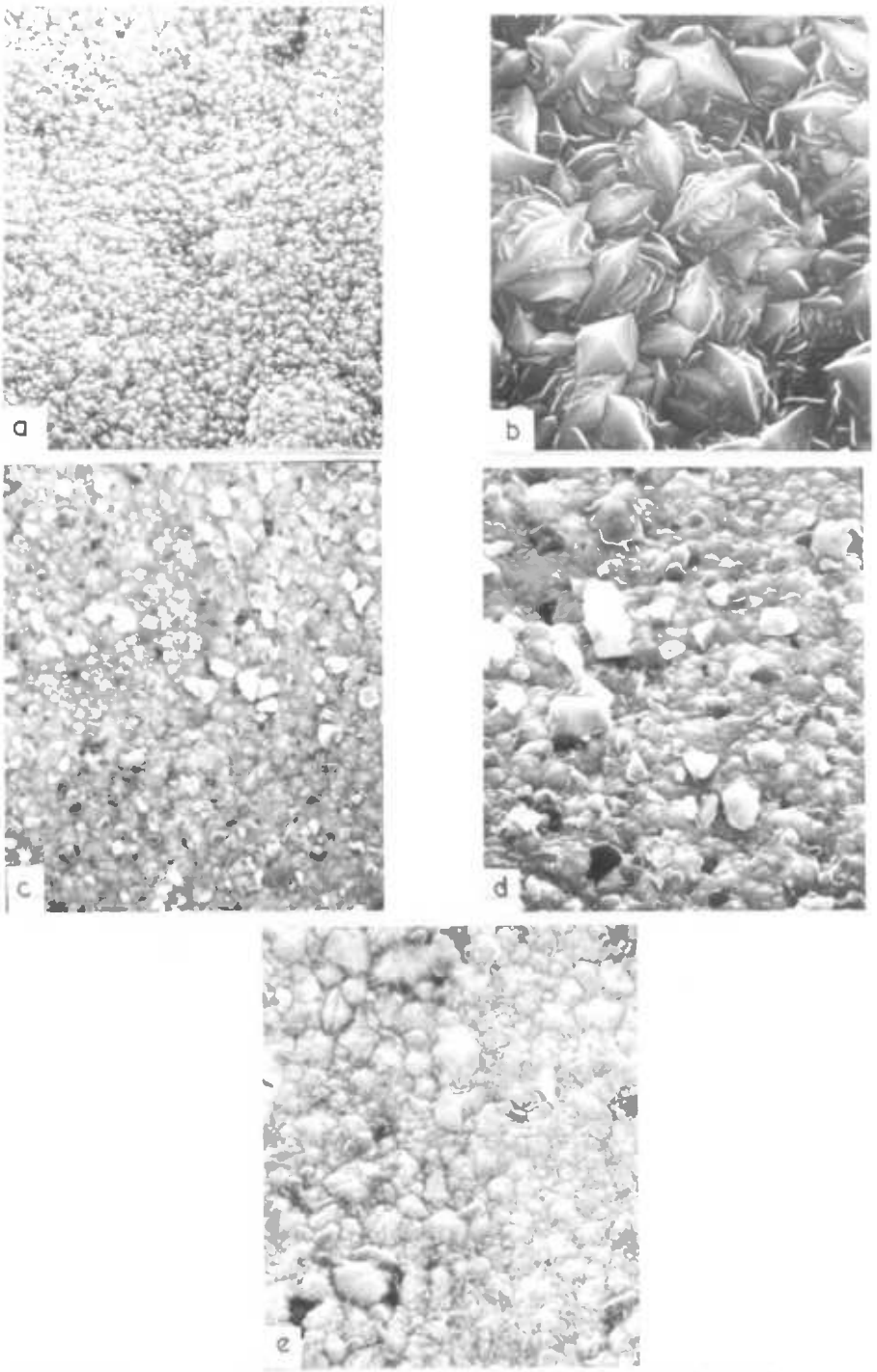

PLATE 3

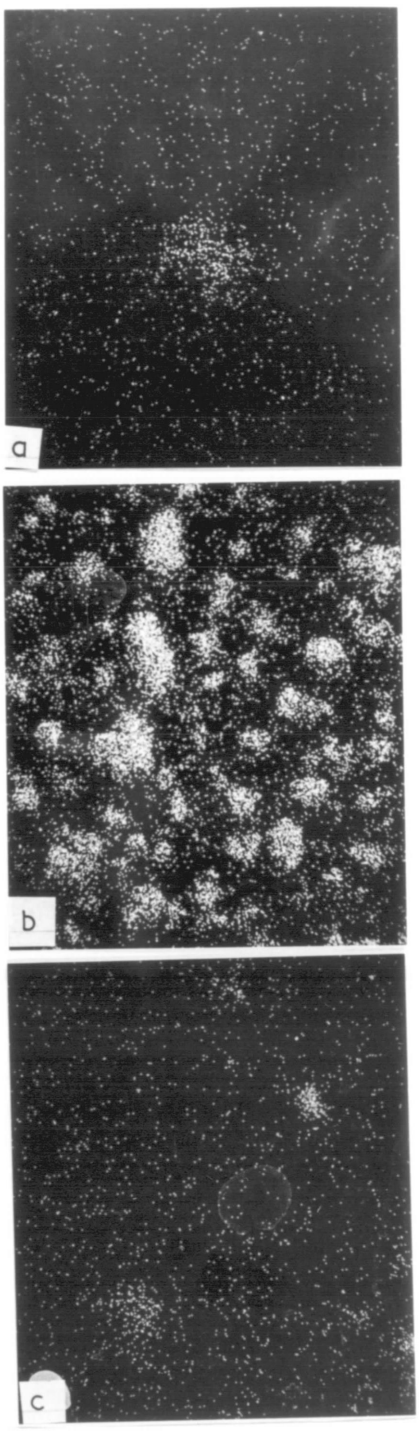

X-ray scanning image of the samples shown in PLATE 3.

a. Distribution of Al, $K\alpha$, x1500.
b. Distribution of Zr, $K\alpha$, x1000.
c. Distribution of Hf, $K\alpha$, x2000.

PLATE 4

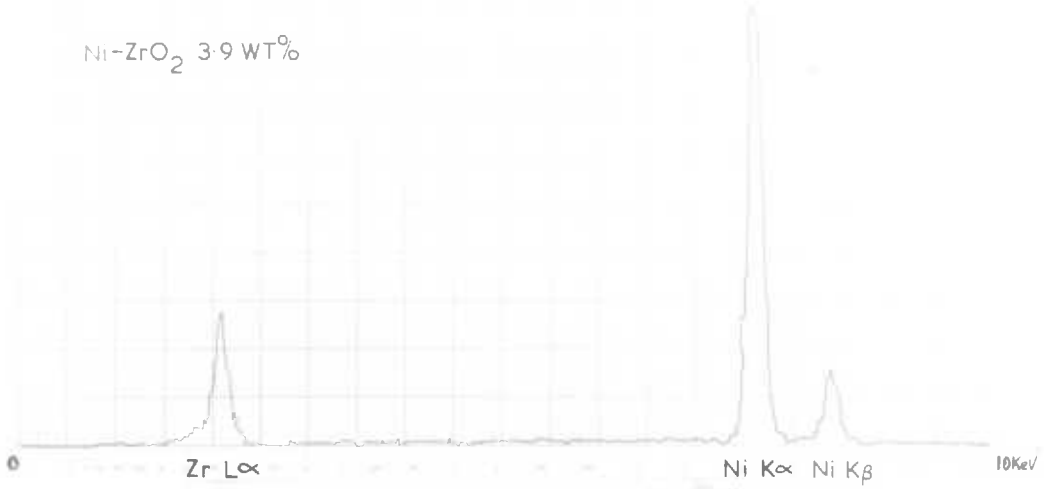

a. X-ray analysis of electrodeposited Ni-ZrO_2 (3.9 wt.%).

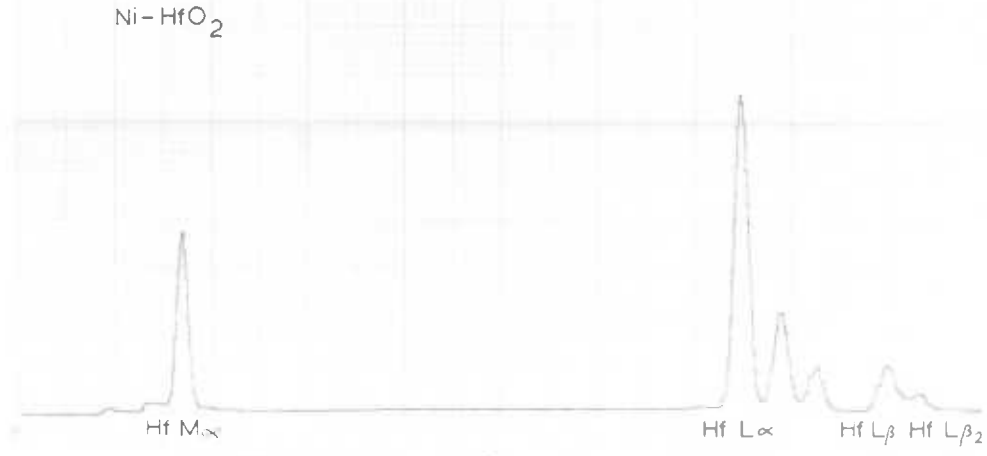

b. X-ray analysis of electrodeposited Ni-HfO_2 (12.5 wt.%).

PLATE 5

TABLE 4 — (see appendix A)

Wt of Al_2O_3, in bath (g/l)	Wt% Al_2O_3 in deposit	Vol % Al_2O_3 in deposit
2	0.47	1.66
4	0.83	2.92
8	1.64	5.74
10	2.02	7.07

TABLE 5

Wt of ZrO_2 in bath (g/l)	Wt % ZrO_2 in deposit	Vol % ZrO_2 in deposit
5	1.19	6.69
10	1.84	10.33
15	3.60	20.16
20	3.92	21.93

TABLE 6

Wt of HfO_2 in bath (g/l)	Wt % HfO_2 in deposit	Vol % HfO_2 in deposit
2	0.28	2.71
6	1.33	12.87
10	2.35	22.78

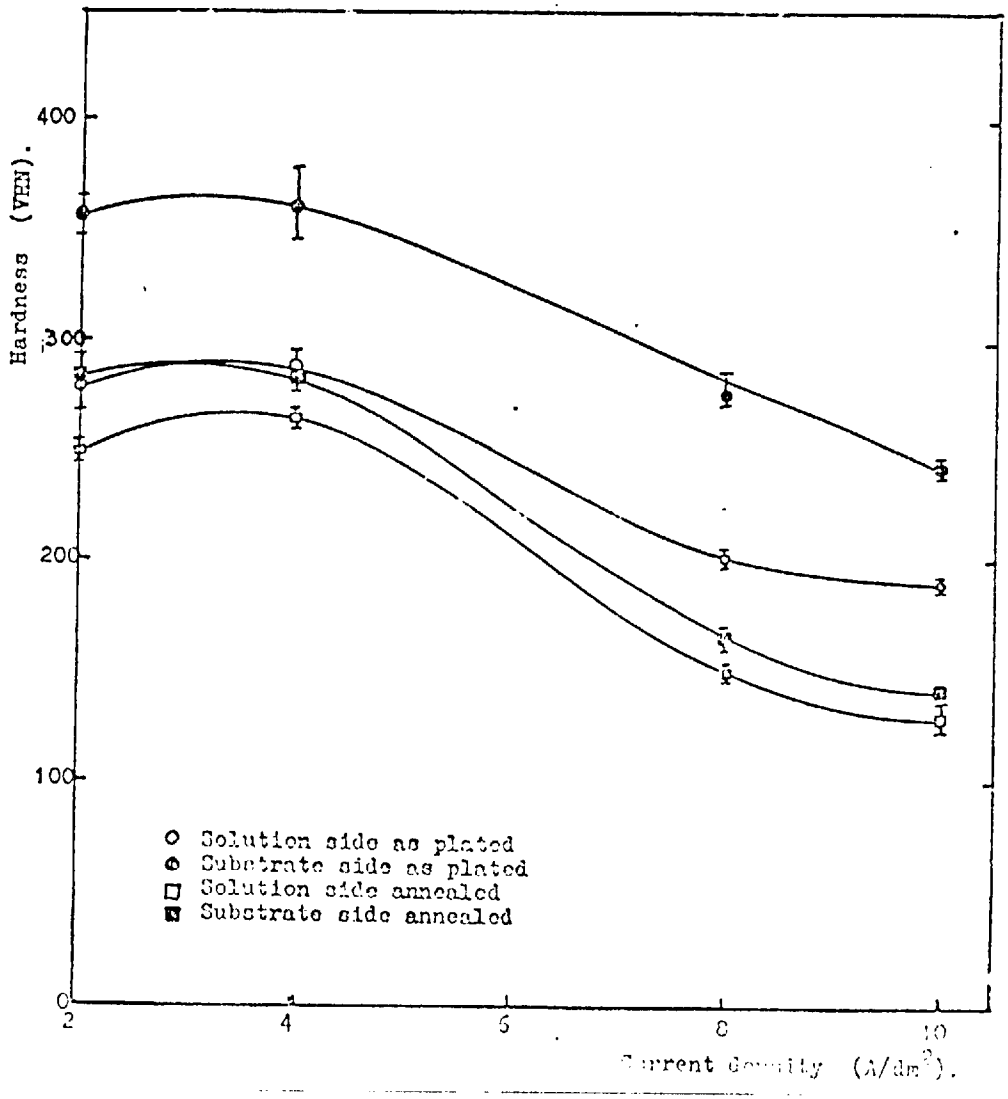

Graph 3. Effect of current density on the hardness of Ni-Al_2O_3 (2.02wt.%) deposit.

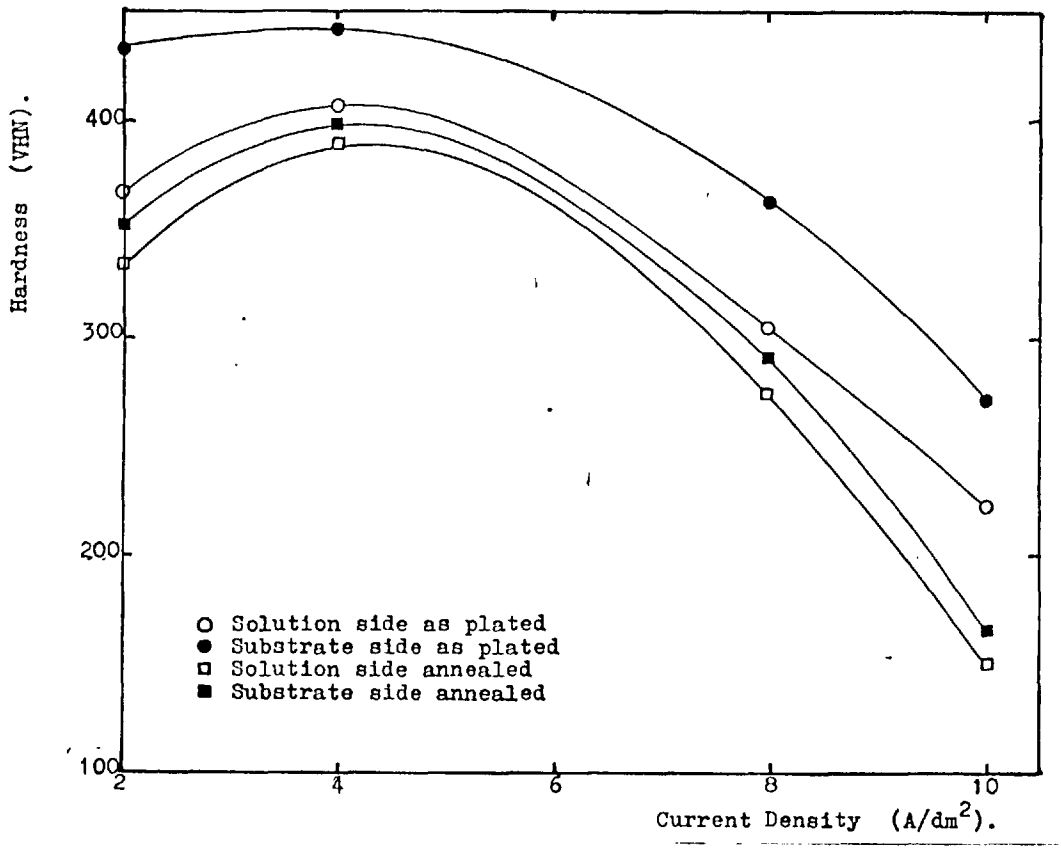

Graph 4. Effect of current density on the hardness of $Ni-ZrO_2$ (3.92 wt.%) deposit.

2. Mechanical properties

Microhardness values for specimens in their as-deposited as well as annealed state at various current densities are given in Graphs 3 and 4, and Tables 7 and 8 show the comparison of the effect of various oxides on the hardness of Ni. The highest average microhardness was obtained at a current density of $4A/dm^2$ for the $Ni-Al_2O_3$ and $Ni-ZrO_2$ specimens. In general, the hardness values decreased as the current density increased, ranging from 277.3 to 179.3 VHN for $Ni-Al_2O_3$ (2 A/dm^2 to 10 A/dm^2, 10 g/l alumina) and 365.8 to 225.3 VHN for $Ni-ZrO_2$ (2-10 A/dm^2, 20 g/l Zirconia).

As can be seen from Graphs 5 and 6, the concentration of the different oxide particles in the electrolytes or the volume percentages of the oxides, influence the hardness of the respective deposits. Hardness increases as the concentration of the oxides increases in the electrolyte, Tables 9 and 10. Similarly, yield strengths also increase with the amount of oxide in the deposit, as shown in Graphs 5 and 6. The yield strength of deposits (25.4 mm x 6.3 mm), 80-120 μm thick, determined after 1 hour anneal at 750°C were 9.4 Kg/mm^2 for Ni; 52.3 Kg/mm^2 for $Ni-Al_2O_3$ (2 A/dm^2, 10 g/l alumina); and 60.4 Kg/mm^2 for $Ni-ZrO_2$ (4 A/dm^2, 20 g/l zirconia). Generally, microhardness and yield strengths of the various nickel cermets decrease on annealing. The decrease is, however, small for $Ni-ZrO_2$ specimens as

compared with Ni-Al_2O_3 deposits. The yield strength values for electrodeposited nickel and nickel composites are shown in Tables 11 and 12. It is seen that the hardness values for the solution side of nickel and nickel composites is much lower than that recorded for the substrate sides.

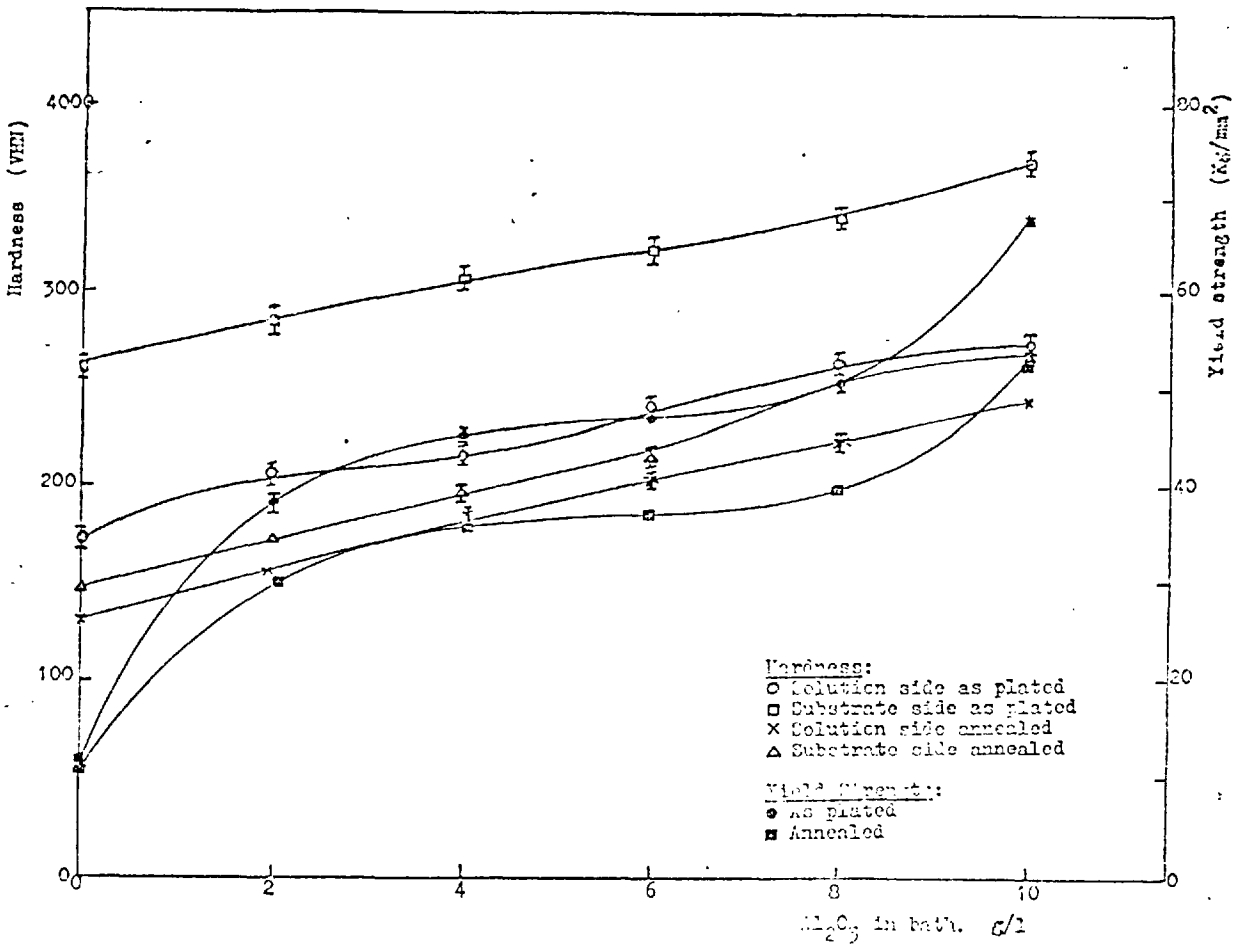

Graph 5. Hardness and yield strength vs concentration of Al_2O_3 particles in electrolyte.

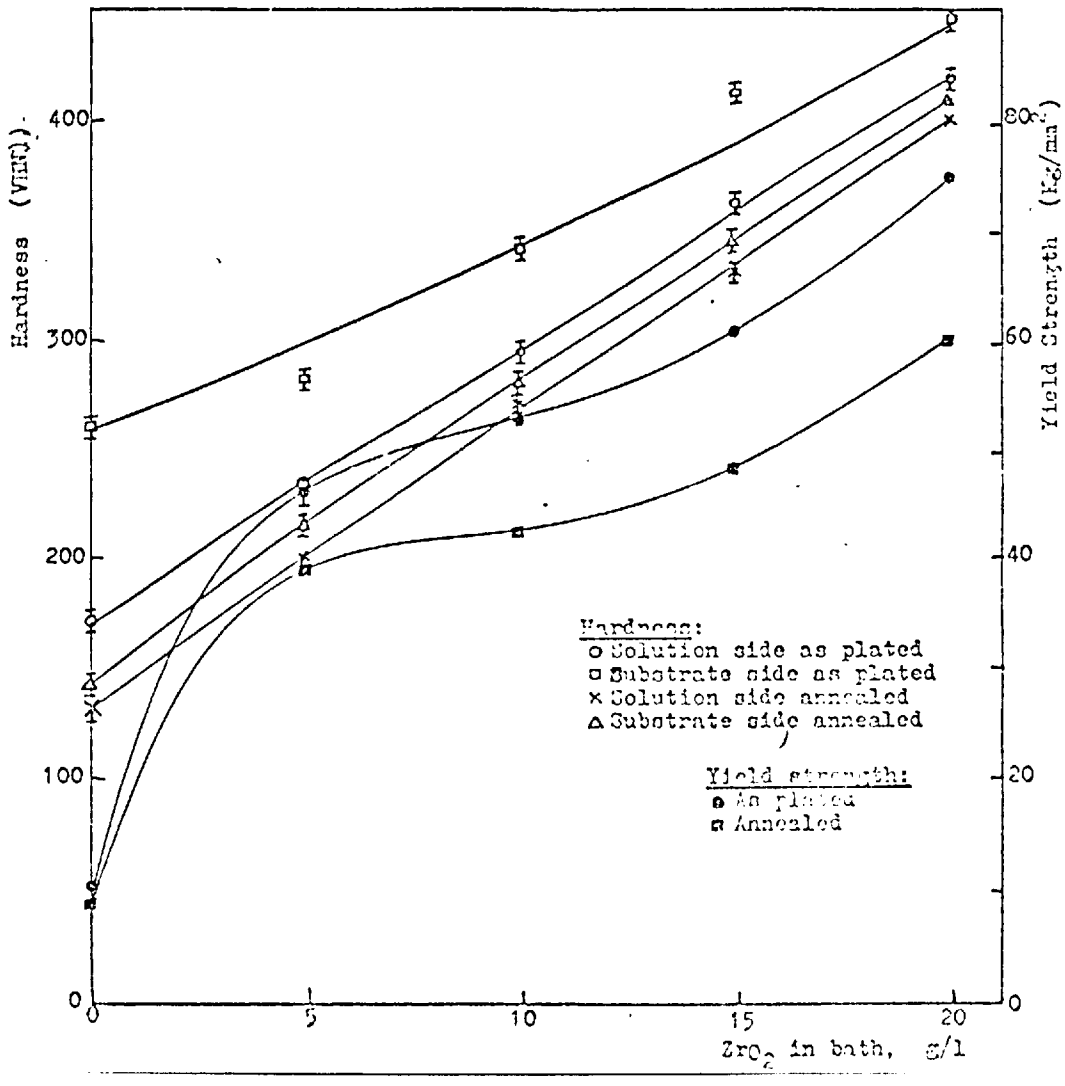

Graph 6. Hardness and yield strength vs. concentration of ZrO_2 particles in electrolyte.

TABLE 7. Hardness Measurements Vs Current Density

Electrolyte : Watts type nickel + 10g/l Al_2O_3 (0.05 μm)

Annealing conditions: Argon atmosphere 1h at 750°C

*Data for plated nickel only. Others are for the Ni-Al_2O_3 cermet (%Al_2O_3 in deposits(2.02 wt %))

Current Density (Amps/dm^2)	Condition	HARDNESS (VHN) Solution Side	Substrate Side
2* (NI - Plate only)	as plated	174.7	258.2
	annealed	130.9	148.4
2	as plated	277.3	358.2
	annealed	249.6	271.8
4	as plated	288.8	363.4
	annealed	263.9	279.0
8	as plated	200	275.6
	annealed	148.8	166.3
10	as plated	179.3	244.5
	annealed	128.3	140.7

TABLE 8. Hardness Measurements Vs Current Density

Electrolyte : Watts type nickel + 20 g/l ZrO_2 (0.1 μm)

Annealing conditions : Argon atmosphere 1 h at 750°C

Current Density (Amps/dm^2)	Condition	HARDNESS (VHN) Solution Side	Substrate Side
2	as plated	365.8	430.5
	annealed	330.8	350.4
4	as plated	405.6	440.8
	annealed	390.2	395.3
8	as plated	308.2	360.4
	annealed	375.0	394.5
10	as plated	225.3	274.5
	annealed	150.2	165.7

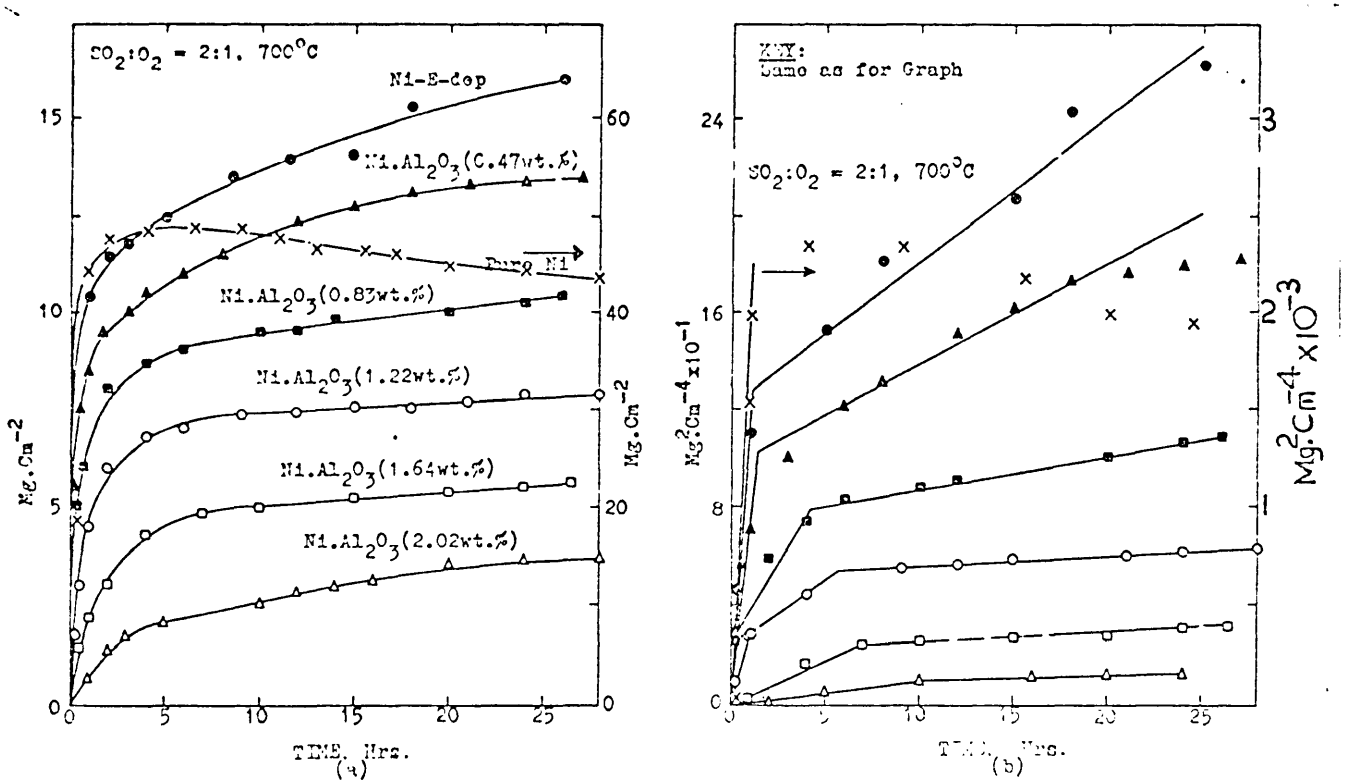

Graph 7. Corrosion kinetics of nickel and Ni-cermets.

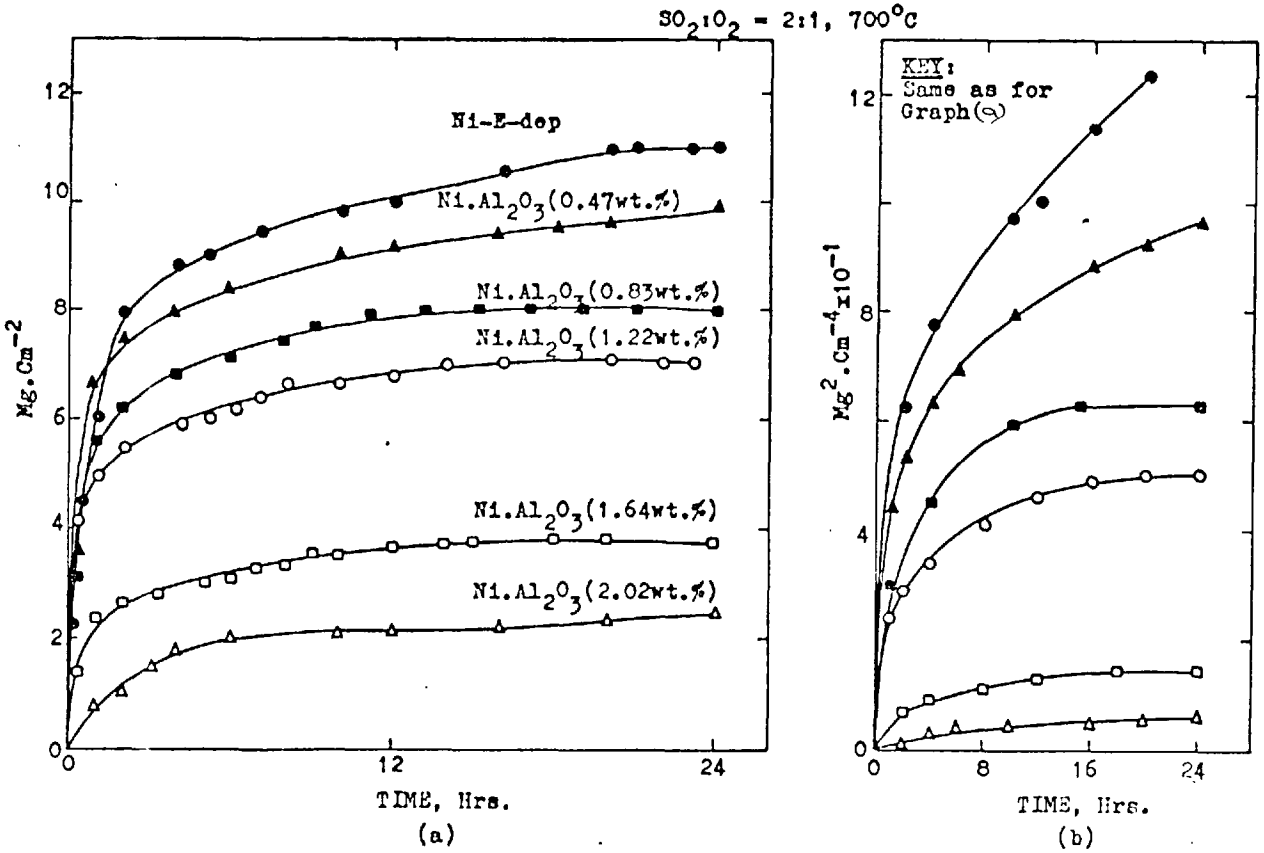

Graph 8. Corrosion kinetics of nickel and Ni-cermets (after annealing for 1 hour at 750°C).

TABLE 9. Micro-Hardness Measurements for $Ni-Al_2O_3$ Deposits

Conditions of plating : Electrolyte : Watts type
Current density 2 A/dm^2 Temp 50°C
Air agitation 1.4 Kg/mm^2

Annealing conditions : Argon atmosphere 1 hr at 750°C.

Concentration of Al_2O_3 in electrolyte (g/l)	VHN as plated		VHN annealed	
	Solution side	Substrate side	Solution side	Substrate side
0	170.8	260.6	130.9	146.9
2	205.0	280.9	157.2	173.0
4	211.7	307.6	186.7	196.3
6	238.4	322.1	203.8	212.9
8	258.1	337.2	224.4	261.7
10	275.4	364.3	247.0	269.0

TABLE 10 Micro-Hardness Measurements for $Ni-ZrO_2$ Deposits

Conditions of plating : Electrolyte : Watts type
Current density 4 A/dm^2 Temp 50°C
Air agitation 1.4 kg/mm^2

Annealing conditions : Argon atmosphere 1hr at 750°C.

Concentration of ZrO_2 in electrolyte (g/l)	VHN as plated		VHN annealed	
	Solution side	Substrate side	Solution side	Substrate side
0	170.6	259.8	130.6	146.2
5	235.6	282.6	204.2	219.7
10	298.3	340.2	270.4	280.8
15	362.8	410.6	334.5	349.6
20	420.4	448.2	408.3	412.6

TABLE II Hardness and Yield Strength Measurements

Conditions of Plating : Electrolyte : Watts type + 10 g/l Al_2O_3 (0.05 μm)
Thickness of Substrate : 0.244 mm. Current Density 2 A/dm^2. Temperature . 50°C.
pH 4.0 - 4.4. Air Agitation : 1.4 kg/cm^2.
Substrate : Passivated brass sheet 50.8 mm x 25.4 mm
Annealing Conditions: Argon atmosphere 1 h at 750°C

Al_2O_3 in electrolyte, g/l	Condition	Hardness (VHN)		Yield Strength (Kg/mm^2)	
		Solution side	Substrate side	As plated	Annealed
0	as plated	170.8	260.6	11.2	9.6
	annealed	130.9	146.9	11.8	9.2
2	as plated	205	280.9	38.2	30.2
	annealed	157.2	173.0	38.6	30.4
4	as plated	211.7	307.6	45.6	35.2
	annealed	186.7	196.3	45.3	36.3
6	as plated	238.4	322.1	47.2	36.8
	annealed	203.8	212.9	47.1	37.1
8	as plated	258.1	337.2	50.8	38.4
	annealed	224.4	261.7	50.2	40.2
10	as plated	275.4	364.3	68.4	52.6
	annealed	247.9	269.0	67.2	52.1

TABLE 12. Yield Strength Measurements for Ni-ZrO_2 Deposits

Conditions of plating : Electrolyte : Watts type
Current density 4 A/dm^2, Temp 50°C
Air agitation 1.4 Kg/mm^2

Concentration of ZrO_2 in electrolyte $(g/l)^2$	Yield Strength Kg/mm^2 As plated	Annealed
0	11.0	9.2
	11.4	9.8
5	46.8	39.6
	46.4	39.8
10	52.6	42.6
	52.8	42.7
15	61.2	48.4
	61.5	48.7
20	75.2	60.8
	75.3	60.1

J Gas Phase Studies

1. Corrosion kinetics in SO_2/O_2 = 2:1 at 700°C

1.1 Nickel and nickel + ceramic coatings

A comparison of the corrision behaviour of various Al_2O_3 - containing nickel electrodeposits in SO_2 : O_2 = 2:1 is given in Graph 7. The curves were fairly reproducible although the times at which sudden changes in corrosion rates occurred varied from run to run. Even though specimens of $Ni.Al_2O_3$ (0.47 and 0.87 wt%) initially gained more weight than electrodeposited nickel and Pure Ni, their overall weight gains were below that observed for both nickel specimens. Increasing the amount of Al_2O_3 dispersoid resulted in a decreased weight gain. The coatings oxidised rapidly initially but after approximately 2 hrs the rate decreased abruptly and the weight of each specimen thereafter remaining more or less constant. After the initial period during which the reaction proceeds at a higher rate, parabolic oxide growth was observed for all the $Ni-Al_2O_3$ specimens. Each of the specimens exhibited two parabolas, the first one originating from approximately zero time and the second setting in after a certain critical time with a lower slope than the first.

It can be seen from Graphs 7 and 8 that on corrosion in SO_2/O_2 environment, the nickel-alumina composites show a substantially low weight gain compared to pure nickel

deposits, in the as-deposited condition and after subsequent annealing for 1 hour at 750°C. Plots of weight increase squared versus time for the annealed specimens showed a deviation from a single parabolic scaling rate similar to that exhibited by the as-deposited specimens. The obvious correlation between alumina content and sulphidation rates can be seen. A sudden reduction in the sulphidation kinetics is shown by the 1.64 wt% and 2.02 wt% Ni.Al_2O_3 specimens. In general, the rates of sulphidation of the heat-treated specimens are significantly slower, by an order of magnitude, than those of the as-plated specimens. The parabolic rate constants achieved under various conditions are listed in Table 13.

The presence of ZrO_2 dispersoid in nickel matrix gave rise to weight gains which were comparable to those observed for Al_2O_3 - containing nickel but slightly higher. Once again, lowering the amount of ZrO_2 dispersoid resulted in an increased weight gain, as illustrated in Graph 9. The variation in performance with dispersoid level in the nickel matrix can be seen. It is evident therefore that a small amount of dispersoid (e.g. less than 0.3 per cent) improves the sulphidation resistance of the nickel matrix. The Ni-ZrO_2 specimens show a two-stage parabolic relationship similar to that exhibited by Ni-Al_2O_3 composites.

Comparative weight changes at 700°C for the as-plated and annealed 2.02 wt % $Ni.Al_2O_3$, 3.92 wt % ZrO_2 and 2.35 wt % HfO_2 specimens are presented in Graph 10. The sulphidation kinetics shows a trend $Ni\text{-}ZrO_2 > Ni.Al_2O_3 > Ni.HfO_2$, The weight gains of both the as-plated and annealed specimens of the $Ni\text{-}ZrO_2$ specimens were considerably higher than those for $Ni\text{-}Al_2O_3$ and $Ni\text{-}HfO_2$ specimens. The kinetics of sulphidation of a number of nickel-cermets at 700°C together with results from pure, and electro-deposited nickel are shown in Graph 11. The specimens of nickel-cermets were selected from those containing the highest dispersoid contents. It is apparent that the rate curves for the nickel-cermets show a characteristic difference in shape and occupy a band of weight gains ranging from 2 to 5 mg/cm^2.

TABLE 13 Parabolic Rate Constants for the Corrosion of Electrodeposited Cermets at 700°C

	SO_2/O_2 = 2 : 1		Na_2SO_4 Coated		Na_2SO_4 + NaCl Coated	
	Time (h)	Kp($mg^2/cm^4/h$)	Time (h)	Kp($mg^2/cm^4/h$)	Time (h)	Kp($mg^2/cm^4/h$)
Ni-electrodeposit	0-5	12.5	0-1	17.24		
			10.20	1.50		
$Ni-Al_2O_3$ (2.02 wt%)	0-8	11.7	0-1	40.0	0-2	127.5
	8-20	2.92	6-24	2.9	5-24	25.0
$Ni-ZrO_2$ (3.92 wt%)	0-3	6.670	0-1	64.30	0-20	80.0
	4-28	0.678	6-24	1.25	12-40	2.0
$Ni-HfO_2$ (2.35 wt %)	0-2	2.400	0-1	7.70	0-3	9.71
	4 20	0.146	6-24	0.44	12-40	0.55

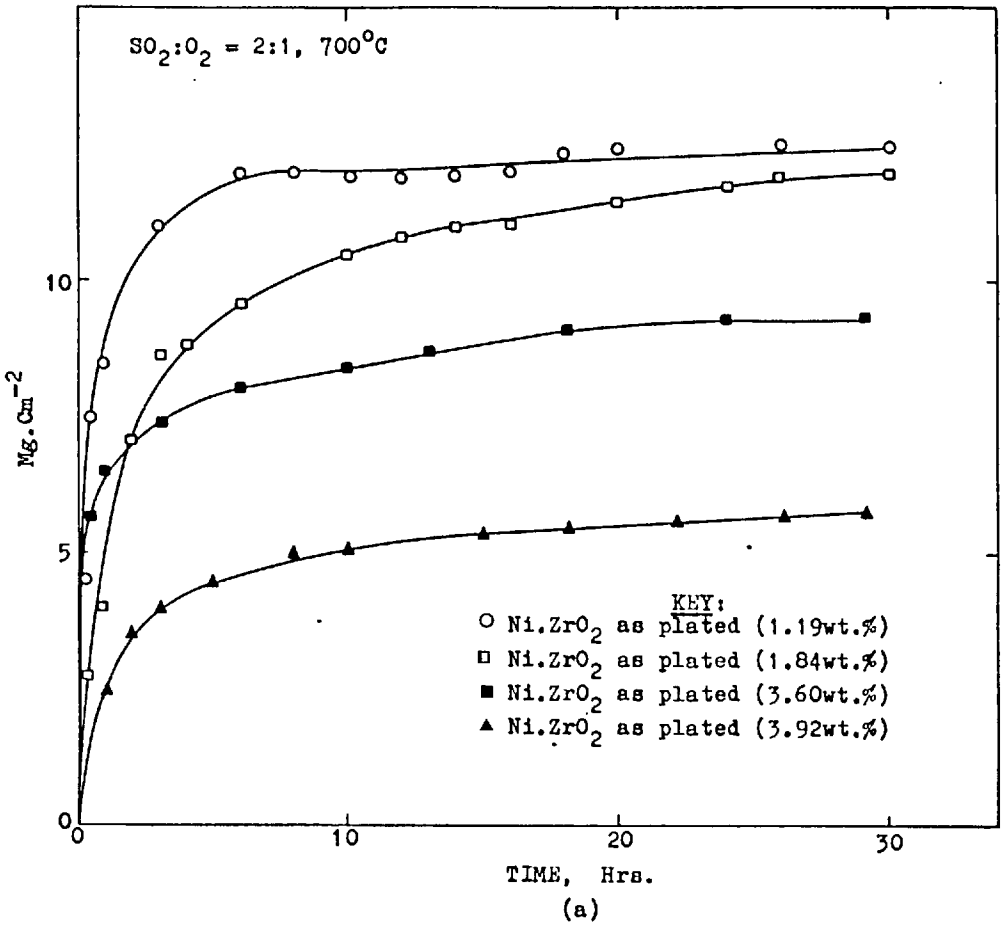

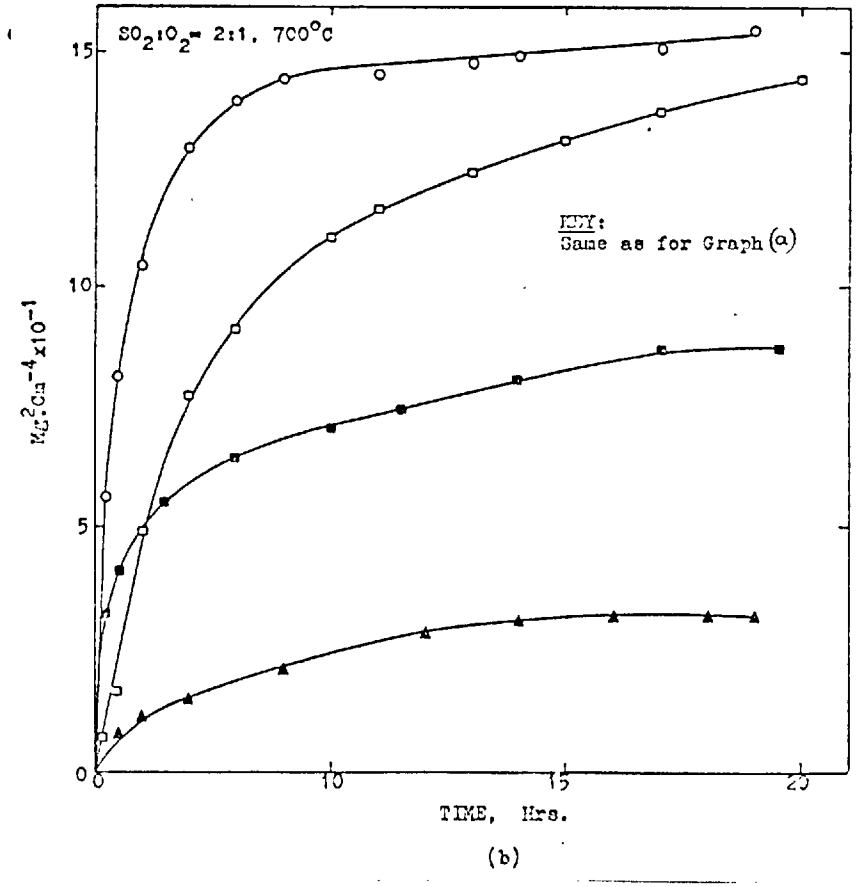

Graph 9. Corrosion kinetics of Ni.ZrO_2 (as plated) deposits with various ZrO_2 contents.

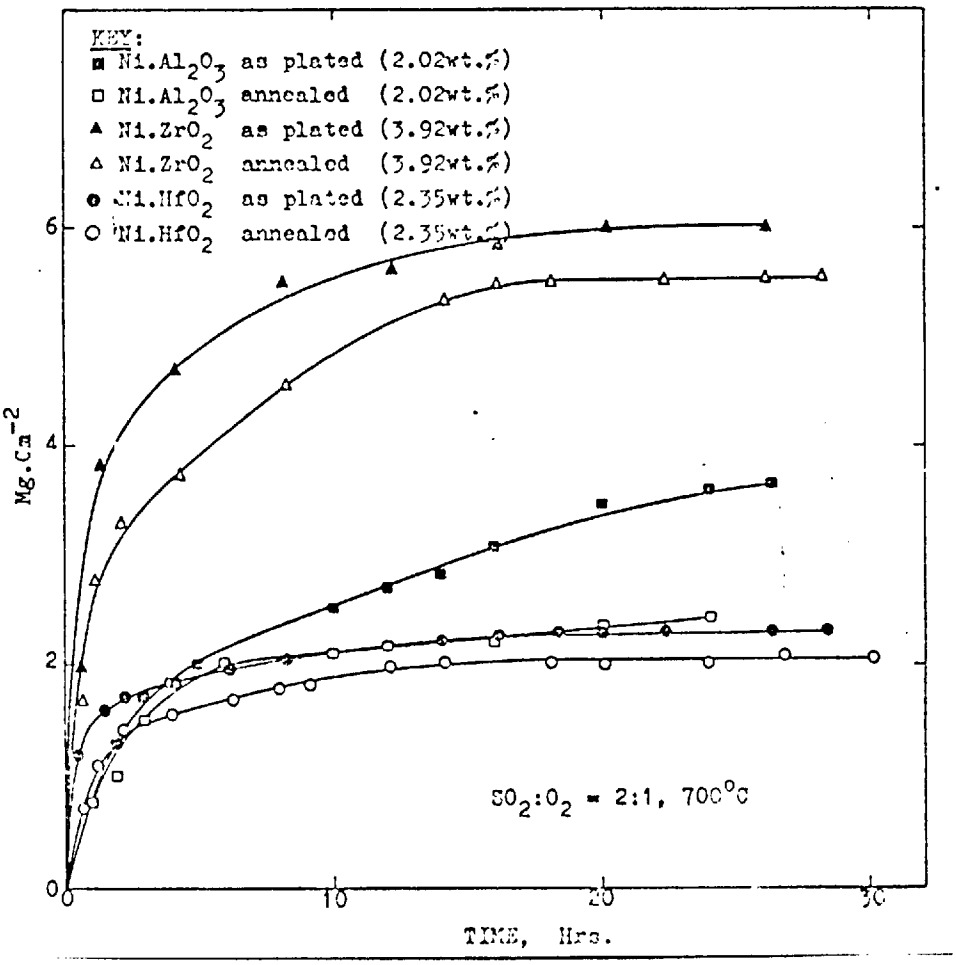

Graph 10. Corrosion kinetics of Ni-cermets before and after annealing for 1 hour at 750°C.

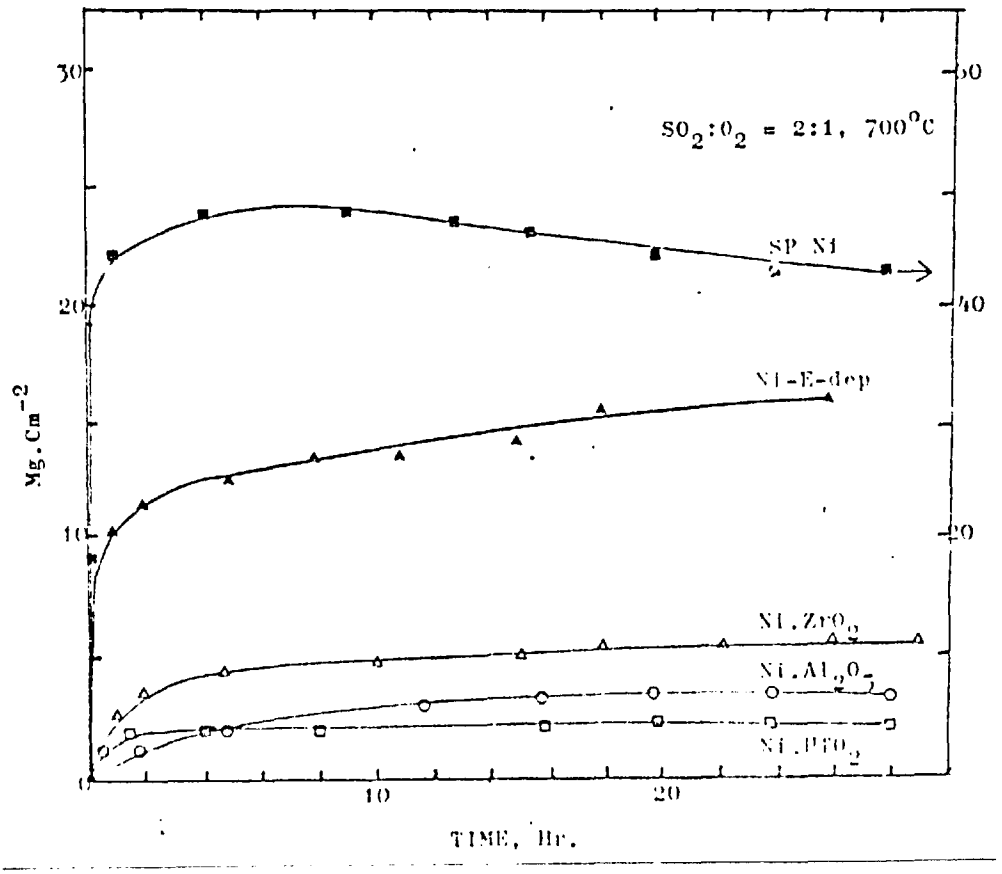

Graph 11. Corrosion Kinetics of nickel & Ni-cermets.

a. Electrodeposited Nickel. 700°C, $SO_2:O_2::2:1$, 28 hrs.. TEMSCAN (x300): Heavy modular growth. with lighter area rich in S.

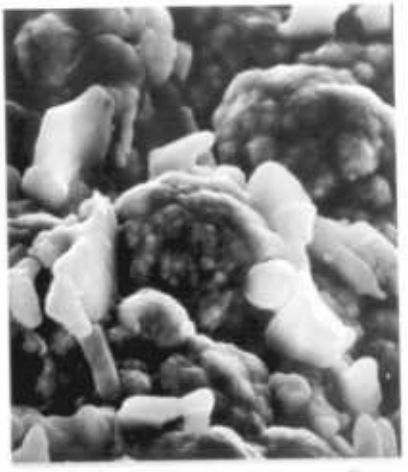

b. Enlargement of similar area as in (a). TEMSCAN(x800).

c. X-ray scanning image of (b); showing the distribution of S, K_{α}.

d. X-ray scanning image of (b); showing the distribution of Ni, K_{α}.

PLATE 6

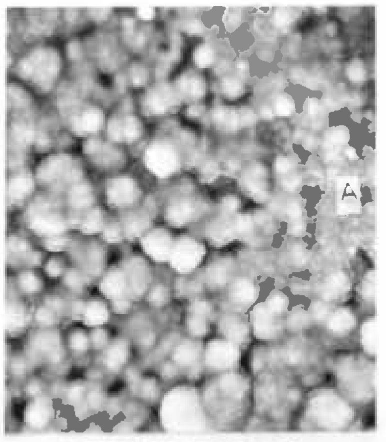

a. Electrodeposited Ni-ZrO_2 (3.92 wt.%), 700°C, SO_2:O_2:: 2:1, 20 hrs., TEMSCAN(x300); Overall structure of corroded surface.

b. Close view of A, (x2000).

c. Enlargement of similar area as in (a). (x500).

d. X-ray scanning image of (c), showing the distribution of Zr, Kα.

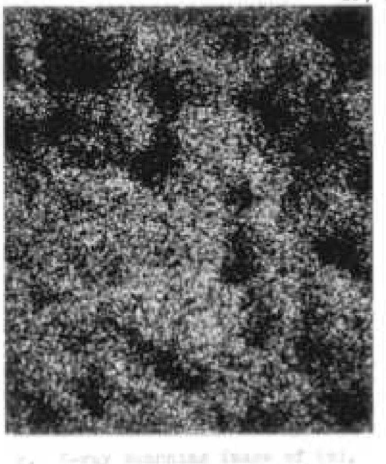

e. X-ray scanning image of (c), showing the distribution of [illegible] Kα.

PLATE 7

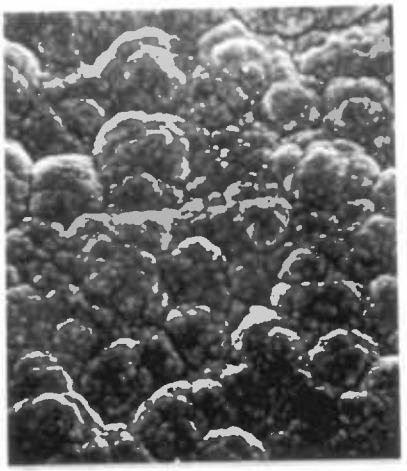

a. Electrodeposited Ni-HfO_2 (2.35 wt.%), 700°C, SO_2:O_2:: 2:1, 28 hrs., TEMSCAN(x300): Heavy modular growth.

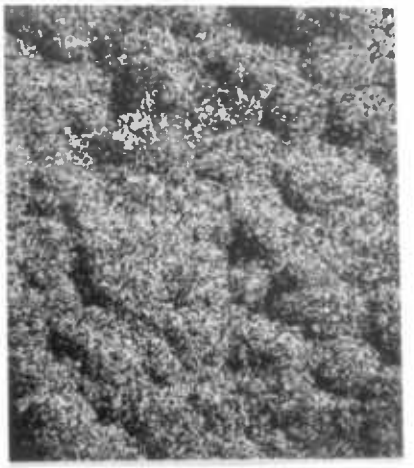

b. X-ray scanning image of (a), showing the distribution of S. K_{α}.

c. X-ray scanning image of (a), showing the distribution of Hf. K_{α}.

d. X-ray scanning image of (a), showing the distribution of Ni. K_{α}.

PLATE 8

1.1.1. Surface topography and structure.

The appearance of the surface oxide formed on electrodeposited nickel after 28 hr at 700°C is shown in Plate 6. The bulk of the surface is dark grey in colour, heavily nodular, with a network of white-appearing oxide, which is rich in sulphur, X-ray mappings show that the nodules consist of a mixture of NiO and Ni_3S_2.

The topography of the dull black scales on Ni-ZrO_2 (3.92 wt %) after sulphidation at 700°C (Plate 7a) shows the presence of pores. Also, from the X-ray scans the ZrO_2 particles are more finely dispersed than as shown in the as-plated specimen (Plate 4b).

The results for a similarly exposed specimen of Ni-HfO_2 (2.35 wt%) is shown in Plate 8. The corroded surface is dull black and nodular, and X-ray mapping (Plate 8b) shows that the oxide scale is heavily sulphated.

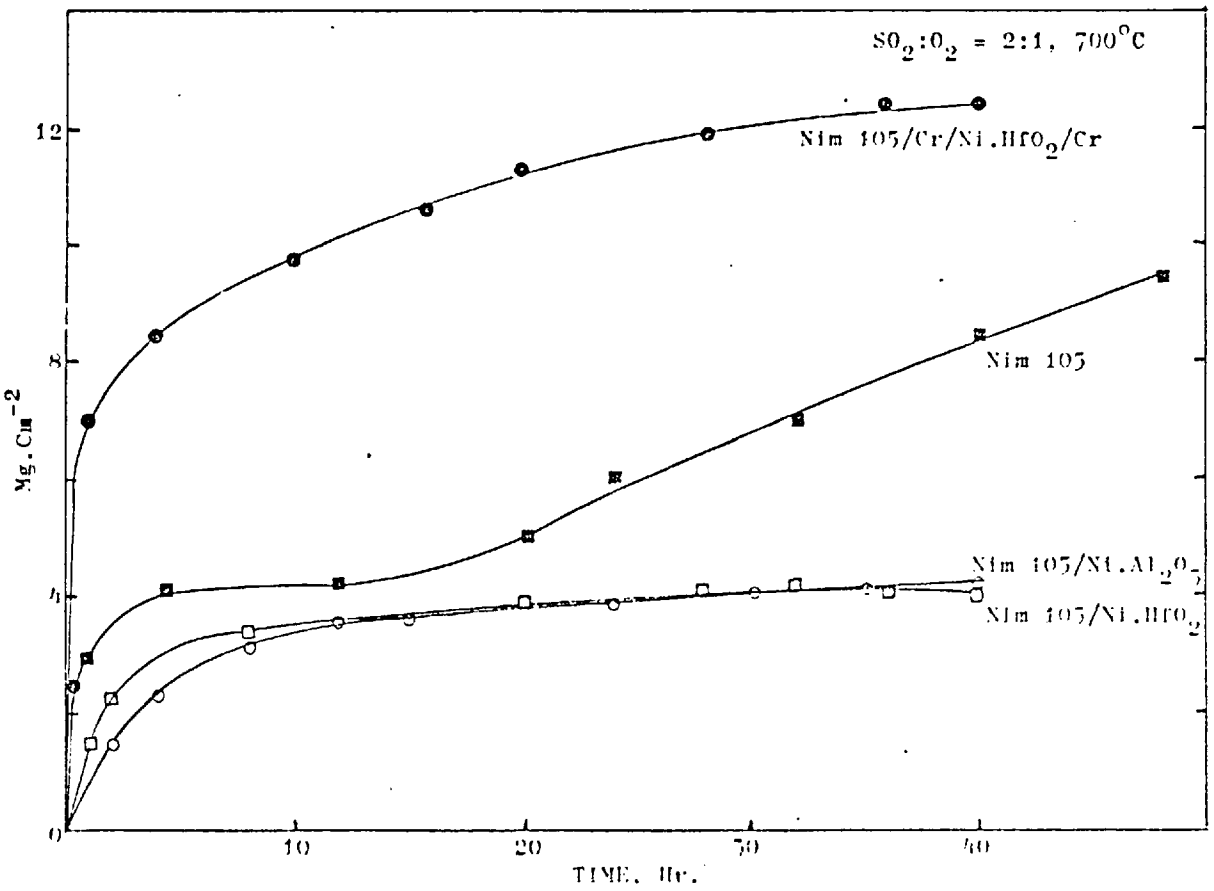

Graph 12. Corrosion kinetics of Nimonic 105 and cermet-coated Nimonic 105.

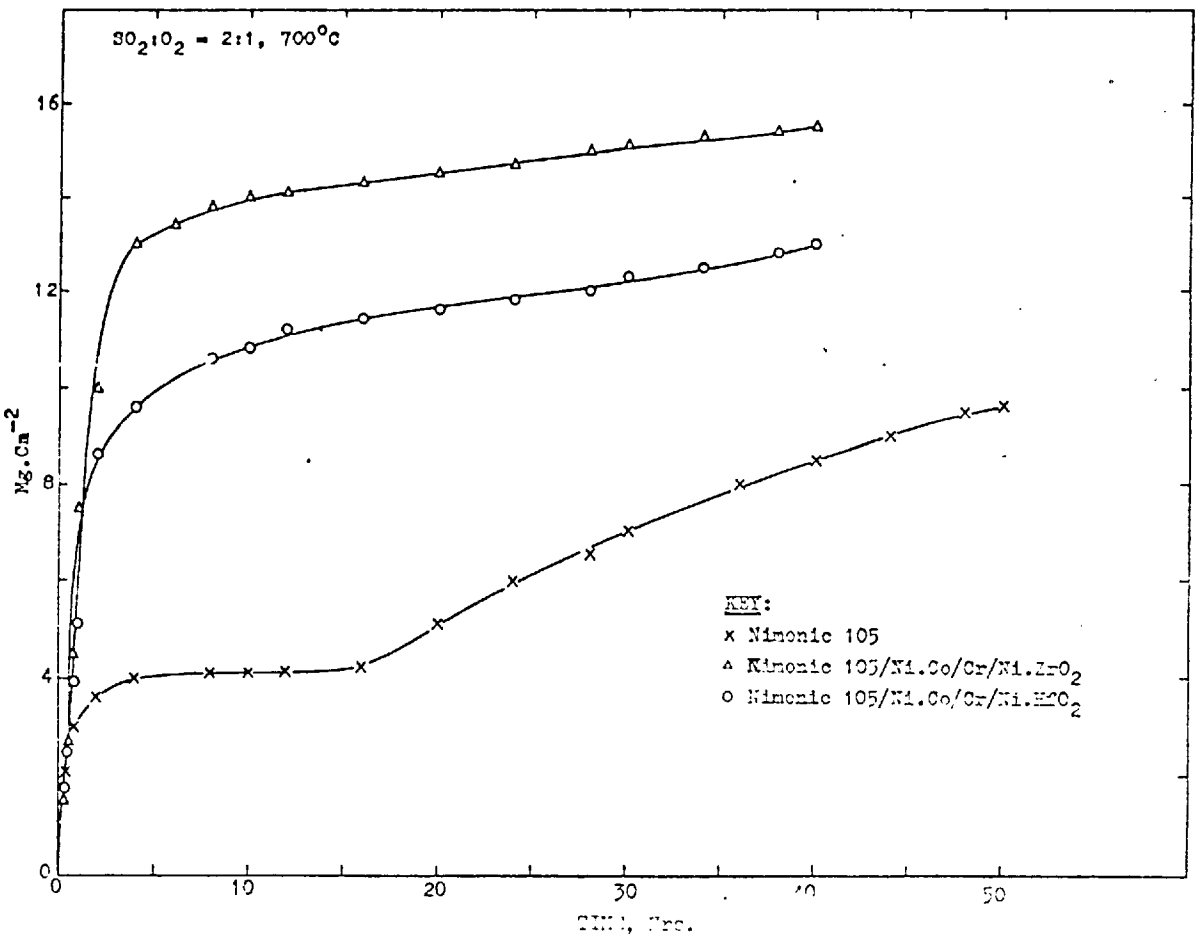

Graph 13. Corrosion kinetics of Nimonic 105 and cermet-coated Nimonic 105.

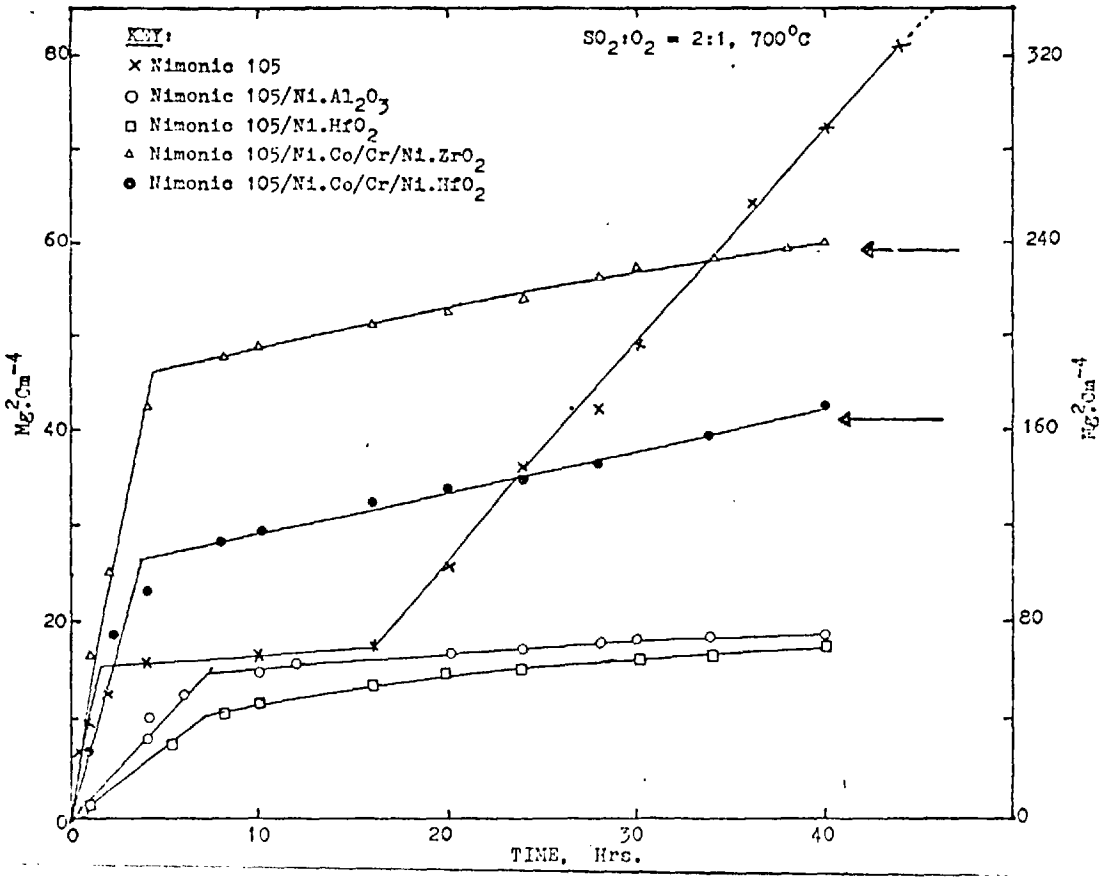

Graph 14. Corrosion kinetics of Nimonic 105 and cermet-coated Nimonic 105.

1.2. Nickel base superalloys - cermet coated.

The corrosion rates of nickel base superalloys, Nimonic 105 and IN 738 at 700°C, as well as that of the alloys coated with various electrodeposited cermets are plotted in Graphs 12-14 and 15-18 respectively. It is seen (Graphs 12 and 14) that the Nimonic 105 corroded relatively faster than alloys electrodeposited with $Ni.Al_2O_3$ and $Ni.HfO_2$. The overall weight increases shown by these other materials were approximately similar to each other, although the Nimonic 105/$Ni.HfO_2$ alloy corroded relatively rapidly during the first few minutes, the rate of weight increases again fell to a relatively low value. The Nimonic 105 alloy showed very irregular behaviour since the initial, substantially rapid rate of corrosion was followed by a period of slow corrosion. However, after some time (typically 15 hrs), the rate increased rapidly and the specimen gained weight relatively quickly. The duplex coated Nimonic 105 alloys (Nimonic 105/Ni-Co/Cr/$Ni.HfO_2$, Nimonic 105/Cr/$Ni.HfO_2$/Cr, Nimonic 105/Ni-Co/Cr/$Ni.ZrO_2$, oxidised faster than the other materials, but the rates decreased somewhat after longer periods. Nevertheless, it corroded faster than the Nimonic 105 during these periods. The kinetic curves illustrate the significant differences in corrosion rates of the alloys incorporated with ZrO_2 oxides as compared to those with HfO_2. The alloys with

ZrO_2 oxide coatings showed a considerably higher corrosion rate than those with HfO_2 oxide coatings.

In all cases the corrosion was found to conform well to the parabolic rate relationship (Graph 14). Each of the specimens showed a deviation from a single parabolic scaling rate, as noted by a departure from a straight line relationship in plots of weight increase squared versus time. The Nimonic 105 alloy exhibited three parabolas, but all the cermet-coated Nimonic 105 alloys showed two. The parabolic scaling constants for the various specimens are listed in Table 14.

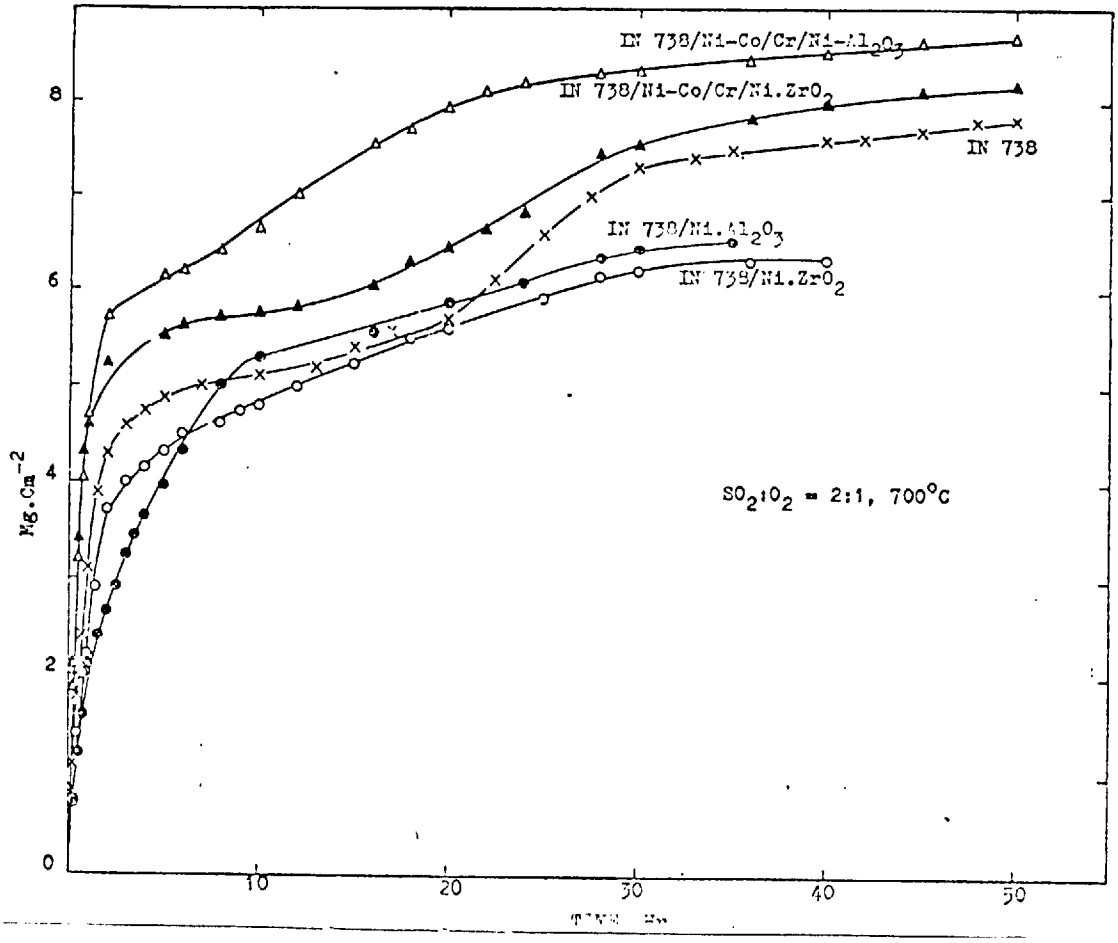

Graph 15. Corrosion kinetics of IN 738 and cermet-coated IN 738

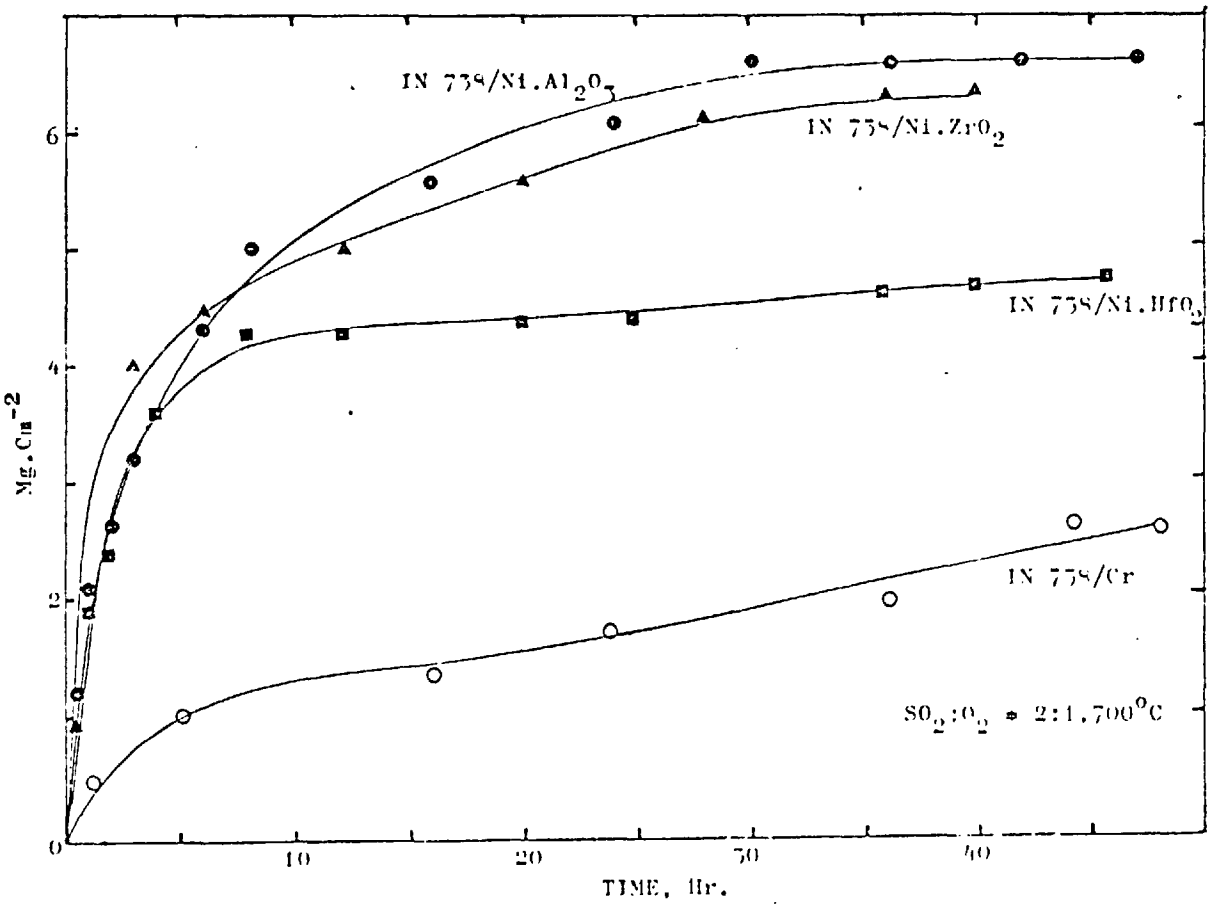

Graph 16. Corrosion kinetics of cermet-coated superalloys.

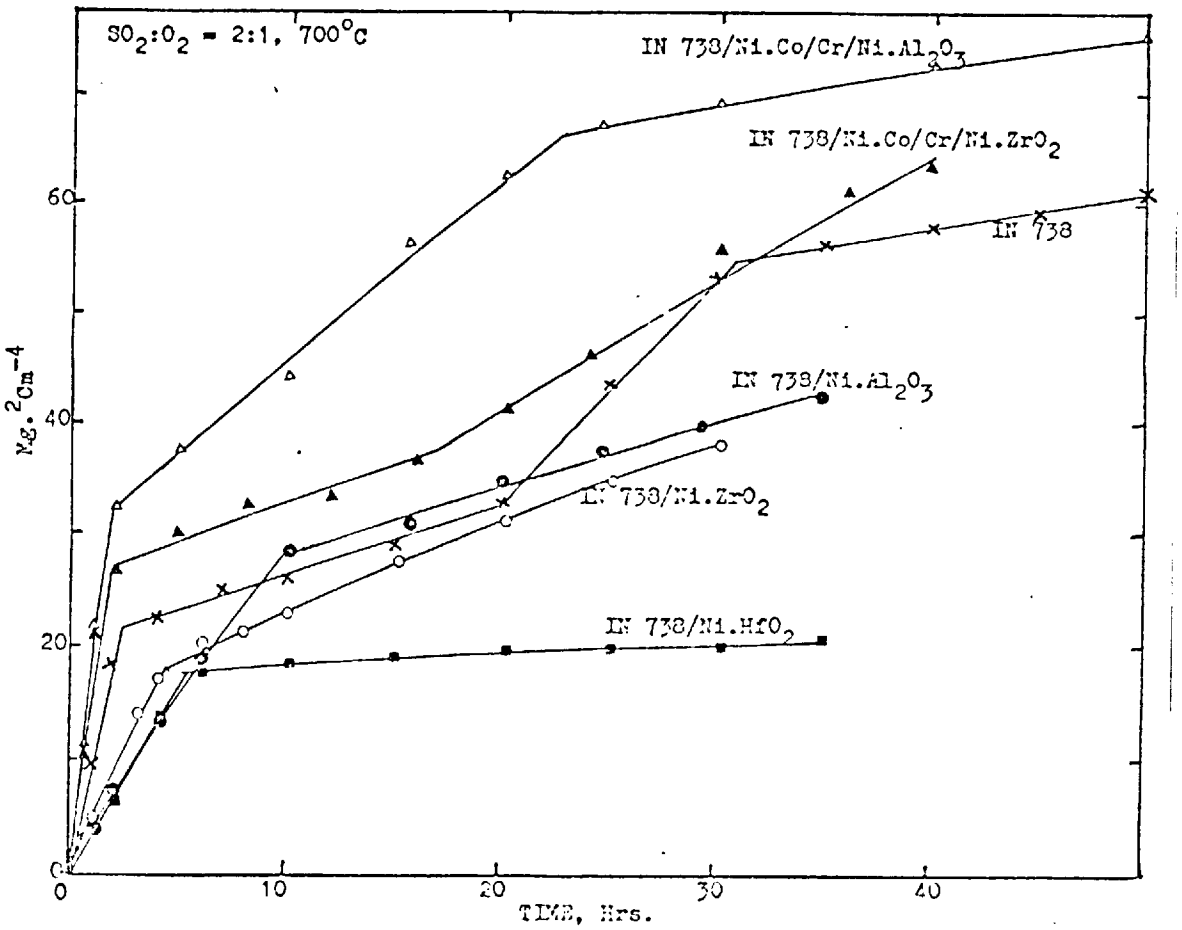

Graph 17. Corrosion kinetics of IN 738 and cermet-coated IN 738.

The kinetic curves for the sulphidation of IN 738 and various electrodeposited composite coatings on IN 738 are shown in Graphs 15-17. The overall weight increases shown by these materials were marginally higher than for those shown by the Nimonic 105 based materials, although significant differences in the shapes of the kinetic curves were apparent. As in the case of Nimonic 105, the corrosion behaviour of IN 738 was very irregular, and as can be seen (Graph 17) the alloy showed a four-fold deviation from a single parabolic scaling rate. The IN 738/Ni. HfO_2 specimen corroded significantly slower than both IN 738/Ni.ZrO_2 and IN 738/Ni.Al_2O_3. In all cases, the corrosion rate was rapid during the first two hours, but the rate decreased somewhat after longer periods. Calculated parabolic rate constants (K_p) are given in Table 15. From this it can be noted that the largest amount of corrosion is experienced by the duplex coated alloys such as IN 738/Ni-Co/Cr/Ni.ZrO_2.

Graph 18 shows the effect of electrodeposited chromium on the corrosion kinetics of Nickel (electrodeposited), nimonic 105 and IN 738 alloys. In this case the minimum effect is with the electrodeposited nickel since the chromium coating on both nimonic 105 and IN 738 further increases their level of chromium (14.6 and 16 wt % respectively), and thus promotes a faster formation of

the more protective Cr_2O_3 scale. However, examination of the specimens after corrosion shows the surface scales to be dark grey in colour, loose and cracked, and predominantly nodular.

TABLE 14. Parabolic Rate Constants of Cermet Coated Nimonic 105 Alloy

Coating	700°C						900°C			
	SO_2/O_2-2:1		Na_2SO_4 Coated		Na_2SO_4+NaCl Coated		SO_2/O_2=2:1		Na_2SO_4+NaCl Coated	
	Time(h)	Kp($mg^2/cm^4/h$)	Time(h)	Kp($mg^2/cm^4/h$)	Time(h)	Kp($mg^2/cm^4/h$)	Time(h)	Kp($mg^2/cm^4/h$)	Time(h)	Kp($mg^2/cm^4/h$
Nil	0-2	10.50	0-2	26.00	0-2	160.0	0-10	0.074	0-6	3.40
	5-15	0.14	5-20	1.09						
	17-50	2.47	23-50	2.96	12.50	0.9	15-45	0.090	12-50	0.34
/Ni.Al_2O_3	0-4				0-3	15.00	0-15	0.066	0-8	0.533
	8-40				8-40	0.55	35-45	0.076	8-18	1.020
/Ni.HfO_2	0-4	2.05			0-25	7.09				
	7-40	0.22			12-35	0.16				
/Ni-Co/Cr/Ni.ZrO_2	0-3	50.0	0-2.5	240	0-3	311				
	8-40	1.6	15-50	11	15-50	13				
/Ni-Co/Cr/Ni.HfO_2	0-3	40.0	0-2	180	0-3	273				
	12-40	1.78	20-50	3	10-40	3.12				

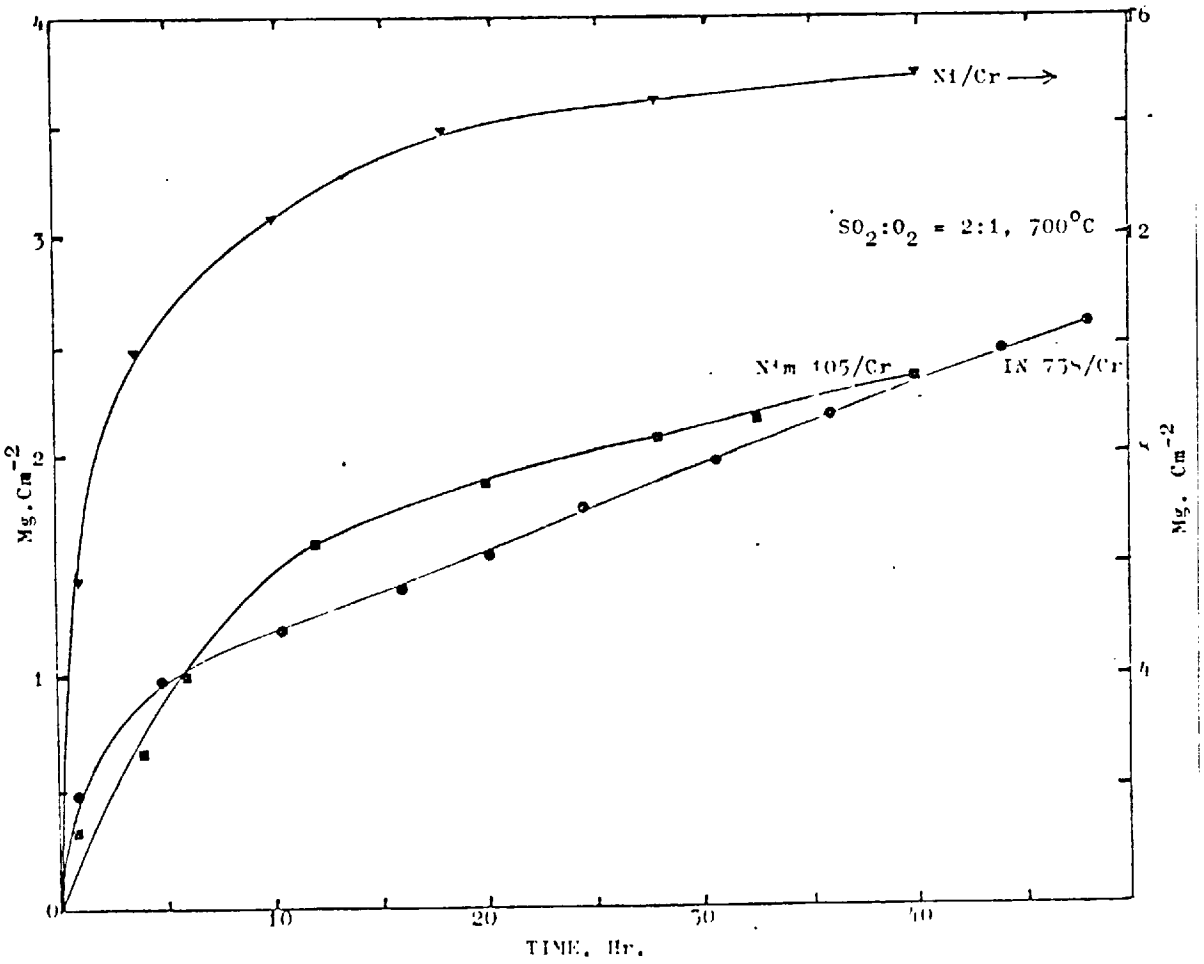

Graph 18. Corrosion Kinetics of chromium-coated superalloys

TABLE 15. Parabolic Rate Constants of Cermet Coated IN 738 Alloy

Coating	700°C						900°C			
	SO_2/O_2=2:1		Na_2SO_4 Coated		Na_2SO_4+NaCl Coated		SO_2/O_2=2:1		Na_2SO_4+NaCl Coated	
	Time(h)	Kp($mg^2/cm^4/h$)	Time(h)	Kp($mg^2/cm^4/h$)	Time(h)	Kp($mg^2/cm^4/h$)	Time(h)	Kp($mg^2/cm^4/h$)	Time(h)	Kp($mg^2/cm^4/h$)
Nil	0-2	9.50	0-2	68	0-4	45	0-30	0.1	0-30	0.75
	5-20	0.56								
	20-30	2.10	5-30	4.5	5-30	23				
	30-50	0.38	30-50	7.5	30-50	8.8	30-50	0.94	30-50	1.47
/Ni.Al_2O_3	0-2	4	0-2	62.5	0-2	35	0-2	0.2	0-2	1.30
							5-20	0.014		
	8-35	0.62	8-27	1.5	10-30	2.1	20-40	0.056	10-28	0.18
/Ni.ZrO_2	0-2	5			0-2	10	0-5	0.045	0-2	1.437
							15-20	0.060		
	8-35	0.7			15-30	1.4	25-30	0.026	2-24	0.111
/Ni.HfO_2	0-2	3.25			0-2	9-5	0-10	0.028	0-2	1.417
	8-35	0.10			8-30	0.29	10-30	0.0097		
							30-45	0.028	2-25	0.044
/Ni-Co/Cr	0-3	14.70	0-3	133	0-3	311				
/Ni.Al_2O_3	5-20	1.65								
			10-50	5.15	10-50	11				
	25-50	0.34								

Cont/.....

Table 15 continued

/Ni-Co/Cr	0-3	15.33	0-2	180	0-3	517
/Ni. ZrO_2	15-30	1.23				
	30-50	0.60	20-50	6	16-40	190
/Cr	0-5	0.24			0-2	70
	5-25	0.05				
	30-50	0.16			30-50	0.08

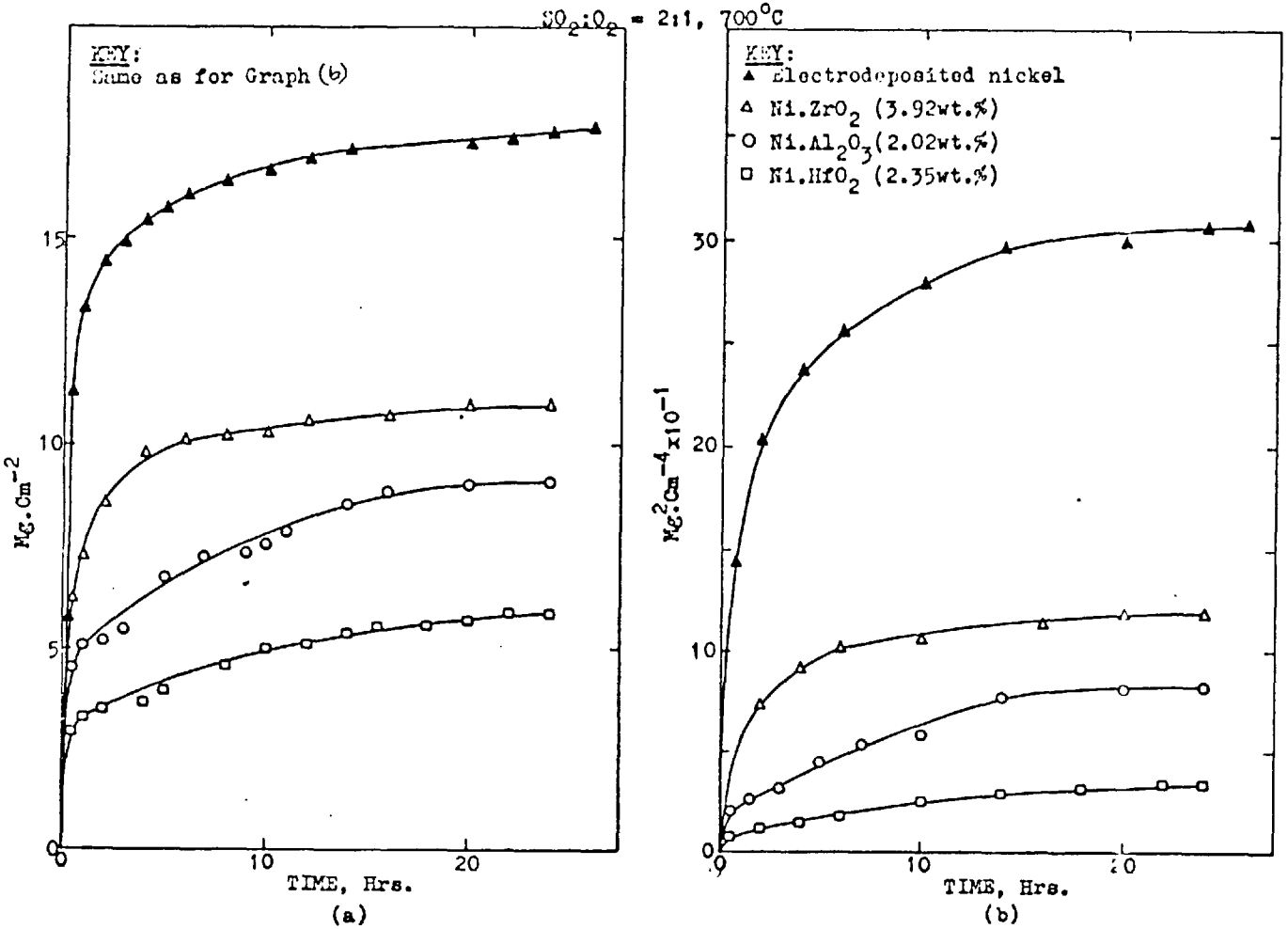

Graph 19. Corrosion kinetics of Ni-cermets coated with 0.1M Na_2SO_4 (1 mg/cm^2).

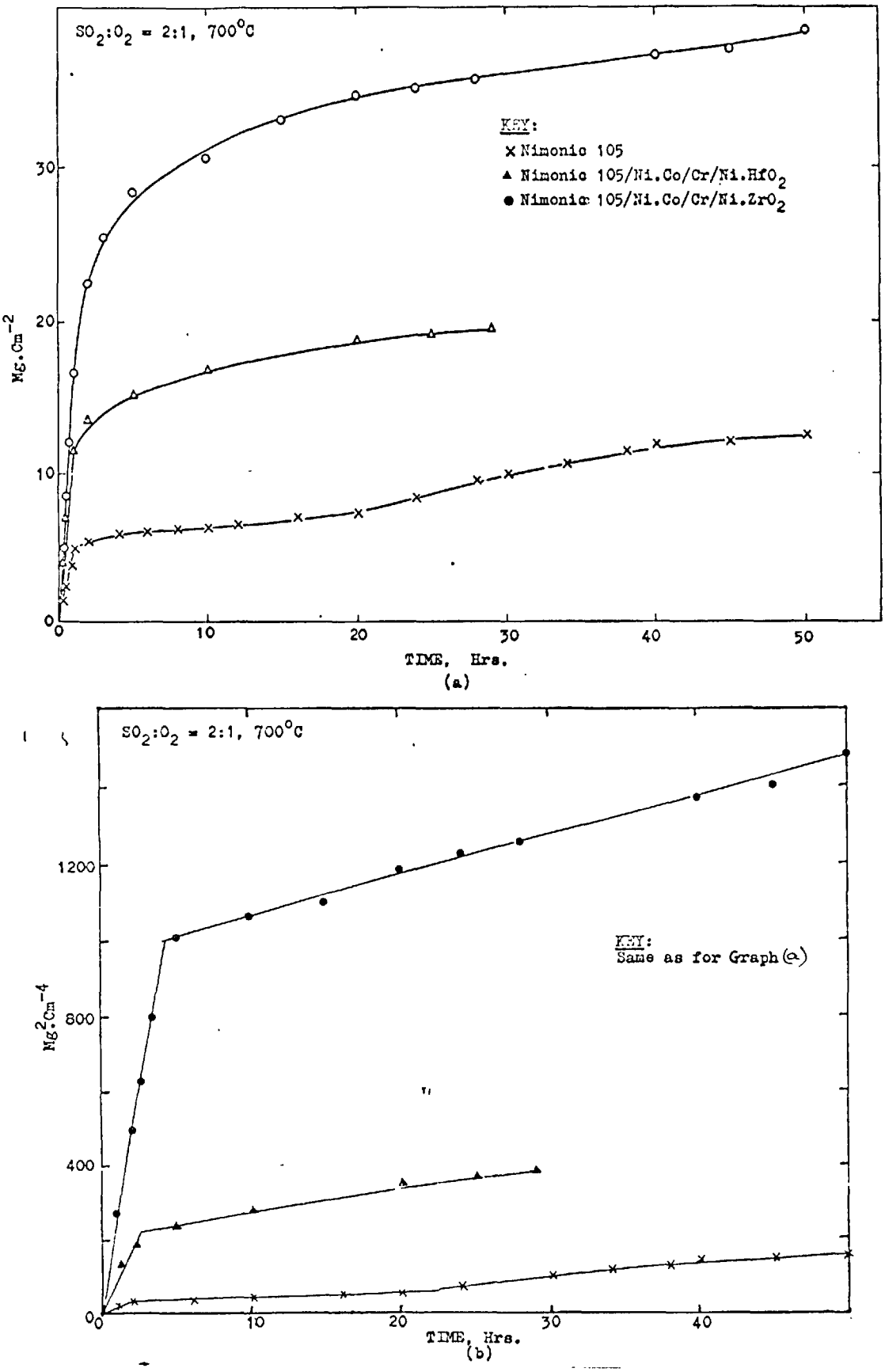

Graph 20. Corrosion kinetics of Nimonic 105 and cermet-coated Nimonic 105 (1 mg/cm^2 of 0.1M Na_2SO_4 salt contamination.)

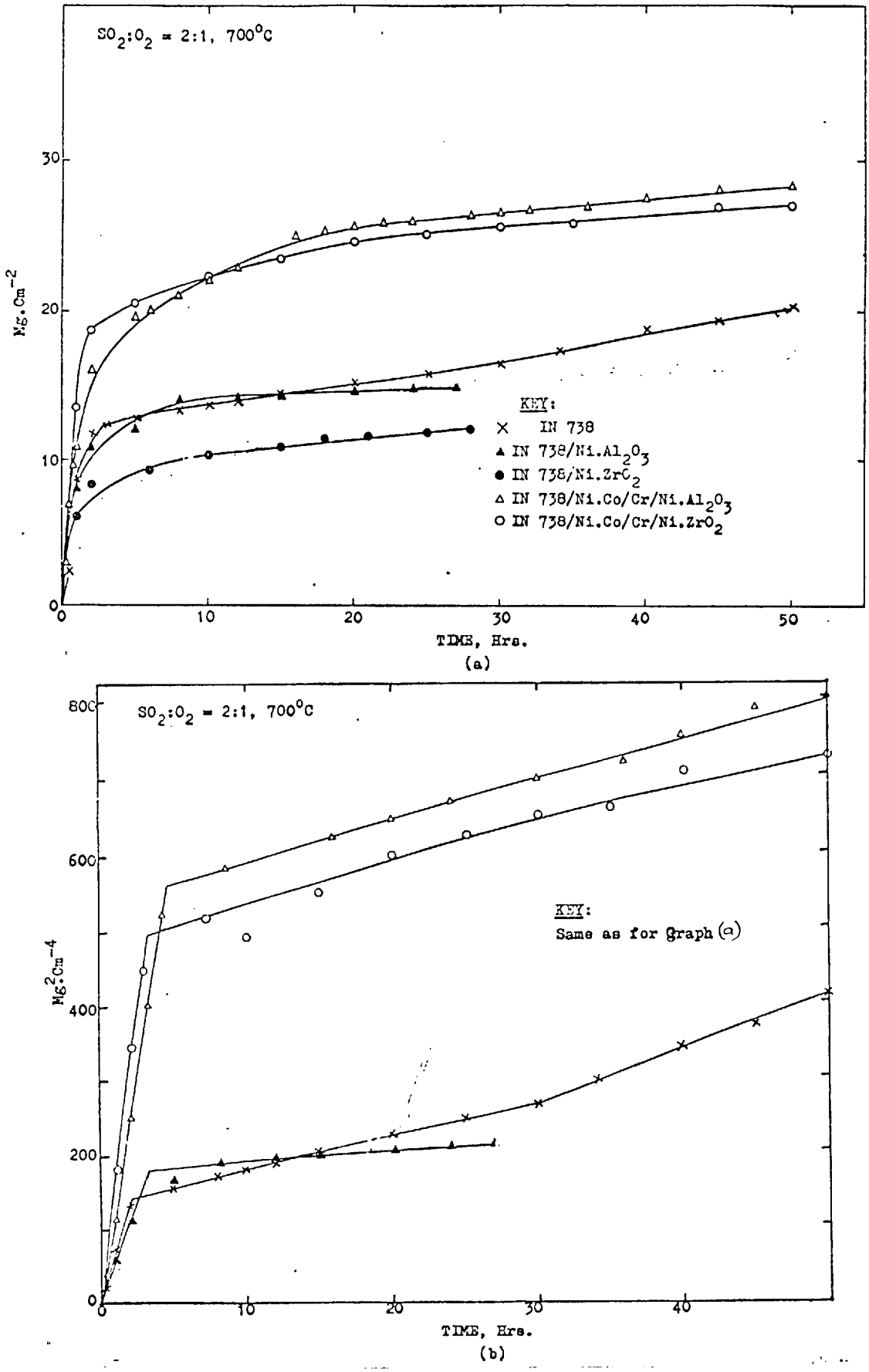

Graph 21. Corrosion kinetics of IN 738 and cermet-coated IN 738 (1 mg/cm^2 of 0.1M Na_2SO_4 salt contamination).

1.3 Na_2SO_4 contaminated specimens

Thermogravimetric curves obtained at 700°C with SO_2 : O_2 = 2:1, show that with specimens contaminated with 1mg/cm^2 Na_2SO_4 (0.1 molar), there are generally two successive periods (Graphs 19; a,b, : 20; a,b,; 21; a,b): a first period (less than 1 hour) during which the corrosion rate is very high; and a second period during which the gain of weight follows an approximately parabolic kinetic law as with the non-contaminated specimens.

In general, the corrosion kinetics of the specimens contaminated with 1 mg/cm^2 Na_2SO_4 show similar trends to those exhibited by the non-contaminated specimens (Graph 19). The electrodeposited nickel corroded much faster than any of the cermet coatings, and the order is Ni. HfO_2 < Ni.Al_2O_3 < Ni.ZrO_2. The increase in the corrosion rates is about two- fold greater than for those of the non-contaminated specimens. The parabolic rate constants for the various electroformed cermet coatings are given in Table 13.

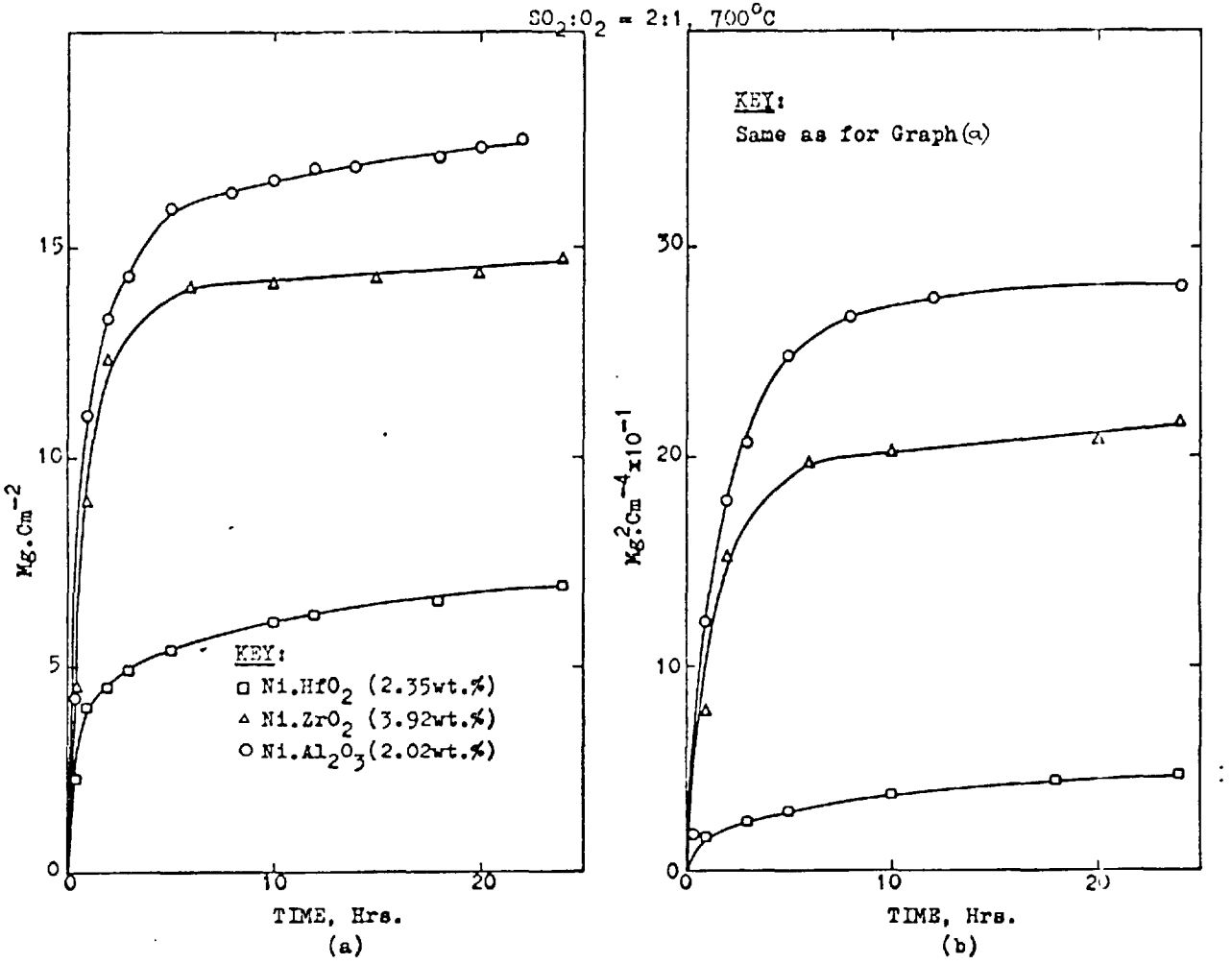

Graph 22 Corrosion kinetics of Ni-cermets coated with Na_2SO_4 + 24 wt.% NaCl (1 mg/cm^2).

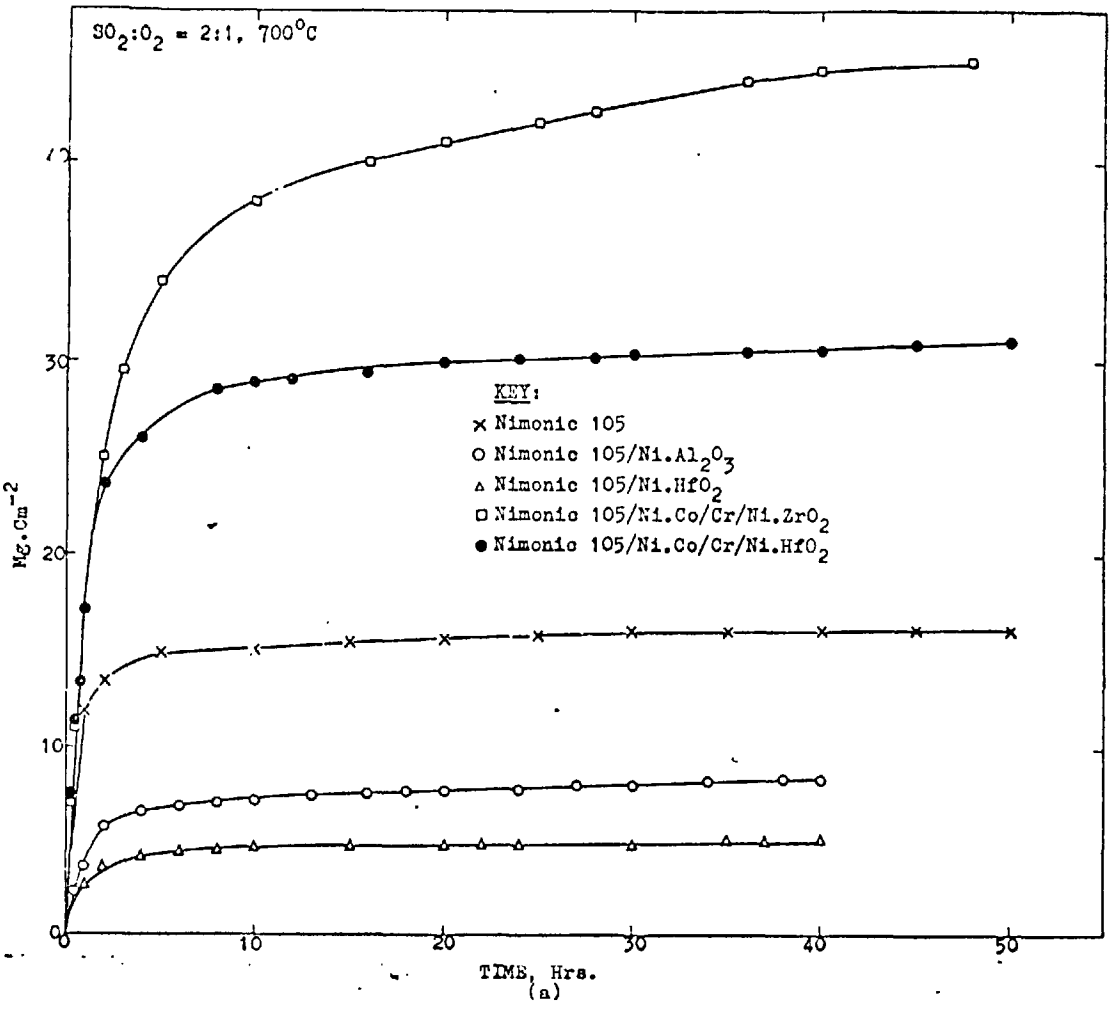

Graph 23. Corrosion kinetics of Nimonic 105 and cermet-coated Nimonic 105 (1mg/cm^2 of Na_2SO_4 + 24wt.% NaCl salt contamination).

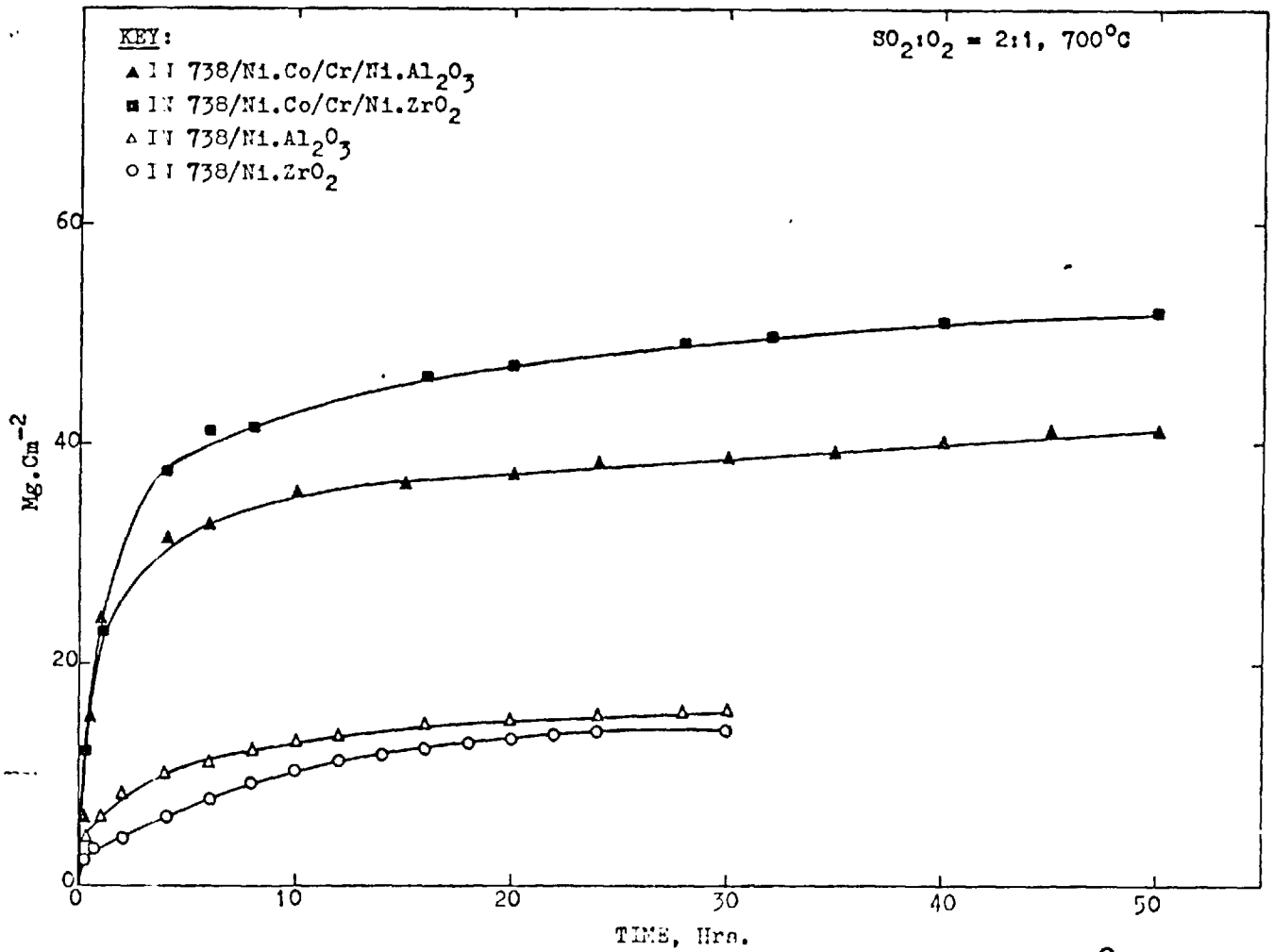

Graph 24. Corrosion kinetics of cermet-coated IN 738 (1 mg/cm^2 of Na_2SO_4 + 24wt.% NaCl salt contamination.)

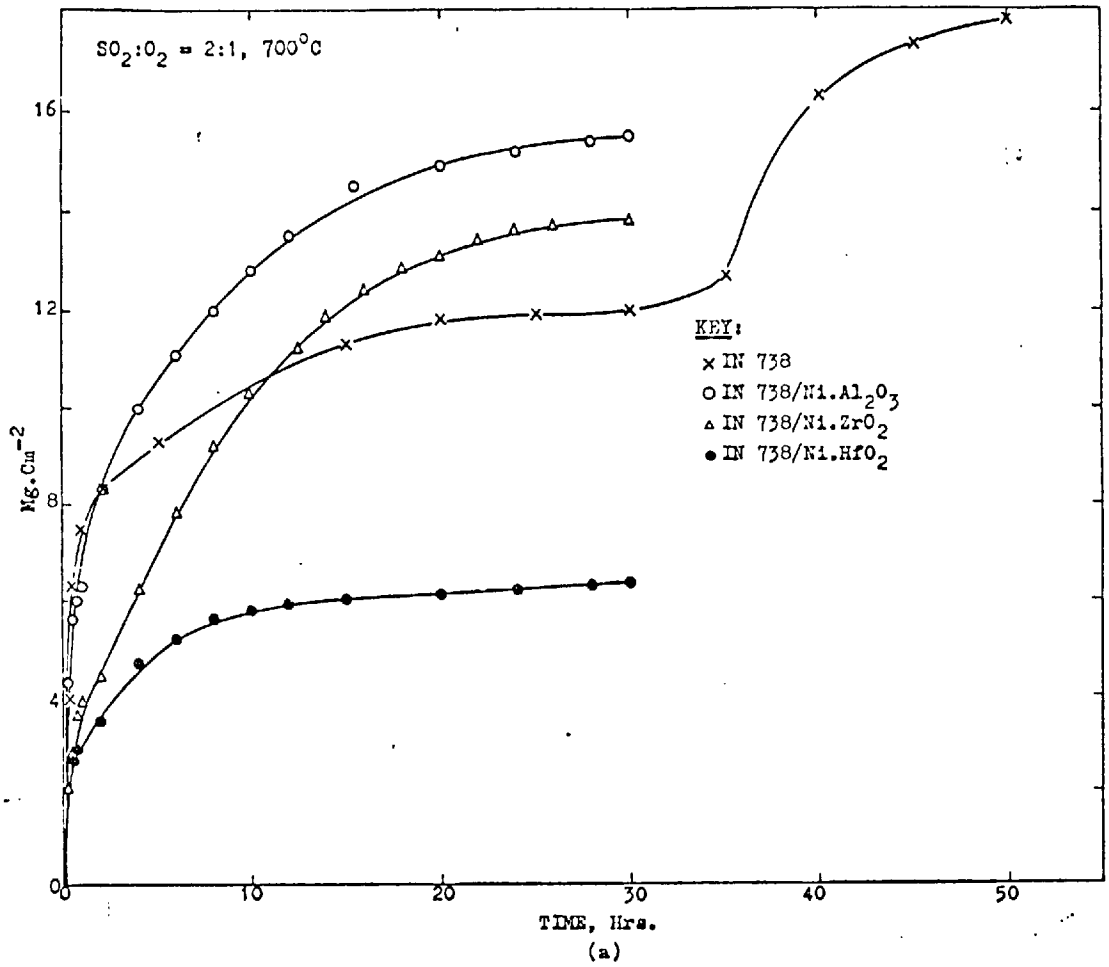

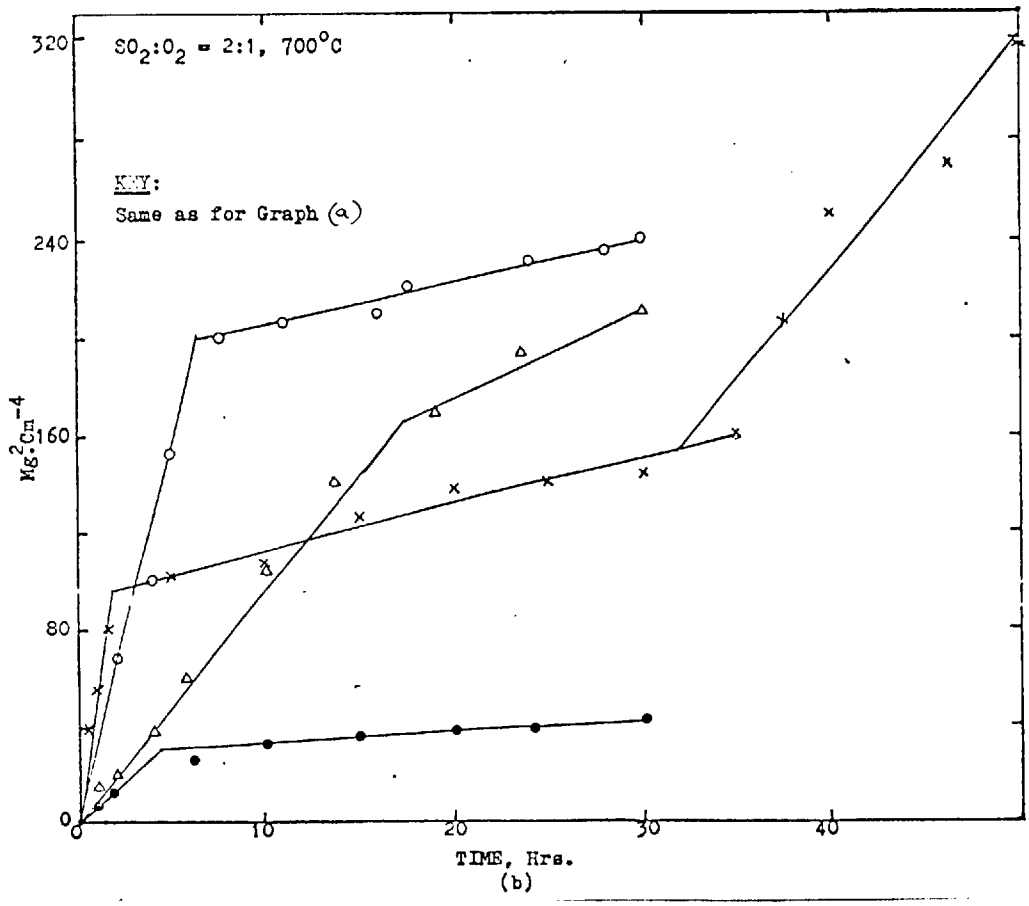

Graph 25. Corrosion kinetics of IN 738 and cermet-coated IN 738 (1 mg/cm^2 of Na_2SO_4 + 24 wt% NaCl salt contamination).

1.4. Na_2SO_4 + NaCl contaminated specimens

Typical results of the sulphidation of test specimens, coated with 1 mg/cm^2 deposits of a mixture of Na_2SO_4 and 24 wt % NaCl, SO_2; O_2; 2:1 at 700°C, are presented (Graphs 22, 23, 24, and 25). The degredations of the duplex electrodeposited (i.e. superalloy/Ni-Co/Cr/Cermet) specimens were more severe than that observed for the same specimens coated with 0.1 M Na_2SO_4. Noteably, there was no significant difference in the kinetics between Na_2SO_4 and Na_2SO_4+NaCl mixtures for cermet coated superalloy specimens (i.e. superalloy/Ni.Al_2O_3, Ni.ZrO_2 or Ni.HfO_2).

In most cases shown in Graphs 22-25, the reaction settles down to a fairly constant rate of attack, usually after an initial period during which the reaction rate increases. Only the IN 738 specimen showed evidence of a breakaway after a period of about 40 hours. Tables 13-15 show the values of rate constants achieved by the various test specimens. With the exception of IN 738, all the test specimens exhibited two parabolas.

a. Electrodeposited Ni-Al_2O_3 (2.02 wt.%), 700°C, SO_2:O_2:: 2:1, 28 hrs., TEMSCAN(x800); fractured x-section showing outer layer and most of inner layer.

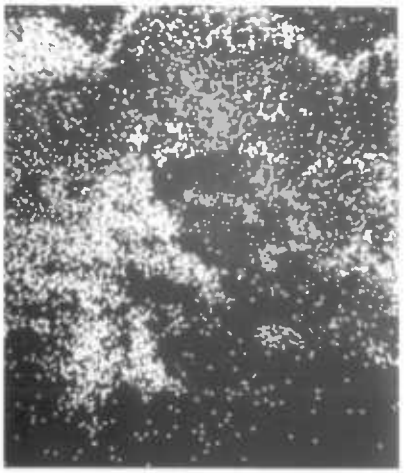

b. Distribution of S, Ka.

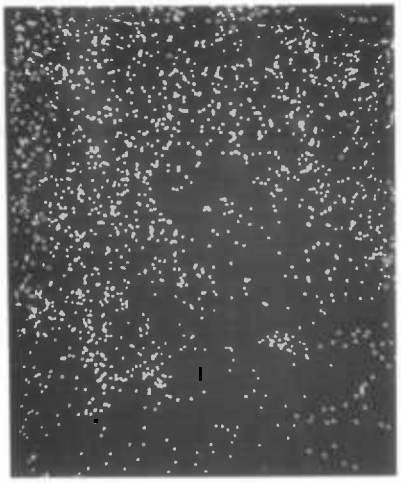

c. Distribution of Al, Ka.

PLATE 9

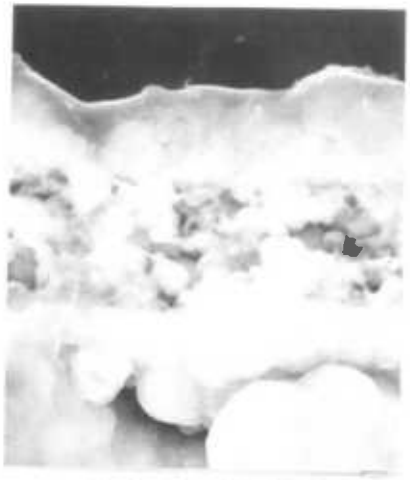

a. Electrodeposited Ni-ZrO_2 (5.92 wt.%). conditions as in Plate 9. 7500AR(x800).

b. Distribution of Ni. Kα.

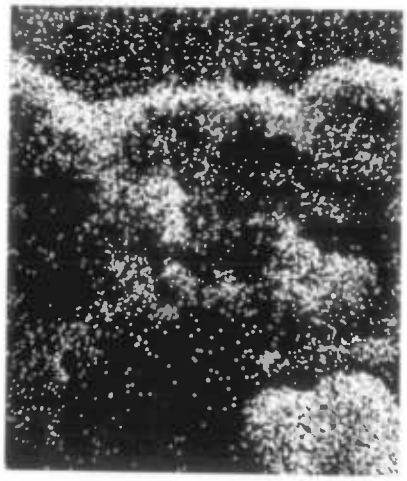

c. Distribution of Zr. Kα.

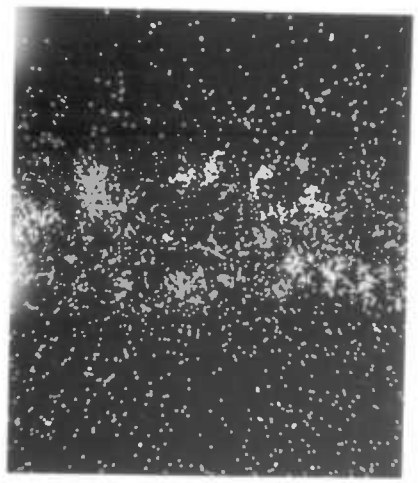

d. Distribution of Cr. Kα.

PLATE 10

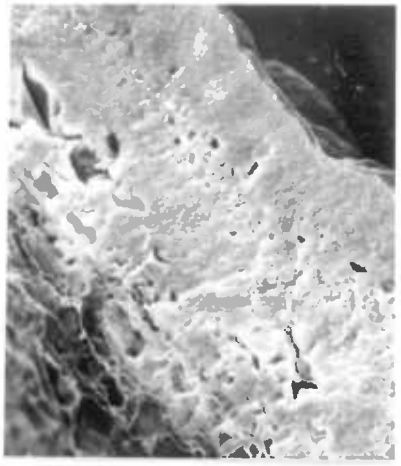

a. Electrodeposited Ni-HfO_2 (2.35 wt.%), conditions as in Plate 9. TEMSCAN(x500).

b. Distribution of Ni, Kα.

c. Distribution of O, Kα.

d. Distribution of Hf, Mα.

PLATE 11

2. Corrosion Kinetics in SO_2/O_2 = 2:1 at 900°C

2.1. Cermet-coated superalloys

The weight-gain curves for a number of cermet-coated superalloys, IN 738 and Nimonic 105, at 900°C (1650°F) in SO_2/O_2 = 2:1 are shown in Graph 26 a,b. In general, the extent of the corrosion attack on the tested specimens appear to be less severe than that observed at 700°C. IN 738/Ni.Al_2O_3 specimen show a discontimuous change in the initial reaction kinetics which can be attributed to the breakaway of the scale formed. Once again, it is noticeable that the rate of corrosion of the HfO_2 containing coating is much slower than that observed for coatings containing Al_2O_3 and ZrO_2. It can be seen that the Nimonic 105/Ni.Al_2O_3 specimen corroded faster than its IN 738 equivalent, even though the initial rate of corrosion (up to 10 hours) of the Nimonic 105/Ni.Al_2O_3 specimen was much slower. Each of the specimens corroded at 900°C showed a deviation from a single parabolic scaling rate. Examples of these curves are shown in Graph 26b, and their parabolic rate constants are listed in Tables 14 and 15.

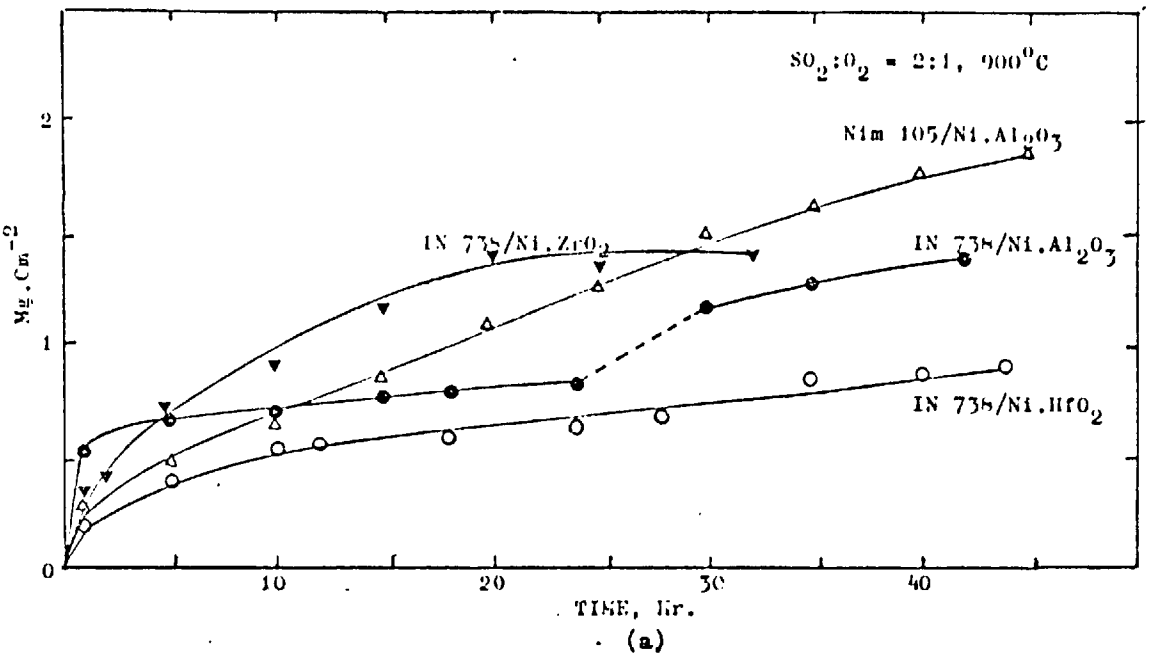

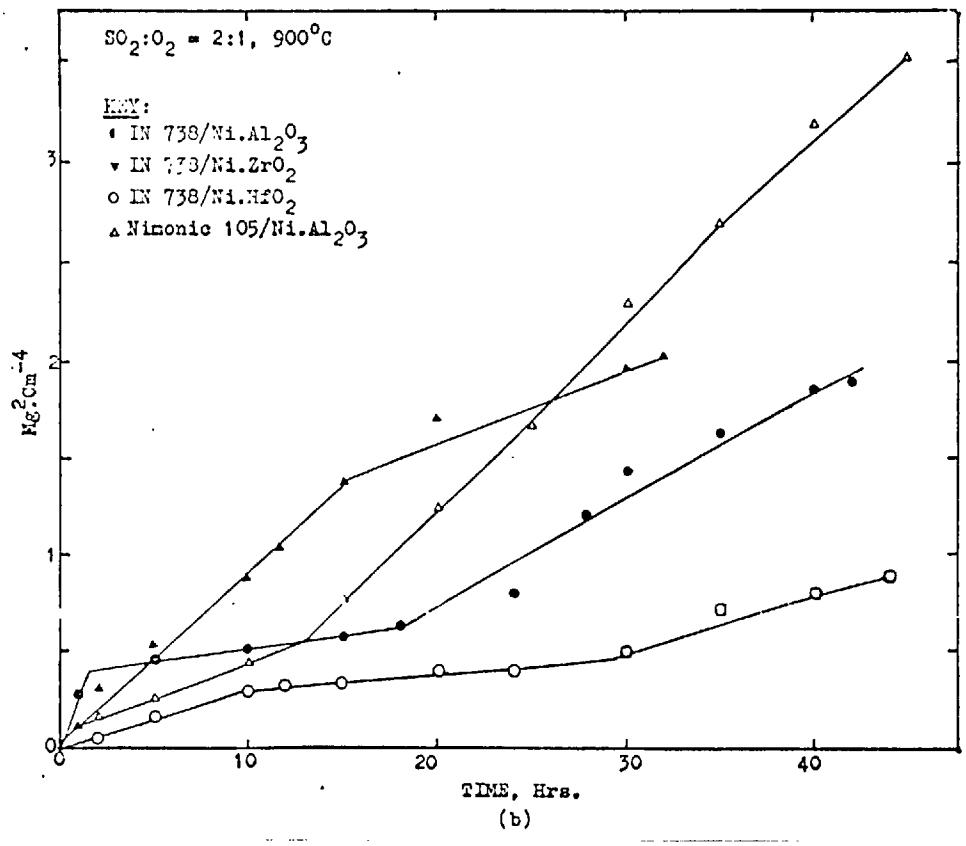

Graph 26. Corrosion Kinetics of cermet-coated superalloys.

2.2 Na_2SO_4 + NaCl contaminated specimens

The thermogravimetric results for IN 738, nimonic 105, and for the respectively cermet-coated alloys at 900°C are shown in Graph 27 a,b. The effect of contamination of each of the specimens with 1 mg/cm^2 of Na_2SO_4 + 24 wt % NaCl mixture is obvious. The corrosion rates of each of the specimens is an order of magnitude greater than that observed for the uncontaminated specimens. Under these test conditions, the overall weight increases for the IN 738 /Ni.Al_2O_3 and IN 738/Ni.ZrO_2 are very similar, although the initial corrosion rate for the latter is much faster. The behaviour pattern of the alloys IN 738 and nimonic 105 are very similar up to a period of 30 hours, after which the nimonic 105 shows a breakaway in the scale formed. As in the case of uncontaminated specimens, each of the specimens exhibited more than one parabolic rate constant (Graph 27b, Tables 11 and 15).

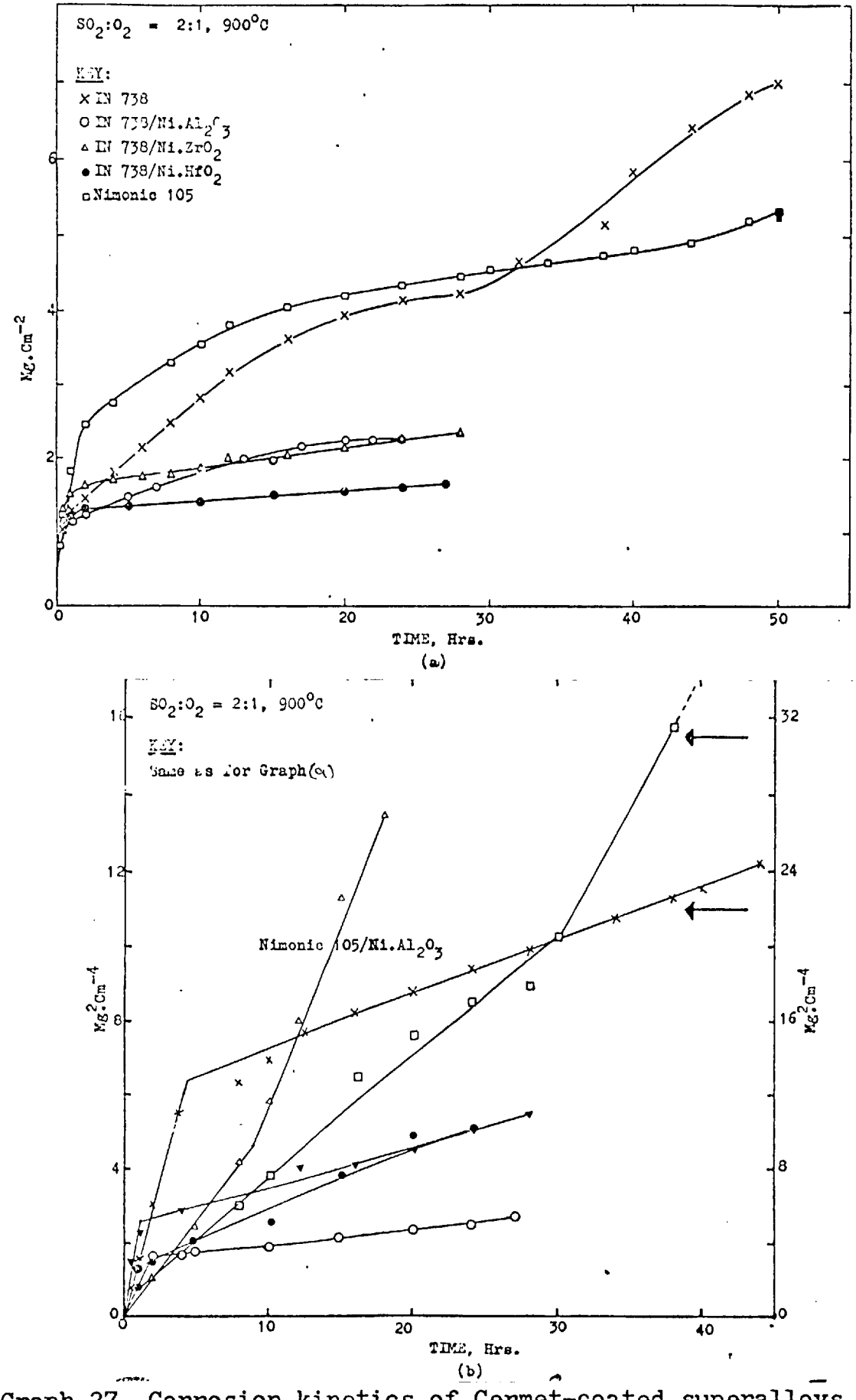

Graph 27. Corrosion kinetics of Cermet-coated superalloys (1 mg/cm^2 of Na_2SO_4 + 24 wt.% NaCl salt contamination).

2.3 Scale morphology, structure and analysis

Plates 9, 10, 11 show the fractured cross-sections of the various electrodeposited cermets of $Ni.Al_2O_3$ (2.02 wt %), $Ni.ZrO_2$ (3.92 wt %) and $Ni.HfO_2$ (2.35 wt %) after corrosion at 700°C for 28 h : the sections through the nodules are apparent. Examination in cross-sections of these fractured specimens show a gradation in the grain size through the sections. The grain size in the outer region of the scales is around 0.5μm increasing to about 5-10 μm at the inner surfaces. This gradual increase in grain size across the scale appears consistent with a scale growth model of inward sulphur diffusion, new oxide being formed at the scale/matrix interface. Plates 9b,c display the electron dispersive analyser scans for the electrodeposited $Ni.Al_2O_3$. The elements displayed are sulphur and aluminium. The Al_2O_3 layer is directly underneath the sulphidation zone Plates 10 b, c, d and 11 b, c, d, show X-ray distributions of nickel, sulphur, zirconium and hafnium, for electrodeposited $Ni.ZrO_2$ and $Ni.HfO_2$ respectively. These X-ray distributions confirm the presence of the ceramic oxide particles below the sulphidation zone, and also show the depths of penetration of the diffused sulphur. The electron images of the various specimens show the presence of voids, formed within the scales, and the voids extend to the centre of the specimen. X-ray diffraction of the

respective scales formed on the cermets ($Ni.Al_2O_3$, $Ni.ZrO_2$ and $Ni.HfO_2$) reveals that the outer layer consists of NiO in which sulphide particles are uniformly distributed through the oxide, and below this layer of oxide is a layer of Ni_3S_2.

Micrographs of the cross-section of corroded nimonic 105 and cermet coated nimonic 105 specimens at 700°C is shown in plate 12. Detailed examination of the alloy/scale interface regions showed complex oxide/sulphide networks and acicular precipitates noticed in various locations in the alloy affected zones of the nimonic 105 alloy (Plate 12 a), and the porous outer scale contains fragments of metal. The morphology of the scale formed indicates the presence of surface cracks and protrusions, and X-ray diffraction reveals the scale to consist of NiO, Ni_3S_2 and inner layer CrS particles.

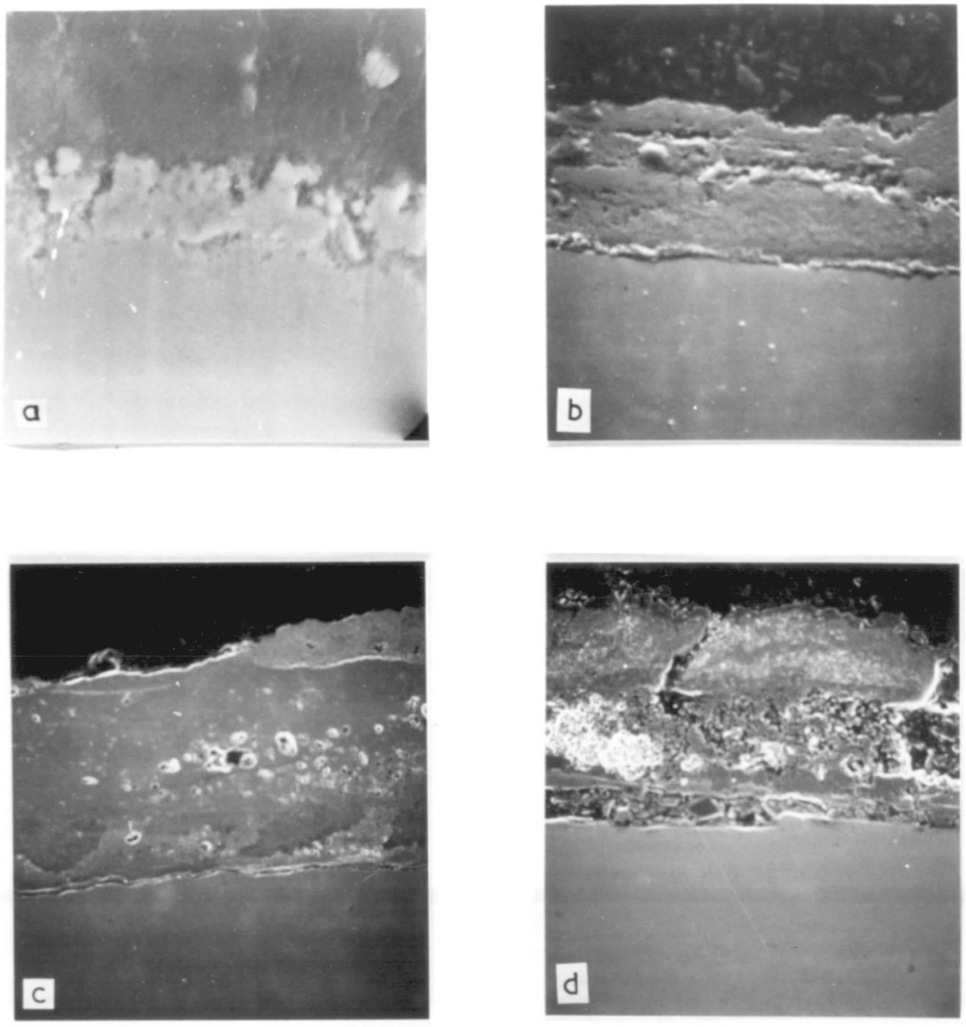

S.E.M. micrographs of the cross-section of corroded Nimonic 105 and cermet coated Nimonic 105 specimens, after exposure in SO_2:O_2=2:1 at 700°C.

(a) Nimonic 105, after 50hr., section(x122).

(b) Nimonic 105/Ni.Al_2O_3, after 40hr., section(x330).

(c) Nimonic 105/Ni.HfO_2, conditions as in (b), section(x120).

(d) Nimonic 105/Ni.Co/Cr/Ni.HfO_2, conditions as in (b), section (x200).

PLATE 12

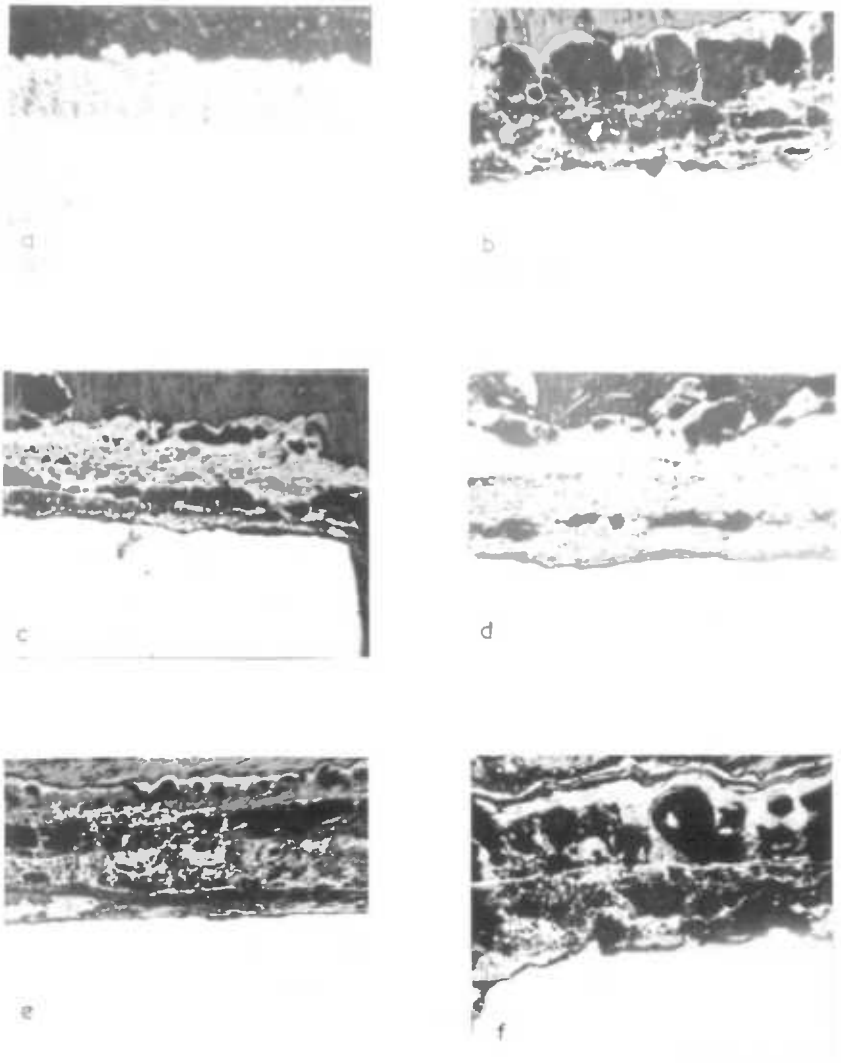

Microgrophs of specimens after exposure in 30_2:10_2:air at 700°C. for 40hr.

(a) 21.5rO_2 type coating on IN738, initial condition.

(b) IN738/21.5rO_2, sectional(x100).

(c) IN738/21.4SO_2, sectional(x100).

(d) IN738/21.4Y_2O_3,sectional(x100).

(e) IN738/21.5rO_2+21.4Y_2O_3, sectional(x100).

(f) IN738/21.5rO_2+21.4SO_2, sectional(x100).

PLATE 13

The scales formed on nimonic 105/duplex coat (Ni-Co/Cr/cermet) were porous, the least protective, and sulphides in the coating were somewhat larger as shown by the lighter shade areas in Plate 12 d. In this particular case, cracks which increase in width and depth can be seen. The movement of the cracks being into the base of the coating. No coating breakaway occurred, but the integrity of the coating has been undermined as can be seen from the attack along the coating / substrate boundary. Surface examination of the nimonic 105/duplex specimens after sulphidation at 700°C shows a very nodular, dark-grey scale with patches of pink colour. X-ray diffraction reveals the outer layer to be predominantly NiO_2 with patches of pink Co_3O_4, and the possibility of the presence of mixed oxide of the type $CoCr_2O_4$. Other oxides identified were Ni_3S_2, Cr_2O_3 and Co_9S_8, and the respective ceramic oxide. Plate 12 b, c, show the cross-sections of $Ni.Al_2O_3$ and $Ni.HfO_2$ coated nimonic 105. In these cases the integrity of the coatings are still in tact, and the presence of lighter shade sulphide areas can be seen, as well as the voids present. Cracking in the coating is not evident. X-ray diffraction of the specimens indicate the presence of NiO, Ni_3S_2, Cr_2O_3 and the respective rare earth oxides.

In the cases of cermet and duplex coated IN 738 specimens (e.g. IN 738/$Ni.ZrO_2$ shown in Plate 13a), the

scales in general were very porous and convoluted. No cracking was evident but the presence of large voids can be seen (Plate 13 b-f). The visual observations made for the nimonic 105 based counterparts also apply to the IN 738 based set of materials. Plate 13 b,c,d compare the coating microstructure of the IN 738/Ni-ZrO_2, -HfO_2 and -Al_2O_3 specimens tested at 700°C for 40 hr. The degree of attack is severe compared with the nimonic 105 combinations. The growth rate of the scales formed on these specimens is considerably slower than that of the scales formed on the IN 738. X-ray diffraction of the specimens have identified the presence of NiO, Ni_3S_2, Cr_2O_3, and CrS.

The IN 738/Ni-Co/Cr/Ni.ZrO_2 specimen showed less corrosion resistance than IN 738/Ni-Co/Cr/Ni.Al_2O as can be seen by the degree of attack on the substrates (Plate 13 e,f). Again, X-ray diffraction reveals the presence of Co_3O_4 and Co_9S_8 formed in patches through the pores on the outer layer of the scales. Energy dispersive X-ray analysis of the duplex coated specimen (Plate 13 f) indicates the presence of Ti, which has diffused outwards from the alloy substrate.

The morphological examination of specimens corroded in SO_2:O_2 = 2:1 at 700°C after contamination with 0.1 mg/cm^2 of 0.1M Na_2SO_4 are shown in Plate 14. The effect of Na_2SO_4

contamination on the sulphidation of nimonic 105 alloy can be seen in Plate 14a. The outer porous scales containing fragments of metal are disrupted, and internally oxidised / sulphidised phases can be seen. Detailed examination of the alloy/scale interface regions showed complex oxide/sulphide networks and acicular precipitates noticed in various locations in the alloy affected zones of the nickel-base alloy. X-ray spot analysis revealed the internal phase to be dominated by sulphides and oxides of Cr, Ni, Ti, and Co. Plate 14 b shows the scale formed on IN 738 alloy. The thick porous scale formed shows evidence of disruption, and some internal phases can be seen. The external scale formed consists mainly of Cr oxide but with larger amounts of Al and Ti oxide.

A completely different appearance is given by the cermet and duplex coated nickel base superalloys. The coating integrity of the various specimens appears to be maintained except for cases where there appeared to have been problems with adhesion of the coating with the substrate (Plate 14 c-f). In general, the fine-grained scales are porous and few voids can be seen. X-ray diffraction indicates the scale to consist of NiO, Ni_3S_2, Cr_2O_3, CrS and the respective rare earth oxide.

Often, localised S was present in the outer layers, but it was not possible to associate this S with individual elements and it is probably associated with reduced Na_2SO_4.

At 900°C, the amount of corrosion of the various specimens in SO_2/O_2 = 2:1 for 45 h. was considerably reduced by comparison with that obtained from 700°C exposures. Plate 15 shows some representative photomicrographs. Both the IN 738 and nimonic 105 alloys show major cracks as well as finer cracks in many locations (Plate 15 a,b).

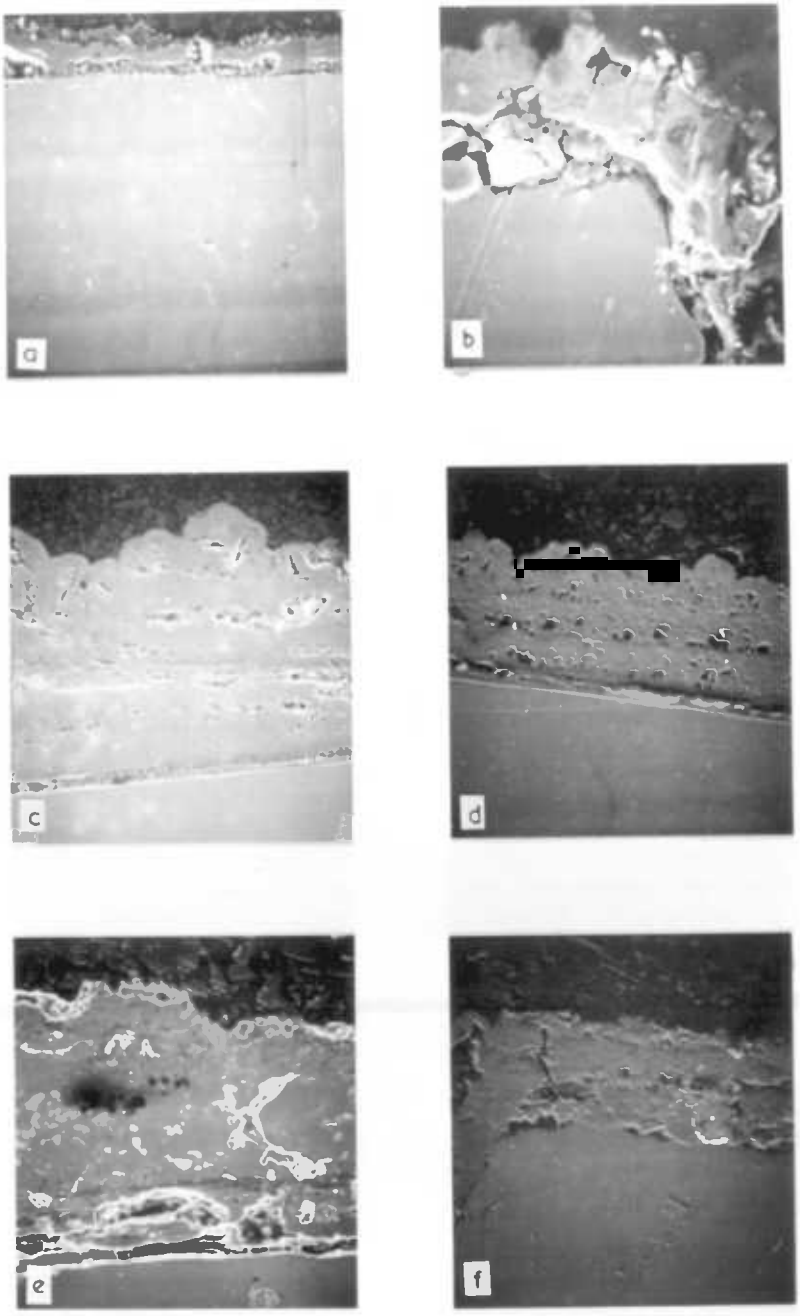

PLATE 14. Cross section of the scales formed on:

(a) Titanic 105, section(x450).

(b) [illegible], section(x800).

(c) Titanic 105/Ti.Os/Cr/Ti.SiO_2, section(x700).

(d) [illegible], section(x480).

(e) Titanic 105/Ti.Os/Cr/Ti.ZrO_2, section(x120).

(f) [illegible], section(x150), sulphidised for 5hr. in $SO_2:O_2=2:1$ at 700°C. after contamination with 1.0mg/cm² of $0.15Na_2SO_4$.

PLATE 14

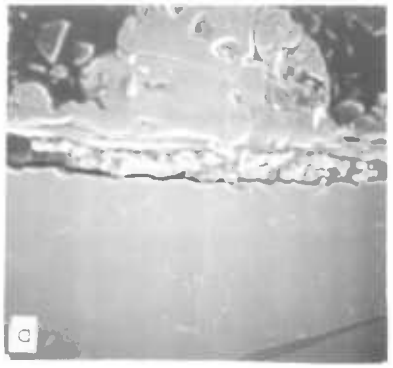

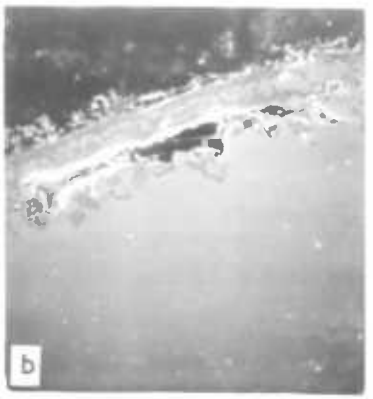

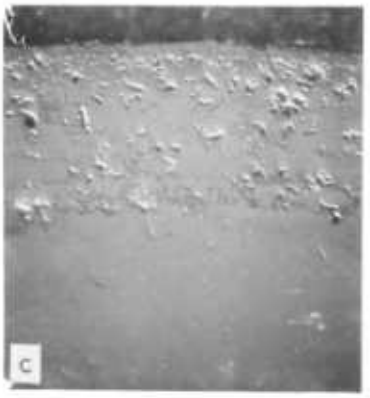

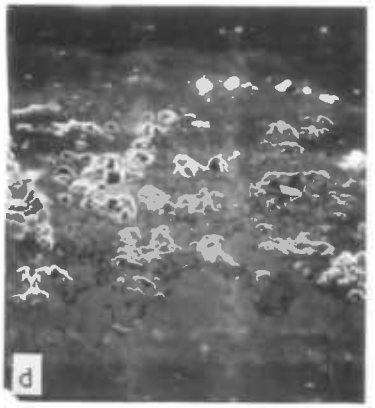

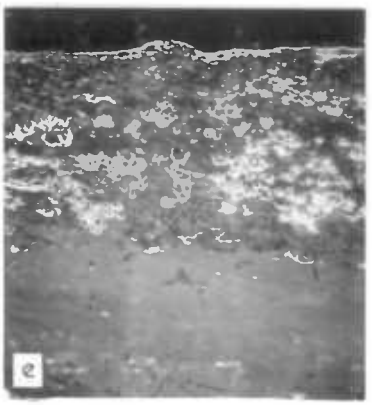

Cross section of the scales formed on specimens sulphidised for 45hr. in $SO_2:O_2$=2:1 at 900°C.

(a) IN738, section(x430).

(b) Nimonic 105, section(x150).

(c) IN738/31.8HfO_2, section(x120).

(d) Nimonic 105/31.4Al_2O_3, section(x190).

(e) IN738/31.4Al_2O_3, section(x190).

PLATE 15

The inner layers of both alloys were dominated by Cr rich oxides and there is essentially no internal sulphur present. Plate 15 c-e show the microstructure in the surface region of IN 738/Ni.HfO_2, nimonic 105/Ni.Al_2O_3 and In 738/Ni.Al_2O_3 respectively, after 45 hr at 900°C. The protective oxide layers are more uniform and the network of pores, and in certain cases, voids are evident. As at 700°C the fine grained cermet coated specimens appear to have suffered less attack. Energy dispersive X-ray analysis of Ni, Cr and S for coated Ni-base alloy (IN 738/Ni.HfO_2) is shown in Plate 16. The outer layer is rich in Ni with Cr and S present, and there is a depletion zone below the Cr which is occupied by the ceremic oxide. The amount of sulphur was considerably reduced by comparison with products obtained from 700°C exposures, and was present as very fine precipitates.

Micrographic examination of specimens sulphidised at 700°C for 40 hr after contamination with a 1.0 mg/cm^2 Na_2SO_4 and 24 wt % NaCl mixture (Plate 17) show the extent of the severe degradation suffered by the specimens. The coating free specimens of IN 738 and Nimonic 105 (Plate 17 a and b) respectively show considerable attack with cracked and spalled oxide scale. The porous oxides formed on both alloys are isolated from the substrate by a continuous layer of oxides composed essentially of Ni(Cr,Al)$_2$

O_4, Cr_2O_3, Al_2O_3 and TiO_2 while internal sulphidation involving chromium, titanium and aluminium is visible in the perturbed underlying zone. In the case of nimonic 105 alloy, there is also precipitation of molybdenum oxide preceded by a sulphide front.

The cermet and duplex coated nickel base alloys (Plate 17c-f) show considerable corrosion attack of the various specimens. The growing oxide scales had cracked locally at edge sites (Plate 17c) and nickel-nickel sulphide eutectic had exuded through the fissures, giving rise to surface warts. In localised areas where a high degree of internal sulphidation of chromium had occurred (plate 17 e,f) the associated large expansion of the coating had caused swelling and localised cracking of the oxide scales.

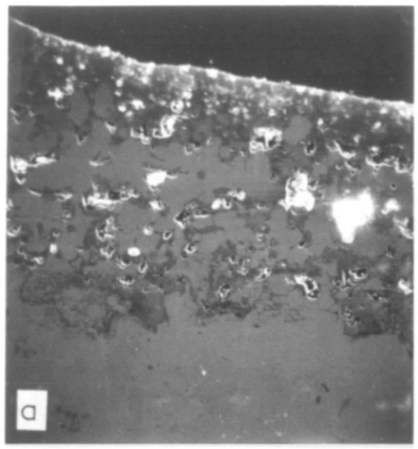

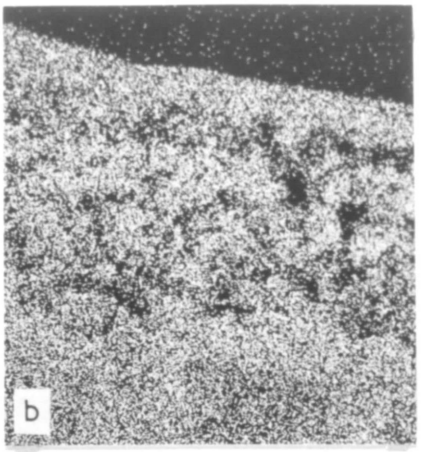

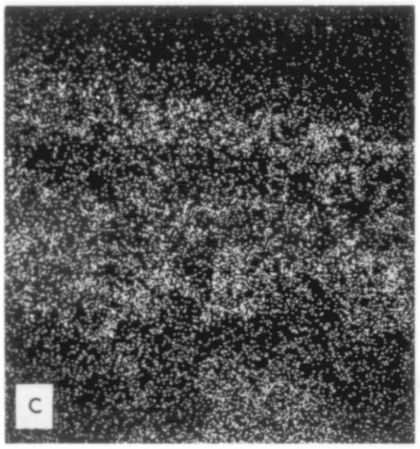

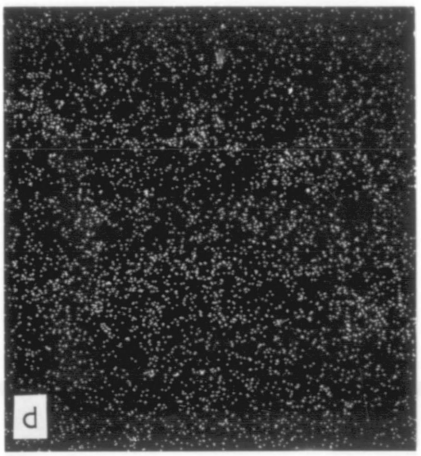

X-ray emission photograph showing element distribution in coated Ni-base alloy (IN738/Ni.HfO_2) following SO_2:O_2 attack at 900°C.

(a) Electron image, section(x180).

(b) Ni,K∝

(c) Cr,K∝

(d) S ,K∝

PLATE 16

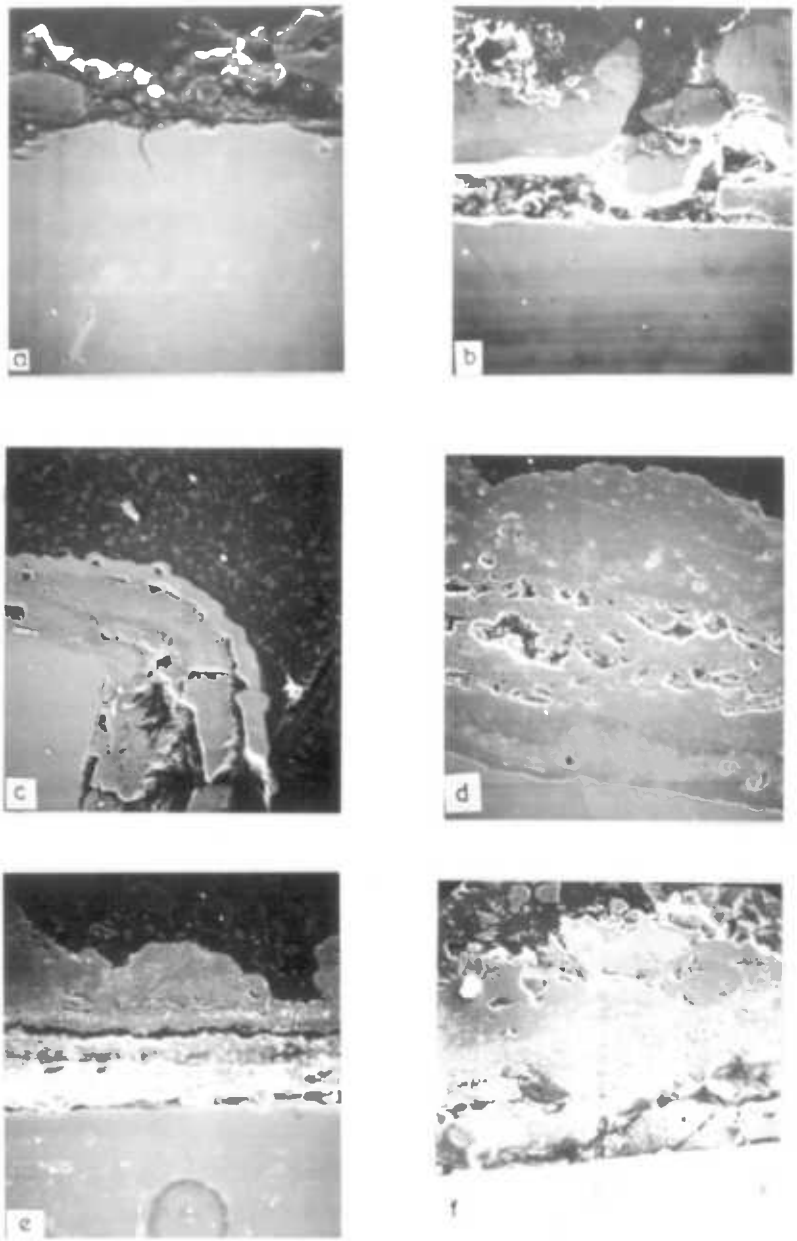

Micrographs of specimens exposed in $SO_2:O_2=2:1$ at 700°C. for 40hr. after contamination with 1.0mg/cm^2 of Na_2SO_4 + 24 wt.% NaCl mixture.

(a) 18750, sectism(x100).

(b) Pinnale 105, sectism(x150).

(c) [illegible], sectism(x50).

(d) [illegible], sectism(x100).

(e) [illegible], sectism(x100).

(f) [illegible], sectism(x50).

PLATE 17

In Plate 18 it can be seen that the sulphidation attack on the various specimens tested at 900°C after contamination with a mixture Na_2SO_4 + 24 wt % NaCl is not as severe as for those tested at 700°C. In general, the internal oxides and sulphides are numerous, and the oxide scale formed consisted of an outer layer which is nickel-rich (NiO) surmounting an inner layer of nickel-chromium oxide (Plate 19). The composition of the chromium rich areas probably approximating to that of the spinel $NiCr_2O_4$.

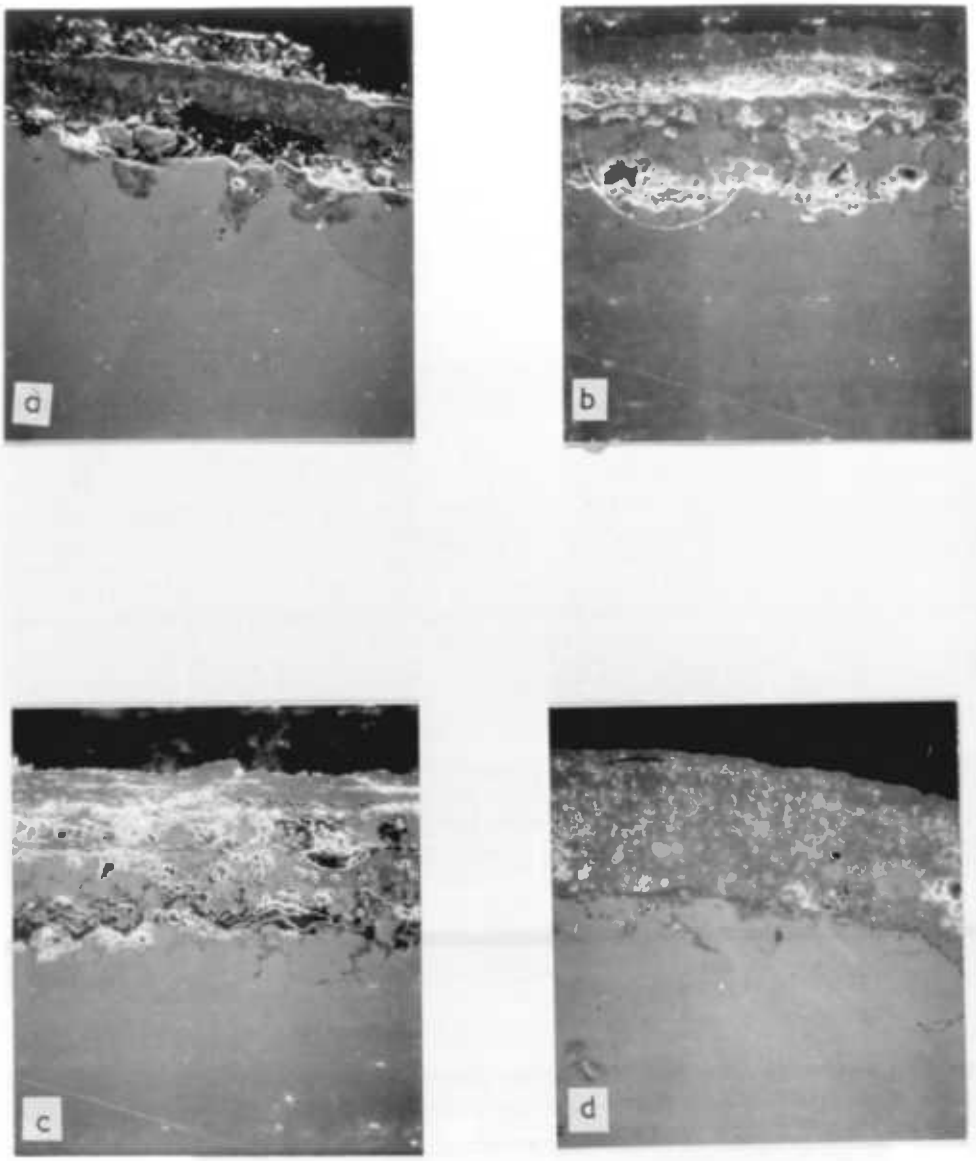

Cross section of specimens sulphidised in $SO_2:O_2=2:1$ at 900°C for 30hr. after contamination with 1.0mg/cm^2 of Na_2SO_4 + 24 wt.% NaCl mixture.

(a) Nimonic 105, 50hr., section(x180).

(b) IN738/Ni.Al_2O_3, section(x120).

(c) Nimonic 105/Ni.Al_2O_3, section(x120).

(d) IN738/Ni.HfO_2, section(x150).

PLATE 18

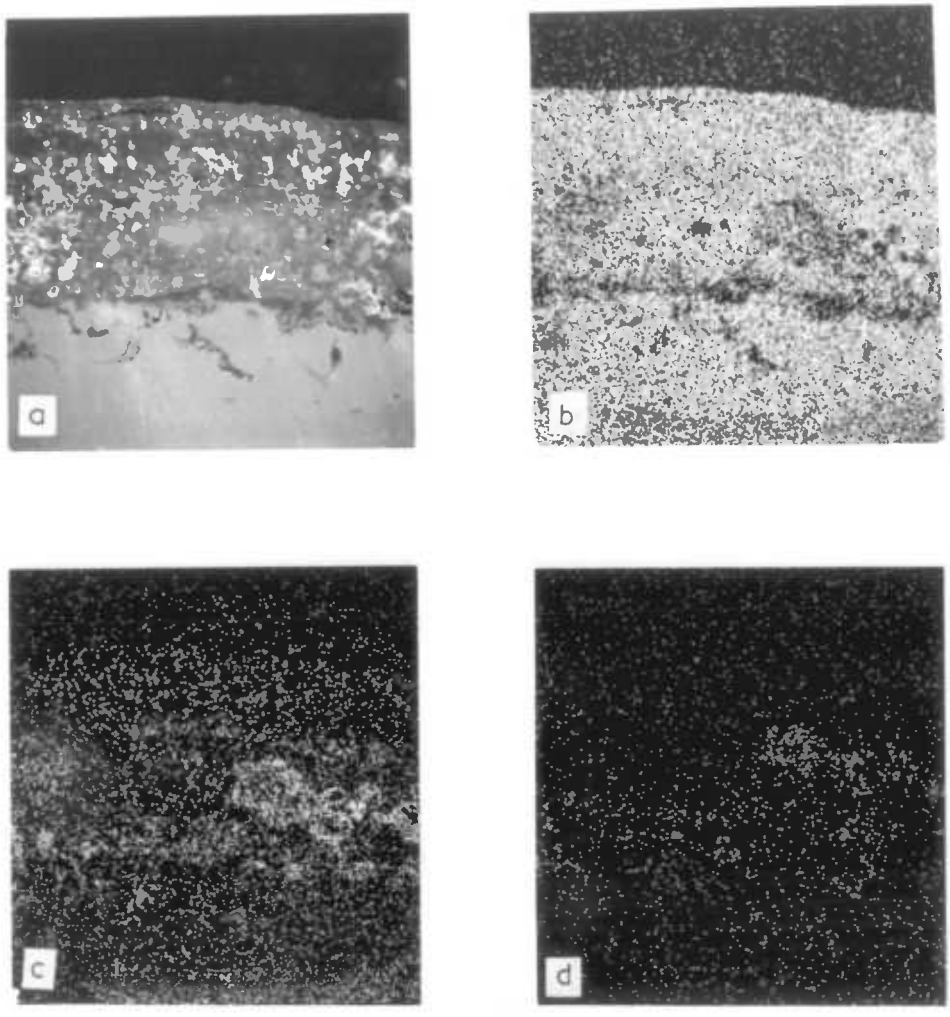

X-ray scanning image of sample shown in Plate 18.

(a) Electron image of IN738/Ni.HfO_2, section(x180).

(b) Distribution of Ni.Kα, section(x180).

(c) Distribution of Cr.Kα, section(x180).

(d) Distribution of O .Kα, section(x180).

PLATE 19

K. Electrochemical Studies

1. Electrodeposited cermet coatings

Graphs 28, 29 and 30 show the results of the assessment of the protectiveness of the oxide film formed on the surface of the cermet coatings at 700°C and 900°C in Na_2SO_4 with and without NaCl (5 wt %) additions. Under the conditions of the experiments, the cermet coatings ($Ni.Al_2O_3$ and $Ni.ZrO_2$) did not exhibit the critical peak current observed with pure metal. The maximum anodic current was $30mA/cm^2$.

There seems to be a small region of passivity when $Ni.ZrO_2$ (Graph 30) is polarised into the noble direction in pure Na_2SO_4. The passive film however, appears to be destroyed by localised attack on further polarisation. This localised attack led to perforation of the specimen expecially around the areas where the specimen is spot-welded to the platinum wire holder.

The effect of the Cl^- ion was quite distinct on anodic polarisation curves. In general, the starting (first forward) potentials are more negative in all cases, and only the electrodeposited nickel generated multiple peak currents over the same potential domain. The cermet coatings did not show much disturbances to the oxide film during the polarisation studies.

The results of free corrosion potential measurements of electrodeposited nickel and cermets of Al_2O_3 and ZrO_2 are given in Graphs 31 and 32. Measurements of current intensity in the potentiostatic mode (i.e. at constant impressed overvoltage) obtained have been plotted against time (Graph 31). The Ni. ZrO_2 coating appears to be more vulnerable to sulphate melts as far as high corrosion currents are concerned. The i-t trace in chloride-containing melts, however, are far smoother compared to the other specimens tested. In the case of electrodeposited nickel, the oxide formed appear to be more stable in the sulphate melts than in the chloride - containing melts.

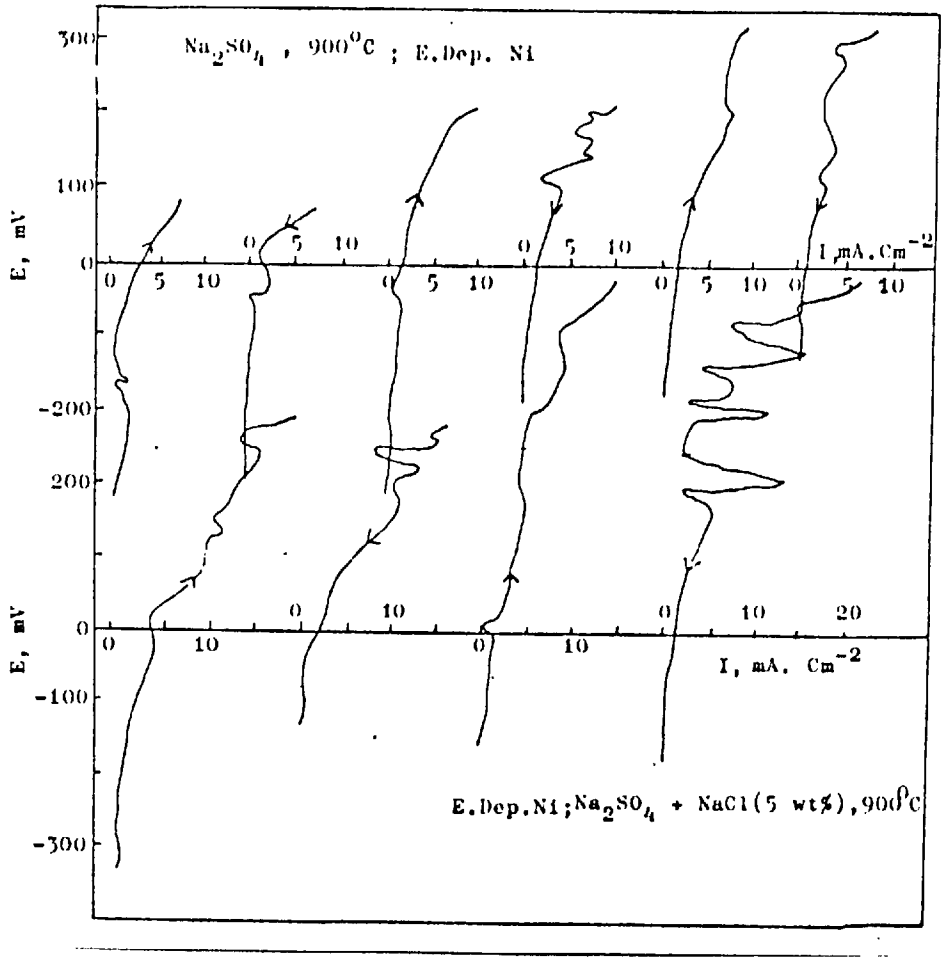

Graph 28. Potentiostatic polarization of Electrodeposited nickel in sulphate & sulphate-Chloride melts.

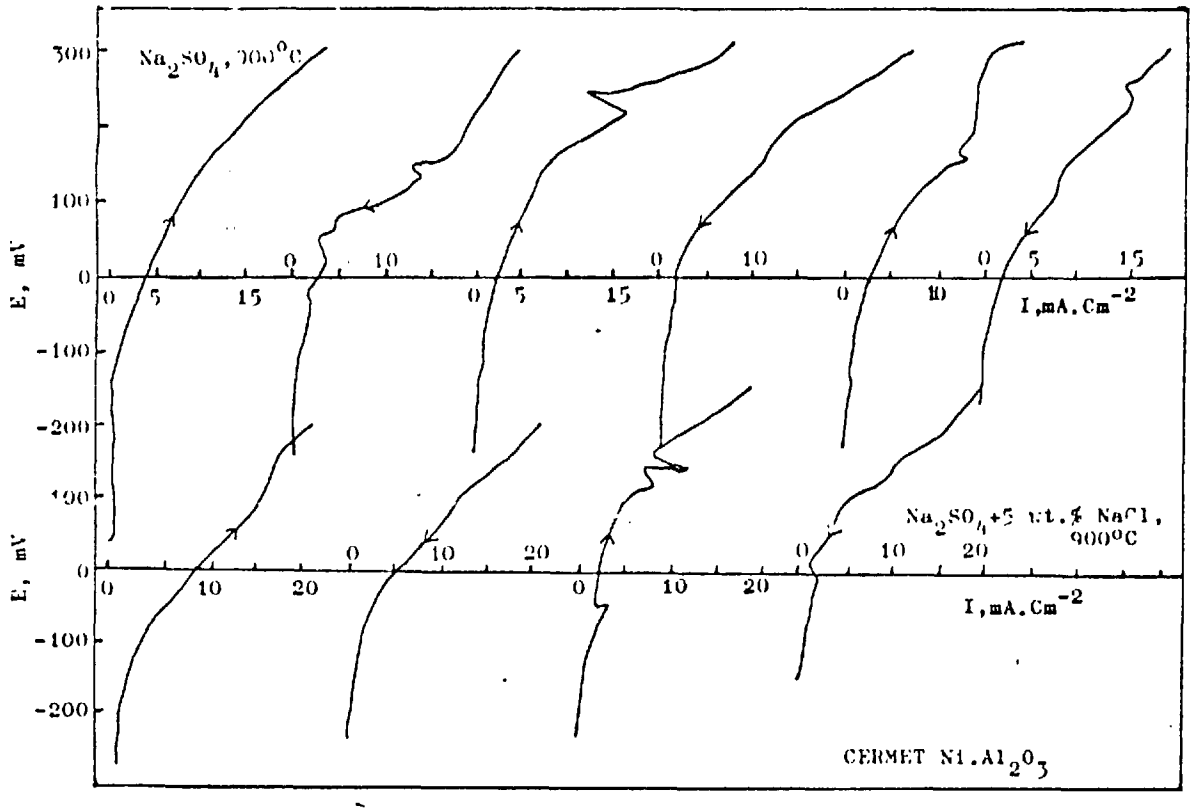

Graph 29 Potentiostatic polarization of Electrodeposited cermets in sulphate & sulphate-chloride melts at 900°C

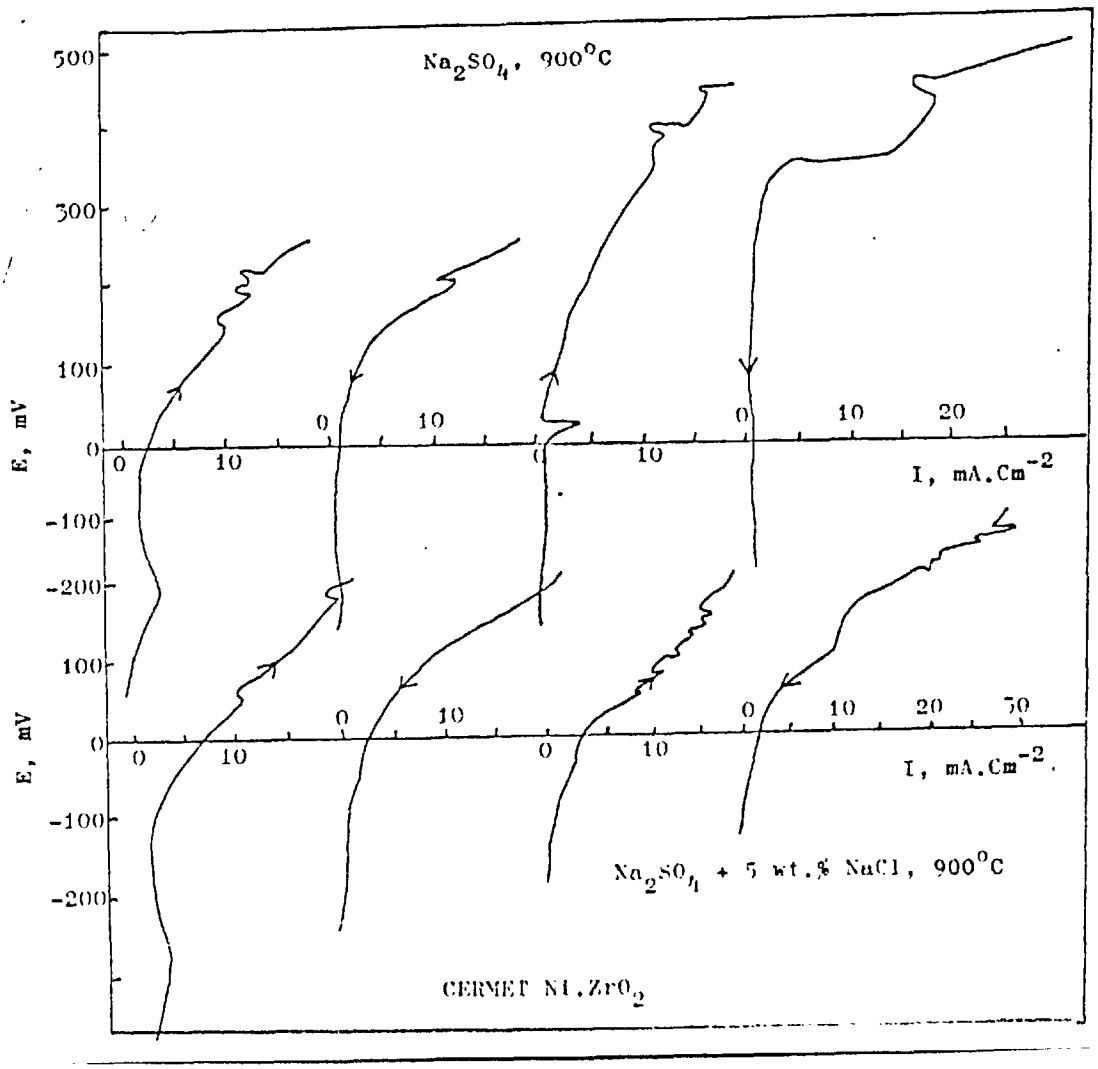

Graph 30. Current-time response of electrodeposited nickel & cermets in sulphate & sulphate-Chloride melts under controlled potential conditions

The curves in Graph 32 summarize the voltage versus time characteristic and its variation with time for electrodeposited nickel, Ni.Al_2O_3 and Ni.ZrO_2 coatings. Peculiar behaviour is observed for the behaviour of the Ni.Al_2O_3 in the sulphate melt. Remarkable ohmic drops and presence of maxima in the polarisation voltage is seen. Electrochemists currently relate the last feature to the presence of two concurrent processes or to the nucleation of new structures. In the present case it can be tentatively related to the beginning of the growth of the duplex scale.

All the coatings exposed to steady-state conditions show a high negative potential at the outset indicating an active metal surface. An adherent corrosion product tends to drive the potential to more positive values. If the product is fluxed out by the melt due to undermining of the coating, a sudden exposure of the coating surface will result in a sudden high negative potential. Negative shifts over 15-80 mV occur as early as 2 hrs in Ni.ZrO_2 and Ni.Al_2O_3 compared to 3-10 hrs in electrodeposited nickel.

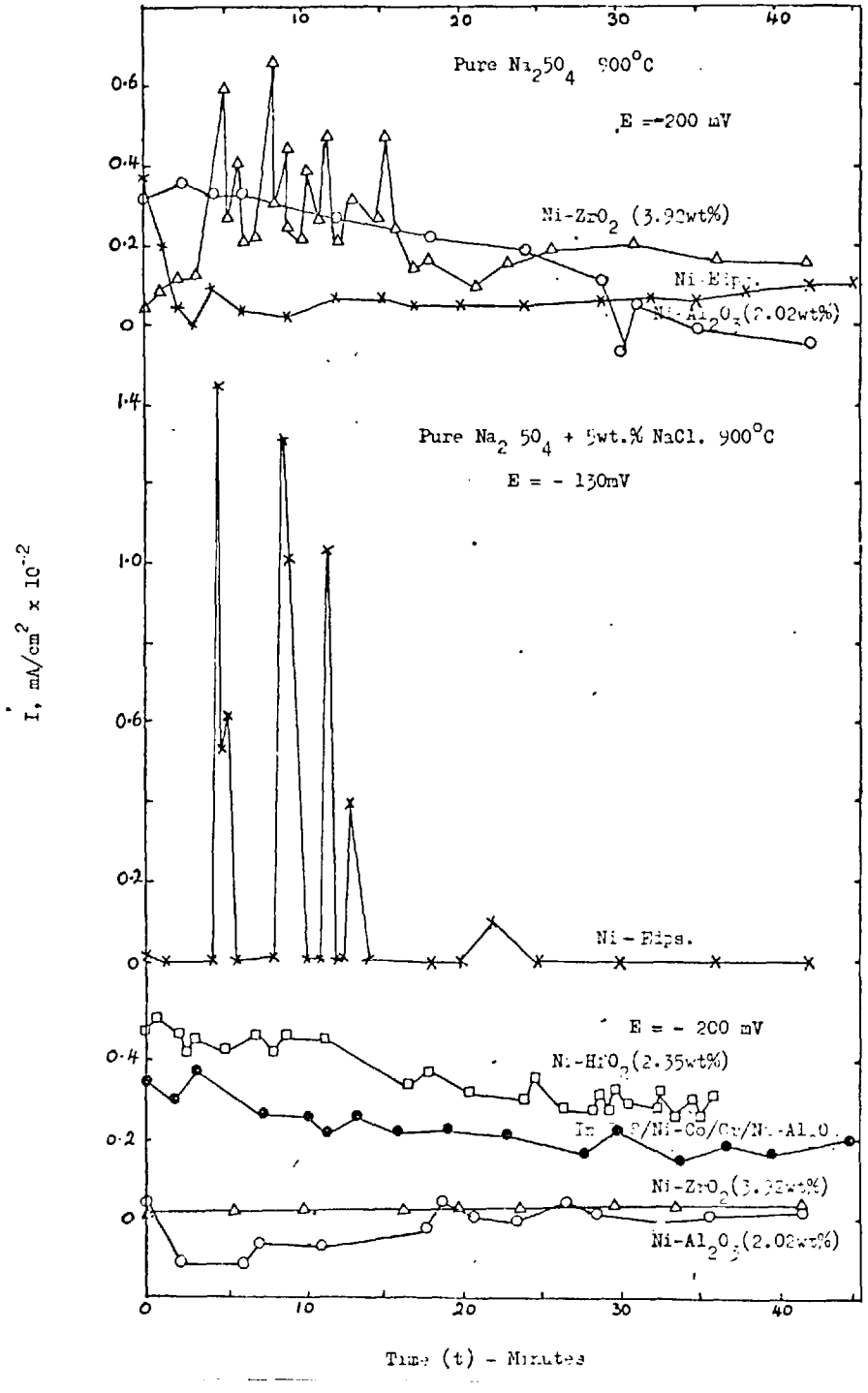

Graph 31. Steady state potential of electrodeposited nickel & cermets in sulphate & sulphate-chloride melts at 900°C.

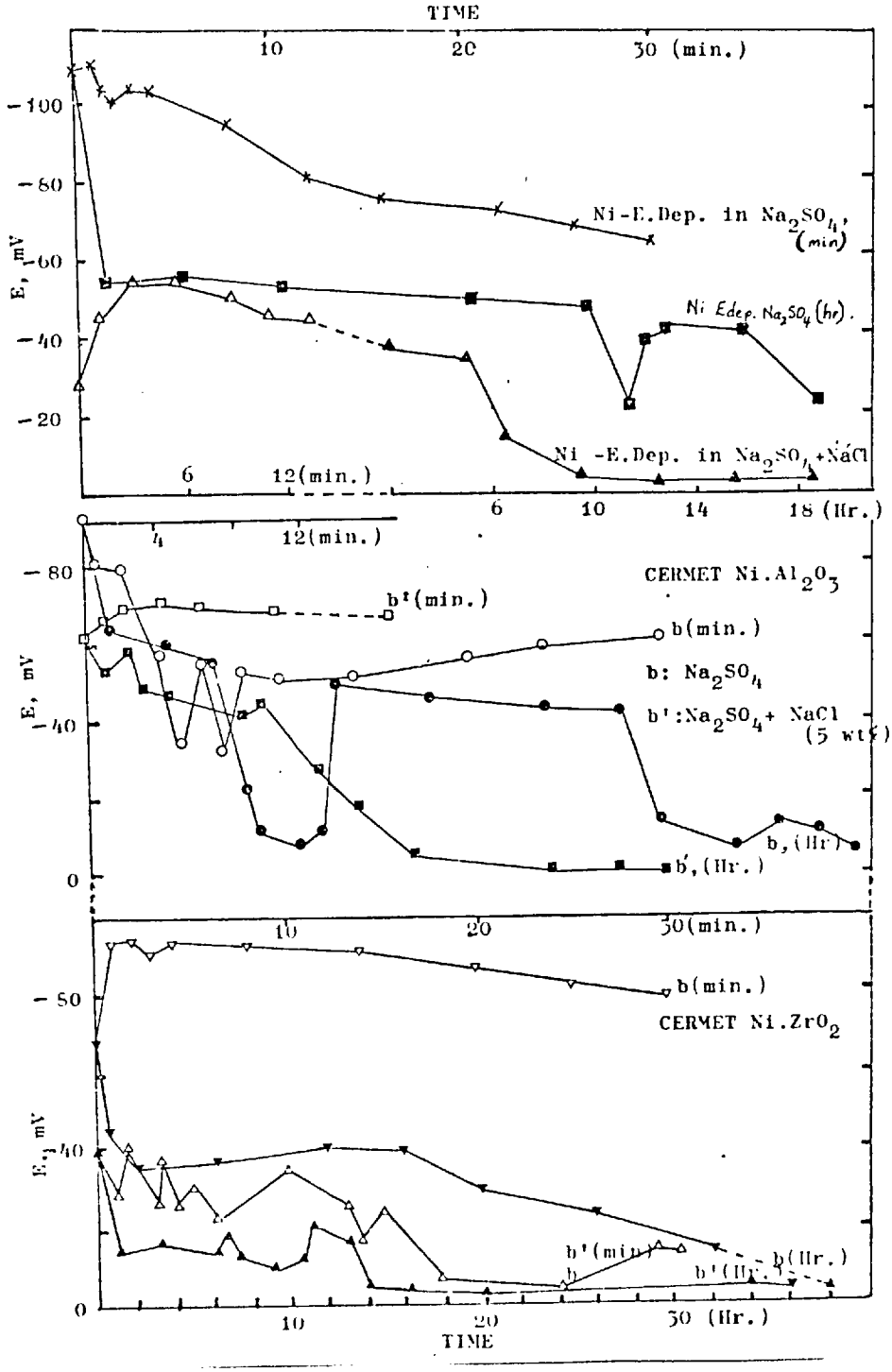

Graph 32. Steady potential of electrodeposited nickel & Cermets in sulphate & sulphate-chloride melts at 900°C.

CHAPTER DISCUSSION

1. Electrodeposition of cermets

The main problem of electrodeposition as a method of producing cermet coatings is the tendency of the particles to form clusters. Ideally, the deposit should consist of a nickel matrix with a uniform dispersion of discrete particles of the ceramic oxide with a spacing less than 0.01 μm, which is considered to be the most effective size for pinning down dislocations. However, owing to the high surface energy of the particles, they tend to form agglomerates in the bath. Various methods have been reported in the literature for preventing particle agglomeration. Dunkerley et al, (1966) evaluated: (1) bubble agitation and mechanical stirring both together and separately: (2) ultrasonic vibration and mechanical stirring combined, and (3) a combination of all three techniques. These workers found that mechanical stirring alone was more effective in depositing higher amounts of dispersed phase for a given particle concentration than when both bubble agitation and mechanical stirring were employed. Ultrasonic vibration plus mechanical stirring showed the same trend. Sautter (1963) using a Waring blender tried three different methods of dispersion of the oxide particles in the electrolyte: (i) dispersing Al_2O_3 directly in the electrolyte:

(ii) dispersing Al_2O_3 in water and adding to the electrolyte; and (iii) dispersing Al_2O_3 in water and adding electrolyte to the dispersion. With the latter technique, Sautter observed a coagulation after adding a small amount of electrolyte to aqueous suspension, but by continuous blending the same grade of dispersion was achieved as by methods (i) and (ii). After preparing the suspension, the electrolyte was stirred for 48 hrs because of entrapment of air by the blending process. Greco and Baldauf found that suspension of particles in a small portion of water and mixing with a blender for five minutes at approximately 15,000 rpm to ensure the break-up of clusters produced specimens with improved mechanical properties when compared to those prepared by immersing the particles directly into the electrolyte and mixing with a magnetic stirrer.

Review of the observations on various methods used to disperse particles in the plating bath indicates the significance of blending the suspension before preparing the composites. The data on mechanical properties of specimens prepared from unblended bath showed considerable scatter and this can be attributed to high degree of clustering or non-uniform dispersion of particles.

It can be seen from Graphs 1 and 2 that with increasing oxide particle content in the electrolyte up

to 20 g/l, the percentage of oxide particles incorporated in the deposit increases linearly. According to Sinha et al (1973), further increase in the Al_2O_3 content above 100 g/l in the electrolyte does not appreciably change the alumina content in the deposit. According to Sautter (1963), the alumina content of the deposit showed a steady rise up to a concentration of 150 g/l of Al_2O_3 (130 g/ Al_2O_3 and TiO_2 quoted by Greco and Baldauf (1968) in the electrolyte. Possibly this difference may be because the bath employed by Sinha et al contained sodium sulphate as an additive. It has been reported by Tomaszewski et al (1969) that the presence of monovalent cations, such as Tl^+, Cs^+, Rb^+, NH_4^+, K^+, or Na^+ in the bath is most effective for greater particle codeposition from a sulphate bath.

The volume percentage of oxide incorporated in the composites examined in this investigation falls within what Jeffries and Archer (1921) have reported as the effective or useful range, which is 2-15 v/o for dispersion strengthening. One may expect that the volume per cent of dispersoids entrapped in an electrodeposit would depend on the number of collisions between the dispersoids and the cathode surface. Therefore, a higher concentration of particles in the plating solution should result in a higher volume per cent in the composite. Low current

densities and increasing flow rates of the solution-particle slurry along the cathode surface may also increase the volume per cent of dispersoids in the matrix. This appears reasonable since both variables should permit a higher number of collisions between the dispersoids and the cathode surface per unit volume of deposited matrix material.

2. Mechanical properties

(i) Hardness

The Ni.Al_2O_3 and Ni.ZrO_2 composites produced by electrodeposition generally exhibited an increase in hardness with an increase in current density up to about 6 A/dm^2. As the current density is increased up to 10 A/dm^2 the nature of the deposit changes, becoming more 'powdery' and hence reducing in hardness (Table 7). From Tables 9 and 10, it can be seen that the hardness of the deposit on the whole, increases with increase in dispersed phase and is about 1½ and 3 times more with 2.02 wt % Al_2O_3 and 3.92 wt % ZrO_2 respectively, compared to pure nickel deposits. The surface of the deposit next to the cathode shows a higher hardness, as usual with all electrodeposited metals, which is probably due to the fine grain size and orientation of the initial deposit (Dhananjayan and Banerjee 1969). The surface of the deposit

facing the solution has a low hardness value compared to the other surfaces due to its comparatively coarser grain size.

It can also be noticed from Tables 7 and 8 that the hardness of the deposits decreases with heat treatment. The tables show a significant increase in hardness of the two alloys as compared with nickel but the difference in hardness between Ni.ZrO_2 and Ni.Al_2O_3 is small for the large difference in wt % of dispersed phase.

(ii) Yield strength

From Tables 11 and 12, it can be seen that like hardness, the yield strengths of the cermet coatings Ni.Al_2O_3 2.02 wt % and Ni.ZrO_2 3.92 wt %, are in order of magnitude greater than that of pure electrodeposited nickel. Composites of 2.02 wt per cent alumina and 3.92 wt per cent zirconia retained a yield strength of 30.2 Kg/mm^2 and 60.8 Kg/mm^2 respectively, after annealing at 750°C. In comparison, the yield strength of similarly annealed, particle-free nickel deposited with similar conditions only 9.6 Kg/mm^2. According to Sautter (1963), nickel - 2.5 wt per cent alumina, annealed at 750°C, showed a yield strength of 35 kg/mm^2. Gillam et al (1966), however, reported slightly higher yield strength (52 kg/mm^2) for a nickel 1.65 wt per cent alumina annealed at 750°C.

These workers found that on annealing at 750°C, though twinning was less prominent, there was no sign of recrystallisation and grain growth as was the case with pure nickel deposits. The particles were situated within grains and had no preference for grain boundaries. On the other hand, on annealing at 1100°C, the alumina particles were found to be redistributed, some forming larger crystals. The grain size of the composite was not increased, however, and the particles did not show any preference for grain boundaries. Nwoko and Shreir (1973) reported that annealing at elevated temperatures (1200-1400°C) resulted in a reduction of dislocation density, and the dislocations were annihilated after prolonged time of annealing. At elevated temperatures, particles became more compact, and particle size increased with time of annealing; however, twinning and grain growth were restricted.

From the standpoint of mechanical properties of the composites tested, the Ni.Al_2O_3 system is most favourable. The yield strength recorded for a specimen obtained from the 10 g/l alumina bath is 52.6 kg/mm^2, whereas, that recorded for a comparable specimen from a zirconia bath is 42.6 kg/mm^2. Similar conclusions have been drawn by Greco and Baldauf (1968) and Nwoko and Shreir (1973).

3. High temperature corrosion resistance

At 700°C the electrodeposited nickel corroded significantly more slowly than the rolled pure nickel (Graph 7). Similar observations have been made for the oxidation rates of annealed electrodeposited nickel compared with those of cold-worked nickel by Hancock and Fletcher (1966), Caplan et al (1972) and Stott and Ashby (1978). These have been explained in terms of formation of heterogeneously nucleated grain boundary voids in the cold-worked nickel lattice (Hancock and Fletcher 1966) which provide adequate sinks for vacancies arriving at the oxide/metal interface as Ni^{2+} ions diffuse outwards through the oxide. In annealed electrodeposited nickel, where the dislocation densities are much reduced, such vacancy sinks are not available, so vacancies tend to accumulate at the metal/oxide interface and the oxidation rate is reduced. Caplan et al (1972) have suggested that the oxide formed on cold-worked nickel is finer-grained than that formed on annealed nickel and the increased oxidation rate is due to the oxide grain boundaries acting as easy diffusion paths for Ni^{2+} through the NiO barrier layer.

From the results in this work (and those of Alcock et al (1969)., Vasantaree (1971), Wootton and Birks (1972), Vasantasree and Hocking (1976)). It is clear that the principal process is the diffusion of Ni^{++} ions through

NiO containing sulphur, which results in the production of NiO and Ni_3S_2 as the main corrosion product at 700°C.

It is apparent that some generalisations can be made concerning the corrosion behaviour of the cermet composites studied. Probably the most obvious of these is that the form of the corrosion kinetics in SO_2/O_2 = 2:1, from 700°C to 900°C, of cermets containing Al_2O_3, ZrO_2 and HfO_2 is very similar, even though large morphological differences can exist in the scales produced (Plates 9, 10 and 11). After an initial rapid rate of weight gain, which can be influenced by relatively minor changes in experimental routine and which lasts up to about 2 hrs, the subsequent rate of weight change is exceedingly small. A most striking feature of the adherent scales grown on these cermet composites is the small grain size which persists throughout severe sulphidation exposures.

It is most instructive to examine the detail data generated in terms of the requirements of the current mechanistic models outlined by Giggins and Pettit (1971), Stringer et al (1971, 1972), for alloys containing dispersed rare earth metal oxides as well as those containing dispersed oxides formed by internal oxidation (see introduction Section A4). Salient features of the models proposed can be summarized below:

(a) The reduction in oxidation rate is attributed to a blocking effect by the dispersoid in the inner layer of the scale.

(b) Pegging of the oxide scale by the oxide dispersion is considered to contribute to the improved scale adhesion.

(c) The dispersoid particles act as nucleation sites for the initally-formed oxides, increasing the number of oxide nuclei and hence accelerating the approach to the steady state scaling condition which with the alloys studied is Cr_2O_3 formation (Stringer et al 1972).

As indicated earlier (Introduction Section A4), the improved oxidation resistance afforded by the presence of the stable oxide dispersion in the alloy seems to be independent of the alloy base and also of the composition of the dispersoid. However, there have not been sufficient systematic investigations to establish whether the size and distribution of the particles were critical.

The present results suggest that the mechanism by which certain rare earth metal oxides (in this case Al_2O_3, ZrO_2 and HfO_2) incorporated coatings protect and influence the sulphidation of nickel based superalloys in the temperature range 700°C to 900°C is as follows. The presence of dispersoids in the coating exert a physical as well as chemical effect on the overall isothermal

sulphidation process. According to Seybolt (1970) the rare earth oxides serve as getters which promote the production of oxi-sulphides. From Table 16, it is interesting to note that the percentage oxidation related to a pure metal specimen show a trend $Ni.HfO_2 > Ni.ZrO_2 > Ni.Al_2O_3$ (88. 86 %, 81.84% and 29.79% respectively). This is in conflict with the kinetic results obtained for the various cermet specimens. The weight-gain versus time curves show the more protective materials to be those with HfO incorporated. However, in terms of the physical blocking barrier, the $Ni.Al_2O_3$, composite is more effective than the Ni.ZrO or $Ni.HfO_2$ because of the higher volume percentage presence of the oxide. Hence, the presence of the oxides at the metal/scale interface or within the inner oxide (Plates 9, 10, 11) can have a blocking effect on the outward diffusion of Ni^{-2+} ions through the NiO scale. Also, the rates of corrosion are less for these materials than for the electrodeposited nickel. This is probably due to the blocking effects of the rare earth oxides at the metal/oxide interface and within the inner oxide. However, the corrosion rates never become sufficiently low to suggest the development of a complete barrier layer at the metal/oxide interface. In addition, pores and voids observed in the inner layers of the composites may also act as blocking barriers by effectively reducing the area available for cation diffusion.

TABLE 16. Comprehensive Information on the Cermet Coatings Under Study

Cermet	$Ni.Al_2O_3$	$Ni.ZrO_2$	$Ni.HfO_2$
Electrolyte addition g/l	10	20	10
Particle size, μm	.01 - .05	0.05 - 0.1	0.05 - 0.1
Incorporation wt %	2.02	3.92	2.35
Volume %	2.58	1.42	0.36
Area Occupation per plane, cm^2	10^{-4} - 10^{-2}	10^{-3} - 10^{-2}	10^{-3}
Oxidation related to a pure metal specimen	29.79%	81.84%	88.86%

A second feature attributed to the presence of the dispersed oxide phases in the composites, is the possible chemical influence on the reduction of sulphidation rate. When considering the cermet and duplex coated, the reactions which can be considered are as follows:

$$3\,Ni_3S_2 + 2HfO_2 + 2\tfrac{1}{2}O_2 = 2HfS_3 + 9NiO \qquad (29)$$

$$6\,CrS + 2HfO_2 + 2\tfrac{1}{2}O_2 = 2HfS_3 + 3Cr_2O_3 \qquad (30)$$

$$3Ni_3S_2 + 2ZrO_2 + 2\tfrac{1}{2}O_2 = 2ZrS_3 + 9NiO \qquad (31)$$

$$6CrS + 2ZrO_2 + 2\tfrac{1}{2}O_2 = 2ZrS_3 + 3Cr_2O_3 \qquad (32)$$

$$3Ni_3S_2 + 2Al_2O_3 + 1\tfrac{1}{2}O_2 = 2Al_2S_3 + 9NiO \qquad (33)$$

$$6CrS + 2Al_2O_3 + 1\tfrac{1}{2}O_2 = 2Al_2S_3 + 3Cr_2O_3 \qquad (34)$$

(see Appendix C for details)

In general the main products other than NiO and Ni_3S_2 observed in the cermet and duplex coated alloys are CrS and Cr_2O_3. The thermodynamic data (Appendix C) indicate that the reaction of the various oxides with other sulphide-forming metals is not possible. The reaction of Al_2O_3 with Ni_3S_2 or CrS to form Al_2S_3 (equations 33 and 34) is not possible because of the high free energy of formation required. At 700°C, K for the reaction with Ni_3S_2 (solid) and (liquid) is 4.06×10^{-24} and 5.85×10^{-31} respectively, and for the reaction with CrS $K = 1.11 \times 10^{-26}$. Calculations for the formation HfS_3 and ZrS_3 show that the required energies of formation (Equations 29 and 31) are low;

$K(29)_{solid} = 3.97 \times 10^5$, $K(29)_{liquid} = 7.95 \times 10^5$ for HfO_2; $K(31)_{solid} = 2.42 \times 10^9$, $K(31)_{liquid} = 1.08 \times 10^8$ for HfO_2 and ZrO_2 reactions with Ni_3S_2 solid and liquid, respectively. Similar conclusions can be drawn when the reactivity of the oxides with other sulphide forming metals are considered at 900°C. The possibility of the oxides, Al_2O_3, ZrO_2 and HfO_2 reacting to form complex oxides with Ni or Cr can be discarded because X-ray results show no evidence of this. The only complex possible is that of $NiAl_2O_4$ and the formation of this spinel is not possible at the temperatures being considered.

It can be argued, therefore, that the predominant factor in the reduction of the sulphidation attack on materials containing Al_2O_3 dispersoid is the physical blocking effect of the diffusing cation. The marked improvement in behaviour depicted by ZrO_2 and HfO_2 dispersoids is attributed solely to their chemical involvement, although the physical effect, however small, cannot be completely iggored. The mixed effect (physical and chemical) is probably responsible for the slower kinetic rates depicted by these materials.

According to Stringer et al (1972), the influence of a dispersoid on the early, transient stages of oxidation is a direct consequence of the dispersed particles acting

as nucleation sites for the initally formed oxides. This reduces the internuclei spacing thereby allowing the nuclei of the protective oxide phase (Cr_2O_3) to grow together to form a continuous layer before any substanial growth of the baser metal oxides occur. As a further consequence of this, the grain size of the scale is reduced as is observed in both the cermets and duplex coated alloys (plates 13-18).

The observations of a stabilised small oxide grain size of the scales formed on the cermets and duplex coated alloys and of larger-grained scales and grain growth on the nickel base alloys from which the scales eventually fractured and spalled point to presence of the dispersed oxide coatings as postulated by both mechanistic models of Giggins and Pettit (1971), Stringer et al (1971 and 1972). The improved scale adhesion results from the change in location of the scale-forming process, the problem of vacancy condensation being eliminated by this change and the growth stresses of the scale being small. Experience of the effect of rare earth oxides additions to nickel/chromium alloys suggests that limited, but frequent, intrusions of the oxide scale into the alloy are highly effective in 'keying' the scale to the alloy. The resistance of the cermet coated alloys to spalling of the scale may, therefore, be due to limited electrodeposit grain - boundary oxidation on an

extremely fine-scale. Thus, the scale plasticity is improved by included particles of oxide acting as dislocation sources in the scale. It is possible that the improved adherence of the oxide scale may contribute towards improving the corrosion resistance by delaying the access of sulphur compounds to the cermet-oxide interface. Similarly, formation of the double oxide layer, and resultant change in the reaction interface between the two oxides, may further inhibit access of sulphur dioxide.

The corrosion kinetics of all the cermet coated alloys are quite similar, although the Al_2O_3 and ZrO_2 containing cermets oxidised slightly faster than HfO_2 cermets. This may be due to the more uniform oxide pegs formed by the HfO_2 as well as the reduced tendency to form voids (Plates 12, 14, 15), as explained by Stringer et al (1977) for the oxidation of Co-Cr-Al alloys containing hafnium additions.

CONCLUSION

1. The preparation of Al_2O_3, ZrO_2, HfO_2 cermets by electrodeposition techniques is relatively simple; the alloys show promise as a useful coating material.

2. The mechanical properties such as hardness and yield strength of the cermets are found to be superior to those of pure electrodeposited nickel.

3. Electrodeposited nickel and pure rolled nickel corroded significantly much faster than the cermets. HfO_2 - containing cermets are found to show better corrosion resistance than Al_2O_3 and ZrO_2 containing cermets.

4. Corrosion of all the specimens was greatest at 700°C and the effects of salt contamination caused the corrosion to accelerate. In general, the most aggressive environment was that containing sodium chloride.

5. The extent of sulphidation of the cermet and cermet-coated alloys is determined by interplay between various factors such as physical blocking by the oxide particles, pores incorporated into the scale and chemical involvment of the oxide particles by reacting with other sulphide-forming metals.

6. Blocking effects by Al_2O_3 are quite significant, particularly for the $Ni.Al_2O_3$ (2.02 wt.%) composite.

7. Effects such as the preferential formation of chromia scales and improved scale adhesion are greatly enhanced in the presence of a dispersed oxide phase in the coated superalloys. The composition of the dispersed oxide does not seem important, nor does its distribution and size.

Future Work

Thermal cycling of cermet and cermet-coated systems would provide, additional data on the mechanical properties of the scales formed.

The effect of prolonged corrosion attack on the coatings used need more detailed study.

The incorporation of other rare-earth oxides into nickel and cobalt matrix should be examined. The ultimate aim would be towards the electrodeposition of complex alloys containing oxide dispersion such as MCrAl type coatings.

Controlled diffusion of chromium and maybe other additional metals through a more noble metal that does not or not strongly react with sulphur dioxide are also worth investigating.

APPENDIX A Values of Percentage Ceramics in Deposits

(i) Percentage Al_2O_3 in deposits.

Wt. of Al_2O_3 in bath	Wt. % Al_2O_3 in deposit		Vol % Al_2O_3 in deposit		Average Value
2 g/l		2		2	
(1)	0.9995	0.4997	3.498	1.749	
(2)	0.9042	0.4521	3.165	1.583	0.47 wt.%
(3)	0.7440	0.372	2.604	1.302	1.66 vol.%
(4)	0.9198	0.4599	3.219	1.6095	
(5)	1.1310	0.5655	3.958	1.979	
(6)	0.9995	0.4997	3.498	1.749	
4 g/l					
(1)	1.611	0.8055	5.638	2.819	
(2)	1.892	0.946	6.622	3.311	0.8 wt.%
(3)	1.777	0.8885	6.219	3.1095	2.92 vol.%
(4)	1.489	0.7445	5.211	2.6055	
(5)	1.526	0.763	5.341	2.6705	
(6)	1.704	0.852	5.964	2.982	
8 g/l					
(1)	3.322	1.661	11.627	5.8135	
(2)	3.416	1.708	11.956	5.978	1.64 wt.%
(3)	3.229	1.6145	11.301	5.6505	5.74 vol.%
(4)	3.089	1.5445	10.811	5.4055	
(5)	3.290	1.645	11.515	5.7575	
(6)	3.350	1.675	11.725	5.8625	
10 g/l					
(1)	4.016	2.008	14.056	7.028	
(2)	4.046	2.023	14.161	7.0805	
(3)	3.889	1.9445	13.611	6.8055	2.02 wt.%
(4)	3.946	1.973	13.811	6.9055	7.07 vol.%
(5)	4.227	2.1135	14.794	7.397	
(6)	4.129	2.0645	14.451	7.225	

(ii) Percentage ZrO_2 in deposits

Wt. of ZrO_2 in bath	Wt.% ZrO_2 in deposit	Vol.% ZrO_2 in deposit	Average value
5 g/l	1.220	6.832	1.19 wt.%
	1.190	6.664	
	1.180	6.608	6.69 vol.%
	1.210	6.720	
	1.180	6.608	
10 g/l	1.80	10.080	1.84. wt.%
	1.84	10.326	
	1.86	10.416	
	1.90	10.640	
	1.82	10.192	
15 g/l	3.64	20.384	
	3.60	20.160	
	3.56	19.946	
	3.58	20.048	
	3.62	20.272	
20 g/l	3.96	22.176	3.92 wt.%
	3.92	21.952	21.93 vol.%
	3.87	21.672	
	3.96	22.176	
	3.87	21.672	

(iii) Percentage HfO_2 in Deposits

Wt of HfO_2 in bath	wt.% HfO_2 in deposit	vol.% HfO_2 in deposit	Average Value
2 g/l	0.275	2.662	
	0.266	2.575	0.28 wt.%
	0.284	2.749	2.71 vol.%
	0.298	2.885	
	0.278	2.691	
6 g/l	1.333	12.903	
	1.330	12.874	
	1.317	12.749	1.33 wt.%
	1.353	13.097	12.87 vol.%
	1.328	12.855	
10 g/l	2.350	22.748	
	2.330	22.554	2.35 wt.%
	2.381	22.951	22.78 vol.%
	2.375	22.990	
	2.342	22.671	

APPENDIX B Mechanical Properties Data

(i) Micro-hardness measurements

Ni-Al_2O_3 cermet

C.D. = 2 A/dm^2, Temp 50°C, Air Agitation

Conc of ceramic in Electrolyte g/l	VHN as plated		VHN annealed	
	Solution side	substrate side	solution side	substrate side
0	179	257.2	130.9	148.6
	168.2	262.4	130.9	148.6
	166.1	254.4	130.9	145.7
	161.9	264.6	130.9	145.7
	179.0	264.5	130.9	145.7
Average	170.8	260.6	130.9	146.9
2	207.6	278.1	156.9	172.5
	204.3	275.8	157.7	174.1
	201.2	187.4	156.9	171.8
	204.3	275.8	156.9	174.1
	207.6	287.4	157.7	172.5
Average	205.0	280.9	157.2	173.0
4	209.96	301.5	184.9	195.1
	211.3	308.7	189.4	195.1
	209.0	313.9	183.2	199.0
	217.0	299.8	186.6	193,3
	211.3	313.9	189.4	199.0
Average	211.7	307.6	186.7	196.3
6	235.6	324.2	207.6	209.96
	239.96	313.9	203.4	213.4
	234.1	329.1	200.2	208.8
	246.8	319.0	200.2	218.8
	235.6	324.2	207.6	213.4
Average	238.4	322.1	203.8	212.9

Continued.....

APPENDIX B. Continued.

	257.4	335.9	224.6	257.4
	254.1	341.7	228.5	268.3
8	260.8	333.3	220.97	264.5
	260.8	341.7	219.6	261.0
	257.4	333.3	228.5	257.4
Average	258.1	337.2	224.4	261.7
	275.8	357.3	247.7	268.3
	278.1	364.4	247.7	272.0
10	278.1	364.4	244.7	268.1
	266.8	378.2	247.3	264.5
	278.1	357.3	347.7	272.0
Average	275.4	364.3	247.0	269.0

(ii) Micro-hardness measurements

Ni-ZrO_2 cermet
C.D. = 4 A/dm^2, Temp 50°C, Air Agitation

Conc of ceramic in Electrolyte g/l	VHN as plated		VHN annealed	
	Solution side	substrate side	solution side	substrate side
5	235.2	283.0	203.6	220.0
	236.3	282.2	203.5	219.8
	235.9	283.2	204.8	220.6
	236.0	283.2	204.7	219.0
	234.6	281.6	204.6	219.3
	235.6	282.6	204.2	219.7
10	295.2	341.2	269.8	278.8
	298.8	340.0	270.6	279.6
	299.1	339.4	270.8	281.8
	299.8	340.4	269.7	281.9
	298.5	340.2	271.0	281.8
	298.3	340.2	270.4	280.8
15	361.8	410.4	332.5	347.4
	360.4	410.8	336.4	351.0
	363.2	411.6	331.6	347.9
	363.8	409.6	337.8	351.6
	364.8	410.6	334.2	350.1
	362.8	410.6	334.5	399.6
20	420.40	446.2	407.6	410.5
	420.51	449.0	408.6	414.2
	419.92	449.4	407.8	412.8
	420.80	448.6	409.2	413.0
	420.54	447.8	408.3	412.6
	420.4	448.2	408.3	412.6

Continued/.....

178.9	256.00	130.5	147.3
168.3	260.30	130.9	148.0
166.6	255.40	130.4	145.6
172.0	260.20	130.8	145.2
168.2	267.30	130.4	145.0
170.6	259.8	130.6	146.2

APPENDIX C Thermodynamic Data

	Hkcal	S	
Ni		7.12	
Cr		5.68	
Hf		10.5	
Zr		9.3	
sl		6.77	
Ni O	-57.5	9.1	
Cr_2O_3	-270.0	19.4	
HfO_2	-266.0	14.2	
ZrO_2 l	-259.5	12.1	
Al_2O_3	-400.0	12.2	
Ni_3S_2	-47.5	52.0	Lf 5.3 kcal at 890°C 1063K
NiS_2	-34.0		
CrS	-63.9	19.48	
HfS_2	-140.0	20.0	
HfS_3	-149.0	23.0	
ZrS_2	-138.0	18.7	
ZrS_3	-150.0	21.7	
Al_2S_3	-172.9	27.0	
O_2	0	49.03	

$Ni + \frac{1}{2} O_2 = NiO$ $\quad \Delta G^\circ$ -58450 + 23.55T

$2Cr + 1\frac{1}{2}O_2 = Cr_2O_3$ -267, 750 + 62.1T

Reaction		ΔG^{o}, Cal		K		P_{O_2}	
		973K	1173K	973K	1173K	933K	1173K
$3\ Ni_3S_2 + 2HfO_2 + 2\frac{1}{2}O_2 =$	$Ni_3S_{2(s)}$	-24,921		3.97×10^{5}		5.76×10^{-3}	
$2HfS_3 + 9NiO$	$Ni_3S_{2(l)}$	-26,265	586.98	7.95×10^{5}	7.78×10^{-1}	4.36×10^{-3}	1.1
$6\ CrS+2HfO_2+2\frac{1}{2}O_2 =$ $2HfS_3+3\ Cr_2O_2$		-33,437	-721	3.25×10^{7}	1.36	9.9×10^{-4}	8.85×10^{-1}
$3\ Ni_3S_2+2ZrO_2+2\frac{1}{2}O_2 =$	$Ni_3S_{2(s)}$	-41,770		2.42×10^{9}		1.76×10^{-4}	
$2ZrS_3+9NiO$	Ni_3S, (l)	-43,114	-166.41	1.08×10^{8}	1.26×10^{3}	6.12×10^{-4}	5.75×10^{-2}
$6CrS+2ZrO_2+2\frac{1}{2}O_2 =$ $2ZrS_3+3Cr_2O_3$		-158,366	-148,246	3.77×10^{35}	4.21×10^{27}	5.88×10^{-15}	8.92×10^{-12}
$2\ Ni+O_2=2\ NiO$		-71,072	-61,652	9.25×10^{15}	3.08×10^{11}	1.1×10^{-16}	3.25×10^{-12}
$2/3(2Cr+1\frac{1}{2}O_2=Cr_2O_3)$		-138,218	-129,938	1.12×10^{31}	1.63×10^{34}	8.93×10^{-32}	6.13×10^{-25}
$3\ Ni_3S_2+2Al_2O_3+1\frac{1}{2}O_2 =$ $2Al_2S_3+9NiO$	Ni_3S_2(s)	104,126		4.06×10^{-24}		3.93×10^{15}	
	Ni_3S_2(l)	134,582	149,234	5.85×10^{-31}	1.55×10^{-28}	1.43×10^{20}	1.61×10^{19}
$6CrS+2Al_2O_3+1\frac{1}{2}O_2 =$ $2Al_2S_3+3Cr_2O_3$		115,540	133,616	1.11×10^{-26}	1.26×10^{-25}	2.01×10^{17}	3.97×10^{-16}

REFERENCES

Alcock, C.B., and Hocking M.G. — Trans. Instn. Min. Metall(Sect. C) 75, C27 (1966)

Alcock, C.B., Hocking, M.G. and Zador, S. — Corros. Sci. 9,11 (1969)

Anders F.J., Alexander, G.B. and Wartel, W.S. — Met. Prog. 88, Dec. 1962

Ansell, G.S., Cooper, T.D. and Lenel, F. (editors) — (1966) Oxide Dispersion strengthening Second Bolton Landing Conference, Bolton Landing, New York.

Arkharov, V.I., Konev, V.N., Nesterov, A.F., Andrianovskii, B.P. and Glazkova, I.M.P. — Issled Sharopvr. Splav Inst. Met., A.A. Baikova 10, 239 (1963)

Bartocci, R.S. — Behaviour of high-temperature coatings for gas turbines engine. Hot. Corr. Probl. Assoc. with Gas Turbines, ASTM Special Technical Report No. 421 (Sept, 1967)

Beltran, A.M. and Shores, D.A. — "Superalloys" C. T. Simms and W.C. Hagel, Editors, p. 317. John Wiley and Sons, Inc., New York, 1972.

Bergman, P.A., Beltran, A.M., and Sims, C.T. — Development of hot corrosion resistant alloy for Marine Gas Turbine Service. Final Summary Report to MEL (Oct. 1967)

Bergman, P.A. — General Electric Report, R64, SE10 (1964)

Betteridge W. and Heslop, J. — 'The Nimonic alloys and other Ni based high temp. alloys.' 2nd ed. 1974. Published by Edward Arnold Ltd. London.

Betteridge, W., Sachs, K, and Lewis, H. — J. Inst. Petroleum, 41, 170-180 (1955)

Blum, W. and Hogaboom, G.B. — Principles of Electroplating and Electroforming. 3rd ed. McGraw-Hill, New York, 1949, pp 200-219.

Blum, W. and Rawdon, H.S. — Trans Am. New York 44, 305 (1923)

Bockris, J.O'M, and Mehl, W.	J.Chem.Phys. 27, 817 (1957); Can. J.Chem., 37, 190 (1959)
Bornstein, N.S. and Decrescente, M.A.	Trans.AIME, 245, 1947, (1969)
Bowers, N.K.	ASME Gas Turbine Conf., Paper No. 66-GT/M25 (1966)
Brandes, H.	Z. Physik.Chem. 126, 196 (1927)
Brandes, E.A. and Goldthorpe, D.	Mettallurgia 76, 195 (1967)
Brenner, A., Zentner, V. and Jennings, C. W.	Plating, 39, 865, 1229 (1952)
Broszeit, E., Heinke, G. and Wiegand, H.	Metall. 25 (5) 470-475 (1971).
Brough, B.J. and Kerridge, D.H.	Inorg.Chem., 4, 1353, 1965
Brown, D.S.R. and Gow, K.V.	Plating, 437-439 (1972)
Brown, H. and Silman, H.	TIMF, 1964, 42, 50.
Browning, M.E., Leavenworth, Jr. H.M., Webster Jr. Will., and Dunkerley, F.J.	"Deposition Forming Processes for Aerospace Structures", ML-TDR-64-26 (Feb.1964).
Bunshah, R.F., and Goetzel, C.G.,	"A survey of Dispersion Strengthening of Metals and Alloys", WADC Technical Report 59-414, July 1959.
Caplan, D., Graham, M.J. and Cohen, M.	J. Electrochem.Soc 119, 207, (1972)
Celis, J.P. and Roos, J.R.	J. Electrochem.Soc., 1977, 124, 10, 1503.
Centolanzi, F.J., Probst, H.B., Lowell, C.E., and Zimmerman, N.B.	"Arc Jet Tests of Metallic TPS materials", NASA Technical Memorandum X-62092 (October 1971)
Chapman, D.L.	Phil.Mag., 25, 475 (1913)
Chatterji, D., McKee, D.W. Romeo, G., and Spacil, H.S,	J. Electrochem. Soc. 122, 941 (1975)
Chattopadhyay, B. and Wood, G.C.,	J. Electrochem Soc, 117, 1163 (1975)
" "	Oxid. Metals, 2, No. 4, 373 (1970)
Chen, E.S. and Sautter, F.K.	Plating Surf. Finish, 63, (5) 28-32 (1976)

Cole, S.R.	Masters Thesis, Virginia Polytechnic Inst. 1967.
Conde, J.J.	Specialist Meeting on High Temp. Corr. of Aerospace Alloys. AGARD, Lyngby, Denmark, April, 1972.
Conway, B.E., and Bockris, J.O'M.	Electrochim. Acta 3, 340 (1960).
Cunningham, G.W. and des Brasunas, A.	Corrosion 12, 3896 (1956).
Cutler, A.J.B., Halstead, W.D., Laxton, J.W., and Stevens, C.G.	Trans. ASME Series A93, 307, (1971).
Dalder, E.N.C., Talboom, F.P.	Development of coated superalloy components for gas turbine engine applications. Progress Reports under contract AF33(615)-1938) (1964-65)
Danek, G.J.	"State of the Art" Survey on Hot Corrosion in Marine Gas Turbine Engines," Naval Engineers Journal, Dec. 1965. p. 857.
Davis, H.H., Graham, H.C. and Kvernes, J.A.	Oxidation of Metals; 3 (5) 431 (1971).
Davis, H.J. and Kinnibrugh, D.R.	J. Electrochem. Soc., 117, 392 (1970).
Decker, R.F., Rowe, J.P. and Freeman, J.W.	NACA Tech. Note No, 4049, 34pp (Washington D.C), (1957).
Delimarskii, Yu.K., Markov, B.F.	'Electrochemistry of Fused Salts.' Sigma Press, New York, 1961.
De Crescente, M.A. and Bornstein, M.S.	Corrosion 24 127, (1968).
Doering, H.V.,	J. Mater. 4, 457, (1969).
Dooley, R.B., Kerby, R.C. and Wilson, J.R.	Progr. Rept. No. 2., Defence Research Board Grant No. 7535-14, Queens University, Kingston, Ontario, Canada, Oct. 1971.
Douglas, D.L., and Armijo, J.S.	Oxid Met., 2, 207 (1970).
Dubpernell, G.	Plating 47, 35 (1960).

Dunkerly, F.J., Leavenworth, H.W. and Eichelman, G.E.	"Oxide Dispersion Strengthening" 2nd Bolton Landing Conference, AIME, June 27-29, 1966. New York.
Erdy-Gruz, T. and Volmer, M.	Z. Physik.Chem. A 157, 165 (1931).
Elliot, P.	Corrosion Science, 12, 291-293,(1972.).
Elliott, P. and Hampton, A.S.	Conf. on Deposition and Corrosion in Gas Turbines, C.E.G.B. London, England, Dec. 1972.
Feisel, D.H., and Cochardt, A.,	"Aging characteristics of some simple precipitation - hardened and dispersion-hardened Nickel-Based alloys" Scientific Paper 8-0161-P6, Westinghouse Research Labs., Pittsburgh 35, Pa. Trans. AIME, 1959.
Finch, G.I., Wilman, H. and Yang, L.	Electrode Processes. Discussion of the Faraday Soc. Butterworths, London, 144-158 (1947).
Fishlock, D.J.	Metal Finishing; 57,-48, (Feb. 1959)
" "	" " " " " 57, 55,(Mar., 1959)
Fleischmann, M. and Thirsk, H.R.	Advan. Electrochem., Electrochem. Eng. (eds. Delahay and Tobias), 3, 123 (1963).
Flood, H., Forland, T., and Motzfeldt, K.	Acta. Chem. Scand., 6, 257,(1952).
Fontaine, P.I.	Br. Corrosion. J. 4 154 (1969).
Foster, J., and Cameron, B.	TIMF, Winter 1976, 54, 178.
Foster, J. and Kariapper, A.M.J.	Trans IMF, 1973, 51, 27-31.
Gerischer, H. and Tischer, R.P.	Z. Elektrochem. 61, 1159 (1957); 62, 256 (1958).
Geyer, N. and Lane, P.	A critical look at superalloy coatings, J. Metals 18 (Feb 1966).
Giggins, C.S. and Pettit, F.S.	Trans. TME-AIME 245, 2495-2507 (1969).

Giggins, C.S., and Pettit, F.S.	Trans. AIME 245, 2695 (1969); Pratt and Whitney Aircraft, Advanced Materials Research and Development Laboratory Report No. 68-024 (October, 1968).
Giggins, C.S., and Pettit, F.S.	Metall. Trans. 2, 1071, (1971).
Gilbreath, W.P.	"Preliminary Studies of the Oxidation of TDNi - 20Cr in Static, Flowing and Dissociated Oxygen at 1100°C and 130 N/m^2, NASA Technical Memorandum X-62064 ((August 1971).
Glasstone, S.	Textbook of physical chemistry, p. 1240-1248, D. Van Nostrand, New York, 1946.
Goebel, J.A., and Pettit, F.S.	Met. Trans. 1, 1943, (1970); 1, 3421, (1970).
Goebel, J.A., Pettit, F.S., and Goward, G.W.	Met. Trans. 4, 261, (1973).
Goebel, J.A., Pettit, F.S., and Goward, G.W.	Conf. on the deposition and corrosion in gas turbines, CEGB, London. England, Dec. 1972.
Goward, G.W.	Journal of Metals. October (1970) 31-39.
Goward, G.W.	"Protective coatings for high - temp. alloys", in properties of high temperature alloys with emphasis on environmental effects. pp. 806-823, (1976).
Goward, G.W., and Boone, D.H.	Oxid. Metals, 3, 475 (1971).
Gouy, G.	J. Physique, 9, 457, (1910).
Graham, A.K.	Trans. Am. Electrochem. Soc. 44, 427, (1923).
Graham, A.K. Ed.	Electroplating Engineering Handbook. 3d. ed., Van Nostrand, / Reinhold, Princetown. N.J. 1971.
Graham, D.C.	Chem. Rev., 41, 441, (1947).
Graham, L.D., Gadd, J.D., and Quigg, R.J.	Hot Corrosion Behaviour of Coated and Uncoated Superalloys, Hot Corrosion Problems associated with Gas Turbines, ASTM. Special Technical Report. No. 421 (Sept. 1967).

Graves, A.D., Hills, G.J. and Inman, D.	Advances in electrochem. and electrochemical eng. Vol. 4. Edited by P. Delahay and C.W. Tobias. Interscience Publishers, John Wiley and Sons, Inc. New York. 1966.
Greco, V.P. and Baldauf, W.	Plating, 55, 250, (1968).
Greco, V.P., Wallace, W.A., and Cesaro, J.N.C.	Plating, 262 (1969).
Greenert, W.J.	Corrosion, 18 57t, (1962).
Grisaffe, S.J. and Lowell, C.E.	"Examination of Oxide Scales on Heat Resisting Alloys, " NASA Technical Note D-4019 (February 1969).
Guglielmi, N.	J. Electrochem Soc. 119, 8, 1009, (1972).
Hamilton, P.E., Ryan, K.H. and Nichols, E.S.	Nickel base alloys and their relationship to hot corrosive environments, Hot Corrosion Problems Assoc., with Gas Turbines, ASTM special Technical Report No. 421 (September, 1967).
Hancock, P.	1st International Congress on Metallogical Corrosion, p.193, Butterworths, London, (1961).
Hancock, P. and Fletcher, R.	Metallurgia 6, 1 (1966).
Hancock, P. and Hurst, R.C.	Paper presented at CAPA Cong. "Oxidation and Sulphidation of Ni and Co-Base Alloys", Liverpool, (1971).
Hardt, R.W. Gambino, J.R. and Bergman, P.A.	Marine Hot Corrosion Mechanism Studies, Hot Corrosion Problem Assoc. with Gas Turbines, ASTM Special Technical Report No. 421 (Sept. 1967).
Harris, J.C.	Spec. Tech. Publ. No. 90-E (1960); ASTM, Philadelphia, Pa.
Hocking, M.G., Vasantasree, V. and Nagaraj, B.A.	AML, Progress Report. Jan. 1976.
Hocking, M.G., Vasantasree, V. and Swidzinski , M.	AML. Progress Report. June, 1977.
Hothersall, A.W.	Trans. Electrochem. Soc., 64, 69, (1933); Trans. Faraday. Soc., 31, 1242, (1935).

Hothersall, A.W.	J. Electrodeposition Soc. 13, 12, (1937).
Hume-Rothery, W.	Inst. of Metals (1960).
Inman, D. and Wrench, N.S.	Brit.Corr.J., 1, 246, (1966).
Ipat'ev, V.V. and Zhellukin, D.V.	Metallov. Obrab. Metall. 12, 42, (1958).
Janz, G.J., Ward, A.T., and Reeves, R.D.	'Molten Salt Data', Renssaler Polytechnic Inst., US-AFOSR No. 63-0039, 1964.
Jeffries, Z. and Archer, R.S.	Chem.Eng. 24, No. 24(June 15, 1921).
Johnson, K.E. and Laitinen, H.O.	J.Electrochem.Soc., 110, 314, (1963).
Jorczyk, E.R.	Metal Finishing 55, 46-49, March (1957)
Kariapper, A.M.J. and Foster, J.	Trans. IMF, 52, 87 (1974).
Kedward, E.C.	Metallurgia, 79, (476,) 225-228, (1969).
Kedward, E.C.	Electroplating and Metal Finishing, 25, 9, (1972).
Kedward, E.C.	Cobalt, 66, (3), 53-59, (1973).
Kedward, E.C.	Trans. IMF, Summer 1977.
Kedward, E.C., Addison, C.A. and Tennett, A.A.B.	Trans. IMF, 54, (1), 8-15, (1976).
Kedward, E.C. and Martin, B.	Trans. IMF, 116 (1967).
Kofstad, P.	High Temperature Oxidation of Metals. Wiley. Lond. (1966).
Kramar, O.P.	Galvanotechnik 48, 477, (1957).
Kravchenko, T.G. and Zhuk, N.P.	Prot.Met. (USSR) 5, 549, (1969).
Kubaschewski, O. and Hopkins, B.E.	Oxidation of metals and alloys. Butterworths, London, (1962).
Kvernes, I. and Kofstad, P.	"Studies on the behaviour of nickel-based superalloys at high temperatures," Tech. Rep. AFML-TR-70-103, July 1970.

Lakshminarayan, G.R. , Chen, I.E.S. and Sautter, F.K.	Plating and surface fin., 63, (5), 35-39, (1976).
Lewis, H. and Smith, R.A.	1st International Congress on Metallic Corrosion, London, April. p. 202, (1961).
Leszynski, W. (Editor)	Powder Metallurgy, Proceedings of an International Conference, New York, (1960).
Linford, H.P. and Saubestre, E.B.	Plating, 37, 1265, (1950); 38, 60, 158, (1951)
Littlewood, R.	Electrochim.Acta., 4, 114, (1961).
Liu, C.H.	J.phys.chem., 66, 164, (1962).
Llewelyn, G.	Protection of nickel-base alloys against sulphur corrosion by pack aluminizing, Hot.Corr.Probl.Assoc. with Gas Turbines, ASTM Special Technical Report No. 421, 10, 2943, (September, 1967).
Lorenz, W.	Z.Naturforsch., 9, 716 (1954).
Lowell, C.E.	"A scanning Electron Microscope study of the Surface Morphology of TD-Ni Cr Oxidised at 800°C to 1200°C, " Technical Note D-6290 (April, 1970).
Lucas, G. Weddle, M. and Pierce, A.	J.Iron and Steel Inst., 179, 342, (1955).
Lund, C.H. and Wagner, H.J.	Oxidation of Ni- & Co-Based Superalloys, DMIC Report 214, March 1965.
Lustman, B.	Trans.AIME, 188, 975, (1950).
Lux, H.	Z.Elektrochem., 45, 303, (1939).
Lyons, E.H.	Trans.Electrochem.Soc., 88, 281, (1945).
Lyons, E.H. Jr.	J.Electrochem.Soc., 101, 361, (1954); 376 (1954).
Mansfeld, F., Paton, N.E. and Robertson, W.M.	Met.Trans. 4, 321, (1973).

Martin, P.W. — Met.Fin.J. 399 and 447, (1965).

McKee, D.W., Chatterji, D. and Romeo, G. — Corres.Sci. 16, 4, (1976).

McKee, D.W., and Romeo, G. — Met.Trans., 4, 1877, (1973).

McKee, D.W., and Romeo, G. — Met.Trans., 5, 1127, (1974).

Metal Finishing Guidebook - Directory, Metals and Plastics Publications, Westwood, N.J., Annual.

Metals Handbook, 8th ed. Vol. 11, American Society for Metals, Metals Park, Ohio, 1964.

Michels, T. Harold. — Metall.Trans. 7A, 379 (1976).

Modi, H.J. and Fursteneau, D.W. — J.Phys.Chem., 61, 640, (1957).

Moller, W. — Conf. on Deposition and Corrosion in Gas Turbines, CEGB, London, (Dec. 1972).

Monson, L.A. — Proc. 2nd Bolton Landing Conf. on "Oxide Dispersion Strengthening, 1966". Gordon-Breach Publ., New York, 1969.

Morisset, P., Ostwald, J.W. Draper, C.R. and Pinner, R. — Chromium Plating. Teddington (Middlesex), Robert Draper Ltd., 1954.

Muller, K. — Metalloberflaeche 14, 261, (1960).

Myers, B.S. — Met.Prog., 76, (5, 6), 103, 108, 172, (1959).

Neckarsulm, N.S.U., — Br.Pat. 1, 200, 410, (1970).

O'Connor, D.J., Johansen, P.G. and Buchanan, A.J. — Trans.Faraday Soc., 52, 229, (1956).

Pannetier, G. and Davignon, L. — Ball.Soc.Chim. Fr., 2304 (1964).

Pettit, F.S., Goebel, J.A. and Goward, G.W. — Corrosion Sci., 9, 903, (1969).

Pfeiffer, H. and Sommer, G. — Z.Metallk., 57, 326, (1966).

Posselt, H.S., Anderson, F.J. and Shrode, P.D. — Plating, 55, 833, (1968).

Rapp, R.A.	Proc. 2nd Bolton Landing Conference on "Oxide Dispersion Strengthening 1966,". (Gordon-Breach Publ. New York, 1969).
Read, H.J.	Proc. Am. Electroplat. Soc., 50, 37, (1963).
Reinkowski, D. and Knorr, C.A.	Z. Elektrochem. 58, 709, (1954).
Rice, L.P.,	Battelle Memorial Institute Defence Metals Information Centre. Memorandum 210, (1965).
Romanoff, F.P.	Trans. Electrochem. Soc., 65, 385, (1934).
Roos, J.R., Celis, J.P. and Helsen, J.A.	Trans. IMF, 55, 113. (1977).
Roos, J.R., Celis, J.P. and Kelchtermans, H.	Thin solid films, 54, 173-182, (1978).
Rumyantsev, Y.V. and Chizhikov, D.M.	Isv. Acad. Nauk. USSR Otdel. Tekh. Nauk. 147, (1955).
Sachs, K.	Metallurgia, 57, 123, 167, 224, (1958).
Sadak, J.C. and Sautter, F.K.	Met. Eng. Q., 14, (3), 44-49 (1974).
Samuel, R.L. and Lockington, N.A.	Chemical and Process Eng., 249, (May 1964).
Sanders, W.A. and Barrett, C.A.	"Oxidation Screening at 1204°C (2200°F) of Candidate Alloys for the Space Shuttle Thermal Protection System," NASA Technical Memorandum X-67864 (October 1971).
Saubestre, E.B.	Metal Finishing 59, 65, (March 1961).
Saubestre, E.B.,	Metal Finishing 61, 77, (December, 1963).
Sautter, F.	Metalloberflaeche. 6, B55 (1954).
Sautter, F.K.	J. Electrochem. Soc. 110, 557 (1963).
Schafer, R.J., Quatinetz, M. and Weeton, J.W.	Trans. AIME, 221, 1099, (1961).

Seltzer, M.S., Wilcox, B.A., and Jaffee, R.I.	"Development of Oxidation Resistance in Thoriated Nickel-Chromium Based Alloys," NASA Contractor Report CR-120880 (December, 1971); Metall. Trans. 3, 2390 (1972).
Senderoff, S.	Metal Finishing 48, 59, (July 1950), 71, (Sept 1950).
Serota, L.	Metal Finishing 62, 73-74, 77, (August 1964). US Pat : 2750335-7 2956935 2655471 2846380
Seybolt, A. U.	Trans. AIME, 242, 1955 (1968).
Seybolt, A.U.	General Electric Co. Corp. R & D Report No. 70-C-189 (1970).
Seybolt, A.U.	Oxidation of Metals 2, 119-143, (1970).
Seybolt, A.U. and Beltran, A.M.	High temperature sulphur-oxygen corrosion of nickel and cobalt, Hot. Corr. Probl. Assoc. with Gas Turbines, ASTM Special Technical Report No. 421. (Sept 1967).
Simons, E.L., Browning, G.V. and Liebhofski, H.A.	Corrosion, 4, 505t, (1955).
Sims, C.T.	A contemporary view of nickel-base superalloys, J. Metals, 18, (October 1966).
Sinha, P.K., Dhananjayan, N. and Chakrabarti, H.K.	Plating, 55-59, (January, 1973).
Skelton, E.W.	Australian Patent 166814. (1946).
Snaith, D.W. and Groves, P.D.	Trans. IMF. 50, 95, (1972).
Snaith, D.W. and Groves, P.D.	Trans. IMF. 55, 136, (1977); 56, 9, (1978).
Snavely, C.A. and Faust, C.L.	Electroplating Engineering Handbook, 2nd ed., A.K. Graham, Ed., Reinhold, New York, pp. 176-189, 1962.

Spring, S.	Metal Finishing Guidebook, Metals and Plastics Publications, Westward, N.J., pp. 208-232. (1962).
Stern, O.	Z. Electrochem. 30, 568, (1924).
Stott, F.H., and Ashby, D.J.	Corrosion Sci. 18, 3, (1978).
Stafford, P., Hunt, P.J. Winstanley, G.R., & Harrison, J.M.	Proc. 3rd US/UK Navy Conf. on Gas Turbines Materials in Marine environment, Bath Univ. (Sept. 1976).
Stringer, J.	NCIC Report No..72-08, Battelle-Colombus (1972).
Stringer, J. and Hed, A.Z.	Oxidation of Metals 3, (6), 571, (1971).
Stringer, J., Whittle, D.P., and El-Dahshan, M.E.	Corrosion Science Symposium, Guildford, (1972).
Stringer, J.. Wilcox, B.A. and Jaffee, R.I.	Oxidation of Metals 5, 11 (1972).
Stringer, J., Wright, I.G., Wilcox, B.A. and Jaffee, R.I.	"Oxidation and Hot Corrosion of Ni-Cr and Co-Cr-base alloys containing rare earth oxide dispersions, " Final report to NASC on Contract No. 0019-71-C-0079. (October, 1971).

"Strong new nickel beats superalloys above 2000°F, " Materials in design engineering 56, No. 2, 12-13, (1962).

Stuart, R.E.	"TD Nickel", Materials in Design Eng. 58, 2, p. 81, (August 1963).
Swidzinski, M.A.M.	PhD thesis, London Univ. 1980.
Swofford, H.S. and Laitinen, H.A.	J. Electrochem. Soc., 110, 814, (1963)
Sykes, J.M. and Alner, D.J.	Trans. IMF, 52, 28, (1974).
Tammann, G. and Jaacks, H.	Z.Anorg. Allgem. Chem. 227, 249 (1926).
Tomaszewski, T.W.	Trans.IMF. 54, 45, (1976).
Tomaszewski, T.W., Clauss, R.J. and Brown, H.	Proc.Amer. Electroplaters Soc., 50, 169, (1963).

Tomaszewski, T.W. Tomaszewski, L.C., and Brown, H.	Plating, 1234, (1969).
Tschinkel, J.G.	Corrosion, 28, 161 (1972).
Ubank, R.	Paper presented at a "Colloquium on Hot Corrosion in Marine Gas Turbines". Admiralty Materials Laboratory, (22-23 Sept. 1970). US Patent : 3,159,908, December 8, 1964 assigned to Dupont.
Vasantasree, V.	PhD. Thesis, London University, May, 1971.
Vasantasree, V. and Hocking, M.G.	Corrosion Sci., 16, 5, (1976).
Ver Snyder, F.L.	"Status and future of nickel-base alloys", High Temp. materials, Edited by R.F. Hehemann and G.M. Ault, J.W. Wiley and Sons. (1959).
Vernon, W.H.J.	J.Inst. Metals, 48, 121 (1932).
Volmer, M.	Das elektrolytische Kristallwachstsum, Paris, Hermann, et Cie (1934).
Wallwark, G.R. and Hed, A.Z.	Oxidation of metals, 3, (3), 229 (1971).
Wasielewski, G.E.	Oxidation of nickel and cobalt superalloys, General Electric Report. R68AEG 141, January 1968.
Weiner, R.	Metalloberflaeche, 14, (7), 69 (1960).
West, C.	Metal Finishing, 51, 66, (August 1953).
Wheatfall, W.L., Doering, H. and Danek, G.J.	"The behaviour of superalloy oxide films in molten salts, " Hot Corrosion Problems Associated with Gas Turbines, ASTM STP 421, Am.Soc. Testing Mats., pp.206-222, (1967).
Wilcox, B.A., and Clauer, A.H.	Metal.Sci.J. 3, 26-33, (1969).
Wile, G.J.	Superalloys for aerospace applications, J.Metals 15, (Sept. 1963).

Williams, R.V.	Electroplat. Met. Fin., (March 1966).
Williams, R.V. and Martin, P.W.	Trans. IMF, 42, 182, (1964).
Wilson, G.A.	Met. Finish. 58, (6), 50, (1960).
Withers, J.C.	WAAD Tech. Rep. 60-718, (Jan. 1961).
Withers, J.C.	Prod. Fin. 27, 62, (1962).
Wootton, M.R. and Birks, N.	Corrosion Sci. 12, 11, (1972).
Wright, I.G., Wilcox, B.A. and Jaffee, R.I.	Oxidation of metals. 9, (3), 275, (1975).
Zwilsky, K.M. and Grant, N.J.	"Copper - Silica and Copper-Alumina Alloys, of high - temp. interest. " Trans. AIME 209, pp. 1197-1201, (1957).

****

ACKNOWLEDGEMENTS

I would like to thank my Supervisor Dr. M.G. Hocking for his interest in this work, and for providing facilities for the work. I am also indebted to Dr. V. Vasantastree for her guidance and many valuable discussions throughout this investigation.

Thanks are also due to Mr. P. Cawley (JOEL Ltd) for the use of the TEMSCAN instrument, and Mr. J. Foster and colleagues (Metal Science Division, Polytechnic of the South Bank) for all their assistance.